General Disclaimer

One or more of the Following Statements may affect this Document

- This document has been reproduced from the best copy furnished by the organizational source. It is being released in the interest of making available as much information as possible.
- This document may contain data, which exceeds the sheet parameters. It was furnished in this condition by the organizational source and is the best copy available.
- This document may contain tone-on-tone or color graphs, charts and/or pictures, which have been reproduced in black and white.
- This document is paginated as submitted by the original source.
- Portions of this document are not fully legible due to the historical nature of some
 of the material. However, it is the best reproduction available from the original
 submission.

Produced by the NASA Center for Aerospace Information (CASI)

HEAT AND MOISTURE FLOW IN CONCRETE AS A FUNCTION OF TEMPERATURE

Jürgen Hundt

(NASA-TM-75286) HEAT AND MOISTURE FLOW IN N79-12152 CONCRETE AS A FUNCTION OF TEMPERATURE (National Aeronautics and Space Administration) 214 p HC A10/MF A01 Unclas CSCL 11D G3/24 38487

Translation of "Wärme- und Feuchtigkeitsleitung in Beton unter Einwirkung eines Temperaturgefälles," German Commission for Reinforced Concrete, Report No. 256, published by Wilhelm Ernst & Son, Berlin, 1975, 108 pages.



NATIONAL AERONAUTICS AND SPACE ADMINISTRATION WASHINGTON, D.C. 20546 NOVEMBER 1978

STANDARD TITLE PAGE

1. Report No. NASA: UM-75286	2. Government Acc	ession No.	l. Recipient's Catalo	og No.
4. Title and Sublitle Heat and Molsture as a Function of T	ncrete	Report Date November Performing Organi		
7. Authors) Jürgen Hundt, Fede Naterials Testing,	eral Instit Berlin, b	ute for	. Performing Organi . Work Unit No.	zation Report No.
Germany	-		. Contract or Grant	
9. Performing Organization Name and A Leo Kanner Associate Redwood City, Califo	8.	<u> </u>	NASV -3199 Type of Report on	
12. Sponsoring Agency Name and Address			Translati	
National Aeronautics tration, Washington, 15. Supplementary Notes			i. Sponsoring Agenc	y Code
ter Einwirkung eines for Reinforced Concr Wilhelm Ernst & Son, 16. Abstract Due to temperature, moisture flows in the vessels. These flow made with crushed li of crushed Rhine gra	reactors in the thickwal were stuments.	t No. 256, 975, 108 pa n operation led prestre died in thr	cause head sed reactive beams of	t and or pressure f concrete beams made
are related to the s which can be proved non-evaporatable wat size distribution. ditions also influen strength, changes in thermal expansion an	tructural by series er, the to The local ce the tec length du	development determinati tal porousi temperature hnical prop e to shrink	of the cor on of the a ty and the and moist erty. Comp age and cor	ncrete, amount of pore ure con- pressive ntraction,
17. Key Words (Selected by Author(s))		18. Distribution State	ment	
		Unclassif	ied-Unlimi	ted
19. Security Classif, (of this report)	20. Security Class		21. No. of Pages	22. Price
Unclassified	Unclass	rrred	214	

TABLE OF CONTENTS

		Page <u>/3</u> *
D	Introduction	1
1.	Current State of Knowledge and Presentation of the Problem	1
1.0.	Structure of Concrete	1
1.1.	Hardening of Cement Paste	1
1.1.1.	Structure	l
1.1.2.	Pore Space	2
1.1.3.	Water in the Pore Space	3
1.1.4.	Technological Properties	4
1.2.	Influence of Increased Temperatures on the Behaviour of Concrete	5
1.2.0.	Demands on Reactor Concrete	5
1.2.1.	Heat of Hydration	6
1.2.2.	Heat and Moisture Conductivity	6
1.2.3.	Technological Properties	8
1.3.	Statement of the Problem	10
2.	Our Own Experience	11
2.1.	Materials and Method	11
2.1.1.	Experimental Materials	11
2.1.1.1.	Raw Materials for the Concrete	11
2,1.1.1.	Concretes	16
2.1.1.3.	Matrix Mortar	19
2.1.1.4.	Cement Mortar and Cement Paste	21
2.1.2.	Experimental Conditions, Set-up and Procedure	22

^{*}Numbers in the margin indicate pagination in the foreign text.

		Page
2,1,2,1,	Experiments on the Concrete Beams	22
2,1,2,1,1,	Experimental Arrangement and Procedure	22
2.1,2,1,2,	Procedure	27
2,1,2,2,	Experiments on Test Specimens	28
2,21	Measurements on the Concrete Beams	31
2,2,1,	Temperature	31
2.2.1.1.	Measurement Method, Arrangements and Procedure	31
2.2.1.2.	Measurement Results	31
2.2.2.	Heat Flux	37
2.2.2.1.	Measurement Method, Arrangement and Procedure	37
2.2.2.2.	Measurement Results	38
2.2.3.	Water Content	39
2.2.3.0.	Selection of the Measurement Methods	39
2.2.3.1.	Weighing Method for Determining the Weight Losses	40
2.2.3.1.1.	Measurement Method, Arrangement and Procedure	40
2.2.3.1.2.	Measurement Results	41
2.2.3.2.	Moisture Measuring Elements	43 <u>/4</u>
2.2.3.2.1.	Measurement Method, Arrangement and Procedure	43
2.2.3.2.2.	Measurement Results	48
2.2.3.3.	Neutron Probe	50
2.2.3.3.1.	Measurement Method, Arrangement and Procedure	50
2,2,3,3,2,	Test Results	57
2.2.4.	Linear Expansion	62

The state of the s

-

		Page
2,2,4,1,	Changes in the Overall Length of the Beams	62
2.2.4.1.1.	Measurement Method, Arrangement and Procedure	62
2.2.4.1.2.	Test Results	67
2.2.4.2.	Local Changes in Length in the Concrete	67
2.2.4.2.1.	Measurement Method, Arrangement and Procedure	67
2.2.4.2.2.	Measurement Results	71
2.2.5.	Concluding Measurements on Concrete Samples from Beams 3 and 6	73
2.2.5.1.	Test Specimens, Extent of Measurements and Procedures	73
2.2.5.2.	Measurement Results	74
2.3.	Structural Developments of the Concrete	78
2.3.1.	Dehydration Experiments on Cement Paste	78
2.3.1.1.	Measurement Method and Experimental Procedure	78
2.3.1.2.	Measurement Results	80
2.3.2.	Evaporatable and Non-evaporatable Water	82
2.3.2.1.	Measurement Method and Experimental Procedure	82
2.3.2.2.	Measurement Results	83
2.3.3.	Total Porosity	86
2.3.3.1.	Measurement Method and Experimental Procedure	86
2.3.3.2.	Measurement Results	86
2.3.4.	Pore Size Distribution	89
2.3.4.1.	Measurement Method and Experimental Procedure	89
2.3.4.2.	Measurement Results	93

		Page	
2.4.	Changes in the Mechanical Properties of the Concrete	97	
2.4.1.	Shrinkage, Contraction and Thermal Expansion	97	
2.4.1.1.	Measurement Method and Experimental Procedure	99	
2.4.1.2.	Measurement Results	104	
2.4.2.	Flexural Bending Strength and Compressive Strength of Cement Paste, Cement Mortar and Concrete	1.06	
2.4.2.1.	Measurement Method and Experimental Procedure	106	
2.4.2.2.	Measurement Results	108	
2.5.	Correlation of Characteristic Values Influenced by Heat and Moisture Conditions	108	<u>/5</u>
2.5.0.	Scope of Experiments	108	
2.5.1.	Setting Up the Water Balances	110	
2,5,2,	Length Changes	113	
2.5.3.	Compressive Strength	116	
2.5.4.	Thermal Conductivity and Water Content	116	
3.	Discussion of Test Data	124	
3.1.	Thermal Processes in the Concrete Beams	124	
3.1.1.	Heat of Hydration Effect	124	
3.1.2.	Heating Effect	125	
3.2.	Moisture Processes in the Concrete Beams	127	
3.2.1.	Moisture Content and Chemical Bonding of Water	127	
3.2.2.	Effects of Hydration and Moisture Conduction on Water Content	131	
3.2.2.1.	Changes in a Closed System	131	

		Page	
3.2.2.2.	Changes After the Start of Heating	132	
	Moisture Losses Due to Drying	132	
3,2,2,2,2,	Interpretation of the Drying Curve Under the Effect of a Temperature Gradient	133	
3.2.2.2.3.	Non-evaporatable Water	136	
3.2.3.	Comparison of Results	137	
3.3.	Influence of Heat/Moisture Phenomena on the Fore Structure	138	
3.3.1.	Total Porosity and Open Porosity	138	
3.3.2.	Pore Size Distribution	140	
3.3.2.0.	Evaluation of the Measurement Method	140	
3.3.2.1.	Cement Paste and Aggregates	140	
3.2.2.	Matrix Mortar	141	
3.3.3.	Comparison of Results	144	
3.4.	Change in Technological Properties	147	
3.4.1.	Shrinkage, Contraction and Thermal Expansion	147	
3.4.2.	Compressive Strength	150	
1.4.3.	Thermal Conductivity	151	
١.	Summary	152	
	References	156	
	Appendix	165	
		v	

g "

Ē

Frequently Used Symbols and Abbreviations

```
bulk density
     fresh bulk density
ρ<sub>F</sub>
     dry bulk density (drying at 105°C)
\mathfrak{p}_{\mathrm{tr}}
     density
PO
     compressive strength
\beta_{T}
     bending strength
βB
     linear deformation
\Delta \mathbf{L}
     unit strain AL/L
     temperature
Θ
     linear thermal expansion coefficient
œ
     heat flux density
λ
     thermal conductivity
R
     neutron monitoring rate
     water content<sup>+</sup>) (with respect to the dried material at 105°C)
W
     water uptake
A
     pore volume
u
ŗ
     pore radius
U<sub>t:</sub>
     total porosity
     pore volume measured as a whole with a mercury porosimeter
R.F. relative humidity of the air
N
     number of measured values
     standard deviation
```

t

test size

^{†)}Content of evaporatable and/or nonevaporatable water.

^{*}Numbers in the margin indicate pagination in the foreign text.

HEAT AND MOISTURE FLOW IN CONCRETE AS A FUNCTION OF TEMPERATURE JURGEN Hundt

O. Introduction

In civil engineering, increasingly high demands are being /9 placed on the construction material concrete, both with respect to its function as a component of load-bearing members and with respect to other technological properties, such as thermal insulation, impermeability to liquids and the shielding of radioactive radiation. Taking nuclear power plants as an example, it is clear that the use of concrete as a construction material for nuclear reactor vessels has given rise to extensive development in construction techniques. In the Federal Republic of Germany, with respect to the task of constructing reactor pressure vessels of prestressed concrete, a guidelines program has been set up which, besides safety aspects, above all also entails basic research of concrete technology [8]. This work is concerned with an important subproblem of this program, namely the investigation of heat and moisture conductivity in thermally stressed concrete structures as well as the accompanying structural changes of the hardened cement The temperatures produced during the operation of thickwalled reactor vessels influence not only the heat-moisture equilibrium state attained by the structural member under normal conditions, but also the technological properties of the concrete.

1. Current State of Knowledge and Presentation of the Problem

1.0. Structure of Concrete

Concrete consists of aggregates, hardened cement paste, water and air. During hardening, the relationship of its solid, liquid and gaseous components changes with respect to one another, while as a result of chemical and physical processes, hardened cement paste is formed from the paste produced from mixing water and cement. The volume and quality of the pore space, filled with water and air, of a concrete depends basically on the inherent porosity of the aggregates, the water/cement ratio and the compression of the freshly mixed concrete. The hardening processes in the cement paste can indeed be influenced to a certain extent by special characteristics of the aggregate, but in normal concretes with a dense structure they are basically determined by the water/cement ratio and the curing medium.

1.1. Hardening of Cement Paste

1.1.1. Structure

Portland cements consist up to 80% of calcium silicates which are converted into calcium silicate hydrates and calcium hydroxide after mixing with water. According to Kühl [9] hydraulic hardening, which includes the processes of hydrolysis, hydration and gel formation, takes place as a result of the "dissolution of the starting material" (production of hydration products in accordance with the

¹Guidelines Program, German Research and Development of Prestressed Concrete Reactor Pressure Vessels.

views of LeChateliers), but also in part as a result of direct accumulation of water on the solid phase of the starting material (production of gel coatings according to the views of Michaelis). The calcium silicate hydrates are the main components of the hardened cement paste and largely determine its properties [10, 11, 12, 13]. Fully hydrated cement pastes consists of about 25% by weight of calclum hydroxide and 50% by weight of calcium silicate hydrates of different forms (CSH-phases). According to the structural model of cement paste devised by Powers and Brownyard [14], which has found widespread approval [15] and has also recently been further developed (see, for example, [16]), the solid portion of the cement paste consists of: (1) colloidal components, i.e. the gel; (2) considerably larger crystals imbedded in this gel and (3) capillary pores originally filled with water. The picture based on extensive data on specific surface [17], density, permeability and strength assumes that the cement gel formed from the calcium silicate hydrates involves fine, thin lamellar particles (2-3 molecules thick, corresponding to 2-3 nm) which, because of their large surface areas and the forces thus activated, are responsible for the high strength levels. Because of its nature, the material, also called Tober morite gel, grows into the capillary pores, in the process of which gel pores are formed at their expense. Depending on the stress concentration factor, gel pores have average pore radii between l and 2 nm [14], while capillary pores have larger radii, namely greater than about 4 nm (on this point, also see [18]). Accordingly, just in terms of the way they are formed, gel pores differ from capillary pores.

Furthermore, it is assumed [14] that the capillary pores in fresh cement paste form a network which, during gradual maturing, is increasingly filled with hydration products until the capillary pore space is filled up or all of the clinker grains have been transformed. In contrast to the gel poresspace consisting of the characteristic pore size, which with full hydration is supposed to reach about 28% by volume [19], the capillary pore volume depends /10 on the water/cement ratio and the degree of maturity of the cement paste in question. Since about 25% by weight of the cement in the form of chemically bound water and 15% in the form of gel water are used for complete hydration, it follows [10] that cement pastes with water/cement ratios <0.4 must still contain undecomposed clinker grains even after a very long time. On the other hand, in cement paste with water/cement ratios up to 0.7 in the mature state, capillary pores are accessible only through gel pores. Above this water/ cement ratio, capillary spaces form in the cement paste which, because of their size, can no longer "grow together" with hydration products, so that the permeability of the pore system increases considerably.

1.1.2. Pore Space

Views on the shape and quality of the cement paste components as well as the pore space formed by them differ to some extent. Richartz and Locher [12] found that the crystalline calcium silicate hydrates are mostly in the form of fibers and consist of rolled up

films in the form of small tubes. As the hydration time increases, they form a thick network. Calcium hydroxide, by contrast, forms thin-sheet crystals which envelop already present hydration products with increasing hydration time. Since these tubial-shaped calcium silicate crystals differ in diameter, they also form different pore sizes with a continuous distribution. Winslow and Diamond [20], on the basis of scanning electron microscope studies, are also of the opinion that pore sizes exist between the size of gel pores and capillary pores. Accordingly, the volume to be attributed to the gel pores would have to be <28%, which can also be confirmed with the help of total porosity and penetration measurements.

Independent of these not yet clearly solved problems which, in particular, are also important for the finding of water in the pore space, it must be recorded that the hydration products of the cement paste form a union which becomes denser with increasing age, in the process of which the gel pore space increases and the specific surface reaches values of about 175 m²/g ([17], also see [21]). Since this occurs at the expense of the capillary pore space whose "starting volume" depends on the water/cement ratio, the total pore volume (i.e. total porosity) reached after complete hydration is determined by the water/cement ratio. The changes in volume can be estimated, in the process of which it must be borne in mind that the total volume of cement and water is reduced during hydration ("shrinkage"), and that besides the chemically bound water, about 15% of the cement by weight is accumulated as gel water. These relationships are presented very clearly in [22].

Various methods are available for characterizing the pore space (23, 24]. Besides the optical methods (light and electron microscopy), these are primarily indirect methods, such as the water absorption method, mercury porosimetry or the absorption of different mediums. With these methods, starting with a certain parameter (e.g. pore volume), other properties of the pore space are inferred (e.g. pore size distribution) with the aid of a theoretical model equation. So, for example, permeability measurements provide information about pore shape and arrangement. Because the permeability of the pore system increases much more rapidly than the total porosity with an increasing water/cement ratio, we can infer that the pore radii become considerably larger as the water/cement ratio increases [11].

1.1.3. Water in the Pore Space

Cement paste contains water in liquid form ("capillary water") as well as in the form of water vapor, as adsorptively bound water ("absorbate water") and as chemically bound water. An exact distinction according to bond types is hardly possible using an imperical approach "because the dissociation pressure of the hydration products and the water vapor pressure of the adsorbed and free water are continuously merging into one another" [25]. The experiments reported in [12] have also shown, for example, that the intermediate layer of water stored in the tube-shaped calcium silicate hydrates

is to be attributed to the chemically bound water, although it eyaporates during vacuum drying.

Thus, it has proved to be convenient to follow the suggestion of Powers and Brownyard [14] and subdivide the total water content into evaporatable and nonevaporatable water. In the drying process used by these two waters, which has been further developed by Copeland and Hayes [26], the nonevaporatable water is to be approximately equated to the chemically bound water.

In the method usually used, for practical reasons, for determining the content of "free water" by heat treatment at about 105°C, it is disregarded that [1] the adsorptively bound water is perhaps /11 not completely expelled during the heat treatment and (2) that the cement paste also gives off water at this temperature which is actually to be attributed to the chemically bound water. So, for example, it has been attempted to improve the reproducibility of the process by keeping the drying temperature very constant and specifying the drying time [28].

The forces to be overcome during drying depend on the bond type existing in each case. If we disregard the chemical bond, then on the one hand we are dealing with capillary forces which are determined by the capillary radius as well as the surface tension and the contact angle of the medium. Secondly, we are dealing with VanderWaals forces which hold several layers of water molecules on the surfaces. The special conditions of the pore space are expressed in the absorption isotherms measured by numerous authors (e.g. [29]) to characterize the drying behaviour of cement paste and concretes. In so doing, the water content, according to the theory of capillary condensation, can also be related to filled pore sizes with radii between 0.1 and 50 nm [30].

Besides the method of characterizing the moisture content in cement paste and also in concrete on the basis of weight loss due to heat treatment at 105°C ("gravimetric method"), a wide variety of physical effects are used to measure moisture, the use of which depends largely on the specific experimental conditions involved. Altmann [31] gives a list of the most popular methods (also see [32]).

1.1.4. Technological Properties

Besides the internal interfacial energy forces, external conditions also influence the hardening and state of the cement paste. Just as in the above considerations, it is assumed that the hardening takes place at room temperature of about 20°C and a relative humidity >80%, so that the equilibrium moisture content of the cement paste or concrete necessary for the reaction steps is not exceeded (cf. [29]). For the sake of completeness, we should here point out

²The term "moisture content" used below, which corresponds to the evaporatable water, distinguished the different states. With respect to the term "hygroscopic moisture content" see [27].

that carbonization processes, which likewise cause structural changes, are disregarded here because, in general, they are important only for surfaces with direct access to wear and moreover they proceed very slowly.

Since the strength of the cement paste depends basically on the surface forces prevailing between the gel particles, it increases with age, i.e. as the amount of hydration products increases. Furthermore, both the compressive strengths and the bending strengths are determined by the total porosity, and since this depends on the water/cement ratio, there is a direct relationship between strength and the water/cement ratio [33]. With respect to the pore space of concrete, Pilny [34] points out that the larger hollow spaces, which are to be attributed to defective compression, contribute far more to the reduction in strength than the porosity dependent on the water/cement ratio.

Pore space and moisture balance are closely interrelated to the most important technological parameters of the cement paste and concrete. So the shrinkage following the pouring of the concrete is due to the chemical bonding of water which is initially intense and then becomes slower. By contrast, the reversible shrinkage or swelling is obviously caused by changes in the internal state of stress during the drying or filling of the capillaries. The irreversible deformation due to shrinkage, clearly a function of the porosity, are attributed to structural changes in the cement paste [35,34,11]. Slow displacement of water from the capillaries is also regarded, for example, as the cause of the creep of cement paste occurring under load [34, 36]. Of the many articles on this problem, those by Bazant are to be singled out. He considers the interaction between the surfaces determined by the microstructure and the water, which is absorbed in variable layer thickness, as the determining mechanism for creep (e.g. [37, 38]).

1.2. Influence of Increased Temperatures on the Behaviour of Concrete

1.2.0. Demands on Reactor Concrete

Since concrete offers effective protection against λ and neutron radiation, which are especially dangerous because of their penetration capacity, it is advantageously used in the construction of nuclear reactors [39]. The attenuation of λ radiation is accomplished by the relatively large mass provided by thick walls while the neutron flux is slowed down primarily by the hydrogen atoms present in the cement paste (on this point see for example [40]). The use of concrete in thickwalled vessel structures, however, presupposes precise knowledge on the phenomena to be expected in the pore space as a result of thermal stress. The development of these phenomena is influenced by changes in the heat and moisture conditions. In the context of the prestressed concrete reactor vessel program (cf. [8]), Eibl and co-workers [41] have presented a "Study on the Determination of Special Concrete Properties in the Construction of Reactor Pressure Vessels". This reports on the present state of knowledge. In this

report, a temperature difference of 60°C between inside and out- /12 side is taken as a basis for the "temperature when loaded" of the yessel.

1.2.1. Heat of Hydration

The thermal stress of the vessel will be set at a point in time at which the concrete is already in an advanced stage and has reached a relatively high degree of maturity. Its properties, however, depend on the preceding history of events, within which temperature changes after pouring of the concrete are especially important in the case of massive structural members. The heat released as a result of exothermic reactions during hydration can, as a consequence of thermal expansion, cause permanent deformations in the concrete, which is still not very hard, and also lead to the formation of cooling cracks after cooling and contraction [42]. With suitably large temperature differences, structural stresses must also be taken into account inasmuch as cement paste and aggregate have very different thermal expansion coefficients. Very little is known, however, about the effects of such structural stresses on the association between cement paste and aggregate (cf. [43]).

1.2.2. Heat and Moisture Conductivity

At the time the reactor is put into operation, the concrete of the pressure vessel has assumed the temperature of the surrounding air (about 20°C). A relatively thinkouter layer on the external surface will have adapted itself to the surrounding air by releasing moisture, while the vessel wall in the interior will have the original total water content. The inside of the vessel is sealed by a metal liner so that no moisture can be lost there.

The temperature field which is established in the vessel after being put into operation leads to changes in the original, almost uniform moisture distribution as a result of moisture conductivity in the direction of the heat flow. It has been attempted to simulate these events in experiments using concrete beams of different sizes heated on one side. The special conditions which existed during these experiments are unfortunately reported for the most part only in broad terms, and in many cases there is no data on the composition of the concrete necessary for further interpretation. Browne [44] cites results reported by Ross and co-workers [44] on a beam about 1.50 m long with a temperature load of 80°C as opposed to an ambient temperature of 20°C. Hornby [46] reports on moisture profiles which were measured on a 2.70 m long beam, one face of which was heated to a temperature of 150°C, while the other face had a temperature of 25°C.

For beams measuring between 0.6 and 3.1 m long, which were heated to temperatures of 125°C on the sealed, vaportight face, England and Ross [47] give water content distributions as a function of the heating time.

McDonald [48] reports on experiments on a 2.74 m long beam of concrete with calcite aggregate (fresh concrete bulk density 2.38 kg/dm; water/cement ratio 0.47; compressive strength after 28 days approx. 420 kp/cm²). The heating of the beam, which, taking into consideration the actual shape of a vessel section, tapered towards the inside, was begun at an age of 17 months. Since after 127 days of heating at about 65°C on the hot face, noticeable changes in the moisture distribution could be detected only on the free face, McDonald assumed that with this temperature gradient (44°C/2.74 m) and the other parameters, an adverse effect on the properties of the concrete did not have to be reckoned with.

The expected changes in the moisture distribution in the concrete wall are discussed by Waubke [41] with regard to the usual diffusion equasion (Fick's first law)

 $\Delta f/\Delta t = div (k \cdot degree f)$ (1)

(cf. [49]), which is valid for a steady diffusion current. equation, f represents the moisture content, t time and k the diffusion coefficient (moisture conductivity). With the diffusion equation, the actual relationships can only conditionally be taken into account, since the "internal drying conditions", which are to be measured by the moisture conductivity, are constantly changing. To be sure, evarious equations have been proposed for the dependence of moisture conductivity [29], however Waubke comes to the conclusion that in all studies the temperature dependence has been disregarded and, moreover, corresponding experimental studies are lacking. the study carried out by Bazant [50], Waubke continues, it turned out that the pore structure necessarily takes on decisive importance. Under practical conditions it is to be assumed [41] that a thin shell region drys out on the outside in which the conditions thereafter no longer change considerably. By contrast, in the moist internal regions, as a result of the strong temperature dependency of the moisture conductivity, changes in the moisture profile have to be taken into account which could have an influence on the changes over time of the local temperature conductivity.

Therefore, in agreement with the data given by the authors cited above [44-47], immediate changes are to be expected in the moisture content of the (open) external surface as well as on the heated inside surface of the vessel. Very slowly increasing losses within the moist interior are to be expected only after a longer period. With the mathematical equations available it is not possible to predict the course of the drying process over time, because we do not have the necessary characteristic quantities of the material.

1.2.3. Technological Properties

The above studies [44-48] cover special characteristic values immediately necessary for constructive calculations. With the material changes, above all those concerning pore structure, the heat-moisture events cause deformations as a result of shrinkage/swelling and thermal expansion. Moreover, with a reduction in moisture content we must also take into account a direct impariment of thermal conductivity. In this connection, we can merely mention the thermal effects on creep as well as on the strength properties and the elastic behavior of the concrete.

With regard to the shrinkage phenomena, Ross and Parkinson [51] discuss experiments on pieces of concrete measuring about 1.50 meters hong and made of gravel concrete with a water/cement ratio of 0.6, after three years of heating (heating started at an age of 139 days) the face heated to 80°C at a degree of shrinkage of about 300 µm/m and the open face (23.8°C) had a degree of shrinkage of about 150 µm/m, while the interior, which remained moist, remained largely free of expansion. According to [44], based on studies reported in [45], a degeree of shrinkage of about 400 µm/m is to be expected for the concrete on the face heated to 80°C. In [41] it is pointed out that these relatively high values may be caused not only by drying processes, but presumably they are also attributable to the decompostion of hydration products at temperatures above about 60°C.

According to the mechanical theory of heat (cf. [52]) molecular kinetic phenomena are responsible for the thermal capacity, the thermal conductivity and the thermal expansion of a material. The thermal expansion of solids is thought to be caused by the increasing kinetic energy, resulting from an increase in temperature, of the molecules or atoms oscillating in the space lattices, i.e. the thermal expansion behavior depends first of all on the nature and structure of the materials. In the case of concrete, besides this type of expansion, volume changes occur which are related to moisture phenomena. According to Pilny [53], linear deformation occurs if, for example, as a result of changes in the hygroscopic equilibrium, water is condensed out of the large pores into the gel pores.

In a fundamental work on the thermal expansion of cement paste, rocks and concretes, Dettling [54] distinguished the "true thermal expansion", which is measured as the overlapping of thermal expansion with mechanical expansion, and the "apparent thermal expansion", which occurs as an inevitable result during temperature changes due to rearrangements of moisture. Thus, in the dry and water—saturated state, cement paste has expansion coefficients differing only slightly from one another on the order of $\alpha=10.0\cdot10^{-6}/^{6}$ C. Compared with this, with moisture contents

between 70% and 45%, depending on the age, maximum expansion coefficients between 21 and 23.10-6/°C result due to the contribution of the apparent thermal expansion.

Dettling, who has evaluated the extensive data of various authors (e.g. [55]), gives equations for calculating the linear thermal expansion coefficients of concretes in which the dominating influence of the aggregates on the expansion behavior is expressed [56]:

$$\alpha = (\alpha_{ze} - \alpha_{z}) \cdot C(b) + \alpha_{z}$$
 (2)

In this equation $\alpha_{\rm ge}$ represents the expansion coefficient of the cement paste as a function of the moisture content, age and temperature; $\alpha_{\rm ge}$ represents the expansion coefficient of the aggregate, if necessary as a function of temperature; the factor C (b) takes into account the composition of the concrete. For temperatures between 20 and 80°C, the dependence of expansion coefficients of concretes on temperature is small and might perhaps produce a noticeable effect if limestone is used as the aggregate [57].

With respect to the state of latent stress created in concrete as a result of increased temperature it is pointed out [58], that a considerable portion of the amount of expansion is prevented by the amount the thermal expansion coefficient of the cement paste exceeds that of the aggregate. The resulting structural stresses may well lead to plastic deformations of the cement paste. As to the question of to what extent this is related to consequences for the pore structure of the cement paste and, for example, also for the mechanical properties of the cement as a function of the state of maturity in question, no data could be found in the literature.

Krischer [59] has theoretically analyzed the relationships between "heat transport and material transport" in porous substances for temperatures up to about 100°C. According to him, besides the heat conductivity of the solid components, moisture content and temperature are also decisive factors, since considerable quantities of heat can be transported during vapor diffusion processes, In this connection, Cammerer [60] states that, to be sure, the theoretical principles have largely been worked out, but that many practical empirical values are still lacking.

The overview presented by Rieche [41] on the heat conductivity of heavy concrete, which takes into account the studies of a wide variety of authors, indeed contains a number of values, but in some cases these differ considerably from one another and do not take into account at all, or only insufficiently, the effect

/14

of moisture content and temperature. Above all, this may be due to the fact that the so-called stationary measuring methods usually used for studying thermal conductivity against variable moisture contents and variable temperature are not suitable.

With regard to thermal conduction of the solid components of hardened concrete, it is the view of Missenard [61] that first of all the type of cement as well as the cement content, the mineral structure of the aggregate and the compression of the fresh concrete are important. According to Marechal [62], the thermal conductivity of concrete is possibly more influenced by the shape and arrangement of the aggregate granules than by the "intrinsic conductivity" of the rock. With the aid of a theoretical model, Harmathy [63] has calculated the thermal conductivity at room temperature for different compositions of concrete. Accordingly, for 85% by weight of quartz aggregate in concrete he arrives at $\lambda \approx 2.5$ W/m·K, and for about the same proportion of feldspar aggregate he obtains $\lambda \approx 1.3$ W/m·K (also see [41]). This may explain the limit values to be expected as a result of different aggregates.

In [41], Rieche states in summary form that for concrete in a moist state at temperatures above 60°C, a considerable increase in thermal conductivity (40-50% in comparison with the dry state) should have to be taken into account. In the case of massive structural members, he adds that only very slow drying and correspondingly slow alteration of thermal conductivity are to be reckined with. For calculating temperature fields, the following limit values are given:

 $1.3 < \lambda < 3.5$ (W/m·K)

1.3. Statement of the Problem

To be sure, the most important relationships in the formation of cement paste are known, but the pore space, which is a determining factor for the binding of the water and for the technological properties, is not yet satisfactorily characterized. In particular, there is a lack of data on the actual pore shapes as well as on the three-dimensional arrangement and distribution of the pores. Likewise, very little has been reported in the literature on the influence of aggregates on the pore space of mortars and concretes.

The internal, interfatial energy forces are a function of the properties of the pore space and also of the wetting behavior of the water contained therein. By changing the external conditions, the heat-moisture balance is disturbed. The temperature directly affects the development processes, and,

presumably at temperatures above about 60°C, already causes structural changes in the cement paste.

Data is available from studies of moisture conductivity in massive structural members under heat stress which allow us to draw qualitative conclusions. According to this data, we must briefly consider changes in the moisture content on the open external surface and on the heated internal surface. The moisture distribution in the interior, by contrast, changes slowly only in the course of several years of heating.

Depending on the type of concrete, the degree of shrinkage on the heated and largely dried internal surface is expected to be on the order of 400 µm/m. The thermal expansion coefficients of the concretes are not only strongly dependent on the type of aggregates used but also on the moisture content, and if the expansion characteristics of the cement paste and aggregate are known, these coefficients can be predicted. At temperatures below 100°C, the thermal conductivity depends largely on the moisture content and temperature. Although the theoretical relationships are clarified to a large extent, there is a lack of practical measured values, or more precisely the data given in the literature differ widely from one another.

The data given in the literature on heat and moisture conduction in massive structural members acted upon by heat are only spotty and are not sufficient for representing the development processes. The same is also true for the technological properties affected by changes in the heat-moisture conditions. In order to make possible quantitative information, it was therefore necessary to study in detail heat and moisture conduction in concrete while varying the determining parameters and verify the findings experimentally. At the same time, the material changes decisive for the technological properties had to be determined and related to the processes in the binding agent matrix.

2. Our Own Experiments

2.1. Materials and Method

2.1.1. Experimental Materials

2.1.1.1. Raw Materials for the Concrete

For the heat and moisture conduction experiments, as far as possible the same concretes were to be used as in parallel

/15

programs of the prestressed concrete reactor vessel project being carried on elsewhere [8]. Accordingly, two types of concrete were to be studied. These differebasically in the type of aggregates, one of them involving crushed limestone and the other sand and gravel. The aggregates and the cement were obtained with the cooperation of the Fried. Krupp GmbH Co., Universalbau, Essen, from the same deposits and manufacturing batches respectively so that by using substances which were obtained of produced at the same time under the same conditions the comparability of the results could be guzzanteed.

The crushed limestone material, referred to below as calcite aggregate (in analogy to the term calcitic concrete etc.) was supplied by the Rhine limestone works in Wülfrath in fractions of 0/2, 2/5, 5/8, 8/12 and 12/16 (the classification corresponds to the square aperture fractions as per the "Memorandum for Granulations from Crushed Natural Rock (Rock Material)" of the the Research Association for Highway Construction). It was dried at 105°C and subdivided by sifting into 8 fractions and 3 gapped gradings. The aggregate mixture composed of the groups for making the "calcite" concretes (beams 1, 2 and 3) corresponded to the grading curve as per DIN 1045 as shown in Fig. 1 [1]. The grading curve includes the limestone powder to be added according to the recipe. This powder was also obtained from Wülfrath and its aggregate grading is shown in Table 1.

Table 1 Aggregate grading of the rock powders used.

A Gesteins-	В	5		
nehl	0/50	50/100 /1	100/2:0	>250
D (marzwehl Okalksteinmohl	64.4 31.8	26.2 27.0	9.0 32.4	ប.4 ម.8

Key: A. Rock powder

B. Proportion in % by weight of the fractions

C. Limestone powder

D. Quartz powder

* Test screens as per DIN 4188 [4].

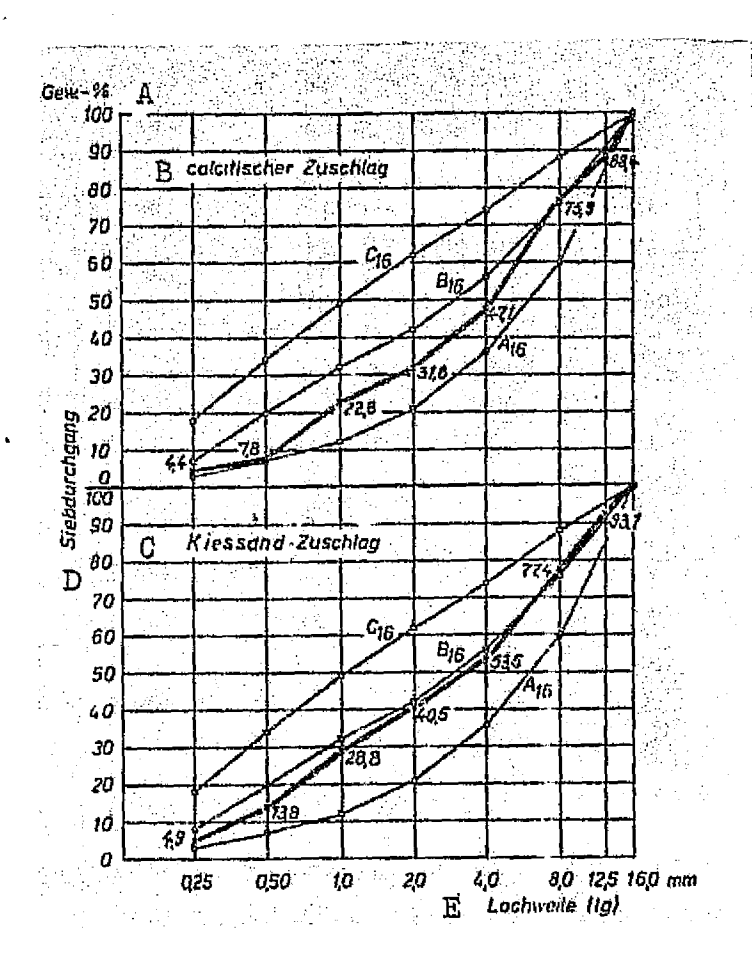


Fig. 1. Grading curves for the calcite and gravel-sand aggregates used for making the concretes for beams 1, 2, 3 and 4,55, 6 respectively with a maximum grain size of 16.0 mm. Aperture sizes and grading curve ranges are in accordance with DIN 1045.

Key: A. % by weight

B. Calcite aggregate

C. Gravel-sand aggregate

D. Undersize

E. Aperture width

The uncrushed material, ranging in shape from round granules to wafers and consisting for the most part of quartz or granules with a high proportion of quartz below referred to as gravel-sand aggregate (analogously, gravel-sand concrete and so forth), came from the Heinrich Elskens AG Co., Duisburg. The name given to it by the company was "Schifferstrasse" and it was delivered in the fractions 0/3, 0/15, 7/15 and 15/30 (classification as per DIN 1045, July 1952 edition). After drying at 105°C the material

was subdivided into six fractions and a gapped grading by screening. The mixture composed of the fractions for the concretes with "gravel-sand aggregate" (Beams 4, 5, 6) corresponded to the lower grading curve shown in Fig. 1 as per DIN 1045 [1] which includes the quartz powder used according to the recipes for making the concrete. The quartz powder was obtained from Dr. Müller GmbH West German Quartz Works, Dorsten (manufacturer's brand:name: "Silicite") and its aggregate grading is shown in Table 1.

The binder used was a Portland cement with a high initial strength of the strength class PZ 450 F DIN 1164 [3]. The cement, delivered in sacks, came from the Dyckerhoff Zement-werken AG in Neubeckum and carried the brand name "Mark II". Random sample analyses (cf. section 2.1.1.4) of the cement to characterized its properties revealed the following characteristic values:

Composition, DIN 1164, page 3 [3] Satisfies the requirements; cf. Table 2.

Fineness of grinding, DIN 1164, page 4
Remainder on the test screen fabric
0.2 DIN 4188
0.4% by weight

specific surface using=the air permeability method 3470 cm²/g

Setting, DIN 1164, page 5
Start of setting measured with a needle device 97 minutes

Soundness, DIN 1164, page 6
The results of the boiling test satisfied the requirements.

Strength, DIN 1164, page 7
The specifications of strength class 450 F were satisfied (cf. section 2.4.2.2.).
Compressive strength after 28 days on average 50.5 N/mm²

Heat of hydration, DIN 1164, page 8

273 J/g (= 65 cal/g)

The evolution of heat for Portland cement with higher initial strength in comparison with that of a blast-furnace cement with slow initial hardening is illustrated in Fig. 2 using temperature measurements made in a glass dontainer insulated with polystyrene foam. For each substance the container was filled with 160 g of pure paste with a water/cement ratio of 0.4.

Density 3.10 g/cm³ determined as per [64].

Table 2 Chemical analysis of the cement.

A Bestmatotic		B C	glunverlust- frei B [JonA]
Lillaverlant, 1000 °C darin darin darin darin darin darin darid	CO.	2,59 2,10	
unibeliaher Mickernal		1,36	1,40
sitistamiloxid H	J10 ₇	19,08	19,59
Alumintumogid G	i. ,0	5,20	5,43
Lisonexia H_	PopO3	3,65	2,11
Titandierid +	Tica	0,63	0,03
Guiselmaxia T	हेताहुँ हैं जन्म	6.58	V (5)3
engangiumania Li	Net.	63,39 1,03	65,08 1,66
Ruliumenti M	K-C	0,90	6,92
Transporta N	H1 ₂ t	6,15	0,13
0.01/06	i Eu	3,22	3,31
ent screecherd po	10.00	1	1
getorid O	193b _q	SE SE	(0,01
Want Intant martem R		6.53	U MG
Same		16666	1:0,00
C €3.0	hverlustfre	Liewsil B	
	C ₃ 5 66	.,4	
f patentiello T	ិខ្លួល i		
retsungt	23A	949 940	
U Kalimbananet -		GaO .	
		1120 + 0.65 i	mate.
fonordomedul -			***
	A. A.		
W silivatmodul	10,	э д	
والمرابع أأأأ أأأنا المارات	يهاره، د	•	

Key:

- A. Ingredients
- B. Percent by weight
- C. Without loss on ignition
 D. Loss on ignition, 1000°C
 carbon dioxide contained therein
- E. Insoluble residue
- F. Silicon diexide
- G. Aluminum oxide
- H. Iron oxide
- I. Titanium dioxide
- J. Managanese oxide
- K. Calcium oxide
 L. Magnesium oxide
 M. Potassium oxide
- N. Sodium oxide
- 0. Sulfate
- P. Corresponding to calcium sulfate

- Q. Chloride
- R. Remainder (not determined)
- S. Total
- T. Potential phase composition
- U. Limestone standard
- V. Iron-alumina ratio W. Silica modulus
- +) Sample preparation, analysis and calculation as per [65]

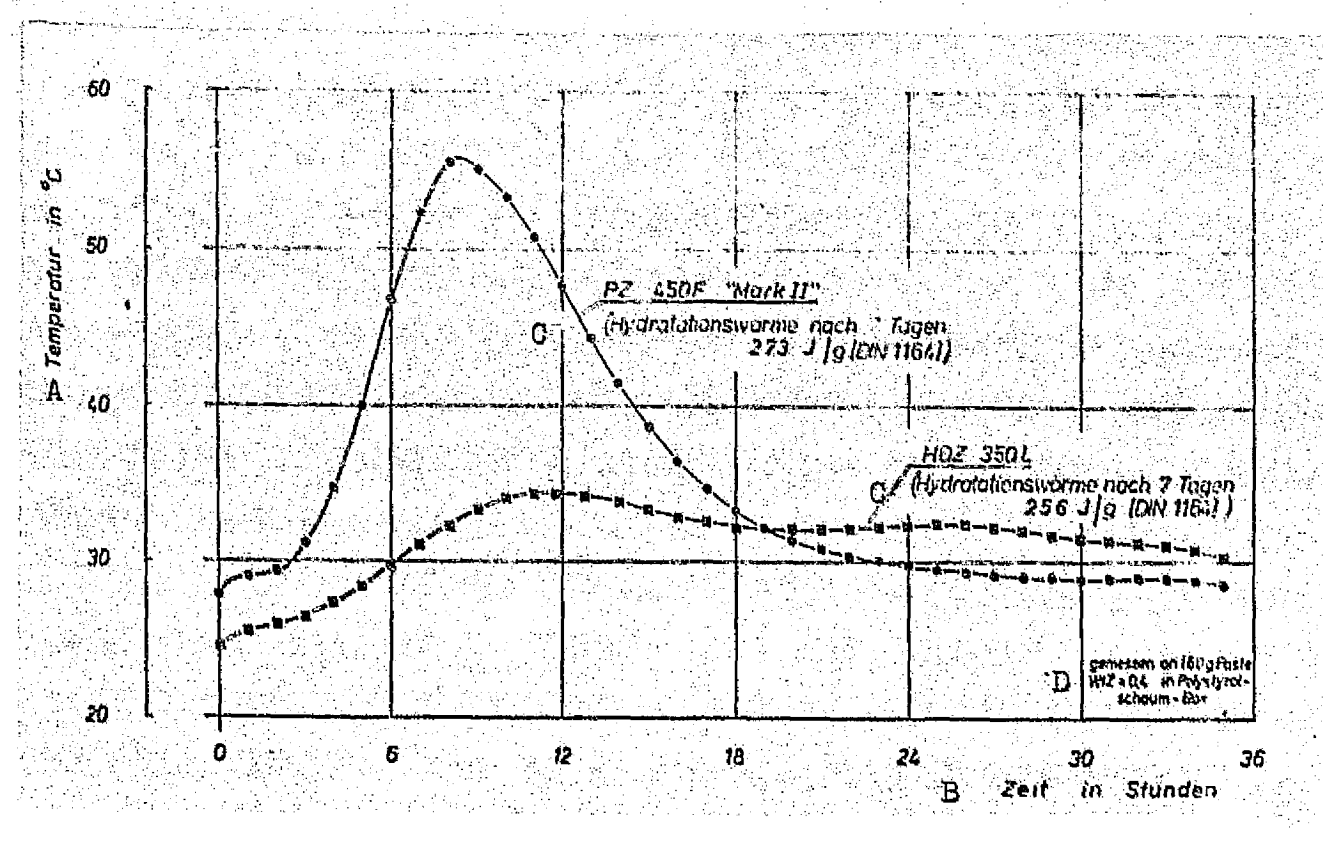


Fig. 2. Change of temperature over time of "Mark II" PZ 450 F Portland cement in comparison to HOZ 350 L blast-furnace cement. Measured in a glass container insulated on all sides, for each sample filled with 160 g of pure paste with a water/cement ratio of 0.4.

Key: A. Temperature

B. Time in hours

C. Heat of hydration after 7 days

D. Measured on 160 g of paste, water/cement ratio=0.4, in a polystyrene foam box

2.1.1.2. Concretes

As far as possible, the concrete compositions were adjusted to the recipes used by Fried. Krupp GmbH Universalbau Co. [8]. Complete agreement in the properties of the concretes could not have been achieved in principle even using the same starting

materials, because of inhomogeneities of the aggregates, different manufacturing and processing conditions etc.

As is obvious from Table 3, for the two types of concrete, differing in terms of the aggregate, three different mixtures were made, yielding beams 1, 2, 3 and 4, 5, 6 respectively.

Table 3
Characteristic data for the fresh concretes with calcite aggregate (beams 1, 2, 3) and gravel-sand aggregate (beams 4, 5, 6).

A	TO SERVICE AND THE PARTY.	[20]			B _{Beton} mit Kiessand -Zuschlag C Balken Nr.			
	1	2	3	4	5	6		
D Zuschlag kg/m ³	1928	1903	1878	1927	1906	1892		
E Zement (FZ 450 F) kg/m ³	341	337	333	305	301	299		
F w/Z-wert	0,50	0.565	0.63	0,52	0.575	0,63		
G Verdichtungsmaß nach Walz	1,40	1,27	1,14	1,22	1,11	1.10		
H Luftporengehalt Vol%	1,3	1.3	1,5	2,3	5.5	2,6		
I Frischbetonroh- kg/dm3	2,44	2,43	2,42	2,39	2,38	2,38		
Druckfestigkeit im J Alter von 28 Tagen N/mm ² (Lagerung nach DIN 1048)	52.5	46,0	39,8	51,2	49,5	43.0		

Key:

- A. Concrete with calcite aggregate
- B. Concrete with gravel-sand aggregate
- C. Beam number
- D. Aggregate
- E. Cement
- F. Water/cement ratio
- G. Degree of compaction using the Walz method
- H. Air/space ratio, % by volume I. Fresh concrete bulk density
- J. Compressive strength at an age of 28 days (curing as per DIN 1048)
- +) Average values of cubes measuring 20 cm on an edge. Commas should be read as decimal points.

17

First of all, the compositions for concretes 2 and 5 had to be established by means of calibration experiments with a specified aggregate mixture, With approximately the same water/cement ratio and a different cement content, in particularly because of the specific properties of the aggregates, the degree of compaction using the Walz method was on the border between consistency ranges K 1 and K 2 as per DIN 1045 [1] in the case of beam 2, and in the case of beam 5 it was on the border between consistency ranges K 2 and K 3. Both concretes had good worked ability and at an age of 28 days they reached the compressive strength levels shown in Table 3. (cubes measuring 20 cm on a side). Using as a basis the mixtures for beams $\bar{2}$ and 5, the compositions for beams 1 and 4 were obtained by decreasing the water/cement ratio, and for beams 3 and 6 by increasing this ratio. As is obvious from the degree of compaction of 1.40 for beam 1, this mixture was close to the limit for practical workability. The degrees of compaction of the mixtures for beams 3 and 6--1.14 and 1.10 respectively--were about at the transition between consistency ranges K 2 and K 3. regard to the sedimentation of fresh concrete during pouring, a greater addition of water would not have been suitable, in particular in the case of beam 6.

Since the scope of the project could not be expanded at /18 will; the experiment had to be limited to varying the water/cement ratio parameter important for the formation of the pore space. The composition of the concretes for beams 2 and 5 was adjusted to the practical demand for good workability with a low water content. From the standpoint of workability, larger gradations of the water/cement ratios would not have been appropriate.

The concrete was mixed in a 150 liter compulsory type mixer. Altogether, for each beam--including the test specimen for the compressive strength tests and the accompanying technical analyses--five mixer loads of the following composition were necessary:

Concrete with calcite aggregate

Aggregates as defined by the grading curve in Fig. 1 (composed of 11 fractions)	205.80 kg
Limestone powder	4,20 kg
Cement	37.20 kg
Water (beam 1	18.60 kg
beam32	21.03 kg
beam 3)	23.42 kg

Concrete with gravel-sand aggregate

Aggregates as defined by the grading curve in Fig. 1 (composed of 7 fractions)	201.60 kg
Quartz powder	8.40 kg
Cement	33,20 kg
Water (beam 4	17.27 kg
beam 5	19.10 kg
beam 6)	20.91 kg

The concrete for the cylindrical test specimens (df. section 2.1.2.2) and for the reference samples for setting up evaluation nomograms (cf. section 2.2.3.2) etc. were made later on in additional loads.

During the pouring of the beams, the concrete was poured in layers of about 5 cm thick into the form formed by the vapor lock (cf. section 2.1.2.1.1) and compacted by tamping and by vibrating with an immersion vibrator 3 cm thick. The amount of fresh concrete used in each beam was determined by weighing. The weighing was also used to estimate the bulk densities and total water contents listed in Table 4. The sample cubes for the compressive strength analyses and for the experiments to determine the technical concrete characteristic values (Table 3) were prepared according to DIN 1048 [2]. DIN 1048 specifications were also followed in preparing the cylindrical test specimens and the reference specimens, and so forth.

2.1.1.3. Matrix Mortar

From the results of the preliminary experiments it was concluded that the structural development could not be sufficiently characterized solely by means of cement paste analyses. Rather, it was to be expected that precisely the type of aggregates used would be important with regard to the pore space. However, because of the equipment used for certain tests, in particular for the pore size distribution test, only small samples can be used, concrete itself was excluded as a test specimen. As a rule, concrete has a low proportion of cement paste which, moreover, would deviate sharply in small samples, In order to be able to determine the special features of the pore space caused by the aggregate, as well as to adequately adjust the sample material to the demands of the measurement method, the structural development tests were performed on mortars. With the exception

Table 4 Bulk densities and total water contents of the concretes compressed in the beams and the accompanying matrix mortars.

A Eigenschaften	C Beton mit calcitischem Zuschlag EBalken Nr. 3			B Beton D mit Kiessand -Zuschlag E Balken Nr. & 4 5 6			
des Balkenbetons F Trockenrohdichte G - Q _{tr}	kg/dm ³			2,24			2,22
⊢ermittelt an Proben des Balkenbetons, vgl. H Abschnitt 2.2.5 —				s = ± 0,13			s = ±0,13
(Trockenrohdichte, I abgeschätzt	kg/đm ³)	(2.33)	(2.27)	(2.23)	(2-24)	(2,22)	(2,20)
Gesamtwassergehalt J (vor Heizbeginn) K	The second of the second	14.4 +)	17.6	19.3	14.9	16.0	17.0
des Matrixmörtels I. Frischrohdichte M. Or	kg/dm ³	2.34	2.32	2,28	2.32	2.31	2.31
(Frischrohdichte des zur Mörtelherstellung verwen-N deten Betons	kg/dm ³)	(2.48)	(2:45)	(2.43)	(2,41)	(2,41)	(2,39)
Gesamtwassergehalt ++, J	Gew%	12.8	13,9	14.6	11.6	12,2	13,2
(Gesamtwassergehalt des zur Mörtelherstellung O verwendeten Betons ++,	Gew%)	(7.3)	(8,2)	(9,3)	(7,6)	8,2)	(9.3)
Robdichte P — Mittelwerte der im Alter von 1 Tag in die Balken eingesetzten Probekörper— G	kg/dm ³	2,56	2,32	2,29	2,31	2.29	2,30

Key: A. Properties

relatively large relatively lassons spread of densities

++) Determined by kiln drying, related to the weight of the dried sample

A. Properties
B. Concrete
C. With calcite
aggregate
D. With gravelsand aggregate
E. Beam number
F. Of the beam
concrete
G. Dry bulk density
H. Measured on samples
of the beam concrete,
cf. section 2.2.5

†) Taking into consideration the
relatively large

I. Dry bulk density,
estimated
J. Total water content
K. Before the start
of heating
L. Of the matrix mortar
M. Fresh bulk density
of the doncrete used
to make the mortar
O. Total water content
of the concrete used
to make the mortar
P. Bulk density
Q. Average values of the
test specimens inserte test specimens inserted into the beams at an age of one day

of the large particle size, these mortars match the concretes from which they were obtained by careful sifting of the fresh concrete on a screen with round holes measuring 5 mm in diameter mounted on a vibrating table. Gement grout residues and only a few fine pieces of aggregate adhered to the screening refuse particles. Accordingly, only the coarse aggregate (>5 mm) portion (about 30-40% by weight of the aggregate in accordance with the grading curves in Fig. 1) and the cement paste adhering to the particles retained by the screen were removed from the original concrete mixtures. The mortar obtained as undersize, given practically the same water/cement ratio, has different characteristic technical data than the original concrete mixture, but especially different aggregate/ cement ratio and a different bulk density (of. the bottom half of Table 4). By separating out the course particle portion, the geometric interrelationships of the individual components were changed. However, the properties of the mortar practically matched those of the matrix into which the course particles are For purposes of clearer distinction from the mortar mixtures made using quartz sand as the aggregate, the mortars obtained from the fresh concretes are hereafter referred to as matrix mortars.

After screening, the matrix mortars were once again thoroughly mixed and put into chronical PVC forms with a volume of 26 cm³. The 64 test specimens for each beam were compressed at the same time in a jig attached to the vibrating table. After scraping and weighing, the test specimens were stored at 25°C and almost 100% relative humidity until being inserted into the recesses provided for on the tops of the beams (cf. section 2.1.2.1.1).

2.1.1.4. Cement Mortar and Cement Paste

The cement stored in 40 airtight containers, each containing about 100 kg, was sampled randomly by withdrawing three 25-kg samples. In addition, a collective sample weighing 30 kg was made up by mixing samples from all of the containers.

The cement of the random samples was used to make prisms measuring 4 cm x 4 cm x 1 6 cm out of cement mortar as per DIN 1164, page 7 [3]. These were also to be used to evaluate the uniformity of the properties of the cement.

The cement of the collective sample was used to make prisms measuring 4 cm x 4 cm x 16 cm of cement paste with water/cement ratios between 0.2 and 0.55 in gradations of 0.05. In so doing, the cement paste test specimens, up until

/19

the forms were opened after 24 hours, were treated according to the specifications of DIN 1164, page 7 [3] and then stored until testing in a saturated calcium hydroxide solution.

2.1.2. Experimental Conditions, Set-up and Procedure

2.1.2.1. Experiments on the Concrete Beams

2.1.2.1.1. Experimental Arrangement and Procedure

In view of the complex events connected with heat and moisture conduction in concrete, it seemed necessary to performs experiments directly on large concrete objects, supplementing these experiments -- to the extent needed -- by experiments on small test specimens. In planning the experimental program we proceeded from the premise that a cement wall, for example of a reactor vessel, with a wall thickness of 4-5 meters is heated on one side, while the other side is exposed to normal room temperature. In approximating the actual geometric relationships, it is possible, in order to study the conduction of heat and moisture, to analyze the events in a free cut, beam shaped object whose length corresponds to the wall thickness and the ends of which represent parts of the wall surfaces. In the experiments descrived below, the beam length could not exceed 240 cm for technical reasons. The beam cross-section of 40 cm x 40 cm was made as large as possible in order to keep edge effects small which may perhaps adversely affect the phenomena.

/20

In the experimental setup for the beams, the following conditions had to be taken into account. The temperature of the concrete on the heated face should be 80°C and the temperature on the face exposed to passing air should be about 20°C with a relative humidity of around 45%. So that, in analogy to the heated wall, heat and moisture were transported only from the inside to the outside, i.e. in the direction of the long axis of the beam, external effects had to be kept from impairing the temperature distribution and moisture distribution, i.e. above all, measures had to be taken to prevent the loss of heat and moisture on the long sides of the beams,

Diagrams of the experimental setup are shown in Fig. 3. The entire arrangement is located in an air-conditioned room with an air temperature of 20°C and 45% relative humidity. With the exception of the free face, the concrete beam is surrounded with a vapor seal made of copper sheets 0.2 mm thick soldered together. These sheets are coated with epoxy

ORIGINAL PAGE IS OF POOR QUALITY

resin sprinkled with sharp quartz sand in order to achieve a tight bond between the vapor seal and concrete.

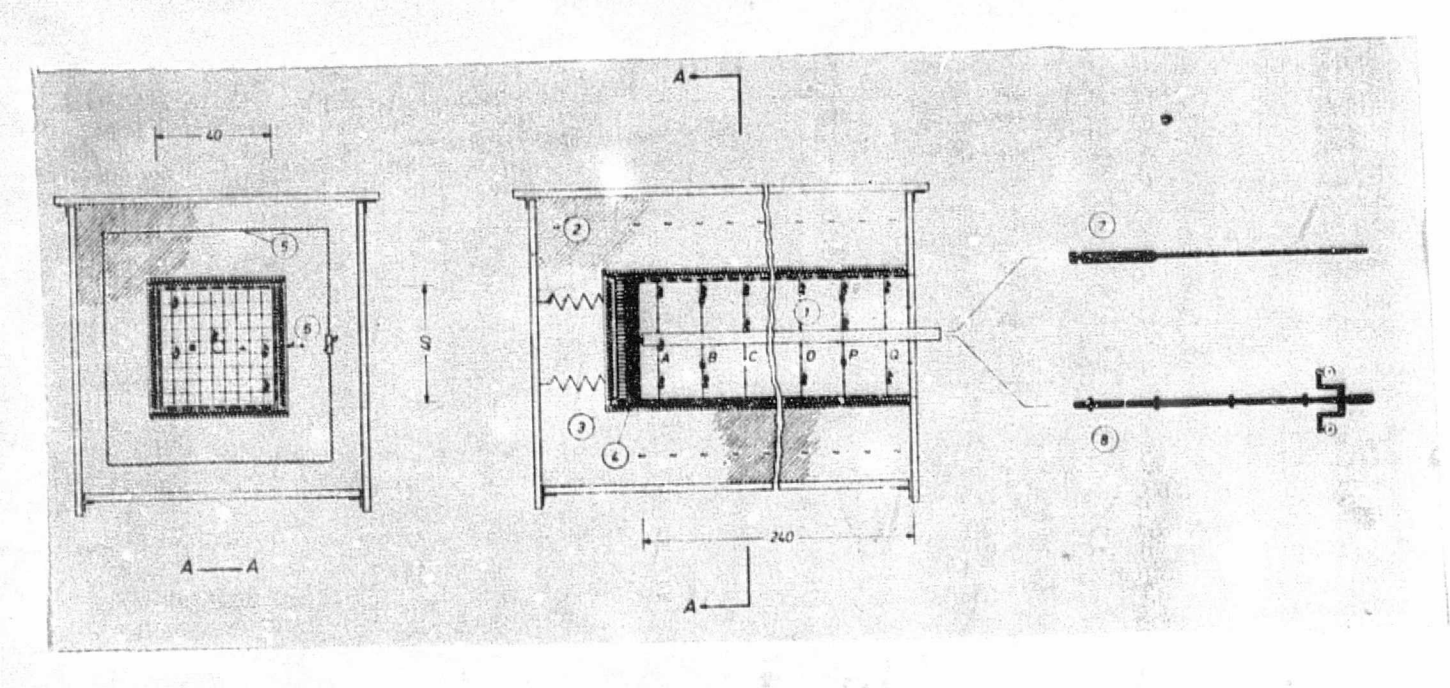


Fig. 3. Schematic representation of the apparatus for studying heat and moisture conduction as well as the accompanying concrete properties of a concrete beam measuring 240 long, 40 cm x 40 cm in cross-section, heated on one face (80°C), with a vapor seal and heat insulation. Conditions on the free face: 20°C; 45% relative humidity.

1. 40 cm x 40 cm x 240 cm concrete beam with measurement planes A to Q_{\star}

Thermocouple

Humidity measuring device

Expansion transducer

with a glass tube arranged along the long axis and a vapor seal next to the heated face and on the long sides.

- 2. Thermal insulation layer, a total of 30 cm thick, made of rigid polyurethane foam and polystyrene foam with an outer casing.
- an outer casing.

 3. Heating plate, 40 cm x 40 cm, pressed against the insulated beam by springs.

4. Heat flux measuring plate, 40 cm x 40 cm.

Counter-heating strips with adjustable resistors.
 Thermocouple for measuring temperature gradients.

7. Neutron probe for measuring humidity.

8. Rule for measuring the length.

A cast iron, electric heating plate is next to the left face of the beam. This is guided over pins and pressed against the beam by springs. Heat is applied to the concrete beams by this heating plate through a heat flux measurement plate, also measuring 40 cm x 40 cm (cf. section 2.2.2) and a 2-mm thick soft copper equalization plate. The heating plate, which weighs about 20 kg and is provided with four separate heating circuits of 1.25 kVA each, is controlled through an electronic two-position controller by means of a contactor, in the process of which the desired value (80°C) on the surface of the concrete is measured with a thermocouple. The heating system and beam are surrounded by 30 cm of thermal insulation, the innermost layer of which consists of rigid polyurethane foam, while polystyrene foam was used for the outer layers. In order to prevent mechanical damage to the vapor seal during the pouring of the concrete, there is a 1-mm thick protective layer of hard PVC between the vapor and thermal insulation on the bottom and long sides of the beam.

Since in spite of the high thermal resistance of the insulating material used and in spite of the thickness of the insulation, heat losses through the long sides have to be taken into account, electric heating strips encircling the beam are positioned in the insulating layers at a distance of 20 cm from /21 the surface of the concrete. These consisteof a 0.5-mm thick Constantan wire insulated with fiberglass and for more efficient giving off of heat they are placed in a folded sheet of copper 2.5 cm wide. Their heat output can be adjusted by means of variable resistors attached to the outer beam casing so that no temperature gradients exist between the surface of the concrete and the level of the heating strip. This compensation is monitored with termocouples, specifically by means of a copper-Constantan-copper element arranged between a heating strip and the surface of the concrete. The joints of the element are 5 cm apart and its thermoelectric voltage difference with a uniform temperature in the cross-section (d 0/d b=0) gces to 0.

The outer casing, which completely surrounds the structure and exposes only the free face through a hole measuring about 41 cm x 41 cm, is made of 25-mm thick board sheets with aluminum foil stuck to them or painted on both sides. The long sides of the sheets are reinforced with steel sections. The top of the outer casing can be unscrewed and is made in three separate parts. The undercarriage consists of a gun-mount type, 2-axle support frame made of I-beams. The entire test assembly (about 1600 kg) can be lifted by the 4 axle ends for weighing (also see Fig. 6).

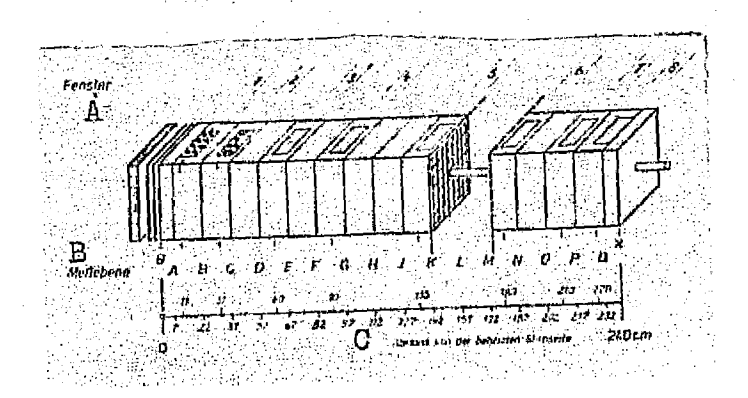


Fig. 4. Concrete beam subdivided into sections by "measurement planes" (labeled A to Q) and arrangement of the "windows" (labeled 1 to 8) on the top of the beam.

Key: A. Windows

B. Measurement planes

C. Distance from the heated face

Fig. 4 shows the 240-cm long beam without casing, thermal insulation and vapor seal. It is subdivided by "measurement planes" into 1% sections which are identified by the adjacent planes 0/A, A/B, ... to Q/X and by the increasing distance from the heated face. Section 0/A is 7 cm thick, Q/X 8 cm thick and all of the other sections are 15 cm thick. wire grids (polyester-coated wire mesh with a mesh size of 50 mm and 2-mm thick wire) arranged in the measurement planes are used on the one hand for anchoring the measurement devices and their feed lines, and on the other hand they indicate the fracture planes when the concrete beams are split after the end of the experiment (cf. section 2.1.). On the top side of the beam there are two "windows" in the vapor seal and the thermal insulation which, after the casing lid has been removed, permit access to the 8 test specimens, arranged on conical recesses, for studying the structural development on the matrix mortar (cf. section 3.3.). Windows 1, 2 and 3 are sealed with steel plates and a silicon rubber gasket pressed between the steel plate and the yapor seal. In the case of windows 4-8, a copper foil is mounted over the window opening onto the vapor seal, with a 3-cm wide band of gasket material stuck to both sides, and pressed tight by the thermal insulation.

The glass tube (inside diameter 41 mm, wall thickness 2.3 mm) placed along the central longitudinal axis of the beam is

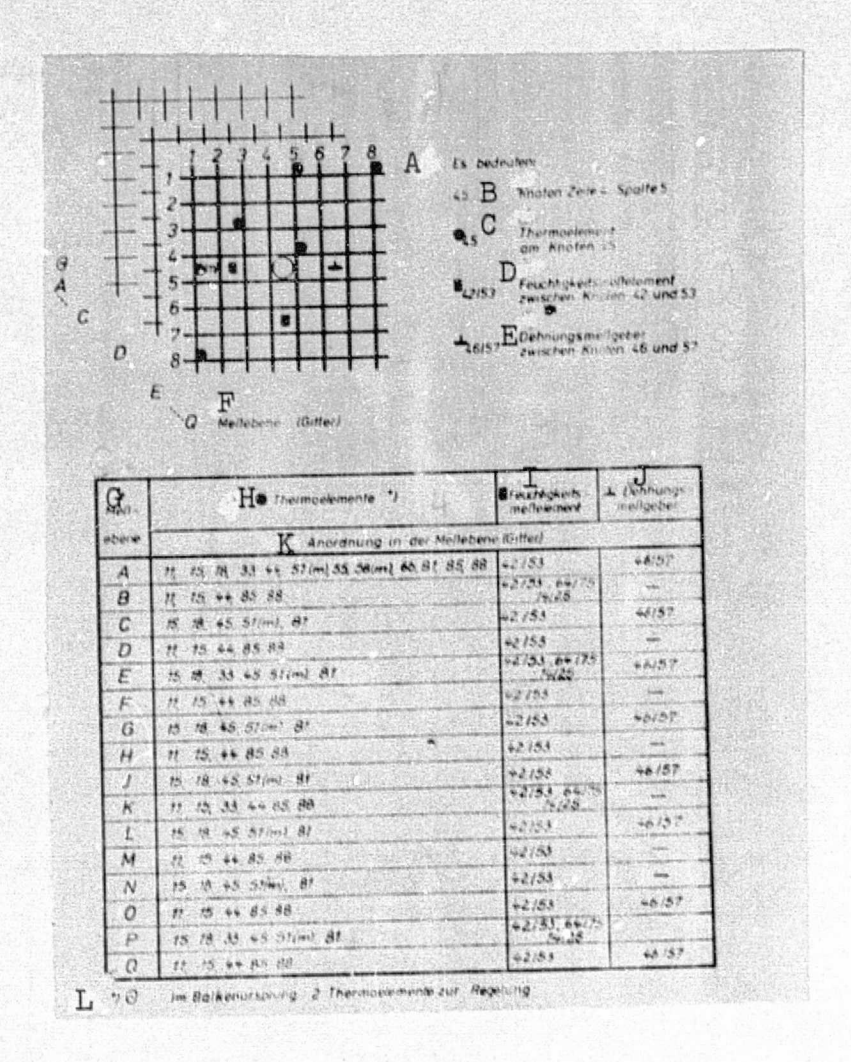


Fig. 5. Arrangement of the thermocouples, humidity measuring devices and expansion transducer in the measurement planes, formed by grids, for the concrete beams (measurement planes A to Q in increasing distance from the heated face).

Key: A. Legend

B. Node line #, column 5

C. Thermocouple at node 45

D. Humidity measuring device between nodes 42 and 53

E. Expansion transducer between nodes 46 and 57

F. Measurement plane (grid)

G. Measurement plane

H. Thermocouples

I. Humidity measuring device

J. Expansion transducer

K. Arrangement in the measurement planes (grid)

L. 0, two thermocouples for control purposes in the origin of the beam

> ORIGINAL PAGE IS OF POOR QUALITY

ORIGINAL PAGE IS OF POOR QUALITY

sealed off at the end towards the hot face of the beam and contains a wooden rod covered with foam material which prevents the transport of heat within the tube by convection and is removed to make the measurements in question.

Fig. 3 and Fig. 5 show the arrangement of the measuring elements and measuring apparatus in the beam.

2.1.2.1.2. Procedure

/22

In keeping with the object of the experiments, it was necessary to prepare 6 test setups like that shown in Fig. 3. Three of these were used for the experiments on concretes with calcite aggregate (beams 1, 2, 3) and three for the tests on concrete with gravel-sand aggregate (beams 4, 5, 6), as already explained in section 2.1.1.

For pouring the concrete, a sheet of metal reinforced with a wooden plate and two U-beams was attached in each case to the "cold" beam faces which would later be exposed to the air. This sheet of metal was sealed at the edges and also around the hole for the glass tube to prevent moisture from escaping. In addition, the test setup was open on top; (Fig. 6). The top portion of the vapor seal, provided with sealed window openings, was placed on the compressed concrete and sealed at the edges. The upper layers of thermal insulation were put in place on the third day after the concrete was poured and in so doing the counter-heating strips were united by a plug connection and the lid was screwed on.

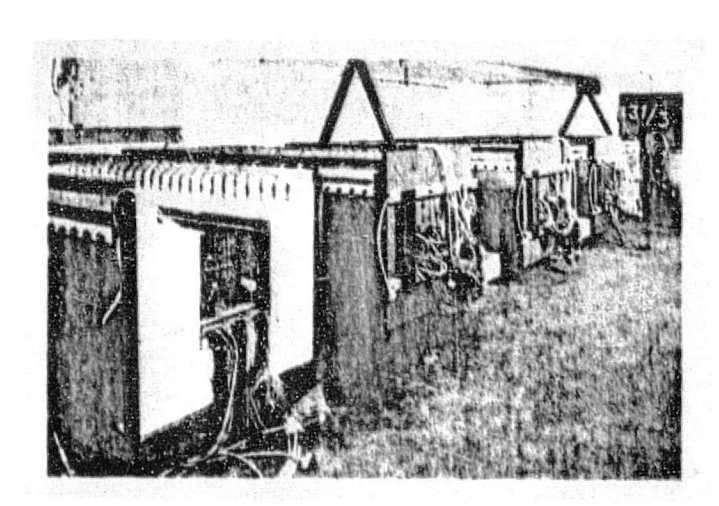


Fig. 6. View of the structures for studying the concrete beams. The left unit is open on top and the face plate is not attached. Measurement wires can be seen coming out of the front of the unit and the heating strips placed through the side wall material.

The concrete for the individual beams and for the accompanying test specimens was poured in each case in one-week intervals. For operational reasons, the making of beams 1, 2 and 3 and 4, 5 and 6 had to be separated by a space of about two months. To this extent, the age of the concrete of the two groups differed. Up to the 28th day after pouning, because of the seal provided on all sides by the vapor seal and the metal sheet on the open face, the beams could not give off any moisture to the air flowing around the test apparatus. On the 28th day, the "cold" face was exposed and heating was begun. To begin with, the heating strips were regulated every 12 hours on the basis of temperature difference measurements in the thermal insulation, and later every 24 hours, and since only slight changes occurred, after about 35 days of heating these could be regulated at intervals of several days.

In view of the external experimental conditions, two periods accordingly have to be distinguished with regard to the measurements made on the beams, namely the period up to the start of heating on the 28th day and the following period characterized by the heating. For various reasons, it was not possible to begin all of the measurements immediately after the concrete was poured. Details on the measurement methods used and how the measurements were performed are explained in section 2.2.

2.1.2.2. Experiments on Test Specimens

-Matrix Mortar Test Specimens-

Since the concrete used to make the beams during the duration of the experiment could not be used for direct analysis of the structural development as well as other properties, tests had to be done on separately produced test specimens.

For studying the content of non-evaporatable water, total porosity and pore size distribution (cf. sections 2.3.1-2.3.3) the matrix mortar provided—as already mentioned in section 2.1.1—was obtained by sifting the fresh concretes of the beams using a screen with round holes measuring 5 mm in diameter. The mortar was poured into conical PVC forms, cured for about 20 hours at 25°C and approximately 100% relative humidity and then removed from the mold and inserted into the matching recesses in the beams accessible through the windows. In this arrangement the side surfaces of the test specimens were in contact with the surrounding concrete and there was an air space about 1-2 mm wide only next to the top surfaces. The

test specimens of the matrix mortar were thus exposed to approximately the same conditions prevailing in the beam concrete, conditions characterized by the respective local temperature and by the moisture content in equilibrium with the surrounding concrete. As shown in the chart in Fig. 7, the test specimens were generally removed in pairs from windows 1-8, weighed, prepared and analyzed. Without taking into account the number of samples for the windows of a beam and the individual age gradations, this chart indicates the type of test done in each case.

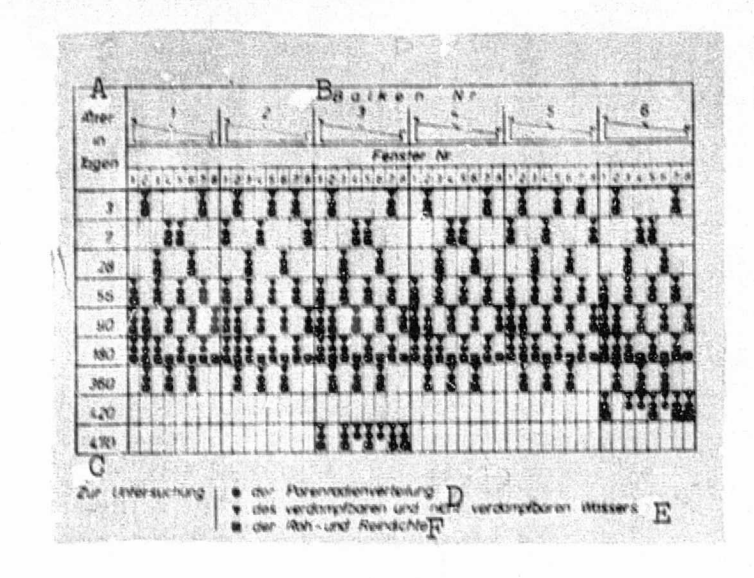


Fig. 7. Coordination of sample-taking points (windows 1-8), age increments (3-470 days) and the type of test performed on the matrix mortar test specimens arrange in beams 1-6.

Key: A. Age in days

B. Beamsnumber

C. For testing

D. Pore radius distribution

E. Evaporatable and non-evaporatable water

F. Bulk density and net density

-Concrete Cubes-

The development of strength is a reflection of the hardening processes in the cement paste. Therefore, compressive strength tests, for example, also provide information on structural development (cf. section 2.3.4.). The conditions given as a result of the thermal load in the beam experiments, however, could not be satisfactorily simulated by curing a larger number of sample cubes, since definite temperature and moisture states changing over time would have involved considerable expense for maintaining them. Apart from this, even in these experiments the results of the compressive strength tests on test cubes can be used only for comparison with the actual strength of the beam concrete. Further influences on the properties of the beam concrete, however, are possible only within limits because of different production and hardening conditions. For these reasons, the only conditions provided for from the outset were curing at 20°C and approximately 100% relative humidity and also at 20°C and 45% relative humidity, where in both cases the test specimens were treated up to an age of seven days in accordance with DIN 1048 [2].

For each beam, i.e. each type of concrete, 12 sets of three cubes measuring 10 cm on a side and six sets of cubes measuring 20 cm on a side were prepared during the making of the concrete for compressive strength tests (a total of 54 cubes per beam). Of the cubes measuring 10 cm on a side, one set was tested with an age of three days and another with an age of seven days. In addition, cut of five sets for each type of curing, one set was provided for testing on the 28th, 90th, 180th, 360th and final day of the experiment. Out of three sets of 10 cm cubes for each type of curing, it was intended to test one set on the 28th, 180th and final day of the experiment.

-Concrete Cylinders-

To investigate thermal expansion behavior as well as shrinkage and swelling, two test specimens were produced for each type of concrete (beams 1-6) in cylindrical, vapor tight, thinwalled sheet metal containers with a diameter of about 100 mm and a length of about 227.5 mm. The curing conditions and the treatment of the test specimens are explained in section 2.4.1. in conjunction with how the measurements were performed.

-Cement Mortar and Cement Paste Prisms-

Frisms measuring 4 cm x 4 cm x 16 cm were used to study the structural development of the cement paste and the strength development of cement mortar, but also especially for evaluating the uniformity of the cement used. The making of the test specimens is described in section 2.1.1.4.

The cement mortar test specimens were cured in accordance with DIN 1164, page 7 [3]. Altogether, 8 sets of three prisms each were available for the flexural tension strength and compressive strength tests at different ages.

All of the 64 cement paste prisms, of which there was one for each water/cement ratio and each age increment, were stored in a saturated calcium hydroxide solution until the flexural tensile strength test and the compressive strength test. The prisms remaining after the tests were used—to the extent required—as test material for the porosity tests and the dehydration experiments.

2.2. Measurements on the Concrete Beams

2.2.1. Temperature

2.2.1.1. Measurement Method, Arrangement and Procedure

NiCr-Constantan thermocouples with a relative differential thermoelectric voltage of 0.059 mV/°C were used to measure the temperature differences. The thermoelectric wires used to make the thermocouples were insulated separately and together with PVC and were from one production batch. The ends of the thermoswivels were welded in protective gas and covered with epoxy resin to protect against corrosion. The dependence of the thermoelectric voltage on the change in temperature was determined in increments of 10°C between 10 and 90°C, with a reference temperature of 0°C, by the Physikalisch-Technischen Bundesanstalt (PTE) [Physical-Technical Federal Institute] in Braunschweig (measurement uncertainty: ±0.010 mV=0.2°C).

The reference points of the thermocouples were placed in glass tubes filled with quartz sand which were immersed in a temperature-controlled bath (0±0.05°C) for the measurement. The total of 94 thermocouples arranged intthe measurement planes of a beam as shown in Fig. 5 (also see Fig. 8) were combined into four 50-terminal plug connections behind the comparison points and connected to a 24-channel potentiometric recorder for the measurement. Thus it was possible to record temperatures at certain measurement points over longer periods and also individually interrogate all of the measurement points.

2.2.1.2. Measurement Results

For all of the beams studied, the temperatures measured under the effect of the heat of hydration of the cement lay within the range shown in Fig. 9 as a function of the age of the concrete. The reference point for the beginning of this range is the end of the pouring procedures in each case. For the temperature rise in the beams, a crucial factor was, above all, that the thermal insulation on the top of the beams was



Fig. 8. View of a section of measurement plane Q before the concrete is poured, with vapor seal on the outsides, wire grid and thermocouples, moisture measuring elements and expansion transducers attached to it.

not applied in each case until after three days in order to keep the concrete from overheating. Insofar as this is concerned, typical temperature developments were not to be expected for the individual concrete beams. As Fig. 9 shows, on the 28th day all of the measurement points in the concrete had again reached temperatures between about 20 and 22.5°C.

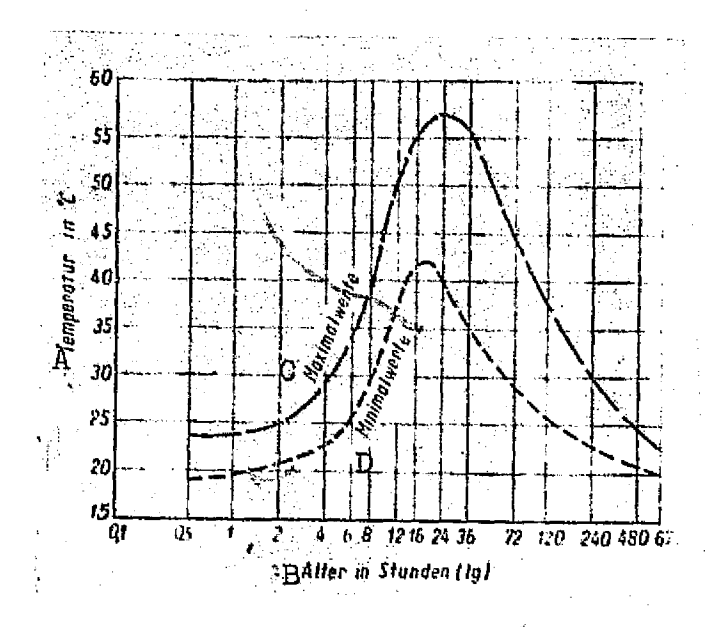


Fig. 9. Limit values for the temperatures of the concrete caused by heat of hydration after the pouring of beams 1-6.

Key: A. Temperature

B. Age in hours

C. Maximum values

D. Minimum values

With the start of heating on the 28th day, the temperatures in the concrete beams again rose, The differences between the temperatures measured at the different points within one beam section was small. For the measurement planes in the hot region of the beams, obviously the least favorable in this respect, the temperatures deviated around the mean value by a maximum of about ±0.75°C, as Fig. 10 shows. The measurement points located in the lower region of the beam showed higher temperatures in some cases with respect to the other measurement points. Apart from this tendency, which presumably is due to the effect of gravity on the moisture distribution in the beam cross-section [66], systematic differences were not detected, so that it seems justified to form mean temperature values for the individual measurement planes. Figs. 11 and 12 show the mean temperature values for measurement planes 0-Q as a function of the age of the beam concretes, beginning with

ORIGINAL PAGE IS OF POOR QUALITY

the 28th day. Fig. 13 shows temperature distributions for different ages of concrete as a function of the beam length and also their differences as a function of the water/cement ratio of the concrete.

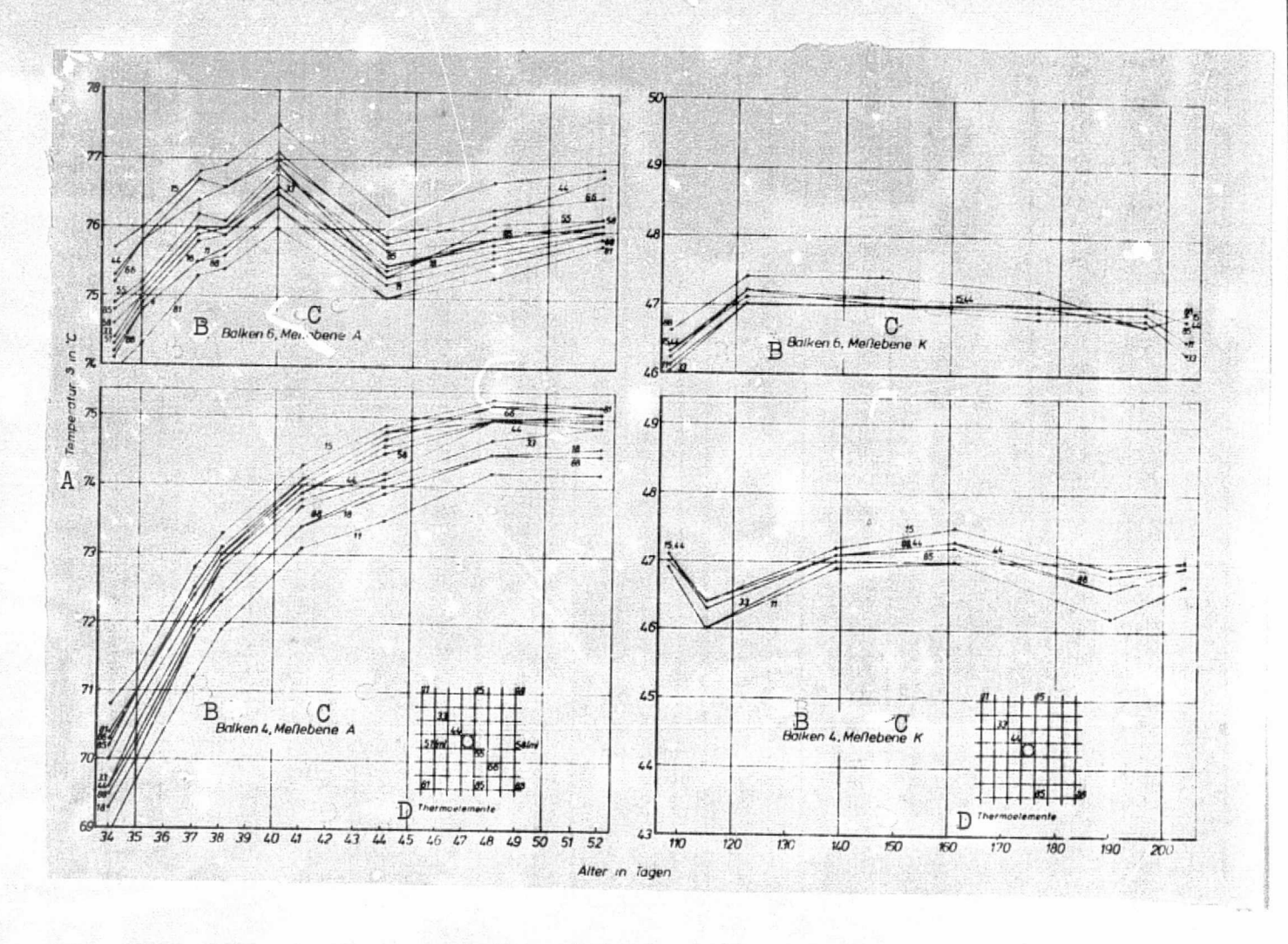


Fig. 10. Examples of the changes in temperature distribution within the beam cross-section (measurement plane A) during the heating phase up to the 52nd day and for greater ages (measurement plane A) for beams 4 and 6.

Key: A. Temperature

B. Beam

C. Measurement plane

D. Thermocouples

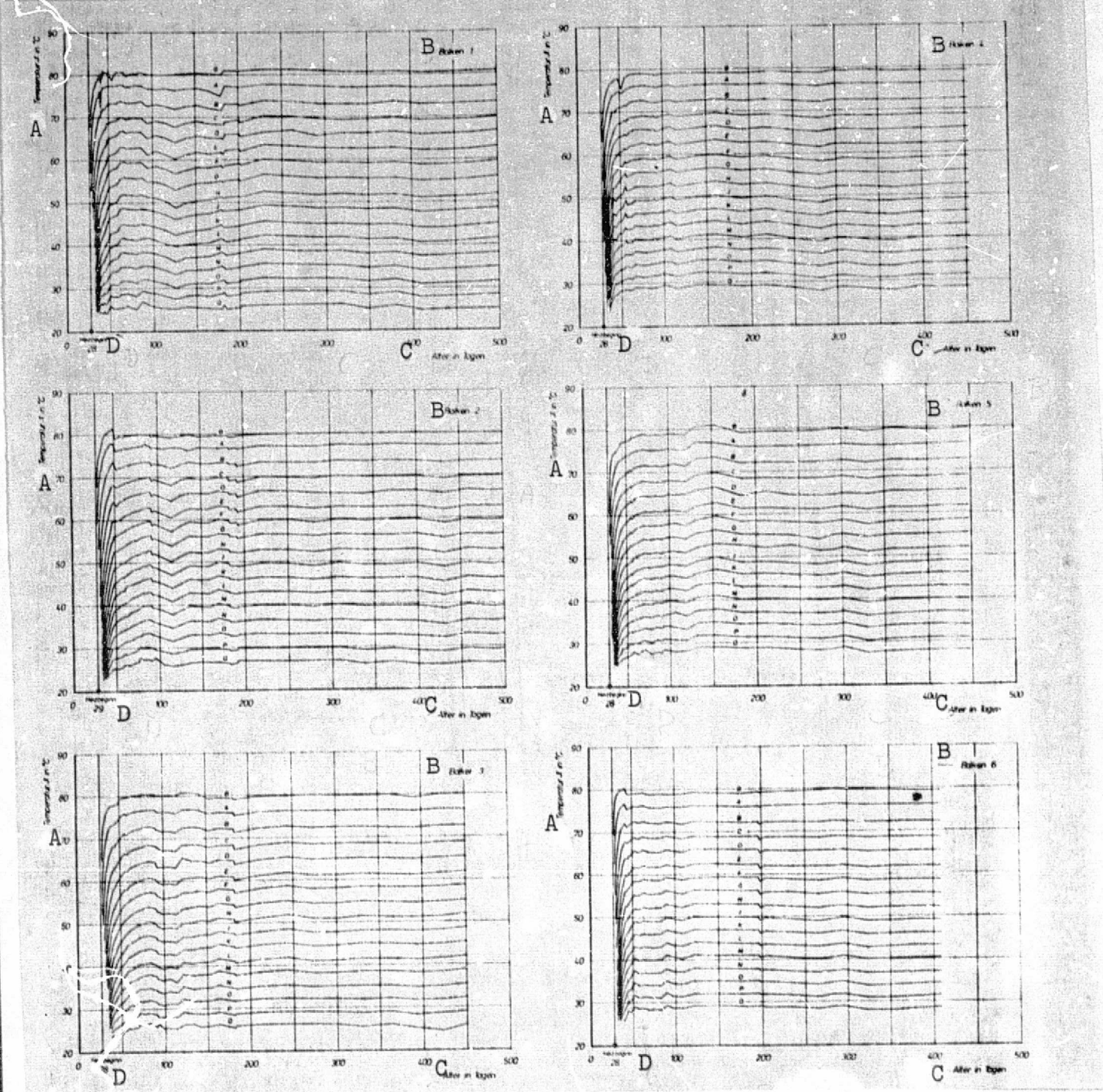


Fig. 11. Mean temperature values in measurement planes θ -Q as a function of age for beams 1, 2 and 3 (concrete with calcite aggregate).

Key: A. Temperature

B. Beam

Fig. 12. Means temperature values in measurement planes θ -Q as a function of age for beams 4, 5 and 6 (concrete with gravel-sand aggregate).

C. Age in days

D. Start of heating

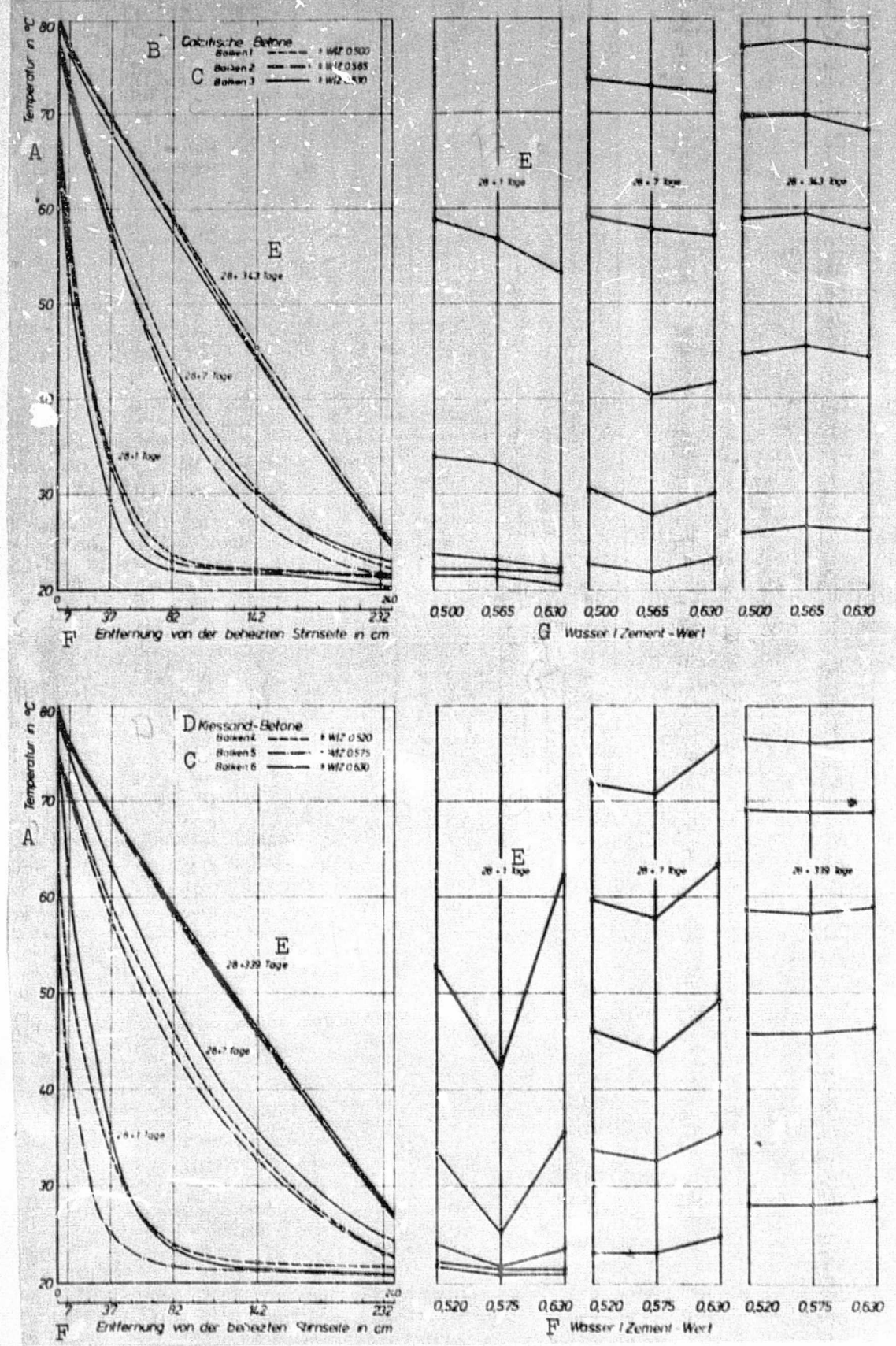


Fig. 13 See caption and key on following page.

Fig. 13. Left: temperature distribution over beam length for various age increments; right: temperatures as a function of the water/cement ratio of the concretes for certain distances from the heated face and for different age increments.

Key: A. Temperature

B. Calcite concretes

C. Beam

D. Gravel-sand concretes

E. Days

F. Distance from the heated face in cm

face in cm OF POOR QUALITY

ORIGINAL PAGE IS

G. Water/cement ratio

2.2.2. Heat Flux

2.2.2.1. Measurement Method, Arrangement and Procedure

The method used to measure the heat flux density on the heated face of the beam (cf. Fig. 3) is based on the equations for heat conduction through solids discussed in section 2.5.4 [67, 68]. Heat flux measurement plates were used to perform the measurement, these contained a large number of thermocouples distributed over the thickness of the plate and connected in series. The temperature difference occurring during the conduction of heat is measured as the thermal stress proportional to the heat flux density. The proportionality factor is the thermal conductivity of the measurement plate (see Eq. (6) in section 2.5.4.).

The five heat flux measurement plates, measuring 40 cm x 40 cm x 0.6 cm, were calibrated in a plate device as per DIN 52 612 [7] for temperatures between 0 and 100° C in 20° C increments. In the range in question, the relationship between the mean temperature of the measurement plate and the heat flux density with respect to the voltage was approximately linear for all of the measurement plates. The sensitivity was between about 8.6 and 7.0 W/m² mV.

The plates were arranged between the heating plate and concrete in beams 1-5, with a sheet of soft copper 2 mm thick between the measurement plate and concrete for better heat conduction. A 12-channel potentiometric recorder was used to measure the thermoelectric voltages, so that the heat flux density on the heated face could be measured simultaneously with the temperatures in the beam.

/25

2.2.2.2. Measurement Results

In the evaluation, the heat flux densities were calculated using the voltages measured, taking into account the average temperatures of the measurement plates. In Fig. 14, the heat flux densities for beams 1-5 are plotted as a function of the age of the concrete. The values measured on the beams immediately after the start of heating (these are not shown in the graph) were around 900 W/m². During the heating and also afterwards, the measured values deviated by about ±0.5 mV (corresponding to about 4 W/m²), which was basically due to the control fluctuations of the heating plate and therefore were not taken into account in the evaluation.

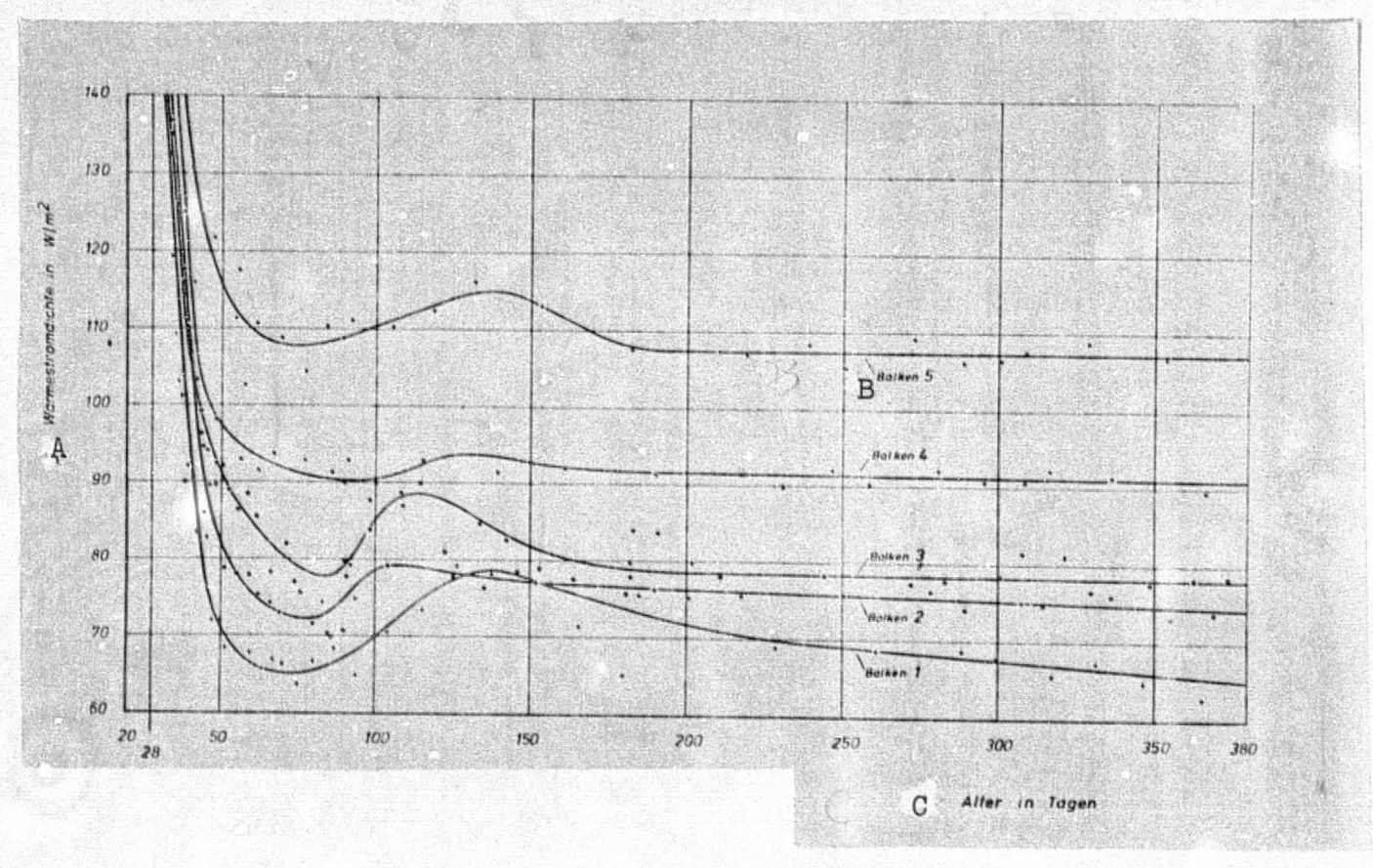


Fig. 14. Changes in the heat flux density as a function of the age of the concrete after the start of heating on the 28th day for beams 1-5.

Key: A. Heat flux density

B. Beam

C. Age in days

2.2.3.0. Selection of the Measurement Methods

Measuring the moisture in concrete poses considerable difficulties, in particular when the influence of temperature is a factor and when the measurements have to be performed over a long period. In view of the scope of the study, besides measurement reproducibility questions and long-term stability problesm, we also had to take into consideration the technical resources and expenses involved by the measurement methods in question.

The final decision as to which methods should be used for making the measurements was made on the basis of results of a survey on methods of measuring moisture in porous materials [69] carried out jointly with RILEM* among relevant scientific institutes. This survey revealed that, because of the specific measurement ranges and the calibration possibilities, it would be better to use several complimentary methods together with the gravimetric method, as a calibrating method, with which the moisture content is determined by drying and weighing.

Therefore, for measuring the moisture content of the concrete beams, the following methods were provided for in addition to the weighing process desdribed in section 2.2.3.2 below, which measures the sum of all of the changes in moisture content as weight losses of the beams:

- the measurement of electrical conductivity in reference specimens (section 2.2.3.3.) which allows changes in the content of evaporatable water to be measured within a certain range;
- the neutron backscattering method (section 2.2.3.4.), with which the sum of evaporatable and non-evaporatable water is measured;
- the gravimetric method (section 2.2.5.), by means of which, after the conclusion of the experiments and after the splitting of beams 3 and 6, samples of the beam concrete are

Reunion Internationale des Laboratoires d'Essais et de Recherches sur les Materiaux et les Constructions [International Association of Testing and Research Laboratories for Materials and Structures].

analyzed for their content of evaporabable and non-evaporatable water.

The first two methods complement one another in that by forming the difference between the total water content and the content of non-evaporatable water, the amount of evaporatable water can be calculated. The gravimetric methods also serves the purpose of a control method.

/29

2.2.3.1. Weighing Method for Determining the Weight Losses

2.2.3.1.1. Measurement Method, Arrangement and Procedure

After removing the front-plate of the outer casing for the start of heating on the 28th day, the beams were able to release moisture from this exposed end. Initially, the moisture loss is determined for the most part by the external drying conditions and as the heating progresses it is increasingly dependent on the amount of moisture transported through the pore space towards the drying front. Since the weight losses of the beam, which is sealed on all sides with the exception of the exposed front face, are therefore causally explained by the events controlling the drying process, it was necessary to directly measure the changes in beam weight as a function of time.

To this end, the entire experimental apparatus was lifted and weighed (cf. section 2.1.2.1.1.). Figs. 5 and 13 [sic.] show the supporting I-beam resting on three supports which spans the test apparatus. The lifting and weighing apparatus (Fig. 15) consists of 2 counterrotating shafts with trapezoidal threads in a manually operated threaded sleeve which is connected by flexible couplings to a "travelling crab" and to a load cell. The weighing beam mounted on the lid of the casing (when the testaapparatus is closed) hang from cables from the lower swivel ring of the load cell. For weighing, we used an electrical load cell with wire strain gauges in a full bridge circuit for compressive and tensile force up to 20 kN, accuracy category 0.1, with a sensitivity of 2 mV/V. This was operated using a manual, high-accuracy potentiometer (measurement rage 100,000 scale divisions correspond to 5 mV/V) as the measuring device. In a test of the measuring apparatus in a precision load machine unit at a temperature of 20°C, the evaluation constant, for the range between 15 and 17 kN, was determined at one scale division corresponds to 0,4895 N.

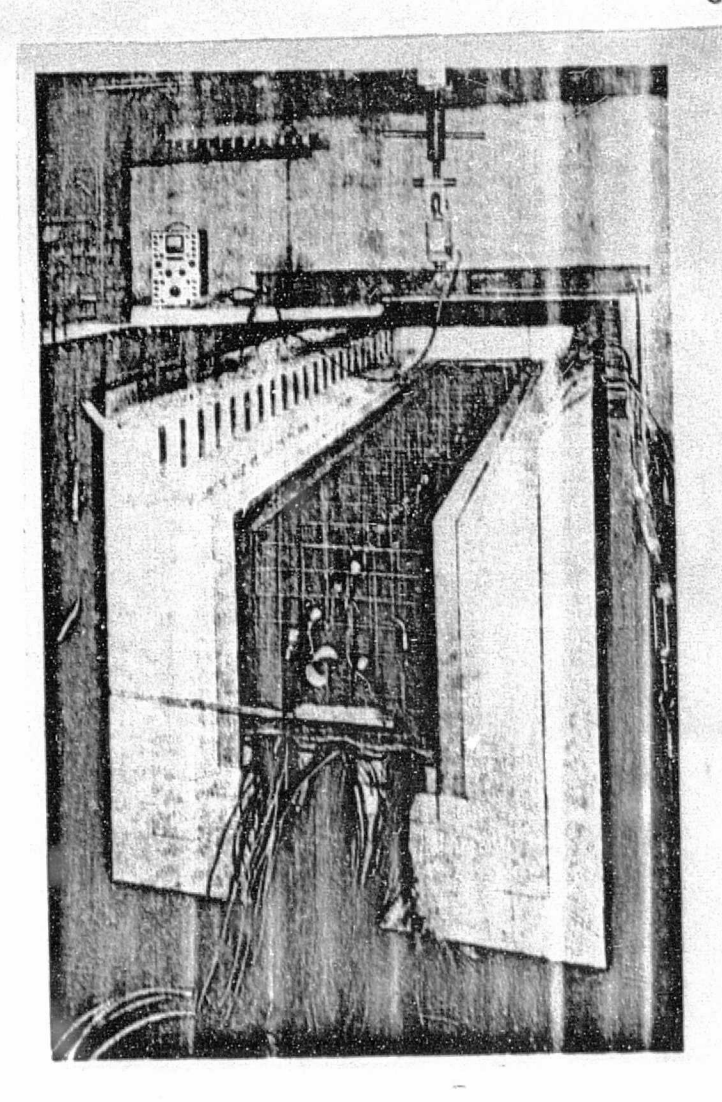


Fig. 15. Frontal view of an experimental set-up without casing before the concrete is poured showing the apparatus for measuring weight losses by means of an electrical load cell flexibly inserted between the supporting beam plus spindle-type lifting device and the weighing beam.

2.2.3.1.2. Measurement Results

Weighing the beams revealed that up to the 28th day there were, as expected, no changes in weight. For the subsequent weighings, the value measured on the 28th day immediately before the start of heating was used as a reference. Based on this value, the weight changes were calculated in each case as the difference with respect to the preceding weighing and added to the total weight loss. Fig. 16 shows the weight losses of the beams due to the release of moisture through the exposed

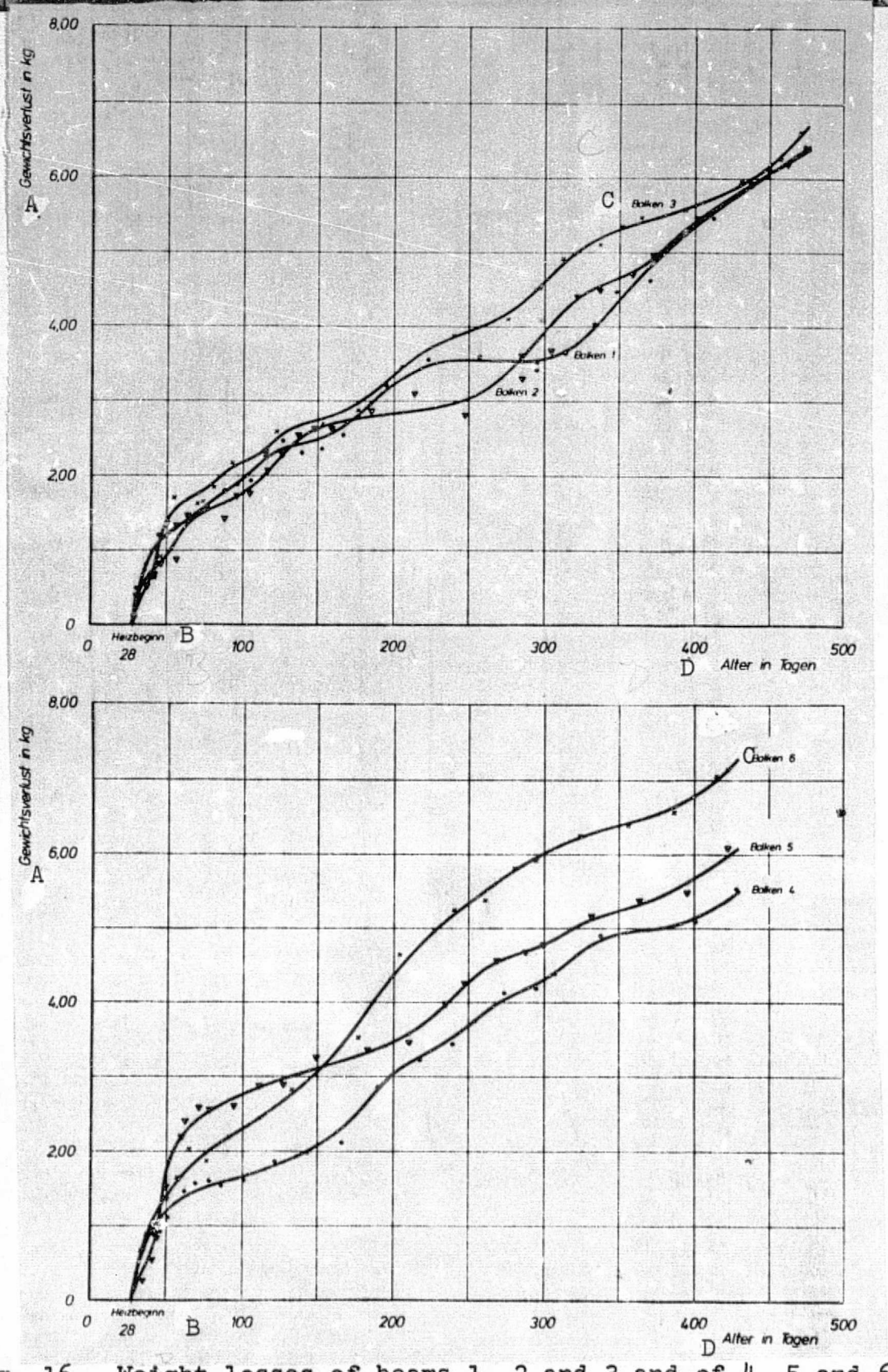


Fig. 16. Weight losses of beams 1, 2 and 3 and of 4, 5 and 6, plotted as a function of the age of the concretes.

Key: A. Weight loss
 B. Start of heating
 C. Beam
 D. Age in days

front face as a function of the age of the concrete. Each plotted value was formed by taking the average of at least three separate measurements.

Based on the spread of the individual measurements, a confidence range [81] of tos / \sqrt{N} = ±0.044 kg was calculated for the mean values with a statistical certainty of 95%.

2.2.3.2. Moisture Measuring Elements

2.2.3.2.1. Measurement Method, Arrangement and Procedure

The method of measuring changes in moisture content based on the change in electrical conductivity has been used for a rather long time with variable success [69, 70]. It is based on the fact that the conductivity of a reference material is changed by the water penetrating into its pores. Measurements are made between electrodes in the form of wires or even hollow cylinders [46]. In order to prevent the formation of an opposing field produced by polarization on the electrodes, alternating current is generally used formaking the measurement. For tests on concrete, reference samples of plaster, cement mortar, fiberglass and ceramic were used, but in this connection the conditions arising in concrete were considered differently. /30 These conditions are the influence of ion concentration in the pore solution on conductivity as well as the variable contact resistances between electrode and reference material.

With the method described by K. Altmann [71, 72], it seemed possible, on the basis of preliminary experiments, to fulfill the special requirements of the measurement task. The cylindrical moisture (diameter 20 mm, length 20 mm) used by him consists of a ceramic material fired at about 1100°C containing platinum electrodes (cf. Fig. 17). By virtue of the manufacturing process and the raw material used, the ceramic piece has a relatively uniform structure with predominantly small pores which are suitable for "excluding the influence of uncontrollable changes in salt content, which also amount to an additional, undesirable change in resistance" [72]. Since the electrodes are burned in, it is also necessary to take into account constant contact resistances between the electrodes and reference material.

During the perliminary experiment it turned out that the measurement expense can be kept relatively small. The voltage used was 11 yolts a.c., 50 Hz, and a commercial a.c. stabilizer was connected in series. The measurement device for the current measurements was a digital multimeter with a nA range and a

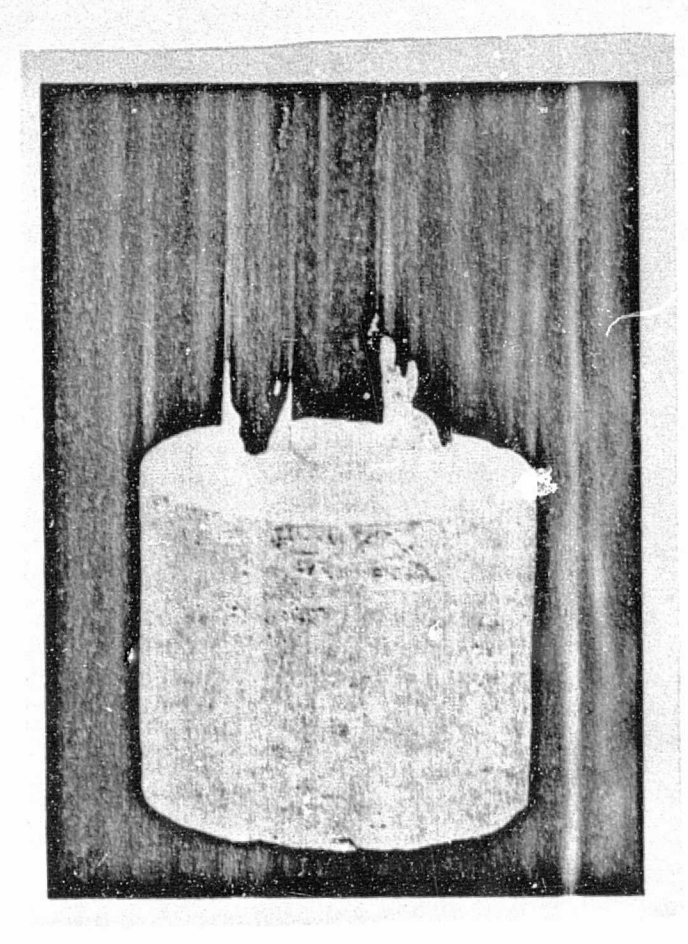


Fig. 17. View of a moisture measuring element (length ca. 2 cm, diameter ca. 2 cm) as designed by K. Altmann, with measurement wires fed in separately.

resolution of 10 pA in the most sensitive range. The making of the elements was contracted out, and it was stipulated that all of the elements should come from one lot. They were delivered without connection terminals and without a metal jacket so that the uniformity of the elements could be evaluated on the basis of current measurements in the dry and water-saturated state as well as by means of water uptake values and the dry bulk density.

The wiring originally intended, with which the two measurement wires were shielded and run as a pair on the bottom of the beam inside the copper casing, had to be changed. It turned out that because of the high temperatures in the hot region of the beam, moisture evidently penetrated into the PVC insulation which caused measurement errors due to bridging between

ORIGINAL PAGE IS OF POOR QUALITY

the conductors. To prevent this, the shielded connections wires were connected separately to the electrode, the protective insulation was countersunk in a hole drilled in the measurement element and the two wires were separated from one another and led out of the cross-section of the beam. Fig. 17 shows one of the ready-to-install elements with protective insulation over the two electrode connections.

Each beam was fitted with a total of 24 moisture measuring elements. These could be connected into the measuring circuits by means of plug contacts. Their placement in the beam is shown in Figs. 5 and 8. Taking into account the influence of temperature, the moisture content is determined from the current intensity measurements made on the beam. For setting up a suitable evaluation nomogram, eight representative elements were selected from the 160 measurement elements available. In this connection, the current intensities, which lay between approximately 20 and 100 nA or 2 and 6 mA, measured on all of the elements after drying at 105°C as well as after saturation with distilled water, were used as the criterion. As described above, the eight measuring elements were provided with connecting wires and, in the water-saturated state, put into rigid steel containers with a vapor-tight screw-on lid and a volume of about 135 cm3. Four containers were provided for the measurements in calcite concrete, and four for these in gravelsand concrete corresponding to the composition of beams 2 and 5 respectively. After the concrete was poured, the closed steel containers were stored for 28 days at 20°C. Then they were kept for 72 hours in a warming cupboard at a temperature of 80°C and afterwards cooled to 20°C in 12°C-increments held in each case for 48 hours. At each temperature stage, several current intensity measurements were made. After the lid was unscrewed, the moisture was removed from the concrete in a vacuum of about 10-1 torr at a temperature of 50°C. This was followed by another temperature cycle like the one described above.

/<u>32</u>

Altogether, six drying stages were necessary to remove the evaporatable water from the doncrete in the steel containers. The last drying process was carried out under atmospheric pressure at a temperature of 105°C;

The data required for the nomograms are shown in Fig. 18, using four measurement elements as an example. The results are shown as a relationship between the lograthmically plotted current intensity and temperature for constant moisture contents (the final two drying stages are not shown on the graphs).

ORIGINAL PAGE IS OF POOR QUALITY

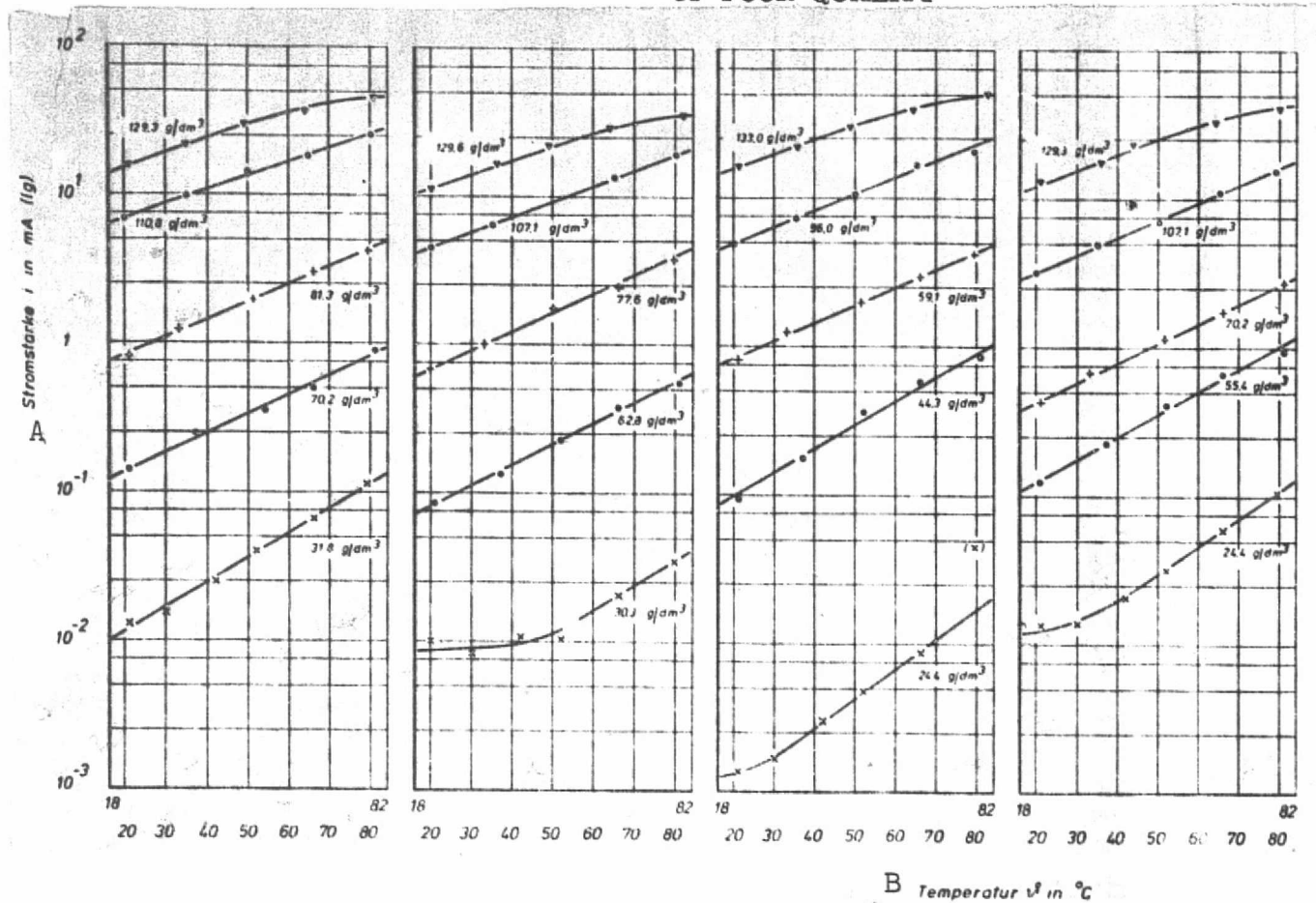


Fig. 18. Relationship between current intensity (i) and temperature (θ) with constant concentrations of evaporatable water for 4 different measurement elements in cylindrical concrete test specimens (conductivity measurement method developed by K. Altmann).

Key: A. Current intensity

B. Temperature

For mean moisture concentrations, all of the measurement elements yielded straight lines which run approximately parallel to one another and differently in absolute values. At high moisture concentrations, in the range of saturation concentrations, a current intensity limit value is to be expected, which is reached all the sooner, the higher the temperature. The curves are similar for low moisture concentrations, however with decreasing temperature they tend towards a limit value.

Fig. 19 shows the evaluation nomogram based on these tests. It is plotted for the temperature parameter and it is valid for the range of about 45-135 g water/dm3 of concrete, and, to be sure, independent of the type of concrete tested.

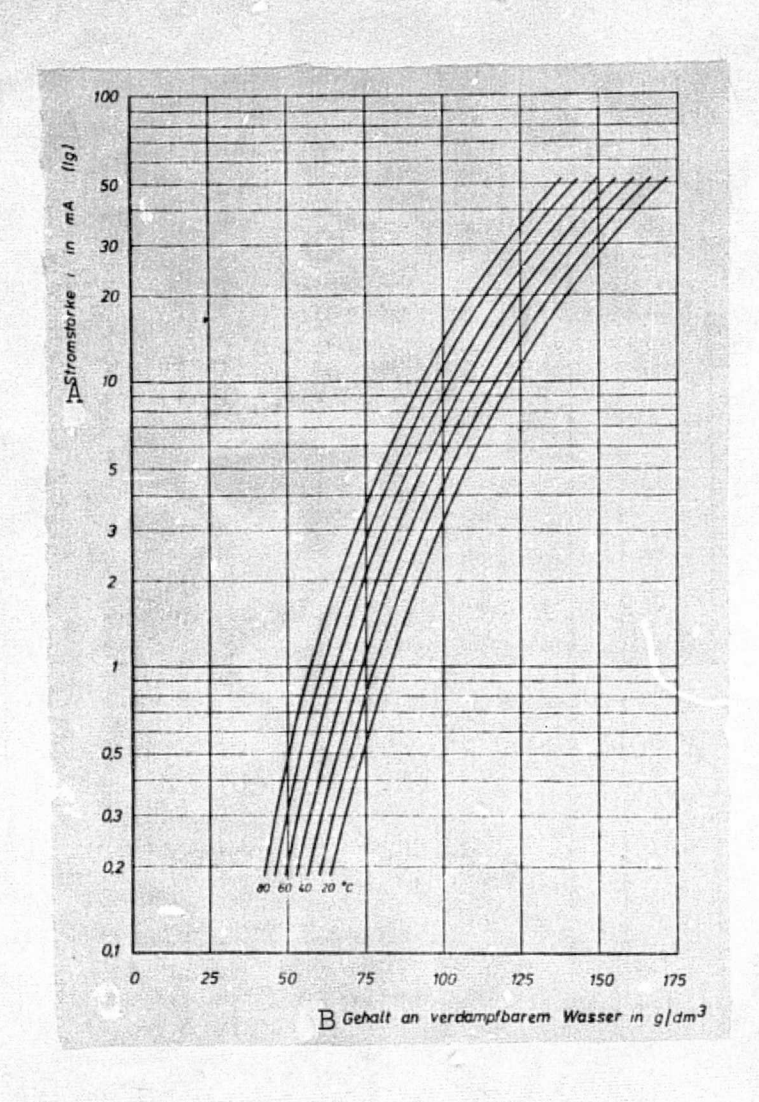


Fig. 19. Relationship between current intensity and the concentration of evaporatable water in concrete at temperatures between 20 and 80°C. Evaluation nomogram for the moisture measuring elements) (conductivity measurement method developed by K. Altmann).

Key: A. Current intensity

B. Concentration of evaporatable water

A comparison with the values given by Altmann [73] does not reveal basic differences if we disregard the greater uniformity of the measurement elements used by him. It may be worthy of note, however, that a higher current intensity or resistance range corresponds to an approximately identical moisture measurement range, which indicates differences in the pore structure of the ceramic material. Finally, it should be pointed out that in the measurements on the beams, as a rule decreasing moisture concentrations and only slight increases in the moisture concentrations, e.g. in the middle of the beam, are to be expected, so that hysteresis effects of the measurement elements—if they exist at all—are insignificant.

2.2.3.2.2. Measurement Results

In Fig. 20 the originally measured current intensities are plotted as a function of the age of the concrete for several elements in characteristic measurement planes of beam 4, for the sake of clarity, the measurement points themselves are not indicated. The information on the right of the graph gives the distances of the planes from the hot end of the beam as well as the ranges of the measurement plane temperatures after the end of the end of the heating phase. Up to the start of heating on the 28th day, all of the measurement elements show a similar behavior. The drop in current intensity up to the 28th day is caused mainly by the cooling of the concrete (compare with this the graph of temperatures after the concrete was poured, Fig. 9), but to a smaller extent it is also caused by the removal of evaporatable water as a result of hydration.

Although all of the measurement elements on the 28th day had to show approxiamtely the same moisture concentrations on the order of 100 g/dm³ (beam 4), current intensities differing from one another between five and 15 mA were measured. In the subsequent heating phase, the measurements show the expected influence of temperature, depending on the position of the element in the beam. In the case of the element in measurement plane A, the temperature effect is evidently superimposed by the already advanced drying effect, which cannot be the case for planes C, D, R, F and H within about 30 days after the start of heating. Rather in these planes, the moisture on the hot side "pushed" by the heating must be taken up or transported. Similar considerations, however taking into consideration the smaller jump in temperature in comparison with the start of heating, also apply for levels N, O, and Q.

48

ORIGINAL PAGE IS OF POOR QUALITY <u>/33</u>

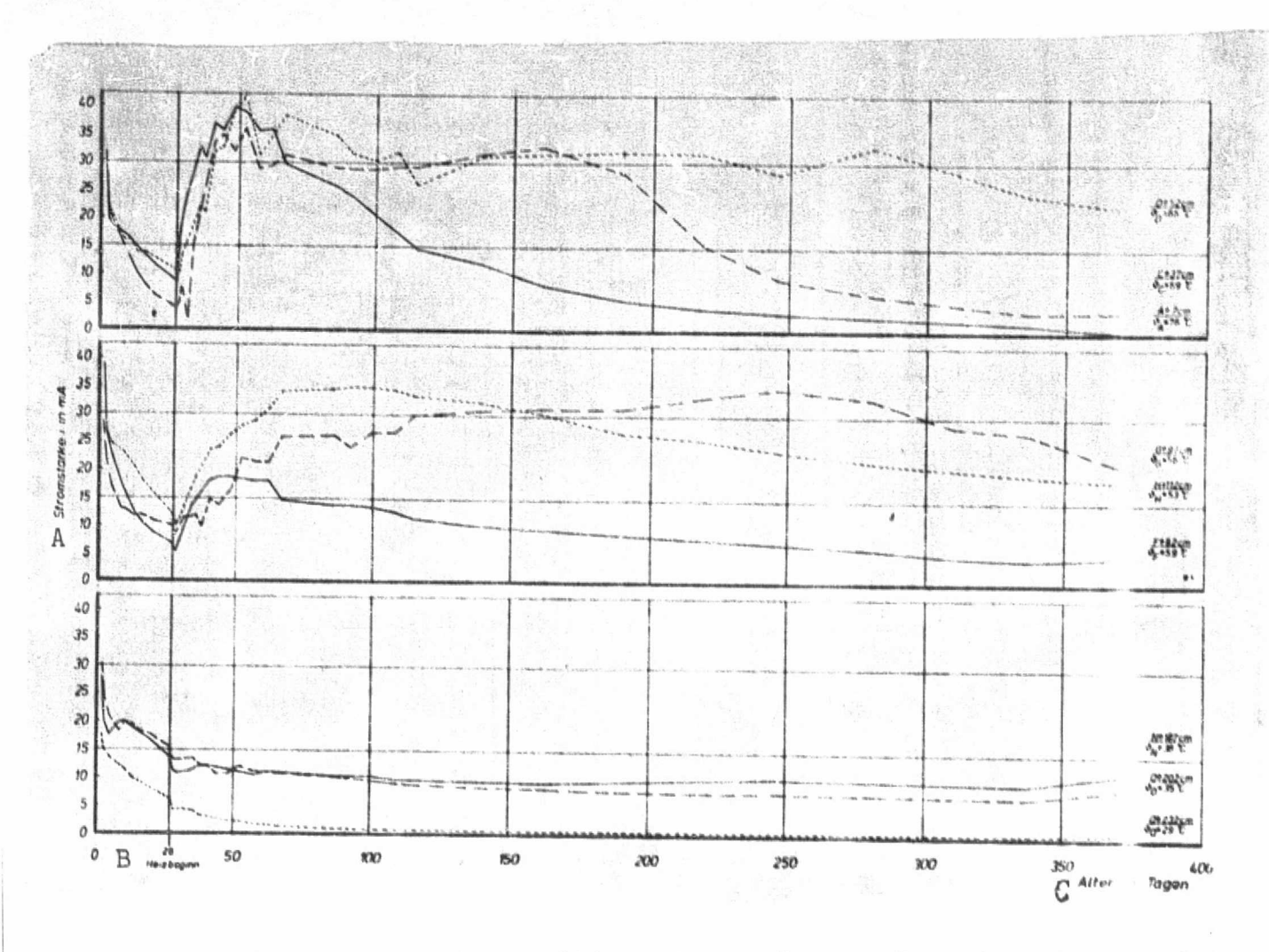


Fig. 20. Current intensities measured as a function of age with the moisture measuring elements in planes D,C, A, G, H, F, N, O and Q.

Key: A. Current intensity

B. Start of heating

C. Age in days

On the whole, it was possibel to infer from the current intensity changes as a function, as shown in Fig. 20 for beam 4, that the elements inserted in the beam also persumably have small differences in the pore structure of the ceramic body, which leads to deviations in the absolute values, but does not have any practical effect on the measurement characteristics.

Thus for the evaluation based on the nomogram shown in Fig. 19, after smoothing the curves, only the relative changes of the current intensities measurements were used, related to the respective mean concentration of evaporatable water at antage of 28 days.

Only a few elements failed. Their unstable behaviors could be easily recognized by means of jump-like changes in the measured values. As already mentioned, however, most of the elements used in the higher temperature ranges of beams 1-3 could no longer be used for evaluation purposes due to the moisture which had penetrated into the connecting lines.

The dotted-line curves in Figs. Al through 12 in the appendix show the changes in the concentration of evaporatable water (moisture content in % by volume) as a function of age for the most important measurement planes of beams 1-6. The measurement planes are identified on the right of the graph with parentheses and the letter for the plane, and also indicated here is the distance from the heated face of the beam.

2.2.3.3 Neutron Probel

/<u>34</u>

2.2.3.3.1. Measurement Method, Arrangement and Procedure

This measurement method is based on the breaking effect for fast neutrons (E>1 MeV) by hydrogen nuclei. If a fast neutron produced by a nuclear reaction ((α , n) - reaction) of a radioactive neutron source (antimony-beryllium, 1245b-Be; amoricium-beryllium, 244 Am-Be etc.) on its way through the concrete strikes hydrogen nuclei, then it loses energy during these impacts until it possesses only thermal energy (α 0,025 eV). With a constant neutron flux, the count rate measured by a detector which records only thermal neutrons is proportional to the hydrogen concentration in the concrete and thus a measure of the water content. The principles of the method, based on nuclear physics, are explained in detail in the literature [74, 75], so that here we need only discuss the important details of the method used.

To be sure, because of their mass which is about equivalent to that of a neutron, hydrogen nuclei primarily take part in the conversion of energy through elastic impacts, since heavy nuclei backscatter almost without loss [76]. On the other hand, however, the influence of heavy nuclei can also be detected in neutron braking [77]. In this connection,

besides the influence of density, particularization must also be paid to the fact that the scattering of hydrogen nuclei occurs in the forward direction, while heavy nuclei are uniformly scattered in all directions, which leads to the dispersion of the neutrons, To this extent, the measured effect is also a function of the chemical composition as well as the density of the material in question.

A cloud of neutrons is formed around the emitter. This cloud decreases in density as the distance from the source increases. If there is a high concentration of hydrogen atoms, then the thermal neutrons are concentrated close to the source and the region measured is small. With a small hydrogen concentration, the sphere of influence is larger [78].

Other factors are the geometrical conditions, i.e. the size and shape of the material in question, as well as effects of adjacent mediums and also the special characteristics of the measurement apparatus with regard to which a distinction must be made between transmission beam methods and backscattering methods. In the first case, the material to be measured is placed between the emitter and detector, and in the second case the emitter and detector are arranged in one unit, e.g. in the form of a so-called immersion probe ("neutron probe"). In this connection, it is also worth mentioning that the braking effect is hardly affected by temperature which, to be sure, may not automatically be assumed for the electrical measuring portions of a neutron probe directly exposed to the influence of temperature.

Neutron probes have been used successfully for some time now, e.g. for moisture and density measurements in soils [75]. For the task at hand, a transmission beam method seemed unsuitable, because the vapor seal, thermal insulation and outer casing would have impaired lateral access to the concrete object. Since the concrete was only accessible from the exposed face, the opportunity offered itself for using a neutron probe for the measurements which could be moved back and forth in a glass tube arranged the long axis of the beam and sealed on the heated end (Figs. 3, 8 and 15).

So as to have as little effect as possible on the measurements, the tube was made of glass which, for example, in comparison with steel has a smaller braking effect with respect to penetrating neutrons [75]. The arrangement has the advantage that the geometrical conditions in a beam from one measurement /35

to the next are identical and that the chemical composition and structure of the concrete measured are always the same with respect to the line of measurement (long axis of the beam) if we disregard the changes caused by advancing maturity.

Based on preliminary measurements on containers with quartz sand of different moisture content and concrete speciments (40 cm x 40 cm x 70 cm) the conditions for the probe to be used on the test beams were determined with a probe constructed in the Federal Institute (1 Ci Am-Be neutron source with a borontrifluoride countertube):

- a) The radiation source should have as homogeneous as possible neutron energy distribution;
- b) Since the emitter and detector are theoretically supposed to be arranged at one point, only a small scintillation counter could be considered for the detector which, in addition, has considerable advantages over a BF3 countertube with respect to the counting accuracy.
- c) The incidence of neutrons in the detector was restricted by Cd apertures in order to obtain the greatest possible resolution.
- d) The diameter of the rod-shaped probe should be as small as possible.

The probe ordered to be constructed to meet the requirements has the following specifications:

Radiation source: 241Am-B

Activity 1 Ci

Neutron yield 5.105 n/s

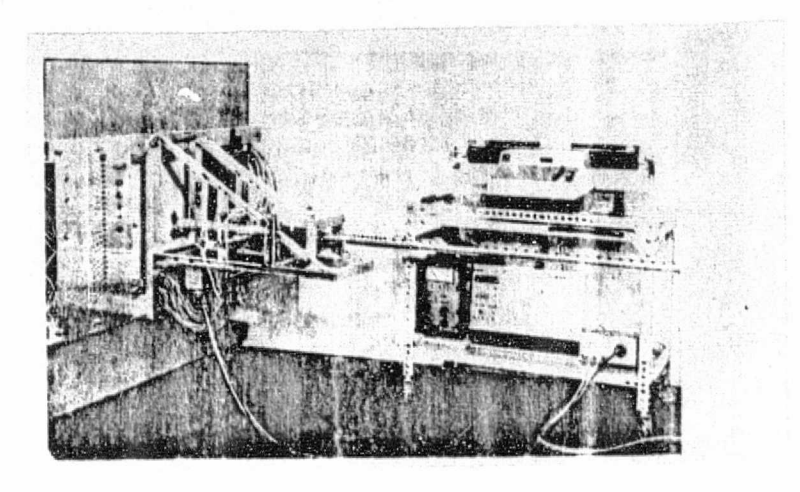
Half-life 458 years

Scintillation counter: Li-glass.

The 36 mm diameter of the probe was determined by the dimensions of the preamplifier.

Fig. 21 shows the complete test set-up developed for automatic operation, The probe, which is carried on a cam rod (in front of the exposed face of the beam) is moved from measurement point to measurement point through the glass tube in the beam by an advancing device controlled by means of light barriers. The measured values are given out by a printer in the form of counting rates (pulses per minute). In each case,

they are correlated with a specified measuring point in the beam by means of the arrangement of the cam on the guide rod. The smallesttprogrammable distance between measurement points or cam settings is 15 mm.



ORIGINAL PAGE IS

Fig. 21. A neutron probe carried on a cam rod with measurement, recording, control and advancing equipment for automatically recording total water content concentration profiles along the long axis of the beam.

In the experiment for setting up the calibration curve, /36 it was assumed that for normal concretes a linear relationship could be expected over a broad range of moisture concentration [74, 75, 79]. In the region of lower water concentrations, where the density distribution of the thermal neutron in the vicinity of the radiation source is decreased and the sphere of influence increased a deviation from the straight line would indeed be conceivable, but with complete drying of the concretes a concentration of non-evaporatable water of at least 4-6% by volume is still to be expected as a minimum value, whereby the sphere of influence still lies approximately within the cross-section of the beam.

It was revealed already in preliminary experiments, and also later, that calibration curves which were determined for sands containing varying amounts of water are unsuitable as a reference for measurements on concrete because of the density difference. Therefore, the counting rates measured up to the 28th day over the length of the beam were averaged and correlated with the water concentrations of the fresh concretes compressed in the experimental set-ups. For beams 4, 5 and 6 we obtained the

curve labelled II in Fig. 22, which runs parallel to curve III for beams 2 and 3. To be sure, the value for beam I lay in the immediate vicinity, but not on any of the curves shown, which is evidently due to the lack of compaction for beam 1.

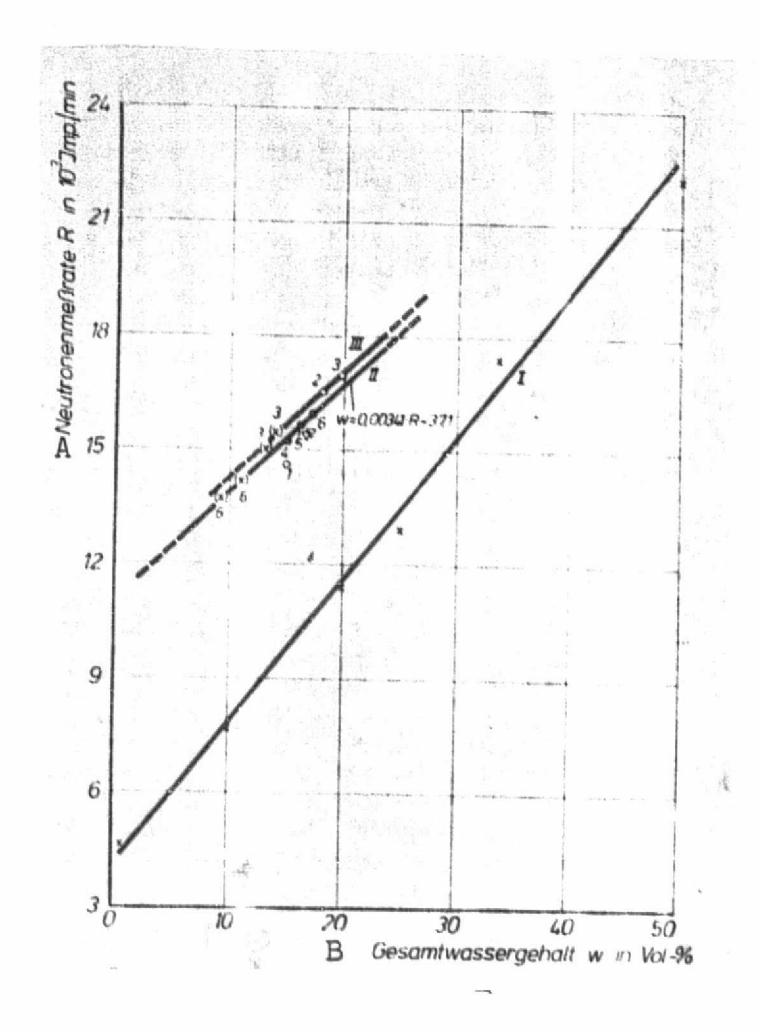


Fig. 22. Relationship between the neutron measurement rate (R) and the total water content (w) for (I) a mixture of quartz sand and ammonium alum; (II) concrete with the gravel-sand aggregate of beams 4, 5 and 6 (with w=0.00341, R=37.1) and (III) concrete with the calcite aggregate of beams 2 and 3.

Key: A. Neutron measurement rate

B. Total water content

- C. Mean values for beams 1-3/4-6 before the start of heating
- D. Individual values for beams 3 and 6 after the beams are split
- E. Individual values of the quarts sand / ammonium alum mixture

At first, no reference values could be determined for the lower portion of the measurement region. This was only possible after beams 3 and 6 were split and the gravimetrically determined water concentrations were available for the edge regions of the beams (cf. section 2.2.5.). These were plotted for control purposes in Fig. 22 with the changes in pulse rates which occurred in comparison with the 28th day measurement (indicated Curve I in Fig. 22 was recorded by the manufacturer of the probe from measurements made on a mixture of quartz sand and ammonium alum NH4A1(SO4).12H2O (bulk density of the mixture about 1.4 kg/dm3). It is shifted with respect to the curves for the concretes and has a somewhat different slope, revealing the influence of density and composition on the position of In plotting the measurements made on the beams, in order to exclude from the outset differences in density and composition of the concrete, the plotting relationship for curve II (w=0.00341.R - 37.1) was used primarily only to determine the relative changes in the total water concentration.

Moreover, it was necessary to determine the geometric reference point of the probe (point of incidence of the thermalized neutrons). This point was outside the center of the detector, offset by a distance of 1.5 mm towards the emitter. Fig. 23 shows the method used to make the correction: two profiles starting from opposite ends were recorded for a concrete beam (40 cm x 40 cm x 70 cm) with a glass tube passing through it along the long axis of the beam. The two profiles are displaced from the center of the detector and relatively to each other by the twofold correction quantity (A).

Even if temperature differences do not significantly influence the backscattering effect, nevertheless an adverse effect on the measurements had to be taken into account due to the heating of the scintillator and the photomultiplier. Aging effects of the electronic components also had to be taken into account. In order to avoid such effects, the main amplifier was equipped with a so-called drift stabilization During measurements in a water bath within the temperature range in question, changes in the pulse rate could not be detected. Likewise, after the measurements, which caused the probe to heat up, the measurement apparatus did not reveal any deviations in the pulse rates measured in a paraffin container before or after the heating. Fig. 24 plots the counting rates regularly recorded before and after each measurement procedure in the container over a period of 300 days. rates do not reveal any significant differences. However, the "container counting rate" has become smaller, which is due to aging effects of the measurement apparatus and must be taken into account in the interpretation of the results.

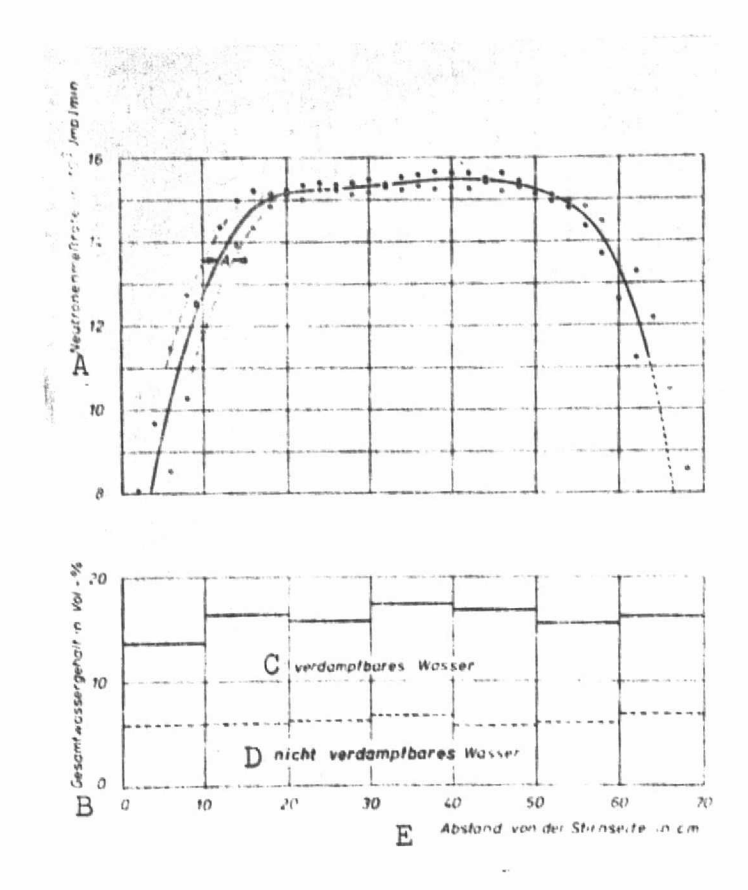


Fig. 23. Neutron measurement rates (10^3 pulses per minute) with the probe advanced counter to the flow and gravimetrically determined water concentrations (% by volume) for a beam (dimensions 40 cm x 40 cm x 70 cm) about 1.5 years old made of gravel-sand concrete, plotted over the long axis of the beam (preliminary experiment on a beam covered on all sides with a vapor seal and one exposed face: heating time, 30 days).

Key: A. Neutron measurement rate

B. Total water content

C. Evaporatable water

D. Non-evaporatable water

E. Distance from the face

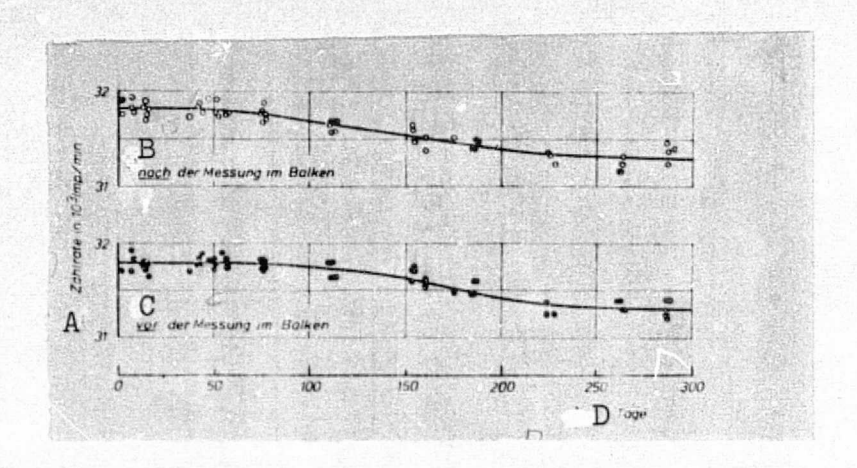


Fig. 24. Counting rates measured with a neutron probe before and after each measurement in a paraffin container (diameter and length: 42 cm), plotted over a period of 300 days.

Key: A. Counting rate

B. Before measurement

in the beam

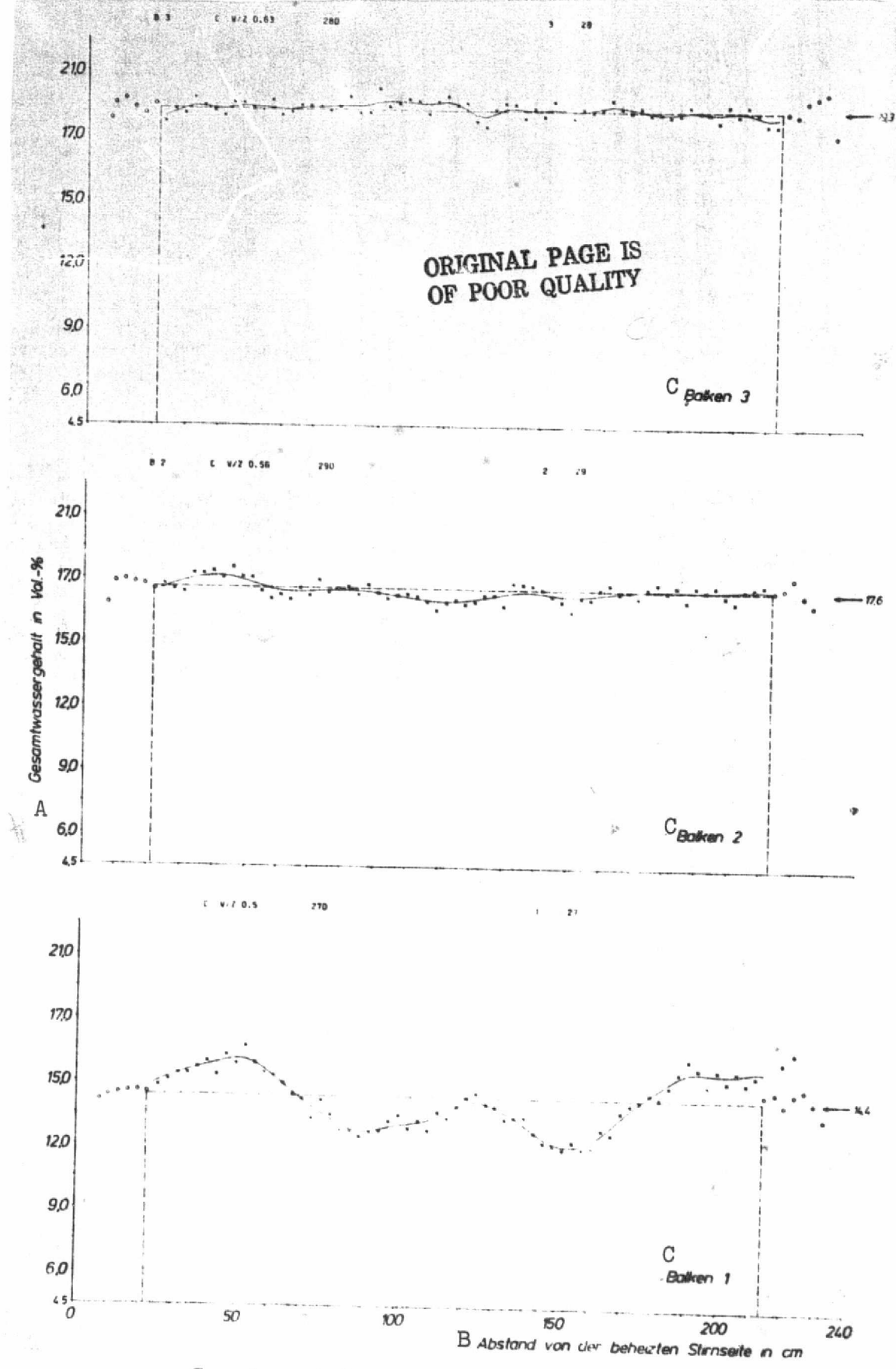
C. After measurement

in the beam

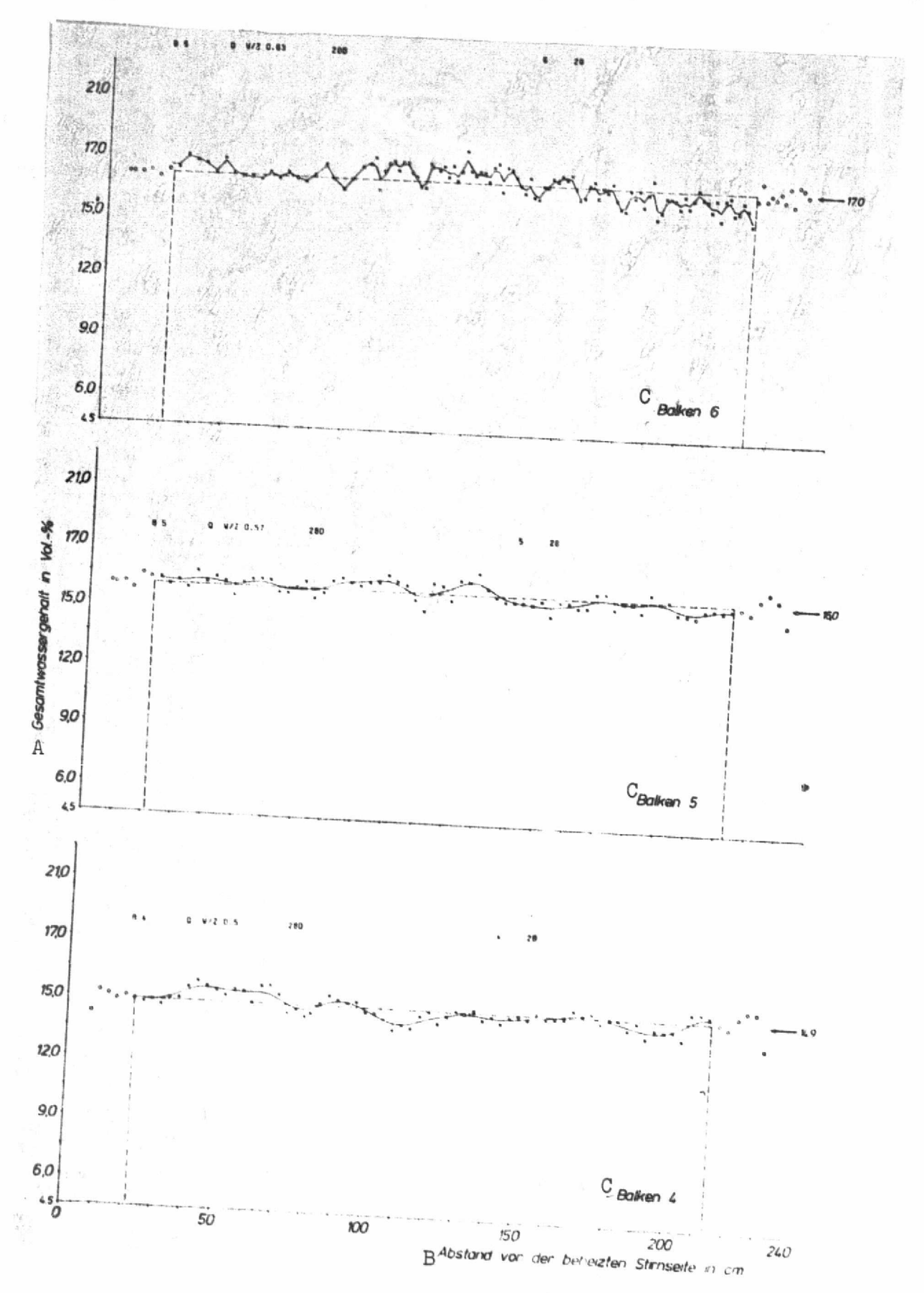
D. Days

2.2.3.3.2. Test Results

Since no moisture could be given off by the beams until the start of heating on the 28th day and since no distinction was made in the neutron measurement between the type of bond for the hydrogen atoms, it was possible to use the measurements made up to that point, without taking into account the age of the concrete, for establishing the plotting relationship (curve II in Fig. 22). In addition, on the 28th day, prior to the start of heating, measurement profiles were recorded for the beams to be used as reference for the experiments after the start of heating. The profiles are shown in Figs. 25 and 26 for beams 1, 2 and 3 and 4, 5, and 6. More details concerning this are given in section 2.5.



See key and caption on page 60.



See key and caption on page 60.

Fig. 25. Total water content distribution profiles recorded by means of a neutron probe for beams 1, 2 and 3, plotted in an automatic plotter after smoothing the measured values using the cubic spline approximation (the distortions in the edge regions were corrected on the basis of the mean values of the total water content).

Key: A. Total water content

B. Distance from the heated face

C. Beam

Fig. 26. Total water content distribution profiles recorded by means of a neutron probe for beams 4, 5 and 6, plotted in an automatic plotter after smoothing the measured values using the cubic spline approximation (the distortions in the edge regions were corrected on the basis of the mean values of the total water content).

For recording the profiles over the long axis of the beams, measurement point sequences were specified by means of the cam rod. At the ends of the beam the distance between the measurement points was cm, and in the interior of the beam they were spaced at a distance of 3 cm. A sequence of measurement points contained a maximum of 84 points, in which the first point was 8.3 cm from the hot face and the last point 230.6 cm from the hot face. In these tests the measurement time was 1 minute per measurement point.

The neutron measurement rates thus recorded in the form of longitudinal profiles at specific age increments of the concrete were first of all converted into total water concentrations using the plotting relationship, and these in turn could be related to the next younger profile and the profile measured on the 28th day following a smoothing calculation.

Fig. 27 shows typical measurement profiles for 4 different age increments. It must be borne in mind that the profiles are not corrected with respect to the geometrical particulars in the marginal regions and that the dotted reference line is only to bring out the changes in the profiles and does not represent a mean value line,

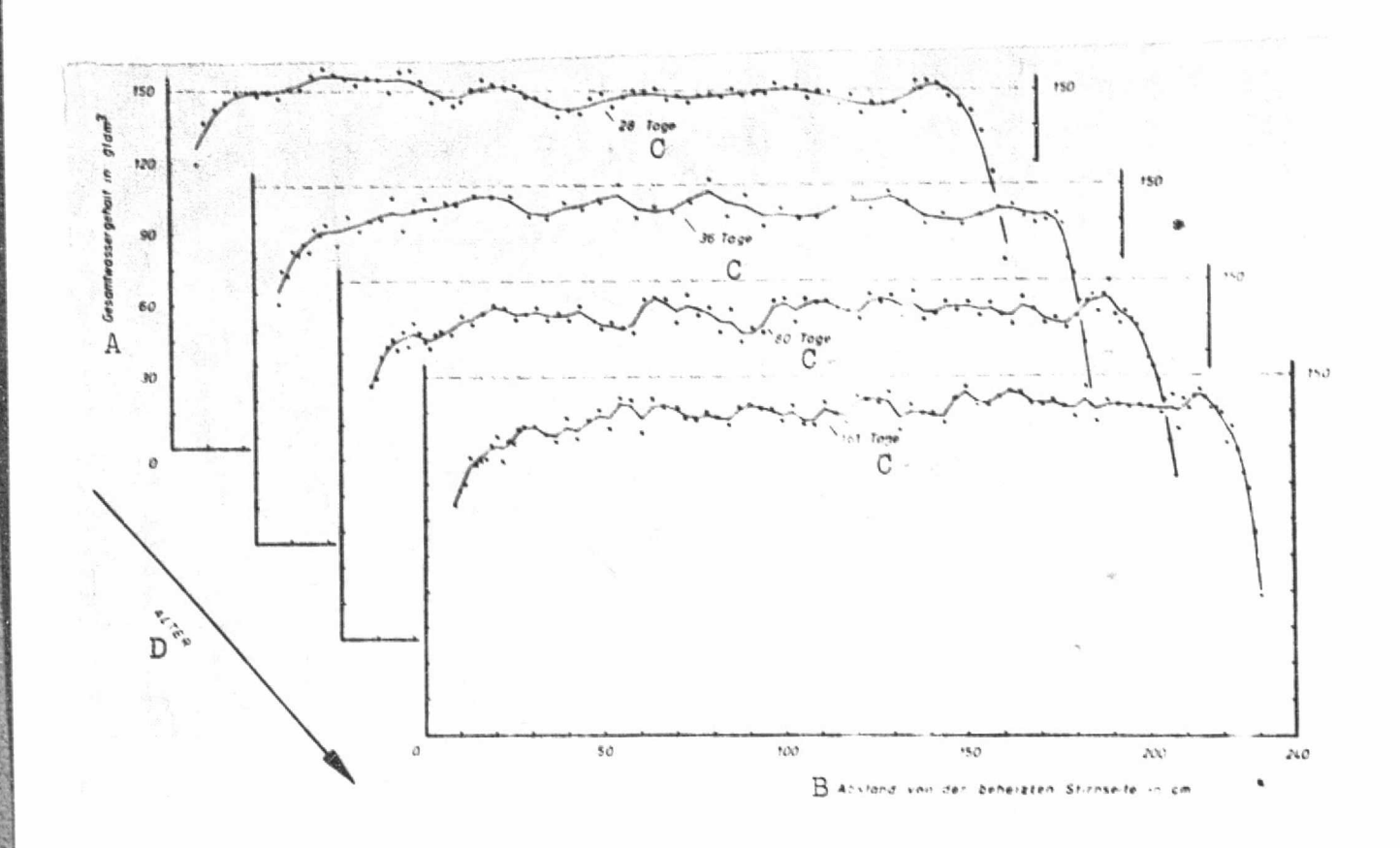


Fig. 27. Total water content measurements smoothed using the cubic spline approximation, plotted over beam length for age increments without taking into account the edge effects (the measurement profiles for the two younger age increments are more severely smoothed in comparison to the two older profiles).

Key: A. Total water content

B. Distance from the heated face

C. Days D. Age

The continuous fitted curve was determined with the "cubic spline approximation" for each measured age increment, a method with which third order polynomials are considered as fitted curves. The fitted profiles were analyzed using a computer

by calculating for 25 selected coordinates the absolute deviation with respect to the next younger profiles as well as the relative change with respect to the profiles for the 28th day and plotting for each coordinate (i.e. the distance from the heated face) over time. As an example, the total water content (% of the value before the start of heating on the 28th day) for every 13 space coordinates is shown as a function of the age of the concrete in Figs. 28 and 29 for beams 2 and 5. The corresponding graphs for the other beams are shown in Figs. A 13-16 in the appendix.

This procedure offers the advantage that necessary corrections can be included without difficulties. Moreover, it is unnecessary to smooth out the distortions of the measurement profiles in the edge regions of the beams caused by the geometry of the test set up. For the graphs in Figs. A 1-12 in the appendix, the percentage proportions were related in each case to the mean value of the measurement made on the 28th day. The continuous curves show the change in total water content as a function of age for the most important space coordinates indicated on the right side of the graphs.

Besides variations in density of the concrete and geometric effects (cf. [80]), systematic errors in the measurement apparatus also particularly affect the accuracy of the results. Fig. 30 shows mean values and confidence ranges for a statistical certainty of 95% which were calculated on the basis of four smoothed measurement profiles recorded in immediate succession for the space coordinates used to plot the graphs [81]. The confidence intervals do not reveal any local variation, so that the deviations of all the single values can be considered jointly. The reliability of the measurements can be evaluated in a first approximation by using the determined standard deviation of s=±0.3% by volume.

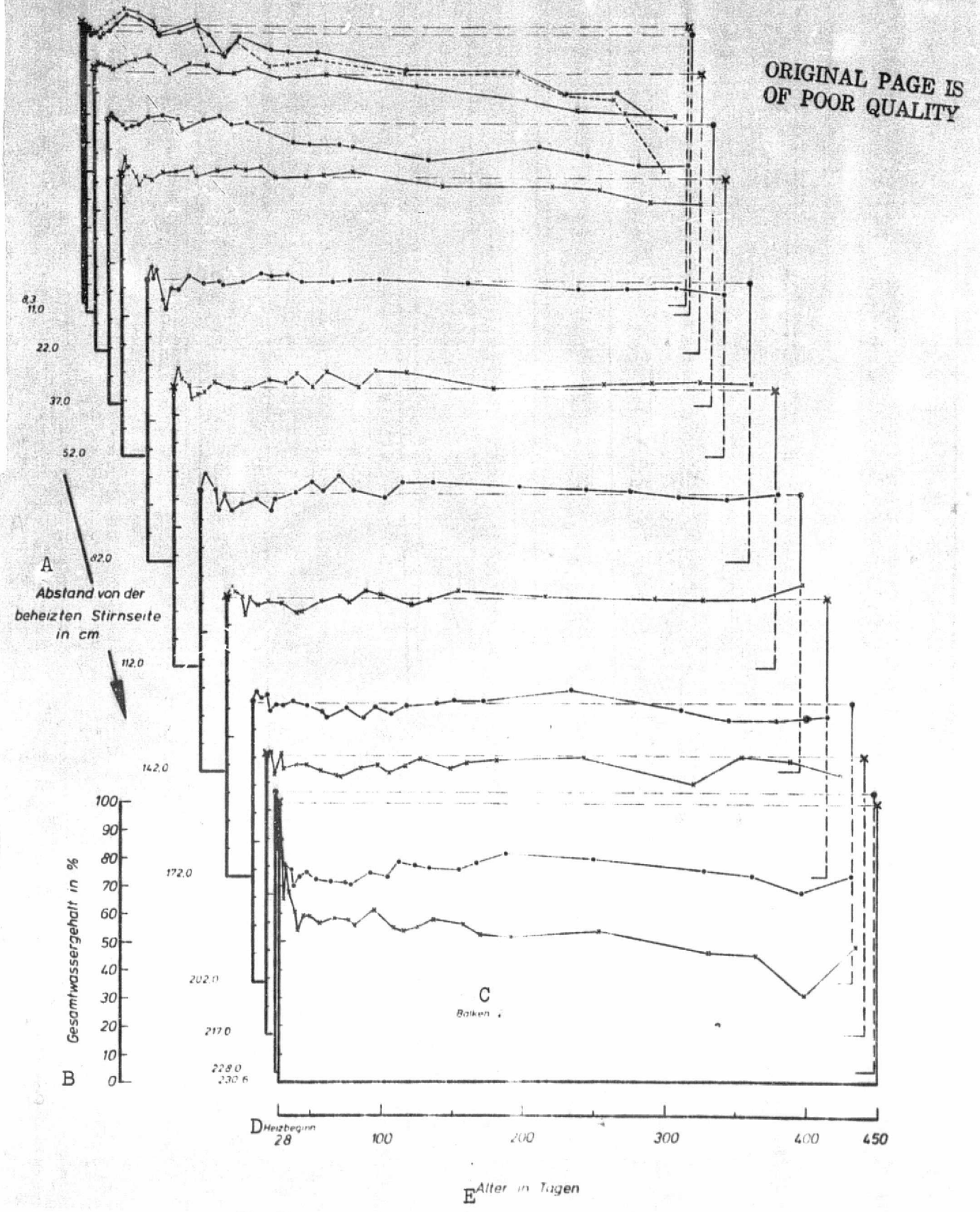
2.2.4. Linear Expansion

/43

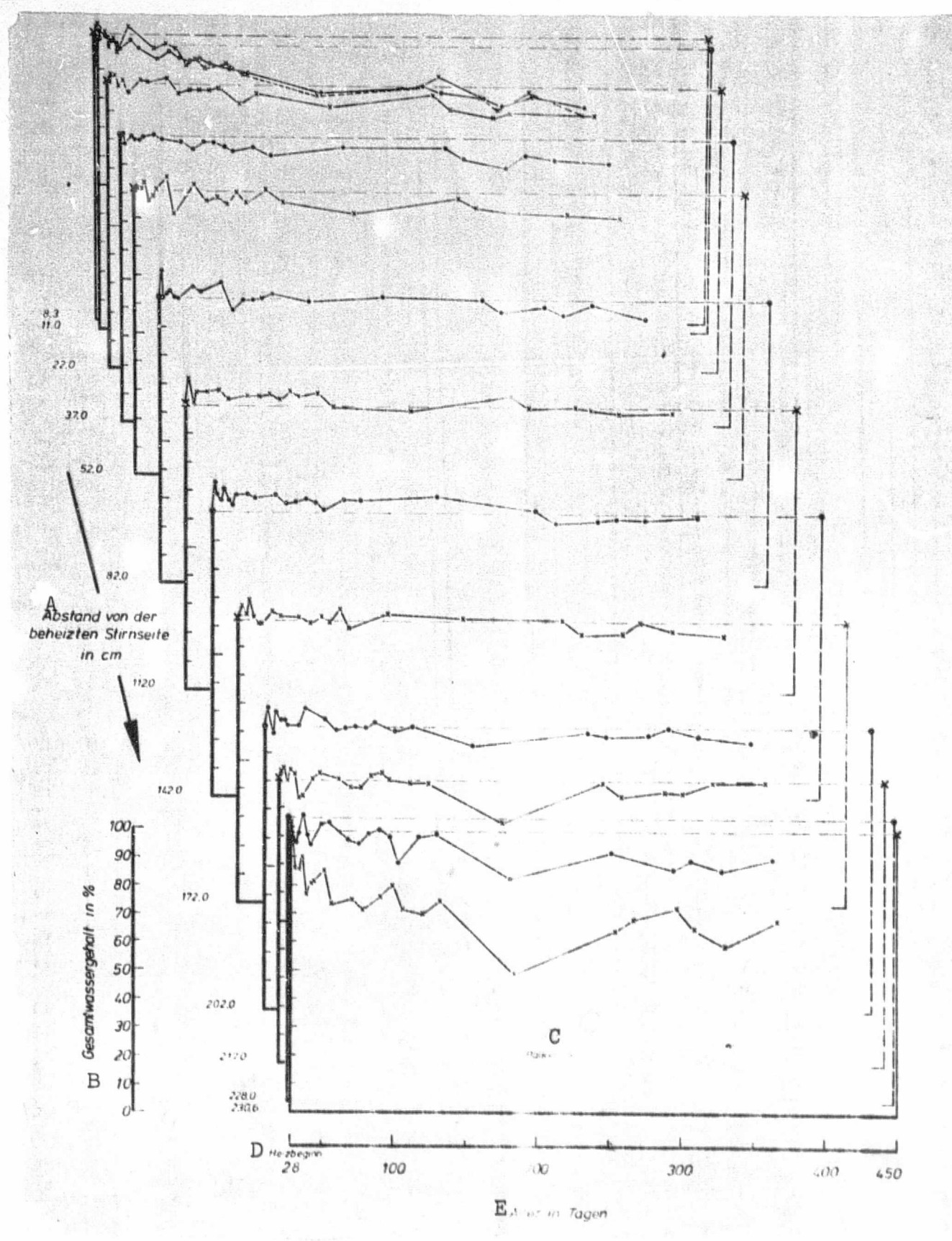
2.2.4.1. Changes in the Overall Length of the Beams

2.2.4.1.1. Measurement Method, Arrangement and Procedure

The beams experience changes in volume, the speed and magnitude of which are a function of the special properties of the cement paste as well as of the aggregates and also of the heat-moisture influences. Altogether, the processes responsible for the changes in volume of the concrete are those termed shrinkage, contraction and swelling as well as thermal expansion (also see section 2.4.1.).



See caption and key on page 65.



See caption and key on page 65.

Fig. 28. Change in total water content (in % of the initial value beofre the start of heating) as a function of the age of the concrete, plotted for 13 space coordinates (distance from the heated face) of beam 2 (also see Figs. A 13 and 14).

Key: A. Distance from the heated face

B. Total water content

C. Beam

D. Start of heating

E. Age in days

Fig. 29. Change in total water content (in % of the initial value before the start of heating) as a function of the age of the concrete, plotted for 13 space coordinates (distance from the heated face) of beam 5 (also see Figs. A 15 and 16).

Key: A. Distance from the heated face

B. Total Water content

C. Beam

D. Start of heating

E. Age in days

The volume changes are measured in terms of linear expansion ($\Delta 1$) or unit expansion (ϵ) in the direction of the long axis of the beam.

The device used to measure the linear expansion of the beams consists of an invar rod with a diameter of 25 mm, onto one end of which is wrapped a steel ball, while on the other end two precision indicators (1 µm per scale division) are attached to a yoke (cf. Fig. 3). The rod carries several PVC rings spaced 30 cm apart over its length. These keep it centered during the measurement process in the glass tube in the center of the beam. In order to keep the uptake of heat from the concrete as small as possible, the beam is wrapped with foam material between the rings. After being inserted into the glass tube, the rod end with the steel ball touches a stop plate arranged perpendicular to the long axis of the beam. This is about 3 cm from the end of the beam and -- for purposes of better fixation in the concrete--it is attached to the stop plate overhanging the outside diameter of the glass tube. The two precision indicators thus press against two of the four nipples arranged cross-wise on the open end of the beam. These nipples also have stop balls and are adjusted by screwing into anchor sockets. The pairwise measurement at two opposite measurement points largely compensates for shifts in the axis of

ORIGINAL PAGE IS OF POOR QUALITY

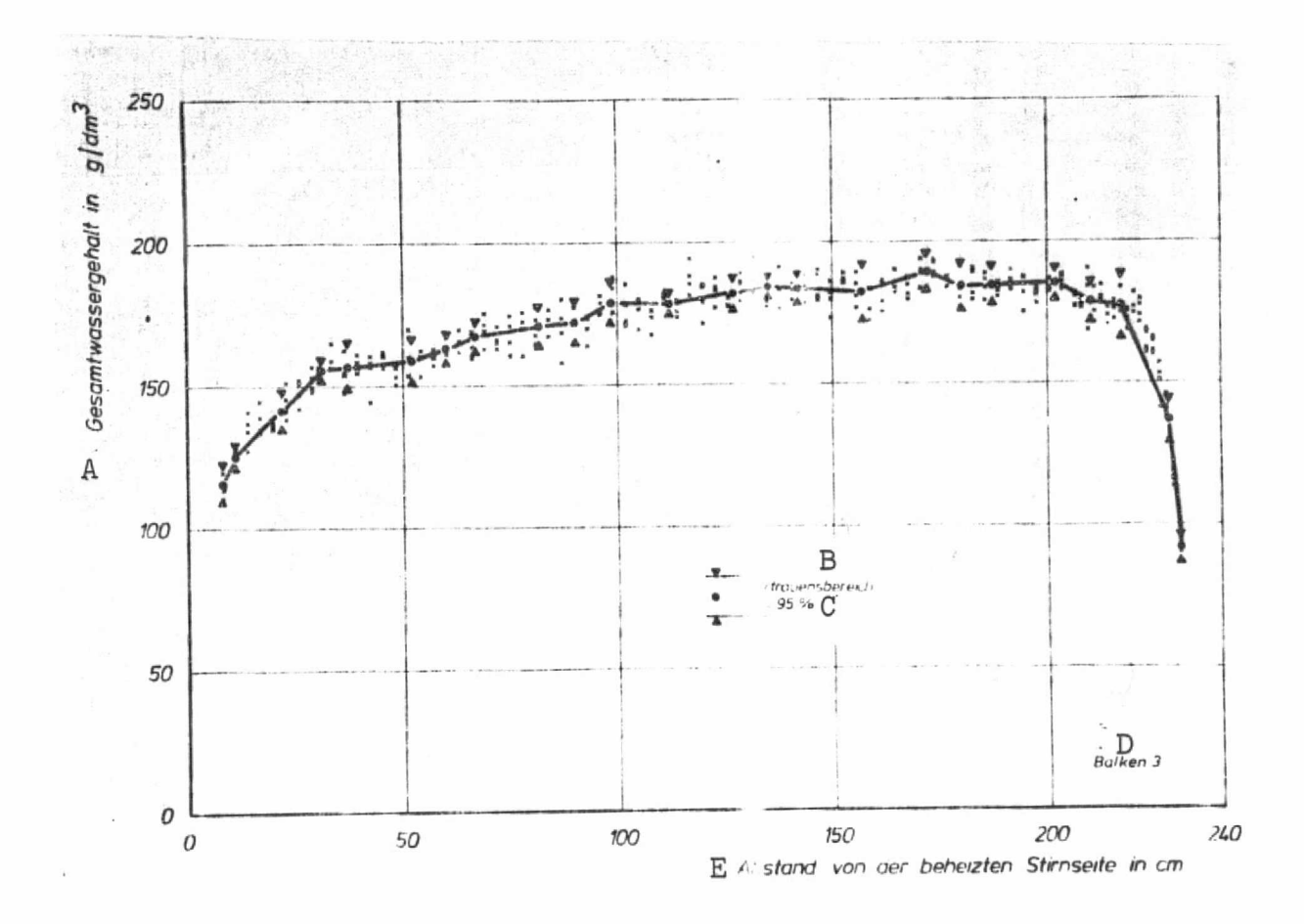


Fig. 30. Confidence intervals ($\pm t \cdot s/\sqrt{N}$) for the total water concentrations in g/dm³ for a statistical certainty of 95% at N=4 measurements (neutron method, beam 3, without taking edge effects into account).

Key: A. Total water content

B. Confidence interval

C. Certainty

D. Beam

E. Distance from the heated face

the rod with respect to the long axis of the tube.

A steel tube, wrapped with polystyrene foam to serve as thermal insulation and a protective jacket, is used to check the rod and for storing it. Like the glass tube, the steel tube also has a stop plate and two nipples attached to a steel plate at the opening of the tube.

Before carrying out the measurements, the measuring rod was first of all checked each time in the steel tube. Then the length of a beam was measured, in the process of which the precision indicators were twice attached to each pair of nipples (a total of 8 individual values for each measurement). For each beam, the first measurement was made between the Ist and 4th day after the concrete was poured. The changes in length were calculatednas differences between two successive measurements.

/44

2.2.4.1.2. Test Results

Figs. 31 and 32 show the results of the measurements using the invar rod on beam 1, 2 and 3 and 4, 5 and 6. They show the total changes in length (Δ 1) of the beams as a function of the age of the concrete, which was related to the value at the start of heating on the 28th day.

Considering the length of the beam, the measuring methods showed relatively high sensitivity. The standard deviation with respect to the individual measured values was s=±6.8 μ m. With a statistical certainty of 95%, the confidence interval [81] for the respective individual values belonging to a mean value was t·s / $N=\pm5.7~\mu$ m.

2.2.4.2. Local Changes in Length in the Concrete

2.2.4.2.1. Measurement Method, Arrangement and Procedure

The total length changes of the beams, measured with the Invar rod, are due to processes which are a function of the temperature and moisture conditions prevailing in the concrete as well as the age of the concrete. In order also to be able to measure local variations in expansion in a beam, expansion transducers were arranged in 8 measurement planes as shown in Fig. 5. The transducers (Fig. 33), which were developed and made by the Federal Institute as so-called interior transducers for measurements in concrete, consist of a

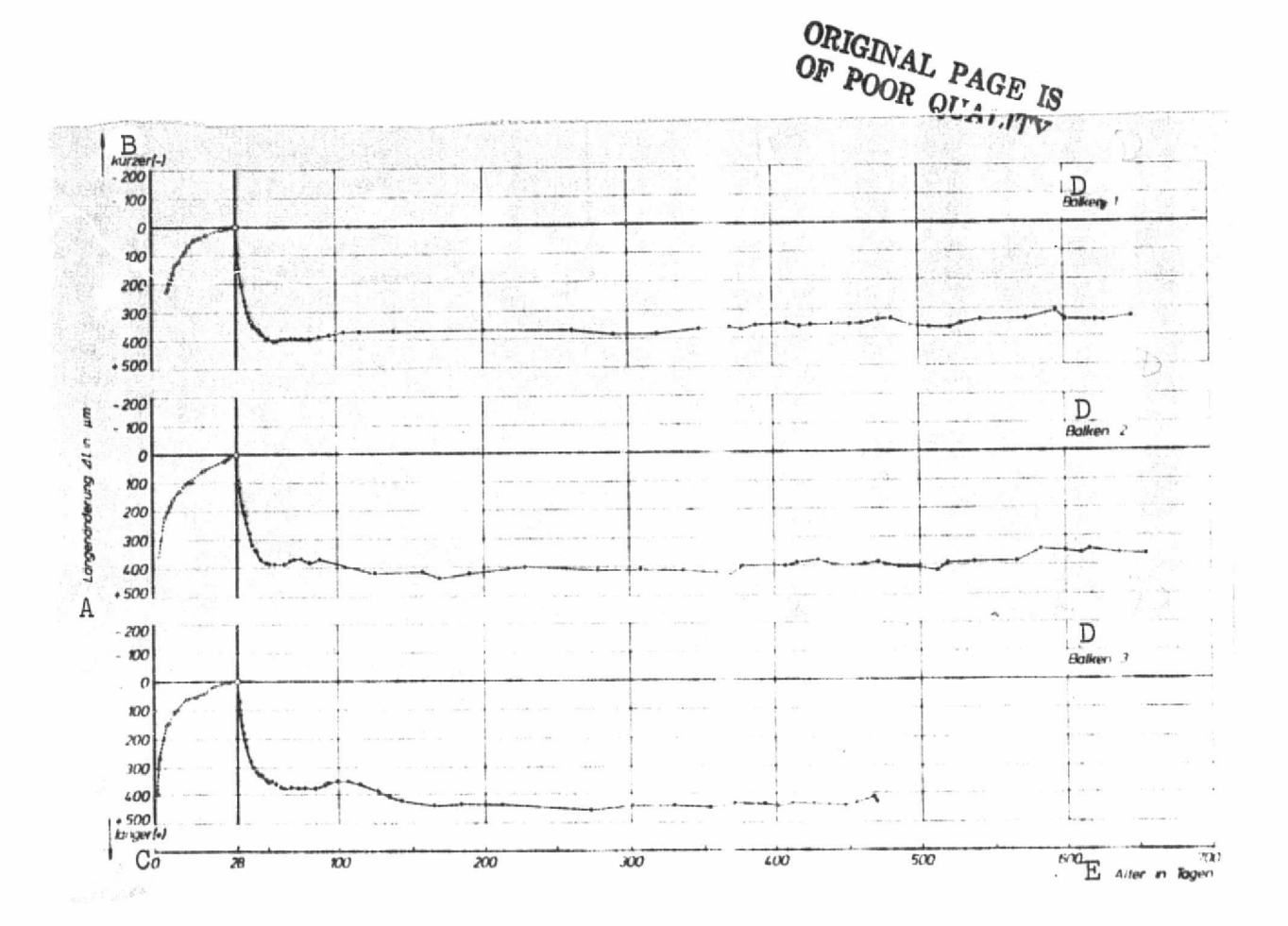


Fig. 31. Changes in total length (Δ 1) for beams 1, 2 and 3 made of calcite concrete as a function of age (reference value: start of heating on the 28th day).

Key: A. Change in length

B. Shorter

C. Longer D. Beam

E. Age in days

commercial strain gauge on a phenolic resin supporting base with a measurement grid length of 60 mm. This was glued under pressure between two 0.1-mm thick spring steel foils and cured at a temperature of 180°C. The strain gauge connection to the measurement wires are located in a copper tube soldered perpendicularly to the strain gauge. This tube is filled with a moisture sealing material and was sealed on the top with a

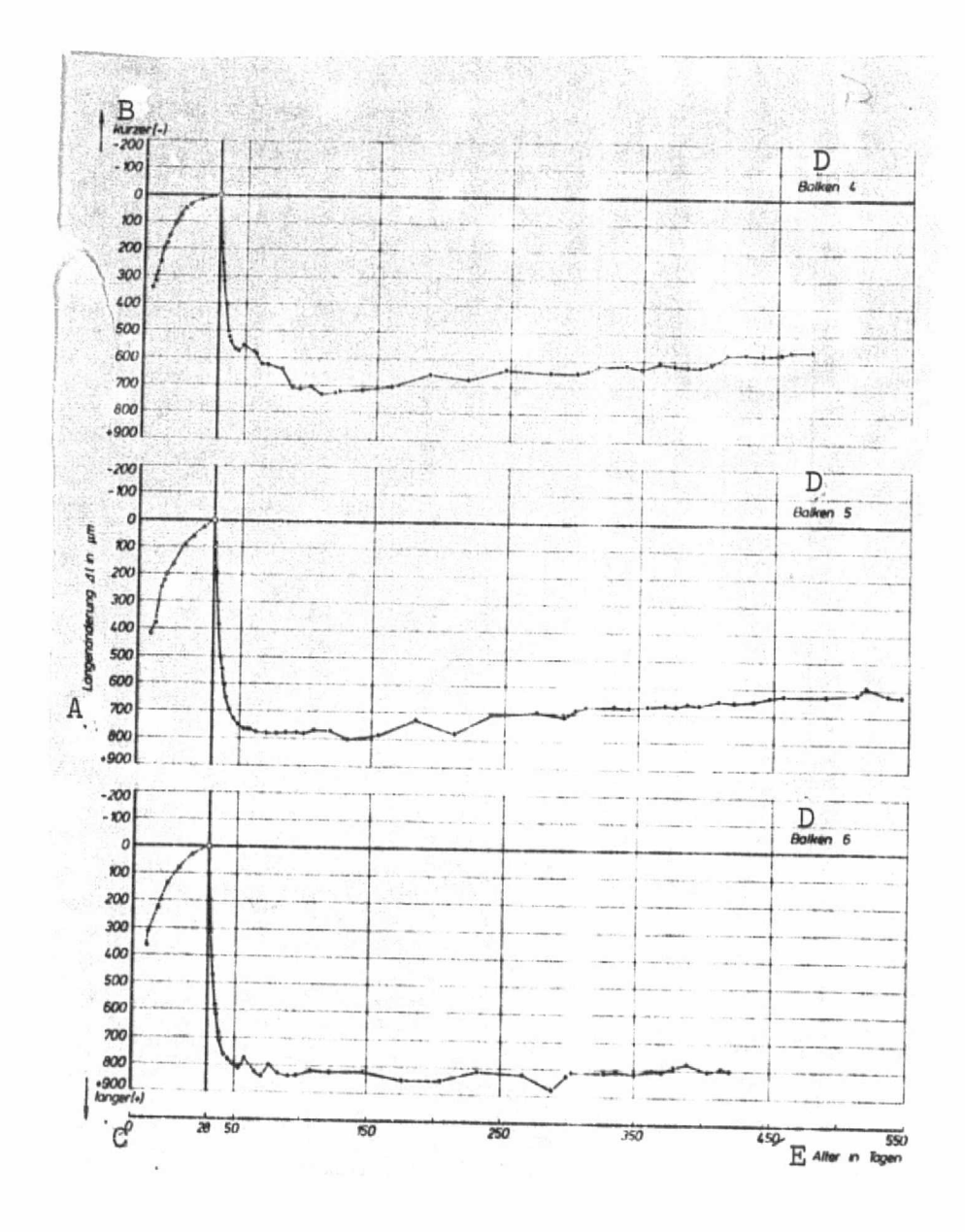


Fig. 32. Changes in total length (Δ 1) for beams 4, 5 and 6 made of gravel-sand concrete as a function of age (reference value: start of heating on the 28th day).

A. Change in length B. Shorter Key:

C. Longer D. Beam

E. Age in days

ORIGINAL PAGE IS OF POOR QUALITY

fast setting cement. All of the transducers were aged for the purpose of stabilizing them by means of several temperature cycles between 20 and 80°C in a warming cupboard.

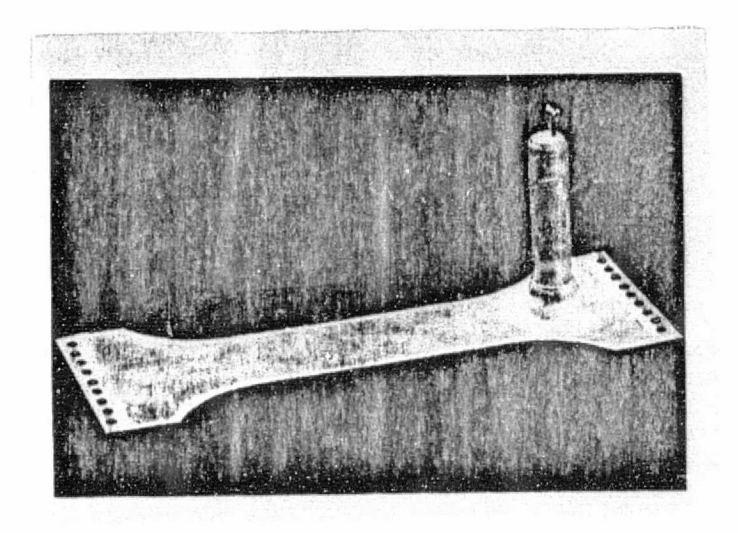


Fig. 33. View of the transducer for measuring local length changes in concrete, consisting of a 60-mm long strain gauge grid between two spring steel foils.

The transducers are placed in the concrete parallel to the long axis of the beam at about the level of the glass tube (Fig. 8). Associated with each active transducer in a semibridge circuit is a passive transducer, which is free to deform on the top side of the beam. By means of this arrangement, in particularly even zero point shifts at the transducers as a result of aging are largely compensated for. The measurement instrument used was a hand-operated potentiometer with 4 measuring points (sensitivity: 1 scale division corresponds to 1 µm/m).

For the measurements of strain discussed below as a result of shrinkage ($\epsilon_{[s*]}$) up to the start of heating on the 28th day, the characteristic curves for the transducers were determined by means of strain measurements under tensile stress. The rigidity values deduced from these measurements were used to make a computer estimation of the temperature changes in

the concrete. Both types of concrete yielded factors (δ_{B2} = /46 6.28 µm/m°C for the calcite concrete and δ_{B5} =1.49 µm/m°C for the gravel-sand concrete) with which, using the temperature changes with respect to the reference value on the 28th day, correction terms could be calculated which accounted for the variable elastic behavior of the strain gauges and the concretes. In checking a pair of gauges, the active gauge of which was located in a test beam, a suitable, linear graph was found in the temperature range between 25 and 75°C after drying the concrete beam.

The strain measurements could be done after putting the thermal insulation and the lid in place. Details of the measurements made after the start of heating, measurements which were expected to reveal, above all, shortening of the concrete due to shrinkage after drying, can only be given after all of the tests have been completed and beams 1 and 2 as well as 4 and 5 have been split.

2.2.4.2.2. Measurement Results

The strains determined as a function of age were summarized both for the calcite and gravel-sand concrete after taking into account the temperature effect. The curves developed from the mean values for the two groups of three beams are plotted on the right hand portion of Fig. 34 (symbols). They connect to the curves for shrinkage or contraction during the first days after the pouring of the concrete. Details on these measurements are given in section 2.4.1.

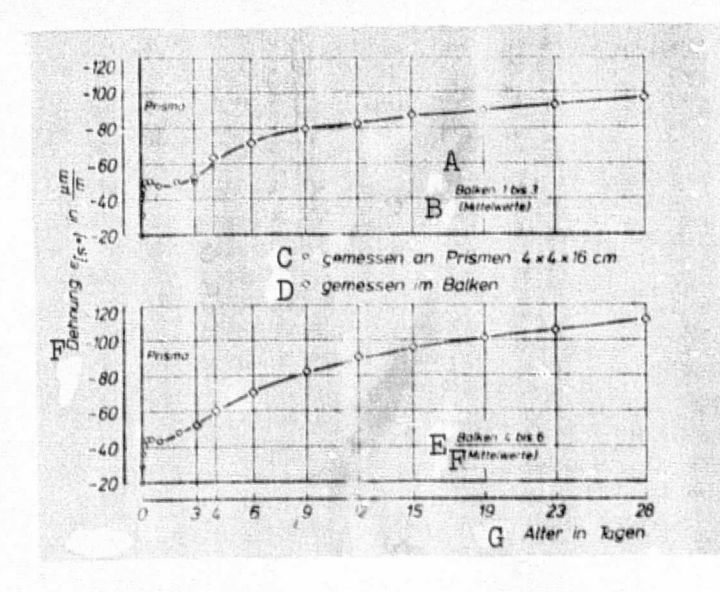


Fig. 34. Strains due to shrinkage and contraction $(\epsilon_{[s*]})$ of the calcite concrete (beams 1-3) and of the gravel-sand concrete (beams 4-6) up to the start of heating on the 28th day.

Key: A. Beams 1-3

B. Mean values

C. Beams 4-6

D. Measured on prisms

E. Measured in the beams

F. Unit strain

G. Age in days

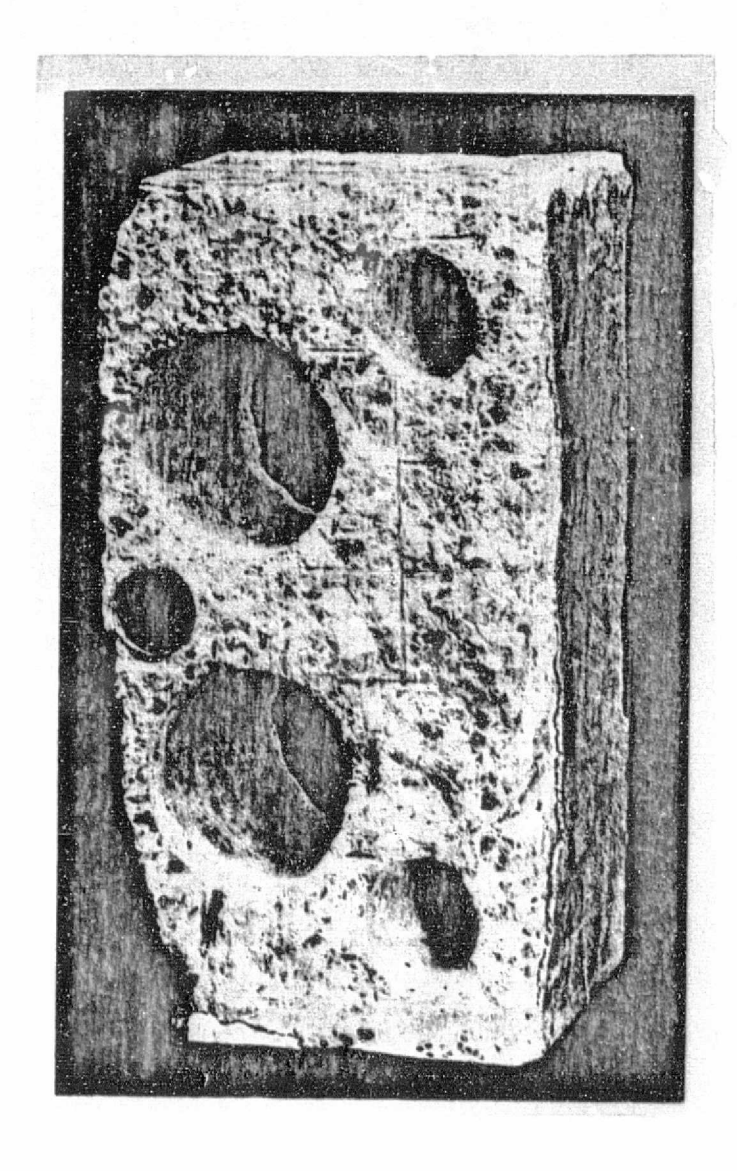


Fig. 35. Partial view of a segment of concrete with cores removed. The segment was obtained by splitting the beam. On the left of the segment, along the horizontal midline, can be seen part of the glass tube running along the long axis of the beam.

2.2.5. Concluding Measurements on Concrete Samples from Beams 3 and 6

2.2.5.1. Test Specimens, Extent of Measurements and Procedure

While beams 1, 2, 4 and 5 are to be heated over a period totaling 3 years, the tests on beams 3 and 6 were stopped when the concrete reached an age of 470 and 421 days respectively to check the reliability of the measurements made with the moisture measuring elements and the neutron probe. This was done by gravimetrically measuring the moisture content of samples of concrete from the beams. In addition, samples were used to study the content of non-evaporatable water as well as the dry bulk density. Moreover, as a supplement to the moisture studies on separately produced cubes (cf. section 2.4.2.), it was necessary to perform compressive strength on cores taken from the beam concrete.

After final measurements on beams 3 and 6, the heating regulator was turned off, the power-supply interrupted and immediately afterwards the case and thermal insulation were removed from the beams so that only the vapor seal was left covering the concrete. When the copper foil was separated from the vapor seal, the layer of epoxy resin remained studk This can clearly be seen on the smooth to the concrete. outer surface of half of a segment of concrete shown in Fig. 35. The segments were obtained by splitting the beams into the planes formed by the measurement grids, using a compression test machine to make the cuts, and then they were immediately cut in half vertically (also see Fig. 4). One half was later used to supply 10-cm diameter core samples, one each from the upper and lower quarter. (The 5-cm cores, the holes of which can also be seen in this photograph, are being used for air permeability tests which are not discussed in this paper.) The other half of the section was used to provide test material for measuring the content of the evaporatable and non-evaporatable water. One sample for each test was taken from the upper and lower quarters of the segment and the test material for determining the dry bulk density was taken from the middle at about the level of the glass These operations were performed rapidly to keep moisture losses as small as possible.

The samples, weighing between 2 and 3 kg, were weighed immediately, crushed, dried at 105°C until the weight became constant and then weighed again. The dry bulk density of the test pieces was determined according to DIN 52 102 [5].

147

The same samples were used for measuring the water uptake under atmospheric pressure as per DIN 52 103 [6]. For purposes of comparison, water uptake under atmospheric pressure and at a pressure of 150 bars was also measured on separately produced samples of calcite and gravel-sand concretes.

The test for the content of non-evaporatable water by means of heat treatment at 550°C of the concrete previously dried at 105°C was done on pairs of samples weighing about 300 grams from beam segments A/B, C/D, F/G, J/K, O/P and P/Q.

The cores used to determined the compressive strength were shortened and the pressure surfaces made plane parallel so that the diameter and thickness were approximately equivalent. Until they reached a constant weight, they were stored at 20°C and 100% relative humidity before they were tested in the surface-dry state.

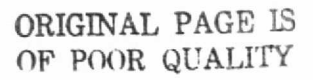
2.2.5.2. Measurement Results

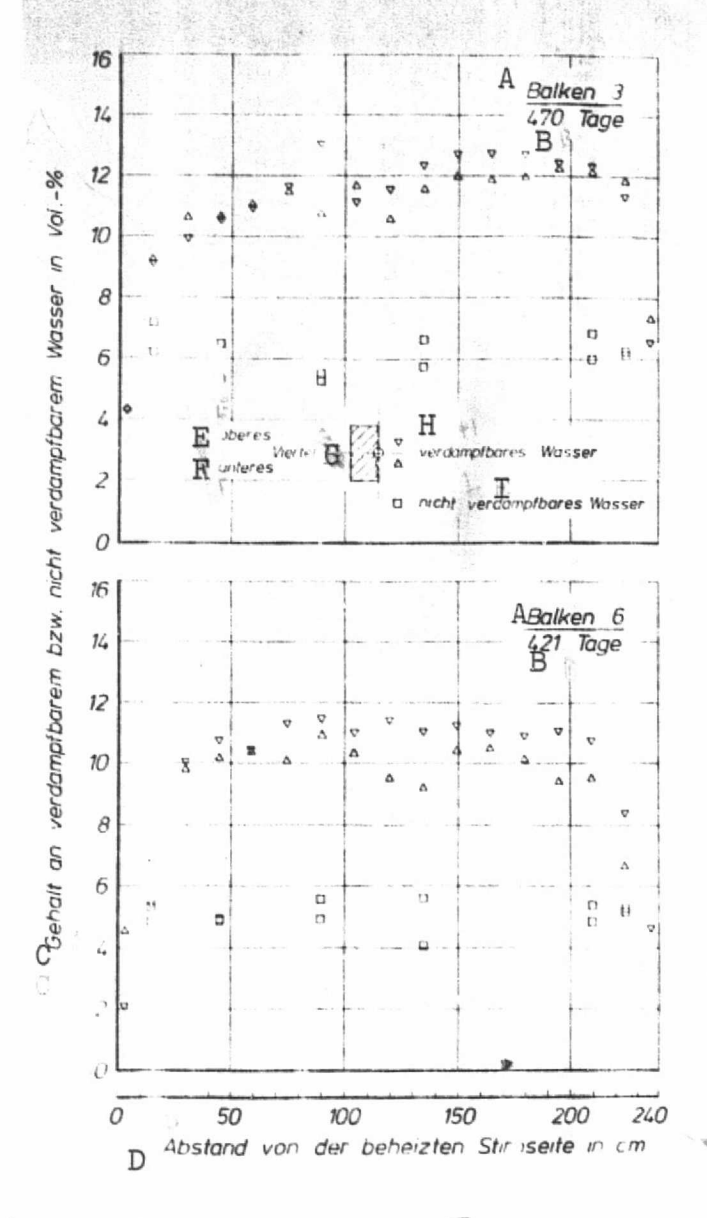
Fig. 36 shows the measured concentrations of evaporatable and non-evaporatable water (converted to percent by volume using dry bulk densities) as a function of the location of the concrete segments in beams 3 and 6. The mean values of two measurements in each case were used to set up the water balances for the two beams in section 2.5.

The dry bulk densities $(\theta_{\rm tr})$ were used in compiling the upper part of Table 4. They do not reveal any local variations. The standard deviation (s) is indicated as a supplement to the mean values.

Fig. 37 (left) shows the water uptake under atmospheric pressure (A) for the specimens from beams 3 and 6 as a function of their position in the beam. Fig. 37 (right) shows the water uptake at atmospheric pressure (A γ) and at a pressure of 150 bars (A $_{dr}$) which was determined on separately produced specimens of all of the concrete.

Fig. 38 shows the compressive strength values (β_D) measured on the cylindrical core samples as a function of their position in the beam. In making these measurements, the influence of the shape and size of the specimens was not taken into account.





Content of evaporatable and non-evaporatalbe water of concrete samples from segments of beams 3 (calcite concrete) and 6 (gravel-sand concrete).

Key: A. Beam

- B. Days
- C. Content of evaporatable and non-evaporatable and non-evaporatable water in % by volume
- D. Distance from the heated face in cm
- E. Upper
- F. Lower
- G. Quarter
- H. Evaporatable water
- I. Non-evaporatable water

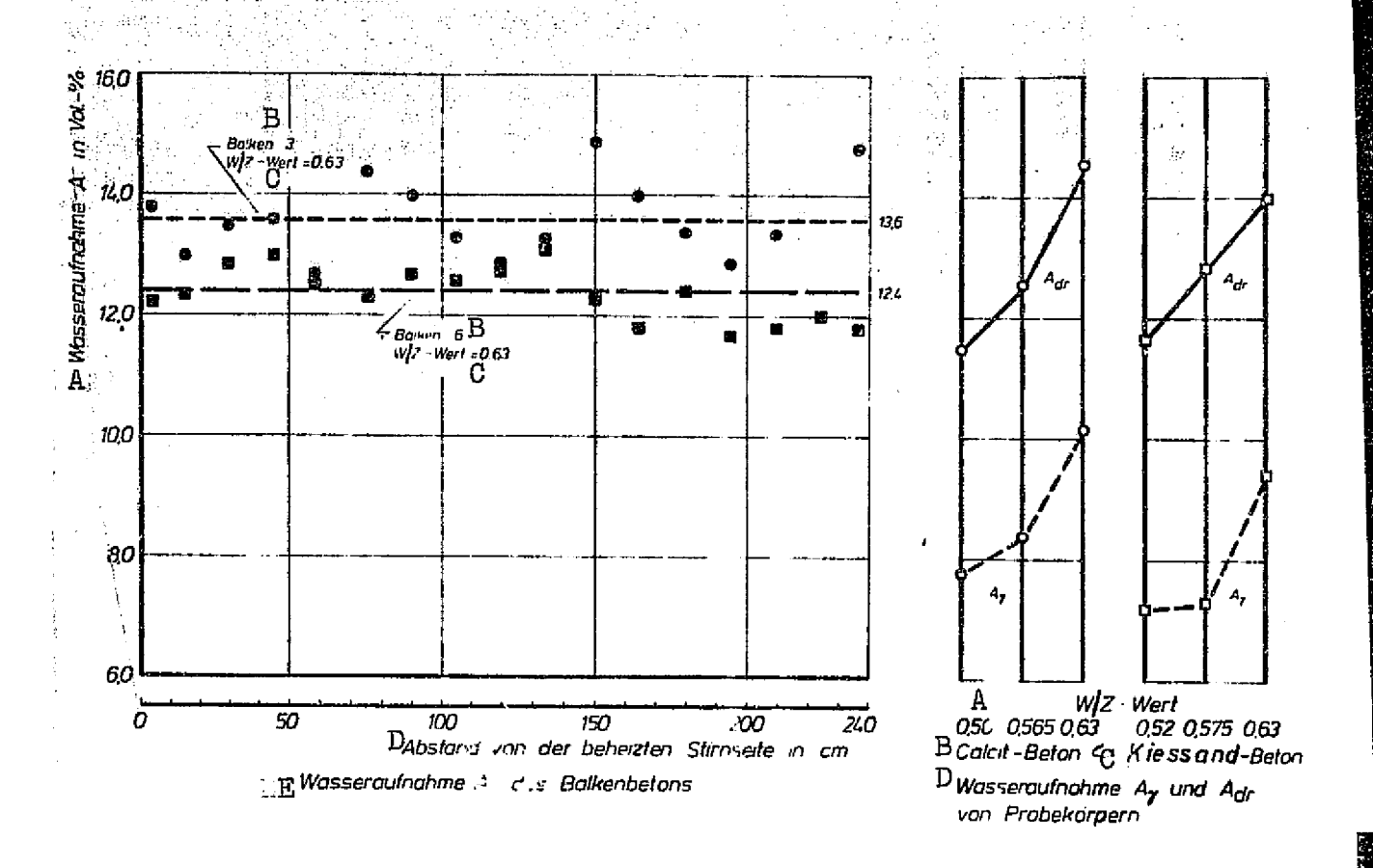


Fig. 37. Left--water absorption (A) of concrete samples from segments of beams 3 and 6, plotted over beam lengths.

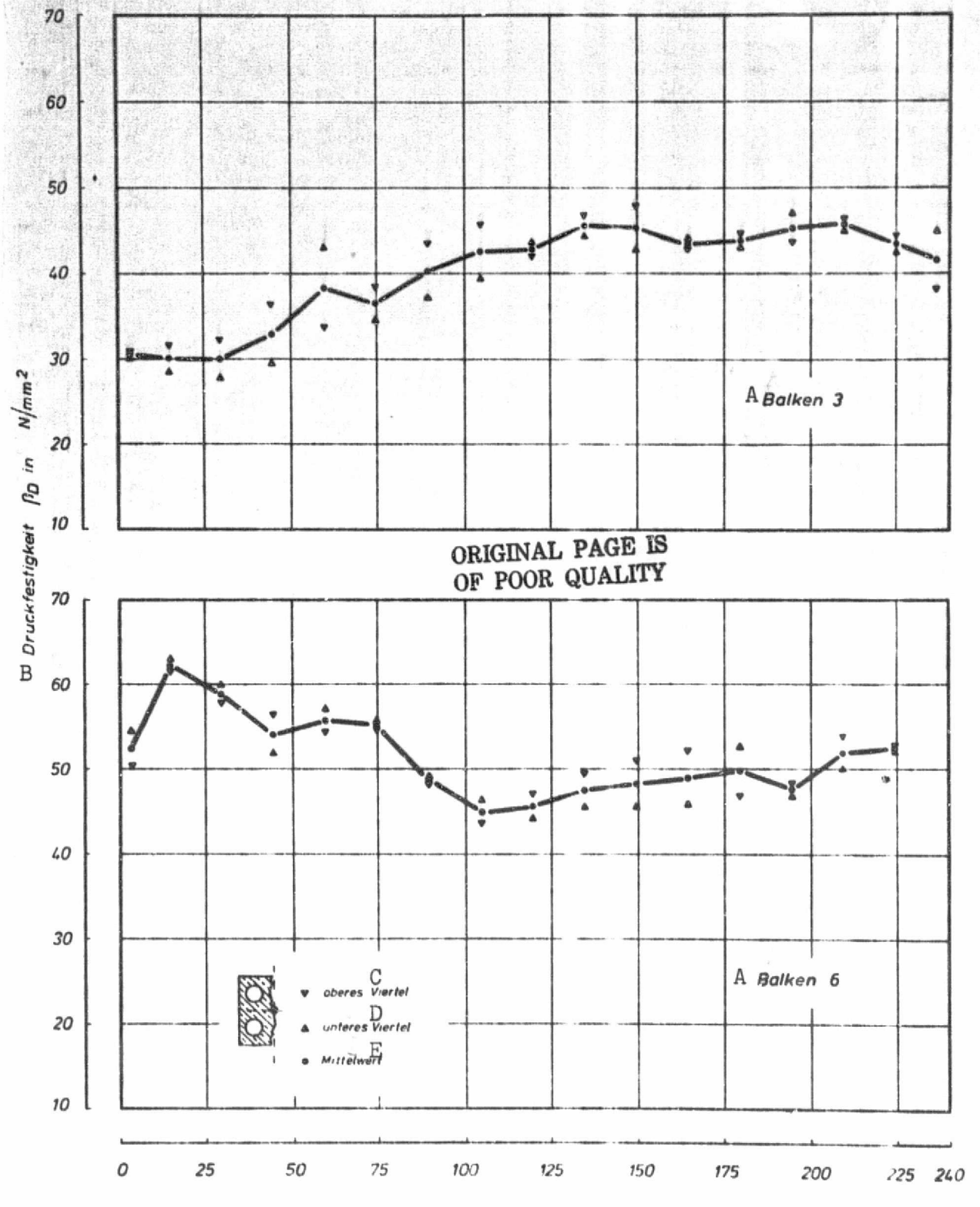
Key: A. Water absorption

- B. Beam
- C. Water/cement ratio
- D. Distance from the heated face in cm
- E. Water absorption A of the beam concrete

Fig. 37. Right-water absorption at atmospheric pressure (A_{γ}) and at a pressure of 150 bars (A_{dr}) of separately producet test specimens of calcite and gravel-sand concretes.

Key: A. Water/cement ratio

- B. Calcite concrete
- C. Gravel-sand concrete
- D. Water absorption \textbf{A}_{γ} and \textbf{A}_{dr} of test specimens



F Abstand von der beheizten Stirnseite in cm

Fig. 38. Compressive strength (β_D) of cores (diameter and whickness 10 cm) from sections of beams 3 and 6, plotted over beam length.

Key:

- A. Beam
- B. Compressive strength
- C. Upper quarter
- D. Lower quarter
- E. Mean value
- F. Distance from the heated face in cm

2.3. Structural Developments of the Concrete

2.3.1. Dehydration Experiments on Cement Paste

2.3.1.1. Measurement Method and Experimental Procedure

According to Powers and Brownyard [14], the water present in the cement paste can be distinguished into three different types, namely, free, adsorptively bound and chemically bound water (cf. section 1.1.3.). The subdivision into evaporatable and non-evaporatable water, made on the basis of defined experimental conditions, assumes that the non-evaporatable water can be approximately equated to the chemically bound water.

In this paper we have adopted the terminology used by Powers by designating, for purposes of simplification the portion of water expelled by drying at 105°C as evaporatable water and the portion given off between 105°C and 550°C as non-evaporatable water. The method used by most authors to determined the content of evaporatable water, i.e. the method of drying in a warming cupboard at temperatures somewhate above the boiling point (also see [18, 28, 63]) measures in addition to the free portion (in the sense of the distinction made by Powers, a portion of the water bound adsorptively to the pore walls, and this as a function of the drying temperature, drying time and pretreatment of the test material). As experiments have shown [82], even under precise drying conditions the weight loss cannot be correlated only with specific temperature ranges, but it also shows a continuous curve, which is primarily due to the fact that the absorption forces, which bind the water molecules in layers and have to be overcome during drying, increase as the molecule approaches the pore wall. In spite of the uncertainty to which the method is subject, it is used in most cases -- including this one -- so as to keep the technical aspects of the experiments from becoming unnecessarily complex. By contrast, the method first used by Powers and Brownyard, and refined by Copeland and Hayes [26], to determine the chemically bound water (i.e. non-evaporatable water) have to be reserved for special experiments [25]. In the experiments described below on samples of cement paste, the heat treatment method at 105 or 550°C used to distinguish evaporatable and non-evaporatable water was compared with the results of thermogravimetric analysis (TGA). Prisms were used for the test material (cf. section 2.1.1.4.). These were stored in a s These were stored in a saturated calcium hydroxide solution until the start of measurement. be able to measure pore-space specific differences, which influence the dehydration behavior, we examined cement paste with

water/cement ratios between 0.20 and 0.55 at increments of 0.05 and also of different ages between 3 and 290 days.

In each case the test material was taken from the interior of the cement paste prisms. For the experiments in the warming cupboard, between 20 and 40 grams of cement paste were used per water/cement ratio and age increment. After weighing, the test material was crushed, dried for 48 hours at 105° C and weighed again. This was followed by heat treatments at 550° C and finally at 1000° C with the appropriate weighing. The water concentrations, with respect to the respective drying temperature (θ^{*}) followed from the difference with respect to the final weight at 1000° C:

$$w(3*) = (\frac{G_3* - G_{1000}}{G_{1000}}).100$$
 in % by weight.

The thermogravimetric analyses were done on samples of cement paste for water/cement values of 0.3, 0.4 and 0.5 at age increments between 1 and 290 days. From the crushed test material, the particle fraction 0.63/1.0 was separated off with test screens in accordance DIN 4188 [4] and 200 mg of this was used as the test material for each test. On the basis of preliminary experiments within temperature ranges, the following heating rates were established:

Temperature (°C)	Range	Heating rate (°C/min)
	·	
20 / 200		2 100
200 / 380		
380 / 540		
540 / 700		- •

In plotting the results, the weight loss curves (df. Fig. 39) were divided into intervals so that these curves include characteristic dehydration phenomena which overlay the more continuous changes. The water concentrations at the temperatures corresponding to the interval limits were calculated according to the above equation, in which the final weight at 700°C was used as a reference value.

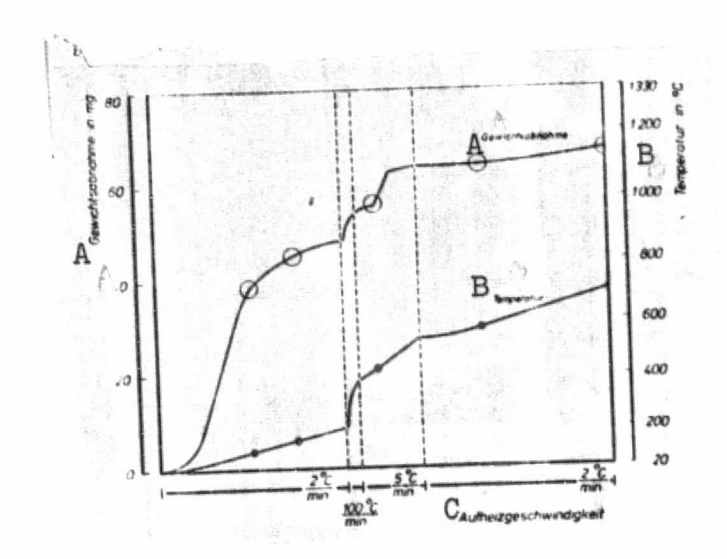


Fig. 39. Thermogravimetric analysis of cement paste: temperature and weight loss as a function of the heating rate (weight of sample: 200 mg).

Key: A. Weight loss

B. Temperature

C. Heating rate

2.3.1.2. Measurement Results

Using as an example a specimen of cement paste with a water/cement ratio of 0.50, Fig. 39 shows the dependency of weight loss on temperature, taking into account the different heating rates. In the weight loss curve, the interval limits used in plotting these graphs were marked by circles which correspond to the temperatures lying vertically below them.

Fig. 40 summarizes the results of measurements expressed as water concentrations of the cement paste at the respective temperatures, as a function of age. Fig. 40 (left) shows the water concentrations determined by means of the heat treatment method. Fig. 40 (right) shows the results obtained by plotting the curves as shown in Fig. 39. For reasons of clarity, individual values are not plotted in the graph.

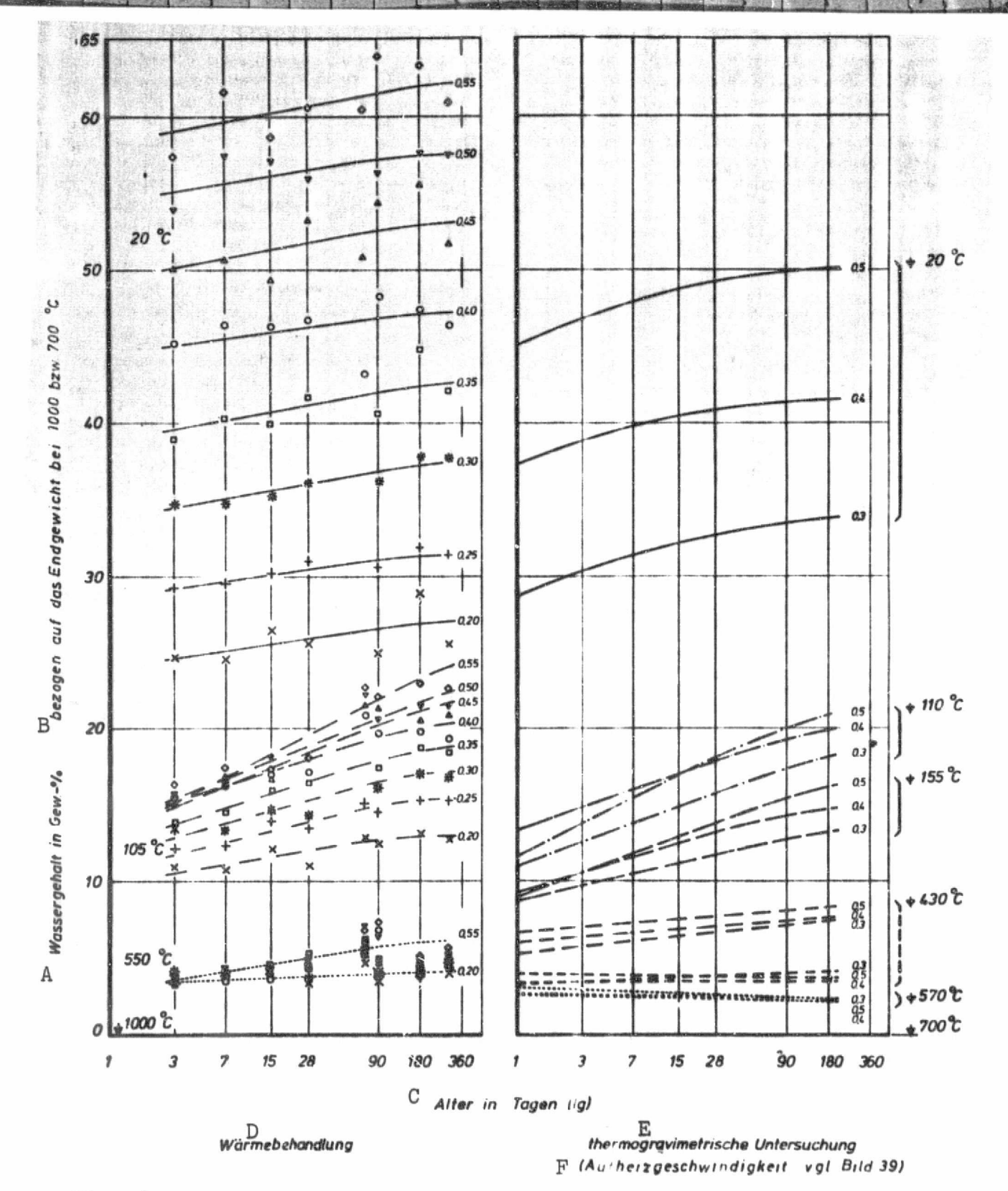


Fig. 40. Water content of cement paste (water/cement ratio 0.20-0.55) as a function of age, determined by heat treatment at 105, 550 and 1000°C and by thermogravimetric analysis.

(See key on following page.)

Key: A. Water content in % by weight

B. With respect to the final weight at 1000°C and 700°C

C. Age in days

D. Heat treatment

E. Thermogravimetric analysis

F. Heating rate, cf. Fig. 39

2.3.2. Evaporatable and Non-evaporatable Water

2.3.2.1. Measurement Method and Experimental Prodedure

The purpose of the tests described below was to determine the effects of heating, i.e. of local temperature and moisture conditions in the beam, on the development of structural properties of the concrete, as far as they are reflected in the ratios of the concentrations of evaporatable and non-evapora-In view of the small sample quantities of matrix table water. mortar, as stipulated by technical conditions, larger deviations were to be expected, particularly in the moisture content determinations, since the ratio of total pore volume to solid volume as well as the pore space essential for water absorption would not be the same for all of the test specimens. also to be expected that in determining the concentrations of non-evaporatable water by heat treatment at 550°C, the measured values would be adversely affected by weight losses of the Thus, these findings could be used primarily only to show development tendencies.

The specimens of matrix mortar, taken in pairs from the beam windows according to the test plan shown in Fig. 7, were weighed immediately after being removed and—to prevent moisture losses—immediately processed as follows:

One specimen was cut in half. One half was used to determine the dry bulk density, which also yielded in each case a value for the concentration of evaporatable water. The other half was used to determine the pure density (cf. section 2.3.3.).

One half of the second specimen was used to measure the pore size distribution (cf. section 2.3.4.), and the other half was used to measure the concentrations of evaporatable and non-evaporatable water. To this end, the material (20-30 grams per specimen) was first pre-dried and weighed to keep evaporation losses at small as possible during subsequent crushing in a mortar. The drying at 105°C lasted 48 hours in each case, a period of time which had been determined to be adequate

in the experiments on crushed material. After weighing, the test material was heated to 550°C and held for 24 hours at this temperature. This is followed by roasting at 100°C, likewise for a period of 24 hours.

As a result of the heat treatment at 550°C, the weight losses caused by the aggregates had to be estimated by means of drying experiments on the particles contained in the matrix mortar. For the calcite mortar, this resulted in a proportion of the content of non-evaporatable water of about 1.3% by volume, and about 1.2% by volume for the gravel-sand material.

2.3.2.2. Measurement Results

Fig. 41 shows the results of the evaporatable water content experiments on matrix mortar specimens for beams 1-6. For setting up the graphs we also used the values measured in determining the bulk density, since these do not show any perceptible systematic differences with respect to the values measured on crushed mortar. For the age stages of 3, 7 and 28 days, 3 or 4 individual measurements in each case could be combined into mean values without taking into consideration the position of the sample-taking point (window) in the beam. For the age stages after the start of heating, distinictions were made according to location, whereby a maximum of two individual measurements could be averaged. These data are interconnected by broken or dotted lines.

The results of the matrix mortar experiments on the content of non-evaporatable water did not reveal any dependencies on the water/dement ratio within a type of concrete. As expected, the values determined for the beams deviated sharply and, after correcting for the weight loss of the aggregate, they were summarized for both types of concrete and shown graphically in Fig. 42. The graph on the left shows the change in concentration of non-evaporatable water for the matrix mortar with caclite concretes (beams 1-3) and the graph on the right for the matrix mortar of gravel-sand concretes (beams 4-6). The data for the three age stages up to the start of heating could be combined into mean values from a maximum of six individual values without taking into consideration local details. The data plotted after the start of heating as a function of age correspond to the mean of a maximum of four individual values. The solid lines indicate the change in content of non-evaporatable water for windows 1-3 after the start of heating, the broken lines combine the points measured at windows 4-8.

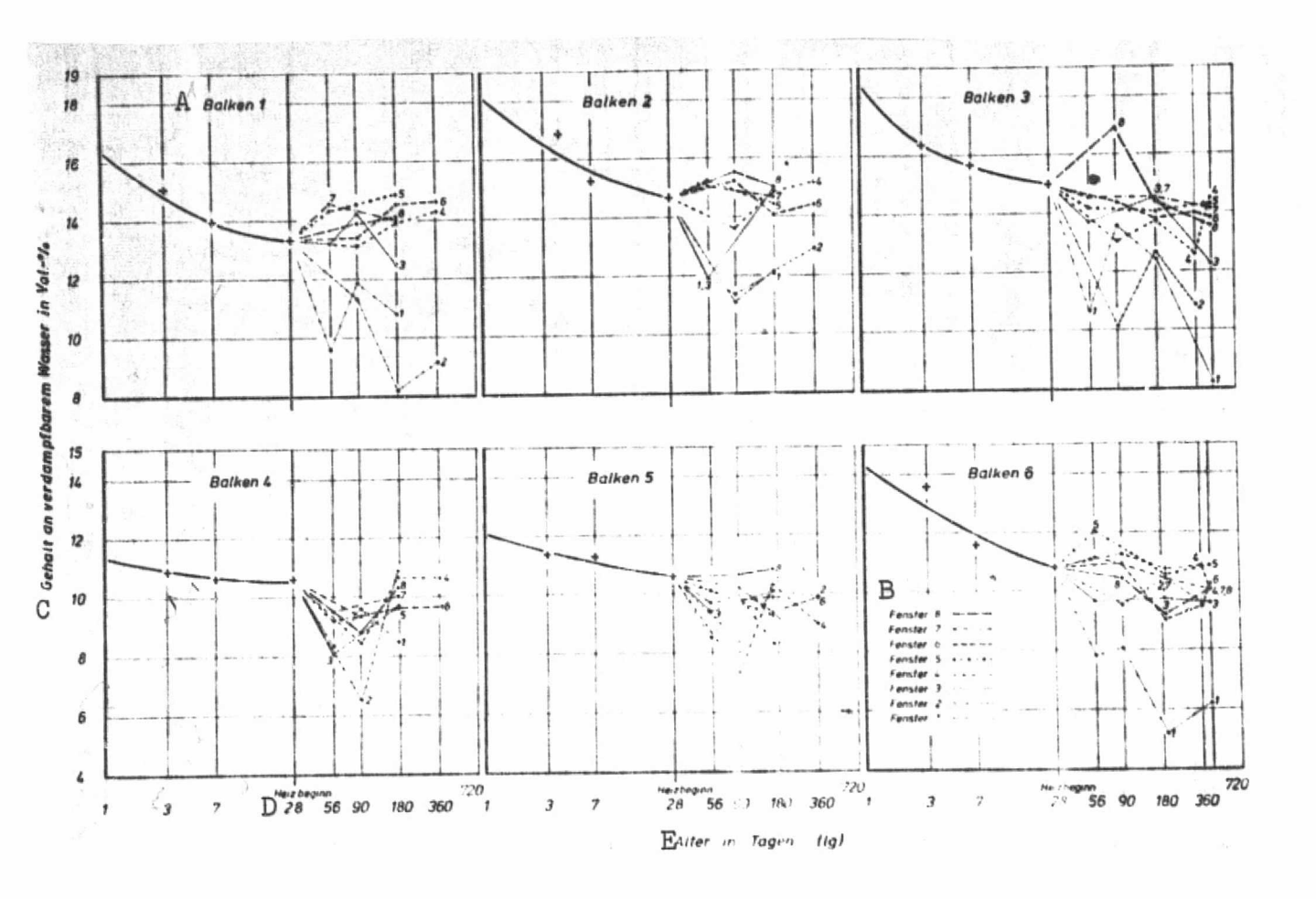


Fig. 41. Content of evaporatable water as a function of age and also of the location in the beam (windows 1-8) after the start of heating, determined on matrix mortar specimens from beams 1-6.

Key: A. Beam

B. Window

C. Content of eyaporatable water in % by volume

D. Start of heating

E. Age in days

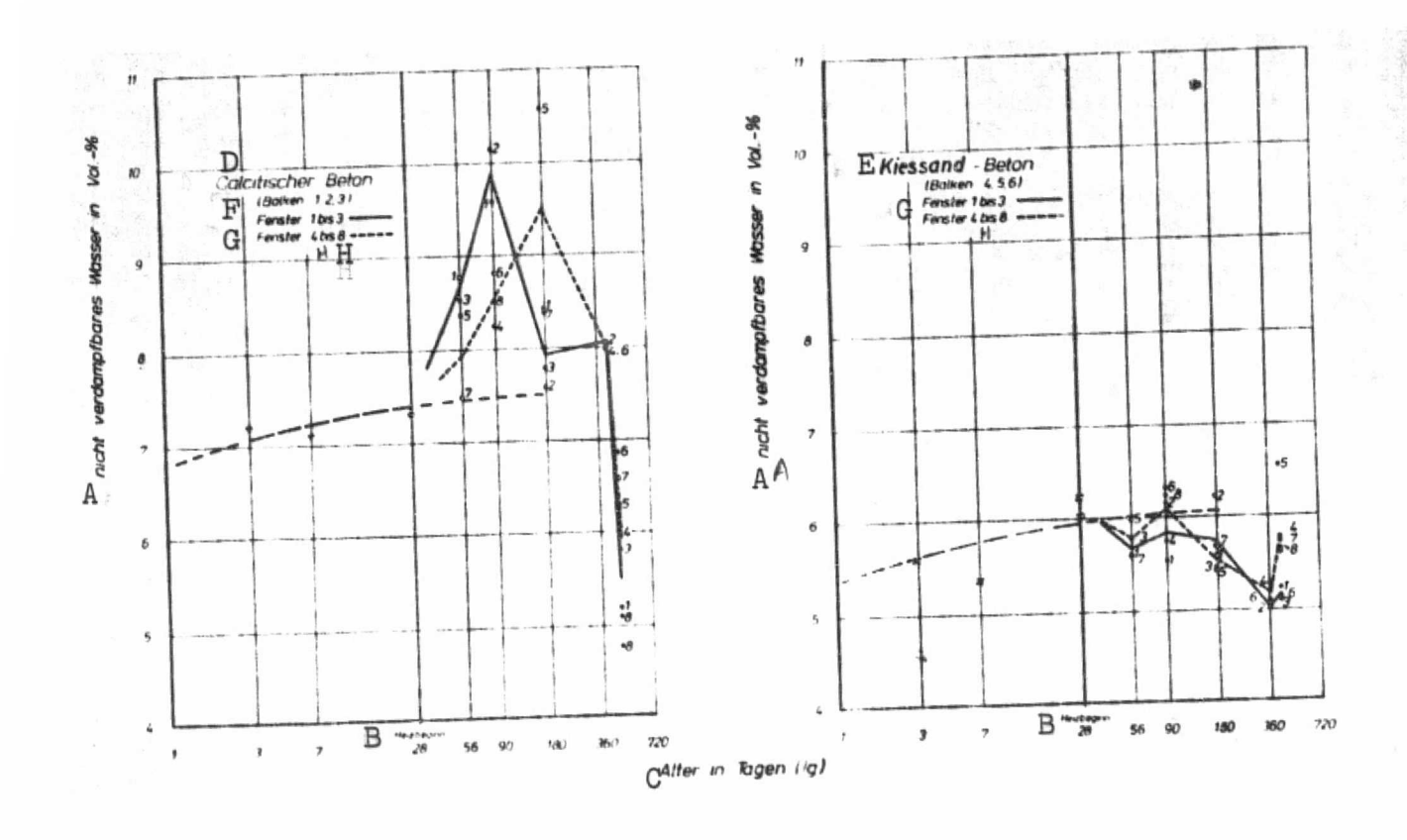


Fig. 42. Content of nonevaporatable water of matrix mortar specimens with calcite aggregate (mean values for beams 1-3 after removal of the aggregate portion), plotted as a function of age and location in the beam (windows 1-8) after the start of heating.

Content of non-evaporatable water of the matrix mortar specimens with gravel-sand aggregate (mean values for beams 4-6 after removal of the aggregate portion), plotted as a function of age and location in the beam (windows 1-8) after the start of heating.

Key: A. Non-evaporatable water
in % by volume

B. Start of heating

C. Age in days

D. Calcite concrete

E. Gravel-sand concrete

F. Beams

G. Windows

H. To

2.3.3. Total Porosity

2.3.3.1. Measurement Method and Experimental Procedure

The structural development of the concrete can be characterized with the help of changes in total porosity (also see [83]). Under normal hardening conditions during the maturation process the total porosity decreases, since the hydration products assume a portion of the originally available pore space. Since the resulting products as well as their strength are dependent on the prevailing temperature and moisture conditions, differences in the development of the pore volume according to the location of the concrete in the beam had to be expected.

The material used for the total porosity experiments was a test specimen of matrix mortar for each type of concrete, the sample-taking of which is described in section 2.3.2.1. As a supplement totthis, measurements were made on cement paste with water/cement values between 0.25 and 0.55 (cf. section 2.1.1.4.). /54 The cement paste prisms were stored until the test age in each case in a saturated calcium hydroxide solution. The tests were carried out according to DIN 52 102 [5]. In each case, half of the test specimen was used to determine the bulk density ($\rho_{\rm tr}$). The other half, after being crushed and dried was used to measure the density ($\rho_{\rm tr}$) with a Beckman comparison air pycnometer with which the volume was determined by adjusting the pressure of two test chambers coupled through a differential pressure meter (cf. [84]).

2.3.3.2. Measurement Results

The total porosity (Ut) is deduced from the values determined for bulk density and density according to the following equation:

Y

To show especially also the influence of heating on the change in pore space, the data for the two types of concrete, differing in aggregate, were compiled in Fig. 43. For the age intervals of 3, 7 and 28 days, it was not necessary to distinguish the location in the beam (window number), so that for these ages six individual measurements were averaged in each case (dashed-line fitted curve). The data for the age intervals after the start of heating, which must be distinguished according to temperature and moisture conditions by indicating

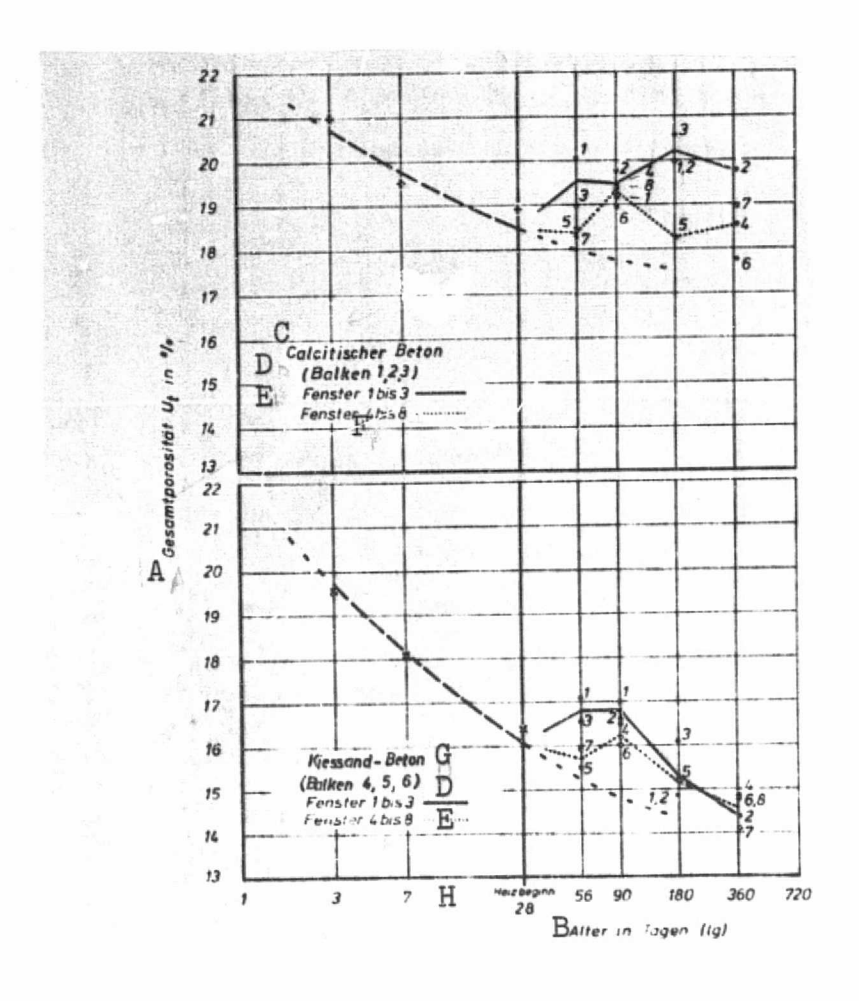


Fig. 43. Change in total porosity (U_t) of the matrix mortar with calcite aggregate (beams 1-3) and with gravel-sand aggregate (beams 4-6) as a function of age and location in the beam (windows 1-8) after the start of heating.

Key:

- A. Total porosity
- B. Age in days
- C. Calcite concrete
- D. Beam

- E. Window
- F. To
- G. Gravel-sand
- H. Start of heating

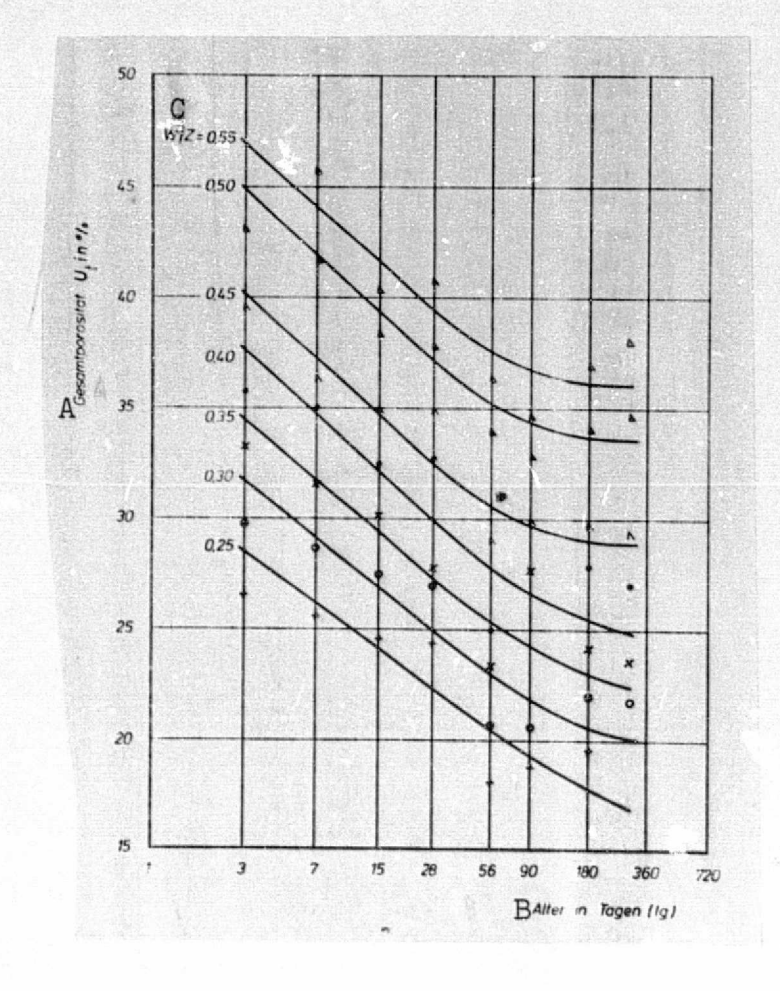


Fig. 44. Total porosity (Q_t) of cement paste stored in water (water/cement ratio = 0.25-0.55) as a function of age.

Key:

A. Total porosity
B. Age in days
C. Water/cement ratio

the window number, in each case respresent three individual values. The solid line after the start of heating combines the results for windows 1-3, the dotted line combines the results for windows 4-8.

Fig. 44 summarizes the total porosity values (U_t) of the cement paste samples. The graph shows the total porosity as a function of the age of the cement paste for water/cement ratios between 0.25 and 0.55.

2.3.4. Pore Size Distribution

or

2.3.4.1. Measurement Method and Experimental Procedure

Besides the chemical and mineralological features of the cement paste as well as of the matrix mortar, we are also especially interested in the pore structure with respect to the technoological properties of the concretes. This structure is characterized by the nature and distribution of the pores. /55 To measure the poresize distribution using the method proposed by Ritter and Drake [85] we used a mercury porosimeter developed by Guyer, Böhlen and Guyer [86] with a pressure range up to 2000 bars (for 4 radii between about 7·10³ and 4 nm). Reference [82] shows a schematic diagram of the instrument built by Carlo Erba Co. This instrument also has an additional device for measuring larger pores with radii between 55·10³ and 7·10³ nm.

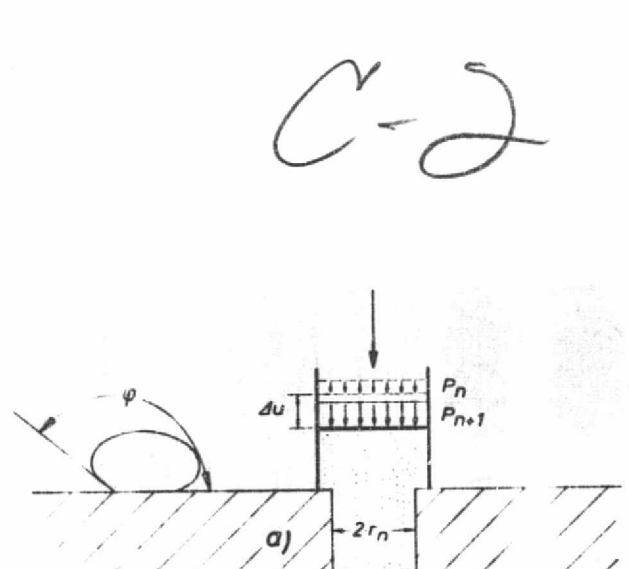
The basic points of the measurement method are described in detail in the literature (e.g. [24, 87, 18]) and these will be repeated here only to the extent necessary for evaluating the results. The method is based on the capillary equation for the equilibrium state

$$p \cdot r^2 \cdot \pi = 2 \cdot r \cdot \pi \cdot G \cos \varphi$$

$$p = \frac{2 \cdot G}{r} \cdot \cos \varphi ,$$

Eq. 3

where p is the pressure, r the radius of the capillary tube, σ the surface tension of the medium and ϕ its angle of contact (cf. Fig. 45).



Schematic diagram of the mercury porosimeter method. Fig. 45.

Key: ϕ . Contact angle of mercury on a nonmetal substance.

a) Series of cylindrical pores with a gradually decreasing radius r

 ${}^{r}_{n}$, ${}^{r}_{n+1}$ radii of successive pores ${}^{p}_{n}$, ${}^{p}_{n+1}$ pressure after filling the pores

change in volume as a result of filling the pore with a radius of r_n+1

b) Pore with bottleneck access

c) Large pore with bottleneck openings

d) Closed spherical pore

For mercury on nonmetallic materials, contact angles are produced which are greater than 90°, and the right side of the equation becomes negative, i.e. the mercury is not wetted and must be pressed into the pore system. Assuming that σ and ϕ are constant variables, namely σ =0.48 N/m for pure mercury and ϕ =141.3° as the contact angle [24], the relationship between the radius of the smallest filled pore and pressure (in bars) turns out to be

$$r = \frac{7492}{P}$$
 in nm. Eq. 4

Winslow and Diamond [20] have determined the contact angle of mercury to be 117° by experiments on cement paste dried at 105°C, and with a surface tension of σ =0.484 N/m they have obtained a modified conditional equation. For example, for the measurement apparatus used here, this would cover a pore radius range of about 2.2-33 x 10³ nm. In view of the objective or studying relative changes in pore size distribution in a complex system, however, the mean values usually taken as a basis for the surface tension and angle of contact were retained [88].

The measurements are carried out in such a way, that first of all by means of compressed air, mercury is pressed in stages into the originally evacuated test material, during which the respective changes in volume and pressure are measured. Then the pressure is gradually increased by means of a multistage hydraulic system in an automatically controlled apparatus, and the pressure and volume are registered on a recording apparatus. The pore radii are calculated in steps using Eq. (4). These are correlated to the pore volume corrected by the compressibility of the hydraulic system.

Eq. (4) is valid in principle only for cylindrical capillary tubes. Accordingly, with step-wise pressure increases, the successive pores must become increasingly smaller (Fig. 45, case a) and not-e.g. like a bottleneck--confine the axis to larger cavities (Fig. 45, case b). Since pore systems, in reality, are considerably more complex, the pore size distributions measured serve only as a model. Indicative of this is the fact that the mercury pressed in does not completely re-emerge if, as a result of gradual decrease in pressure, atmospheric pressure is again obtained. Various reasons for this are given in the literature. While Ritter and Drake [85] attribute this to the bottleneck pores, Hill [89] believes that in very large pores with bottleneck openings (cf. Fig. 45, case c) free mercury levels would form without exterior binding during emptying. On the basis of microscopic examinations of

/<u>56</u>

sample of coke, Jüntgen and Schwuger [87] assume, moreover, that because of the high pressure, mercury in the form of thin films remains stuck for the most part to the wall surfaces of large pores during emptying. Auskern and Horn [90] found that about 50% of the mercury pressed in did not re-emerge from the cement paste; Sellevold [91] gives a figure of 20-45% for his experiments on cement paste. Among other things, Jüntgen and Schwuger [87] also discuss the question of whether the pore structure is not modified at the outset by the strain differences resulting from pressing in the mercury. Repeated measurements revealed a small influence obviously only in the region of larger pore radii.

Altogether the method has a large number of special features which may have a strong effect on the distributions measured and which cause Jung [92], for example, to state that the maximums in the end region of the mercury porosimeter method would often be overestimated. Regardless of these special measurement features, the relative changes in pore space measured with the method allow us to draw conclusions with respect to the development processes.

In this connection, finally the question of the pretreatment of specimens takes on importance. Sellevold [91] informs us that considerable differences have emerged for measurements on pulverized cement paste in comparison with measurements on small pieces of the same material. In addition, the heat treatment at 105°C to expel the evaporatable water from the specimens made from the outset cause a change in the pore space. In the experiments described below, instead of drying at 105°C, the crushed specimens of matrix mortar were dehydrated in a vacuum at about 10⁻³ torr for three days, since dehydration experiments at different temperatures (cf. [82]) as well as comparison measurements had led to the result that, with this drying method, the pore space essentially measured by mercury porosimetry is obviously emptied.

The test material used for the measurements was matrix mortar (cf. section 2.1.1.3.), cement paste (section 2.1.1.4.) and aggregate samples. As explained in section 2.3.2., from one of the two mortar samples removed from the windows of the beams at each age increment (cf. sample-taking chart, Fig. 7), half was split off after weighing, crushed into small pieces measuring about 2-3 mm in diameter and dried in a vacuum at about 10^{-3} torr and at room temperature for three days. From the material prepared in this way and selected by visual examination as being free of courser aggregate, about 3-4 grams were put into a dilatometer container (cf. Fig. 1 in [82]) and measured using the mercury porosimeter method after several

evacuations lasting about two hours. So far, pore size distributions have been measured on 26 test specimens for each of beams 1, 2, 4 and 5, while there were a total of 34 test specimens both for beams 3 and 6. Likewise, cement paste as described in section 2.1.1.4. as well as samples of calcite and gravel-sand aggregate were tested for pore size distribution.

The pressure range up to 1 bar (corresponding to pore radii up to about 7·10³ nm) were measured in eight stages. The recording apparatus graphs were plotted for pressures up to 2000 bars (corresponding to pore radii up to about 4 nm) in 36 stages according to a prepared pattern.

2.3.4.2. Measurement Results

Taking into consideration the correction term for the inherent compressibility of the hydraulic system from the pressure and volume measurements measured in the blind experiment, Eq. (4) provides us with frequency sums of the pore volume (u) as a function of the pore radius (r). These curves were plotted for all of the test specimens over (lg r) (cf., for example, the sum lines in the upper half of Fig. 46 for the test specimens from windows 7 and 8 of beams 2 and 5). The measured pore volumes (UHg) are plotted in Fig. 47 as a function of age and location within the beams (window number). Here the individual values measured up to the start of heating are combined, independently of the sample-taking point.

From the frequency sums (Fig. 46, top) we can directly read the portion of the pore volume as percent of the total volume of all pores with $r < r_i$ for pore radius r_i . Although these sum curves (also called distribution sums) give information on the correstation of the pore volume to the pore radii, it was necessary for purposes of clarity to determine the corresponding frequency distribution (also called distribution densities) with the help of a computer and also plotting over (lg r).

The distributions shown as examples in Fig. 46, center, and also in Figs. A 17-20 in the appendix, are fitted curves for the computer-drawn histograms of the frequency of the pore volume du/d (lg r) plotted over (lg r). Fig. A 17 shows pore volume frequency distributions for the age intervals of 3, 7 and 28 days, measured on samples of matrix mortar of the calcite (beams 1-3) and gravel-sand (beams 4-6) concrete. Fig. A 18 compares the frequency distributions of matrix mortar specimens from windows 2, 7 and 8 from beams 3 and 6 for different age intervals. Figs. A 19 and A 20 show the

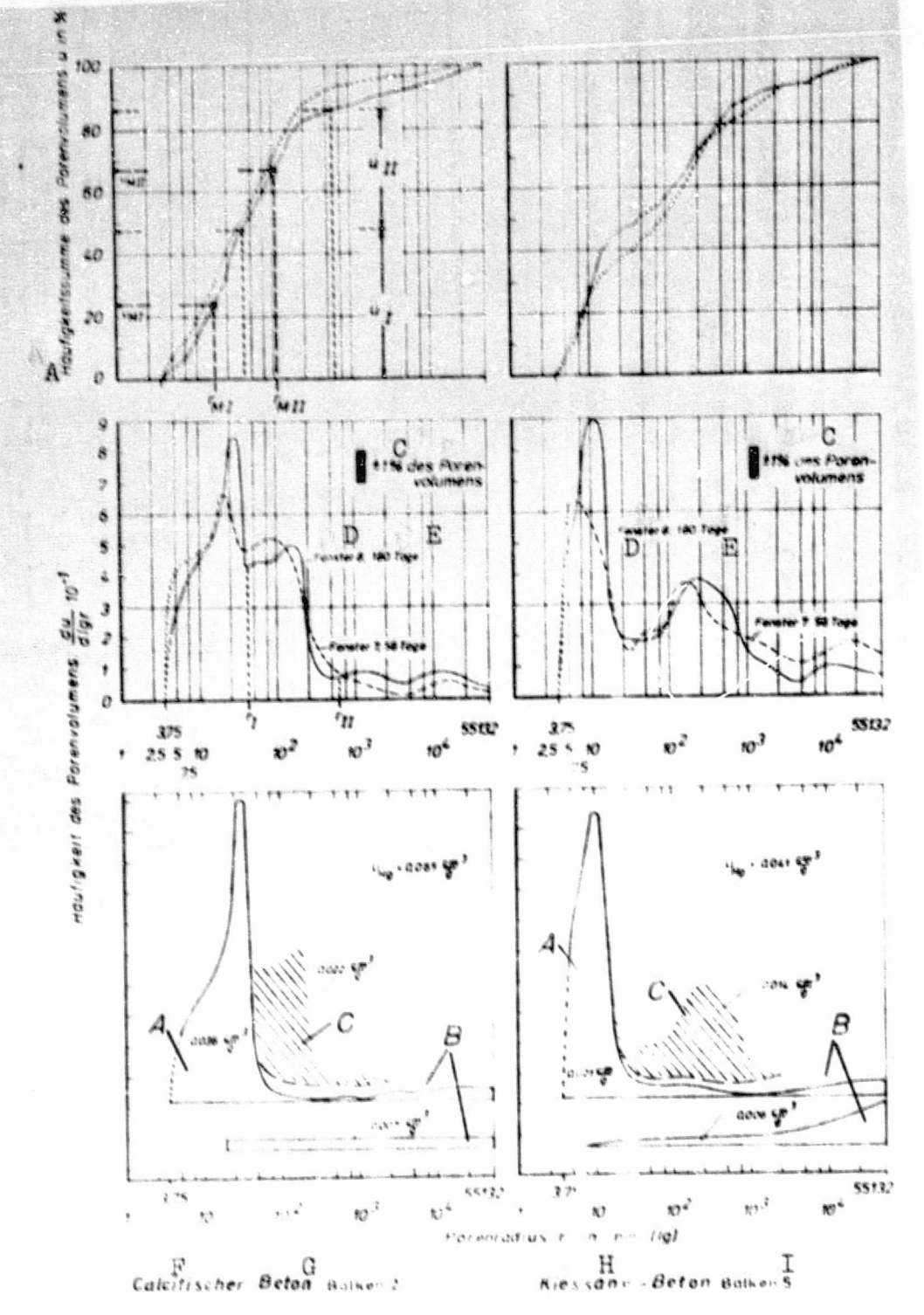


Fig. 46. Graphing methods and elucidation of the relationship, measured using a mercury porosimeter, between the pore volume (u) and pore radius (r) for two specimens of matrix mortars from beams 2 and 5.

See key on following page.

Top pore volume frequency sums as a function of the pre radius (lg)

Center pore volume frequency distributions as a function of the pore radius (lg)

Bottom schematic subdivision of the measured pore volume (UHg) into cement paste porosity (A), aggregate porosity (B) and structure-dependent porosity (C).

Key: A. Pore volume frequency sum in %

B. Pore volume frequency C. 1% of the pore volume

D. Window

E. Days

F. Pore radius

G. Calcite concrete

H. Beam

I. Gravel-sand concrete

frequency distributions of the pore volumes with respect to weight which were measured on cement pastes with different water/cement ratios and ages and also on samples of the limestone and gravel-sand aggregate. With the help of the surface area scale drawn in the figures, we can obtain the proportion of pore volume of the total volume measured between two pore radii. By means of these distribution curves obtained by partial differentiation of the sum curves, changes in the pore volume over the coordinated pore radii are readily Thus, Fig. 46, middle, shows that typical distribuvisible. tion curves for the matrix mortar of the calcite and gravelsand concrete differ considerably from one another in terms of form, which is obviously causally related to the particular features of the aggregates. So in Fig. 46, bottom, taking as an example a specimen of each type of concrete, (from window 8, age 180 days) the proportions of measured pore volume (Un attributed to the components of the matrix mortar as well as the structure-determined porosity are estimated. obtained are based on the distribution curves for cement paste, limestone and gravel-sand aggregates shown in Figs. A 19 and 20 in the appendix.

The distribution curves of Figs. A 17 and 18 in the appendix also reveal that the volume percentages correlated with certain pore radii (in the graphs showing surface area proportions) are obviously shifted with age toward other pore radii. Another goal was to quantitatively determine the

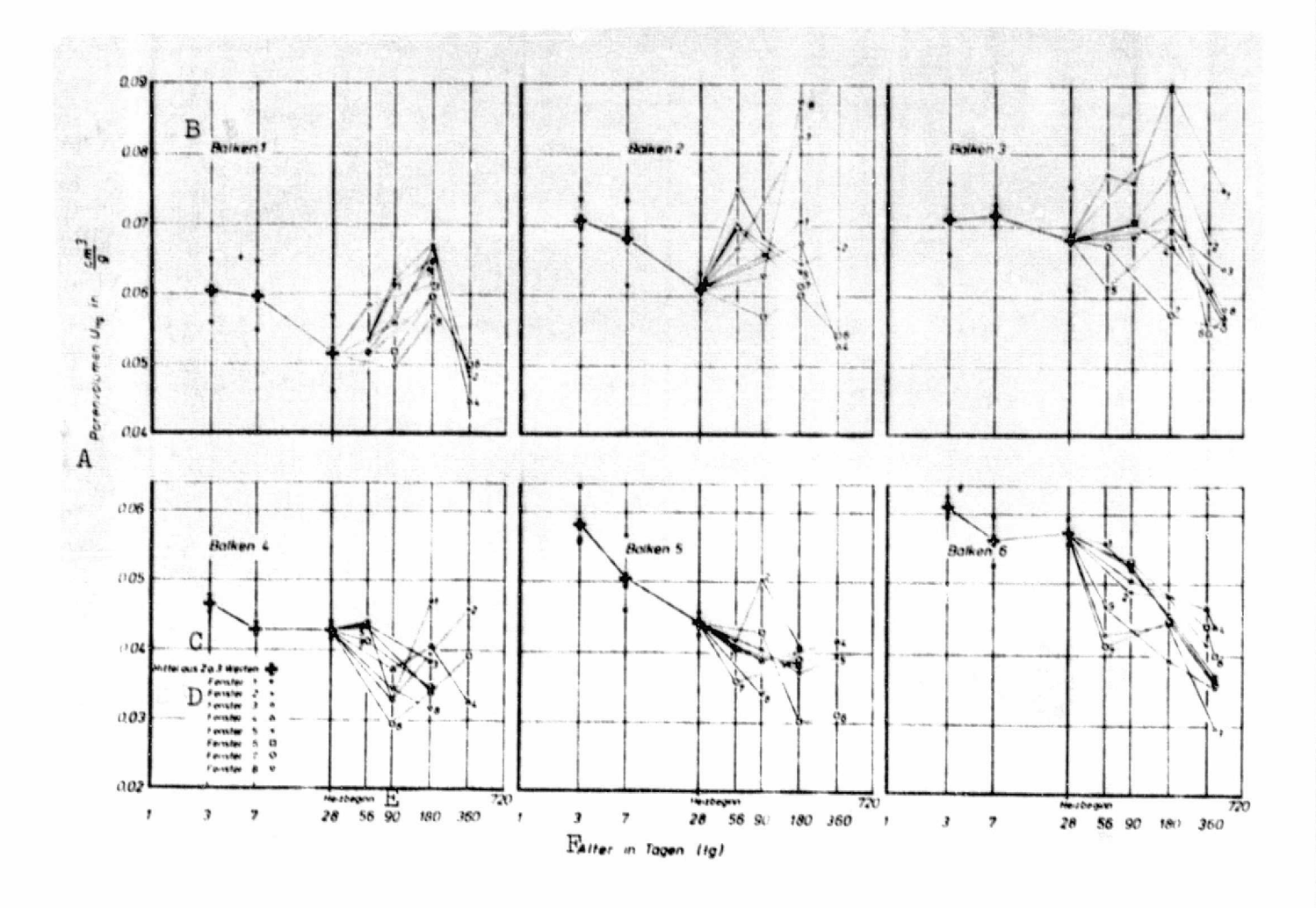


Fig. 47. Pore volumes ($U_{\rm Hg}$) as a function of age and location in the beam (windows 1-8) after the start of heating, measured with a mercury porosimeter on the matrix mortar of beams 1-3 (concretes with calcite aggregate) and 4-6 (concretes with gravel-sand aggregate).

Key: A. Pore volume

B. Beam

C. Mean based on two or three values

D. Window

E. Start of heating

F. Age in days

changes qualitatively visible in the distribution curves. this end, the histograms were separated into surface area segments at characteristic, recurrent minimums. These segments are limited by the smallest or greatest measured pore radii and by radii rI and rIT within the distribution curves (Fig. 46, middle). The limiting radius was characteristic for both types of aggregate, and spedifically for the calcite material a mean value of rr=40 nm emerged and an average value of rr= 52 nm for the gravel-sand material, while ril for both types of aggregates was uniformly determined to be 740 nm. transferring the limiting radii rT and rTI into the frequency sums (Fig. 46, top) the corresponding volume portions u1 and u, turned out to be percentage portions of the measured total pore volume. Their centermost values umI and umII correspond to the "central" pore radii r_{MI} and r_{MII} as marked in Fig. 46, top. The distribution surfaces un and uil were converted by multiphying with the pore volumes (UHg) of Fig. 46 into cm3/g, combined for each type of concrete (three beams in each case) and plotted in the graphs together with the central pore radii as a function of age, taking into consideration the position in the beam or the corresponding temperature ranges. Figs. 48 and 49 show the changes in central pore radii rmT and pore volumes ur for beams 1-3 and 4-6 respectively. In these graphs the location-dependent values up to the start of heating were averaged, while the values for the age intervals after the start of heating were combined for every two adjacent windows (cf. the temperature ranges given in the figures).

The changes in central pore radii r_{MIT} and the accompanying /61 pore volumes u_{IT} are shown in Fig. 50, left, for beams 1-3 (calcite concrete) and right, for beams 4-6 (gravel-sand concrete) corresponding to Figs. 48 and 49.

In Fig. 51, left, the pore volumes up for the age increments up to the start of heating on the 28th day are plotted separately for the matrix mortars of beams 1-3 and 4-6. The identifiable development area for the three concretes in each case has been emphasized by boundary-line curves and right and left slanted shading lines. Fig. 51, right, shows the corresponding graph for pore volumes up.

2.4. Changes in the Mechanical Properties of the Concrete

2.4.1. Shrinkage, Contraction, and Thermal Expansion

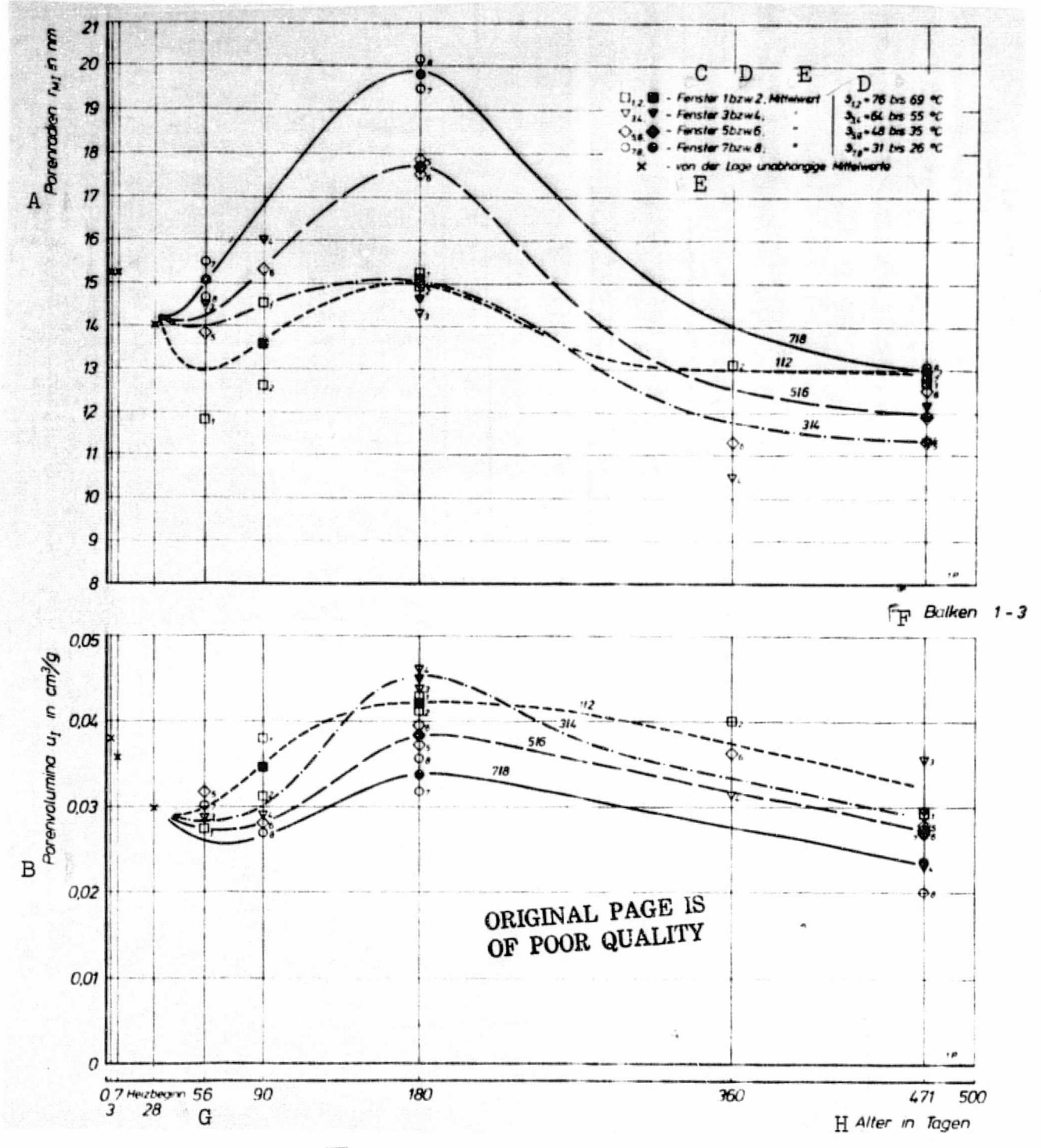


Fig. 48. (Top): Changes in central pore radii (r_{MT}) as a function of age; (bottom): changes in pore volume (u_T) as a function of age measured on matrix mortar from the calcite concrete of beams 1-3. Fitted curves for every two measured values (windows 1/2, 3/4, 5/6 and 7/8).

See key on following page.

Key: A. Pore radii

B. Pore volumes

C. Windows

D. And

E. Mean value

F. To

G. Mean values independent of the location

H. Beams

I. Start of heating

J. Age in days

2.4.1.1. Measurement Method and Experimental Procedure

Besides the measurements of total length changes made on the beams, strain behavior tests were necessary to determine the nature and magnitude of different types of influences.

The reduction in volume as a result of shrinkage and then contraction immediately after the pouring of the concrete, due to hydration phenomena, could not be measured on the beams themselves. After the start of heating, local contraction—induced strains appeared as the beams gradually dried out. These processes are still going on and had to be evaluated on separately produced test specimens. Changes in the length of the beams before and after the start of heating were caused by thermal expansion. To be sure, these changes are included in the sum of all local length changes measured with the Invar rod, however they cannot be measured individually and so even measurements of thermal expansion on separately produced test specimens were necessary.

To investigate the strains in both types of concrete due to shrinkage and contraction in the early stage of hardening we used an experimental apparatus which had already been tested by the Federal Institute for Experiments on Mortars and Pure Pastes. Details of this apparatus are given in reference [93]. It consists of a three-part mold--such as used for making cement mortar prisms measuring 4 x 4 x 16 cm--on whose ends for the two outer prisms are placed inductive displacement transducers. In order to prevent changes in length as much as possible during the measurements, the bottom and the two long sides of the prism molds were each covered with two foils of polytetrafluoroethylene (teflon) sandwiching a lubricating film of oil. To prevent the release of moisture from the concrete to the environment, a glass plate was cemented to the prism molds with ceiling compound and the cavities were filled with wetted foam material. The measurements were made on two prisms each of calcite concrete (corresponding to beam 2) and gravel-sand concrete (corresponding to beam 5) during a 100-hour period after the concrete was poured.

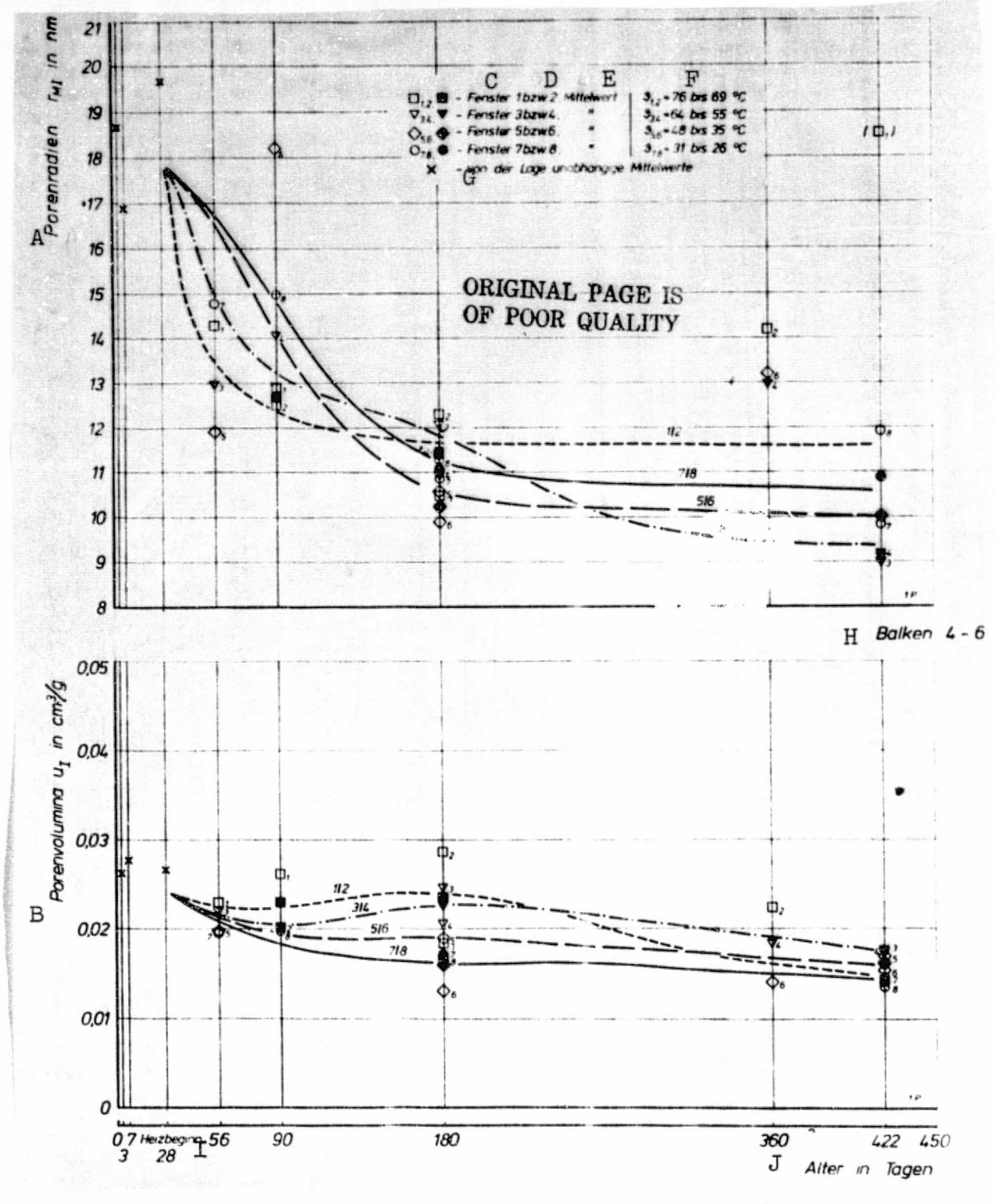


Fig. 49. (Top): Changes in central pore radii (r_{MT}) as a function of age; (bottom): changes in pore volume (u_T) as a function of age measured on the matrix mortar from the gravel-sand concrete of beams 4-6. Fitted curves for every two measured values (windows 1/2, 3/4, 5/6 and 7/8).

See key on following page.

Key: A. Pore radii

B. Pore volumes

C. Windows D. And

E. Mean value

F. To

G. Mean values independent of the location

H. Beams

I. Start of heating

J. Age in days

The linear thermal expansion was first of all studied in preliminary experiments on one beam each of calcite and gravelsand concrete measuring 15 cm x 15 cm x 55 cm. This was done for the temperature range between 20 and 80°C, without taking into account the moisture content of the concrete restricted to the moist and dry boundary states. Based on the practical data obtained in the preliminary experiments, the tests described below were carried out to determine the thermal expansion coefficients and the degree of shrinkage. For each type of concrete and water/cement ratio, two test specimens were poured into cylindrical tin containers measuring 10 cm in diameter and 23 cm long and these were sealed vaportight (cf. section 2.1.2.2.). The membrane-like ends of the containers supported measuring pins which were solidly anchored in the hardened concrete. A thermocouple was arranged approximately in the longitudinal axis of each test specimen. After the concrete was poured, the test specimens were stored for 28 days in a warming cupboard where they were exposed to temperatures corresponding approximately to those which would have occurred in the beams, after the concrete was poured, as a result of heat of hydration (cf. Fig. 9).

On days 3, 7, 17 and 29 the test specimens were cooled to 5°C and maintained at this temperature until the thermocouple indicated that the temperature of the test specimen had reached that of the laboratory. By means of the length changes corresponding to the temperature differences, we obtain the values for the linear thermal expansion coefficients (a). On the 29th day, after the vapor seal (tin casing) was removed from one of the two test specimens for each type of concrete, the temperature was increased to 70°C in a warming cupboard so that one of the two specimens for each concrete could dry out. During the subsequent tests, up to an age of 122 days, the length changes of the specimens were measured for temperature changes between about 70 and 5°C and used to calculate the thermal expansion coefficients.

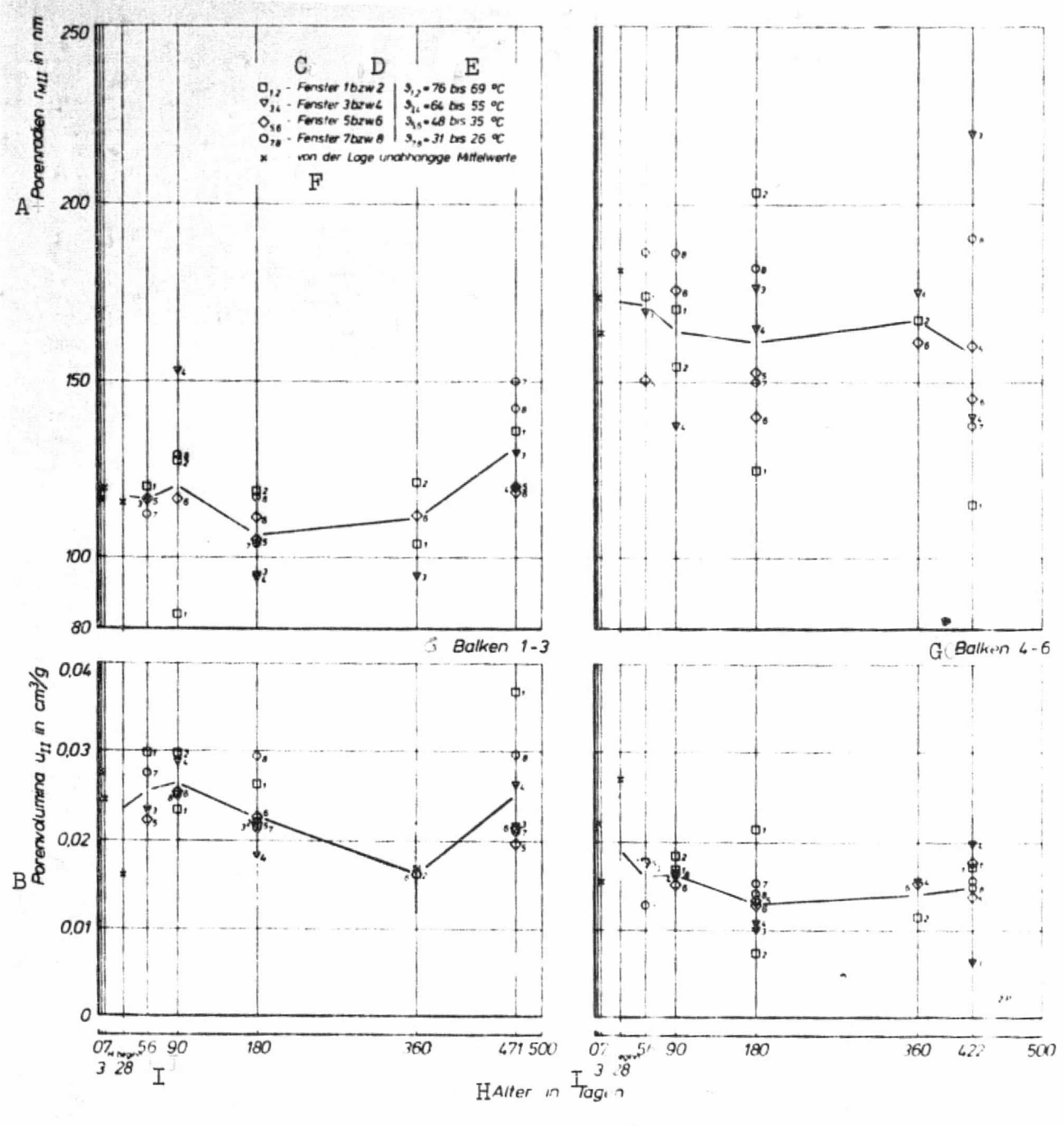


Fig. 50. (Top): Central pore radii (r_{MII}) as a function of age, (bottom): pore volumes (u_{TT}) as a function of age measured on the matrix mortar from the calcite concrete of beams 1-3 (left graph) and from gravel-sand concrete of beams 4-6 (right graph).

See key on following page.

Key: A. Pore radii

B. Pore volumes

C. Window

D. And

E. To

F. Mean values independent of the location

G. Beams

H. Age in days

I. Start of heating

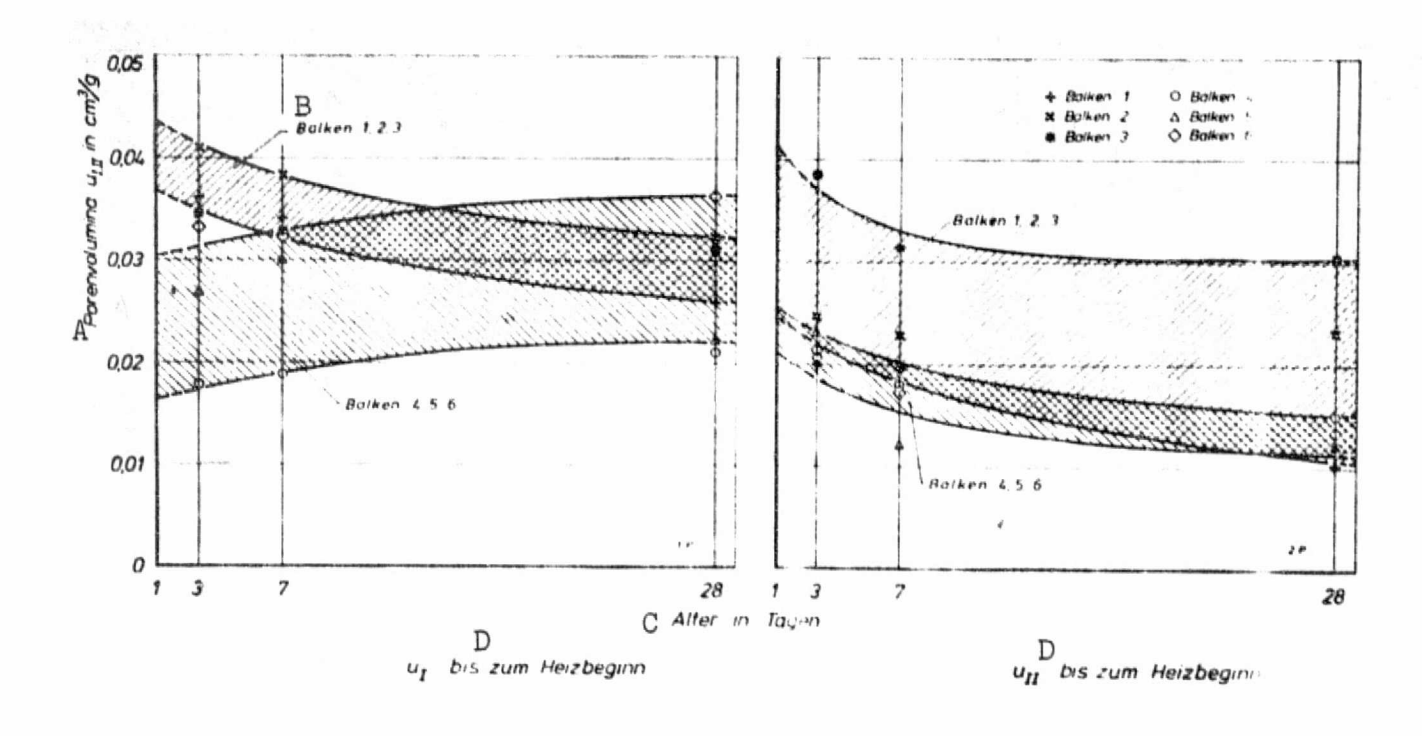


Fig. 51. Development areas of pore volumes $(u_{\rm I})$ and $(u_{\rm II})$ of the matrix mortars from the calcite concrete of beams 1-3 and gravel-sand concrete of beams 4-6 for age increments up to the 28th day.

Key: A. Pore volumes

B. Beams

C. Age in days

D. Up to the start of heating

ORIGINAL PAGE IS OF POOR QUALITY In order to obtain approximate values for the degree of shrinkage for the concretes in the hot regions of the beams characterized by high moisture losses, the vapor seal was removed from the remaining specimen of each pair on the 140th day. Up to this time, these specimens had been stored vaportight at 70°C. The concrete was dried out at 105°C and the contraction caused by the drying was measured. These measurements continued until the concrete had reached an age of approximately 250 days.

Three prismatic test specimens (measuring about 50 mm x 10 mm x 10 mm) were used as samples to determine the linear thermal expansion coefficients (a) for each type of aggregate. These were cut like random samples out of pieces of rock, without taking into consideration the priveleged direction and dried at 105° C until a constant weight was reached. The measurements were made with a dilatometer (a mechanical transducer with a flint glass rod and inductive displacement transducer). The specimens were heated in this device from 20 to 100° C at a constant heating rate.

2.4.1.2. Measurement Results

Linear thermal expansion coefficients (α) between 4.2 x 10^{-6} and 5.3 x 10^{-6} /°C were measured on the test specimens with calcite aggregate and the test specimens of quartzite material yielded expansion coefficients between 11.1 x 10^{-6} and 12.0 x 10^{-6} /°C.

The strains due to shrinkage and contraction (ε) measured on the 4 x 4 x 16 cm prisms are plotted in [s*] Fig. 34 for a period up to 100 hours after the concrete was poured, in this case for concrete with calcite aggregate corresponding to beam 2 and concrete with gravel-sand aggregate corresponding to beam 5. As mentioned in section 2.2.4.2., the results of the experiments with the strain gauges in the beams were used for the connecting values up to the 28th day.

For the concretes corresponding to beams 1, 2 and 3 and 4, 5 and 6, Fig. 52 shows the thermal expansion coefficients (a) determined on the cylindrical test specimens plotted over the age of the concrete. After the 29th day, the values are plotted separately for moist ("with vapor seal") and dry ("without vapor seal") concrete. The two bottom graphs of the figure show the mean values calculated for both types of concrete.

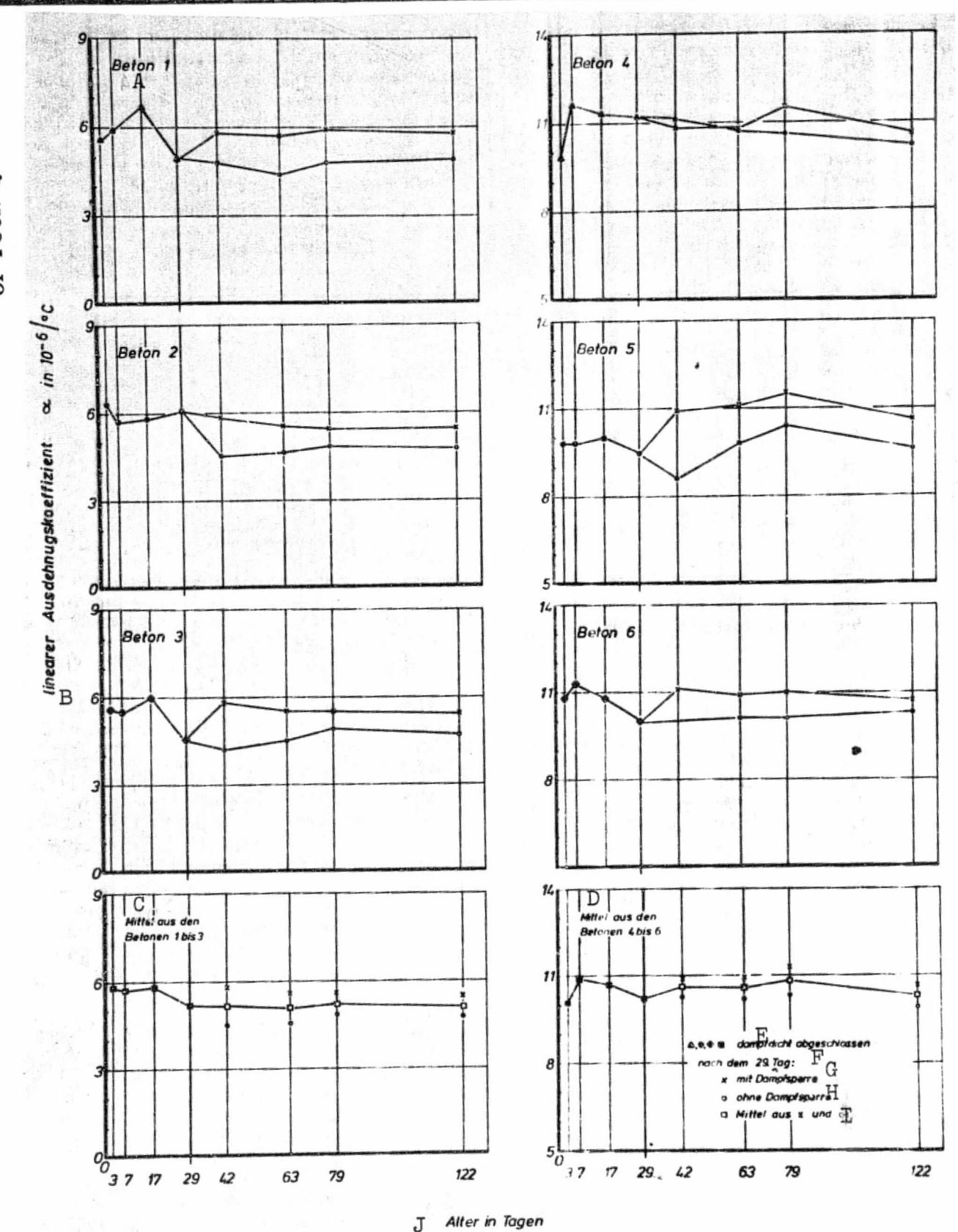


Fig. 52. Changes in the linear expansion coefficient (α) of concrete with calcite (1-3) and gravel-sand (4-6) aggregate as a function of age; determined for temperatures between about 5 and 70°C on moist ("with vapor seal") and dry ("without vapor seal after the 29th day") cylindircal test specimens 20 cm in length.

Key: A. Concrete

B. Linear expansion coefficient

C. Mean for concretes 1-3 D. Mean for concretes 4-6

E. Sealed vaportight
F. After the 29th day
G. With vapor seal
H. Without vapor seal
I. Mean of x and o

J. Age in days

Fig. 53 shows the unit strains due to contraction (ϵ) measured on the cylindrical test specimens. These were obtained by decreasing the total strains by the temperature-induced portion (as described in the first paragraph of this section) whereby the ambient temperature of 20°C and the length measurement on the 6th day were used as reference points. Accordingly, the contractions which occurred due to shrinkage up to this age are not shown in the graphs. The final degree of shrinkage expected for the concrete dorresponds approximately to the shrinkage caused by drying at 105°C between the 140th and 150th day.

2.4.2. Flexural Bending Strength and Compressive Strength of Cement Paste, Cement Mortar and Concrete

/<u>65</u>

2.4.2.1. Measurement Method and Experimental Procedure

In the test on test cubes of concrete it turned out that because of the spread of individual values the development influenced by the processes in the cement paste cannot be adequately analyzed. Therefore, in conformance with the structural development studies, strength tests were also done on cement paste and cement mortar.

The prisms of cement paste (cf. section 2.1.1.4.) for the flexural bending strength test based on DIN 1164 [3] were stored until the test time in a saturated calcium hydroxide solution.

In accordance with DIN 1164, three prisms for each type of cement mortar (cf. section 2.1.1.4.) were used to test a cement sample for flexural tensile strength and compressive strength. The prisms were stored in water until the test dates. The concrete cubes provided for the compressive strength tests measured 10 or 20 cm on an edge. As mentioned in section 2.1.2.2., they differed only with respect to their storage conditions. After the 7th day some of them continued to be stored at approximately 20°C and 100% relative humidity ("moist storage"), the remaining

ORIGINAL PAGE IS OF POOR QUALITY

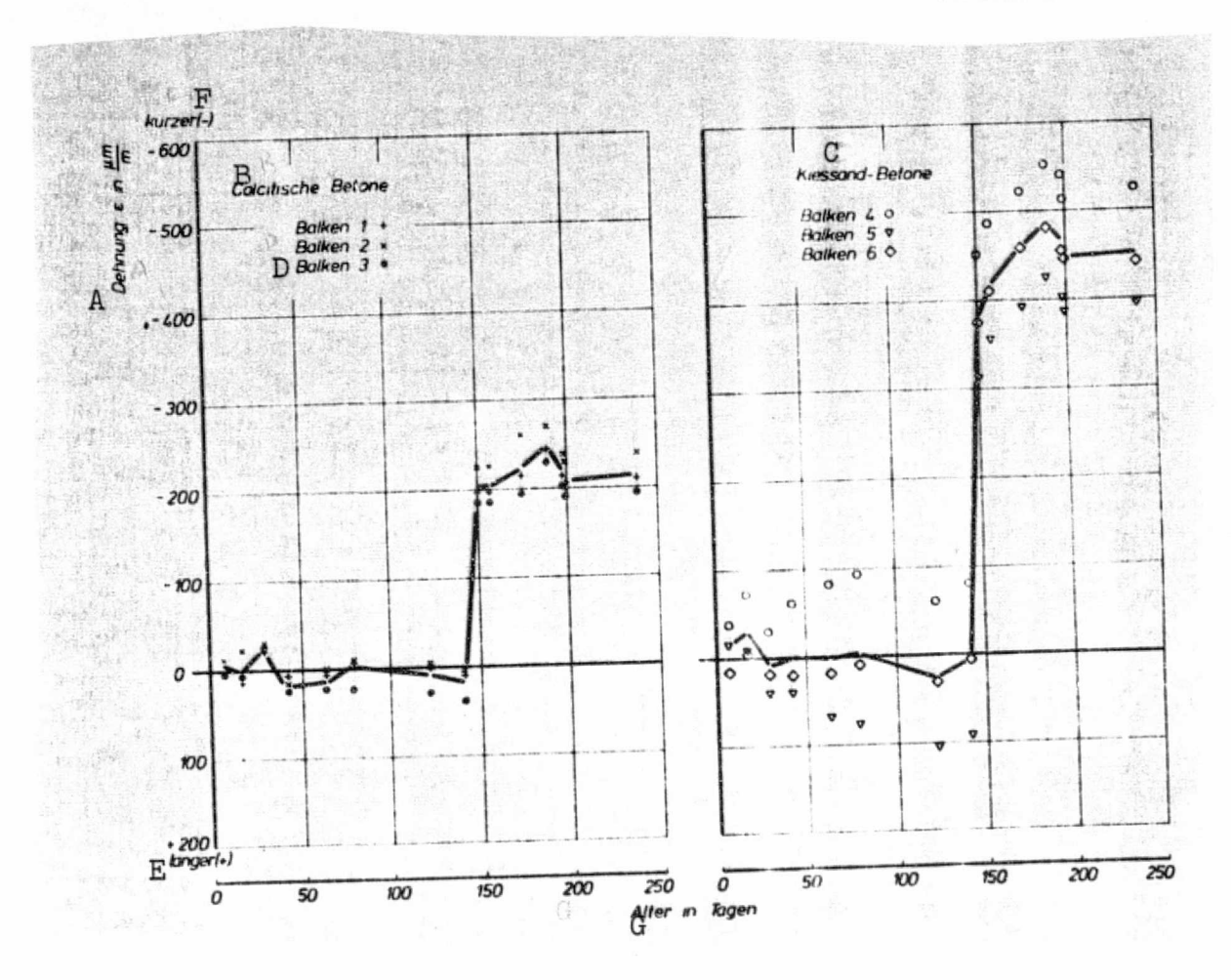


Fig. 53. Unit strains (ϵ) for concrete with calcite (beams 1-3) and gravel-sand aggregate (beams 4-6) due to contraction starting on the 6th day. The cylindrical test specimens were stored in sealed containers at temperatures between 20 and 70°C until the 140th day and then dried at 105°C.

Key: A. Unit strain

B. Calcite concretes

C. Gravel-sand concretes

D. Beam

E. Longer

F. Shorter

G. Age in days

portion was stored at 20°C and 45% relative humidity ("dry storage"). The compressive strength tests were performed on the respective test days on three test cubes in each case as per DIN 1048 [2].

2.4.2.2. Measurement Results

Fig. 54 summarizes the results of the flexural tensile strength (β_B) and compressive strength (β_D) tests on cement paste.

Fig. 55 shows the flexural tensile strength and compressive strength values measured on cement mortars of three randomly sampled cement specimens (cf. section 2.1.1.4.). Each symbol represents the mean of three individual values which, however, do not reveal any noticeable differences for the three cement samples so that mean value curves were drawn.

The individual values of the compressive strength tests (β_D) on the concrete test cubes measuring 10 cm on an edge were adapted to the measurements for the cubes measuring 20 cm on an edge by means of shape coefficients. These were derived individually for each type of concrete from the compressive strength values of 10 cm and 20 cm cubes for ages of 28 and 180 days. The graphs in Fig. 56 summarize the results for the calcite concretes (beams 143) and the gravelsand concretes (beams 4-6). Each symbol represents three individual values. The solid line indicates the change in compressive strength of the 20 cm cubes kept in "moist storage", while the dotted-line curve shows the change in compressive strength for "dry storage" conditions.

2.5. Correlation of Characteristic Values Influenced by Heat and Moisture Conditions

/<u>67</u>

2.5.0. Scope of Experiments

The development of the properties of the concrete in the beams is influenced by heat-moisture processes. Conversely, heat and moisture conductivity are dependent upon the special features of the pore space and the solid structure. This will be illustrated using as an example the influence of temperature and moisture content on the mechanical properties as well as thermal conductivity.

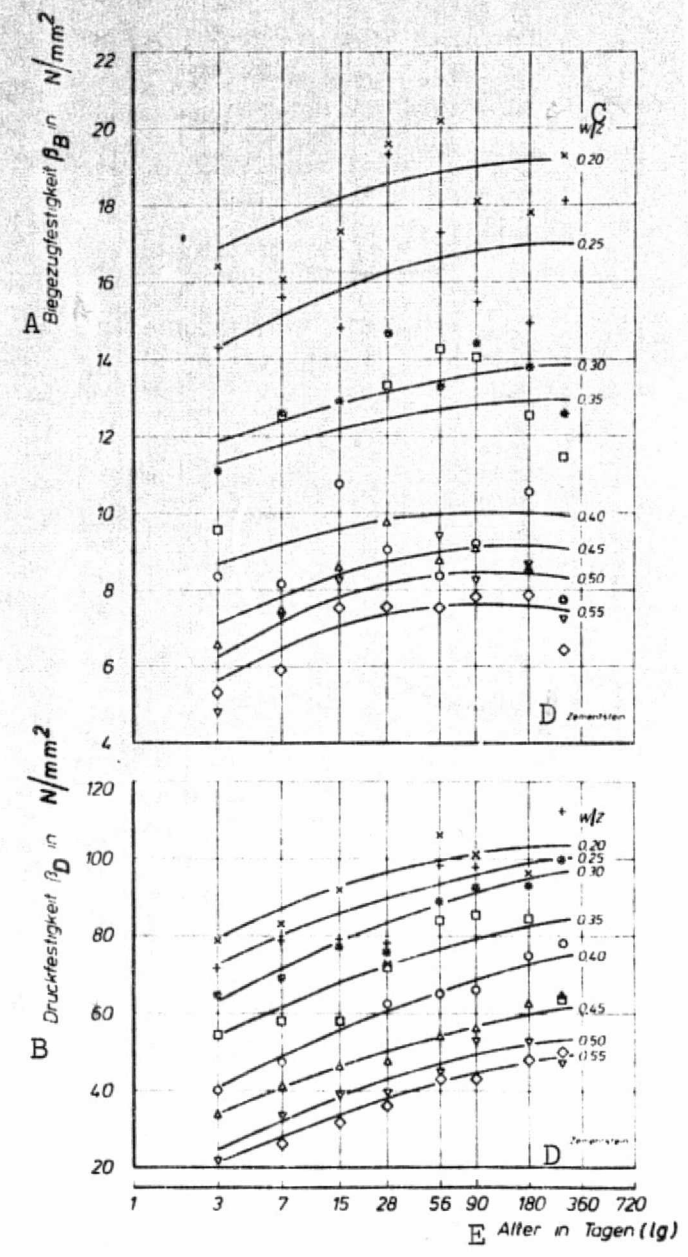


Fig. 54. Changes in flexural tensile strengths (βB) and compressive strength (βD) for cement paste prisms (water/cement ratio=0.20-0.55) stored in water, as a function of age.

Key: A. Flexural bending strength

B. Compressive strength

C. Cement paste

D. Water/cement ratio

E. Cement paste

F. Age in days

ORIGINAL PAGE IS OF POOR QUALITY

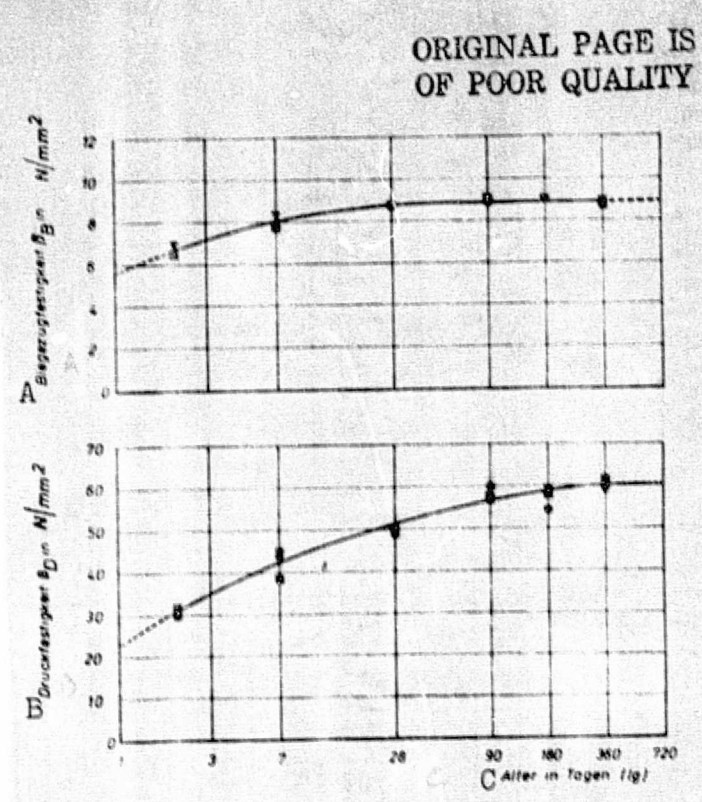


Fig. 55. Changes in flexural tensile strength (β_B) and compressive strength (β_D) for cement mortar prisms as per DIN 1164 as a function of age (three different cement samples).

Key: A. Flexural tensile strength

B. Compressive strength

C. Age in days

2.5.1. Setting Up the Water Balances

With respect to water content, up to the start of heating the beams form a closed system and afterwards, as a result of drying, they can only lose water, but not gain it, at the open face. This makes it easy to combine, in the form of balances, the local changes in water content over time and thus uniformly plot the data from section 2.2.3.

Figs. A 1-12 in the appendix show examples of the change in total water content and in the content of evaporatable water over time--measured at the measuring points for the moste important measurement planes or the immediately adjacent measuring points. These relationships as well as the total water concentrations before the start of heating, which were coordinated with the data in Table 4 for the individual beams, were used to set up the water balances (Figs. 57 and A 21-38 of the appendix) for six age stages in each case.

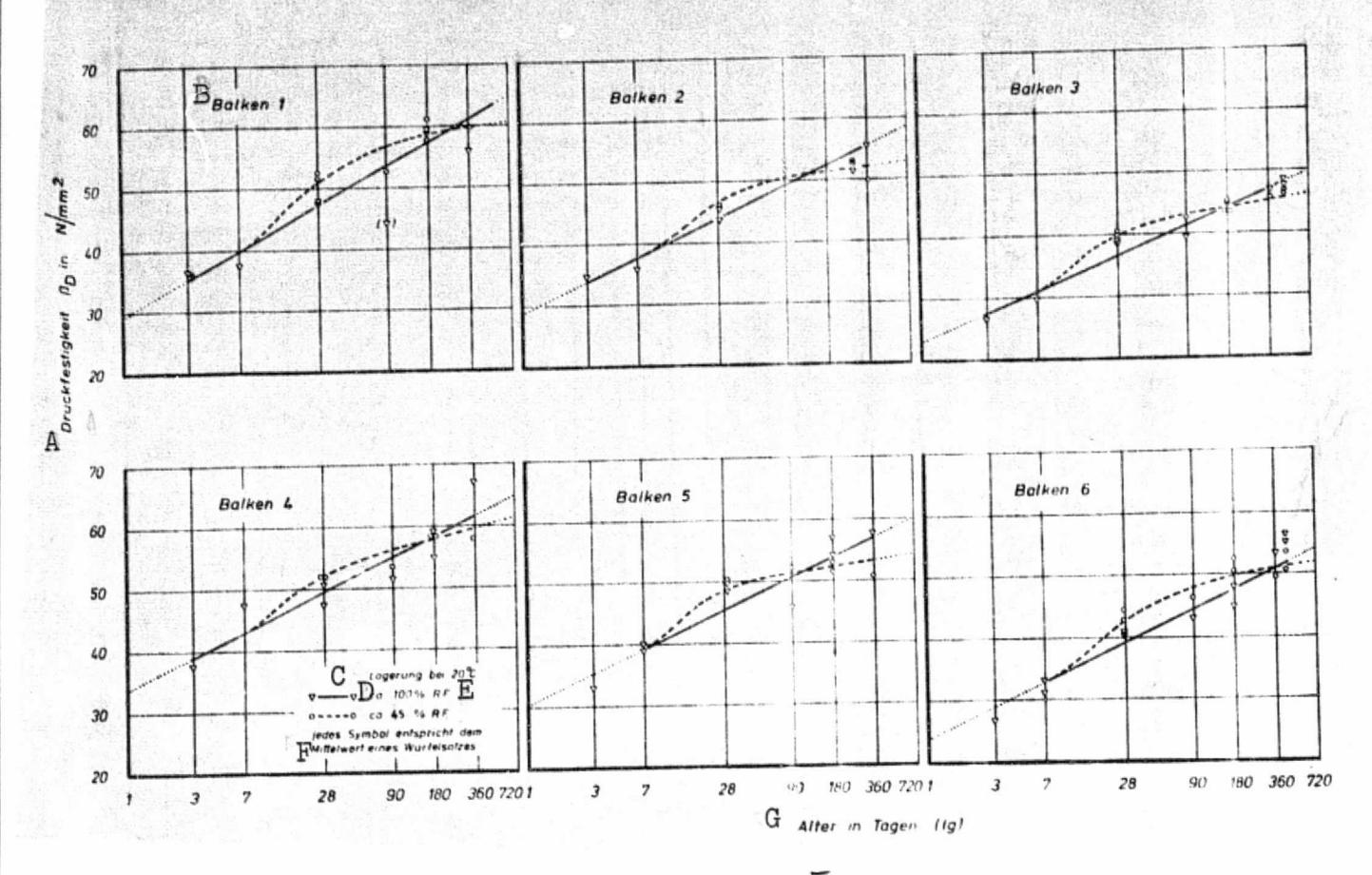


Fig. 56. Changes in compressive strength (β_D) as a function of age during "moist storage" (20°C/100% relative humidity) and "dry storage" (20°C/45% relative humidity) for the calcite concretes of beams 1-3 and the gravel-sand concretes of beams 4-6. Measured on 10 cm and 20 cm cubes.

Key: A. Compressive strength

B. Beam

e at ORIGINAL PAGE IS OF POOR QUALITY

C. Storage at

D. Approximately

E. Relative humidity

F. Each symbol corresponds to the average value for a set of cubes

G. Age in days

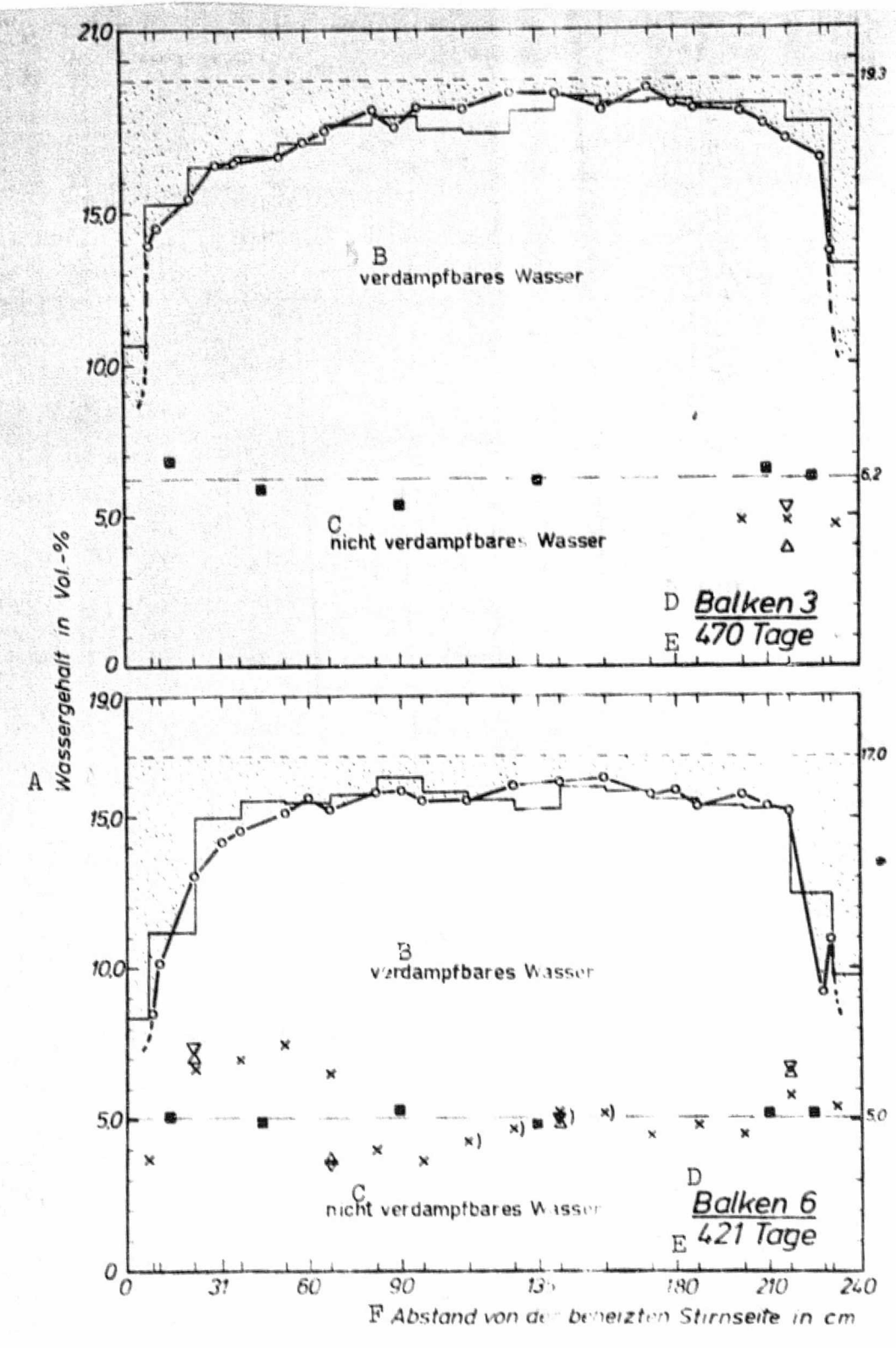


Fig. 57. Water content balances plotted over beam length for beam 3 (calcite concrete) at an age of 470 days and beam 6 (gravel-sand concrete) at an age of 421 days. The upper limit of the shaded areas corresponds to the mean initial water content; marginal regions estimated (also see Figs. A 21-38).

See key on following page.

Key: A. Water content in % by volume

B. Evaporatable water

C. Non-evaporatable water

D. Beam E. Days

F. Distance from the heated face

The total water concentrations at 23 measurement points (measured with a neutron probe) over the beam length were united by straight lines into a distribution curve for this purpose. In the edge regions next to the ends of the beams this curve could only be estimated. (Even by means of the other measurement methods used, however, the quantitative determination of water concentrations in these regions was not without problems.) Since the amounts of evaporatable and non-evaporatable water are added in the distribution curve, the concentration of non-evaporatable water can be deduced by subtracting the evaporatable portion (measured with the moisture measuring elements). The "x" symbols plotted in Fig. 57 for beam 3 (470 days) and beam 6 (421 days) correspond to the data from the measurement points along the middle of the beams, while the " ∇ " and " Δ " symbols represent the results measured with the elements placed /69 above and below this line (also see Fig. 5). In contrast to the graphs in Figs. A 21-38 in the appendix, the water concentrations measured after beams 3 and 6 were split are also plotted in Fig. 57, and in so doing the concentration of evaporatable water for the 17 beam segments examined were plotted in each case above the mean value for the non-evaporatable water (cf. step-like distribution curve). The values plotted for the concentration of non-evaporatable water (symbols) resulted in a mean value of 5.0% by volume for beam 6 and 6.2% by volume for beam 3 (dashed line).

The mean value of the total water content of the beams before the start of heating is plotted above the curves for the evaporatable water. The shaded area serves as a reference value for the water content lost within the time of the experiment. In analogy to this, areas above the dotted mean value line are to be regarded as gains in moisture.

2.5.2. Length Changes

The results of the measurements of the length changes of the beams and of the different influences on the strain of the beams (sections 2.2.4. and 2.4.1.) can be summarized as follows with the help of a systematic graph.

Fig. 58 shows the change in length of the beams relative to the start of heating on the 28th day (zero value). The solid line curve ($\Sigma\Delta 1$) represents the values measured with the Invar rod. It corresponds to the difference in length changes as a

result of temperature ($\Delta l_{[\theta]}$) and due to shrinkage and contraction ($\Delta l_{[s]}$) or contraction ($\Delta l_{[s]}$).

ORIGINAL PAGE IS OF POOR QUALITY

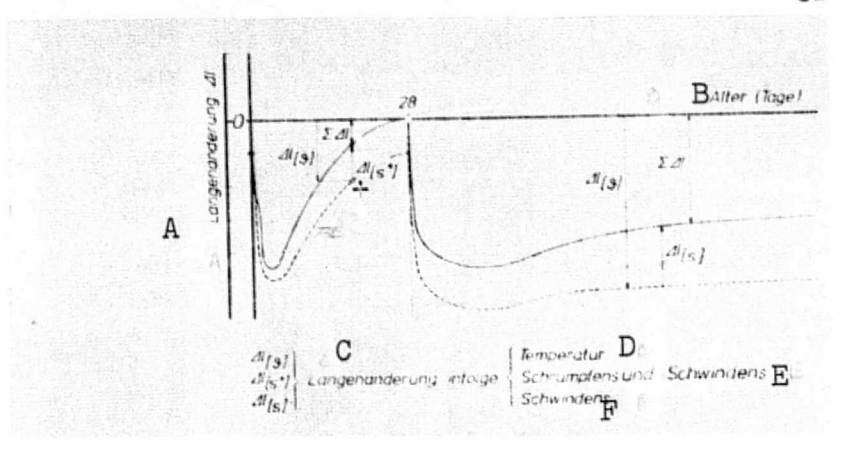


Fig. 58. Graph of length changes (Δ 1) of the concrete beams (reference walue: start of heating on the 28th day). The solid line curve represents the total length changes ($\Sigma\Delta$ 1) measured with the Invar rod.

Key: A. Length change

B. Age (in days)

C. Length change due to

D. Temperature

E. Shrinkage and contraction

F. Contraction

The decrease in volume due to shrinkage and contraction in the period after the concrete was poured is linked with hydration processes which are especially intense at the beginning. Since exothermic reactions are involved, these are responsible for the change in temperature and the resulting strains. From the shift over time of the temperature change maximums for the cement (Fig. 2) and the concretes (Fig. 9) if can be inferred that the temperatures of the concrete and the strains associated with these tempertures lag behind chemical processes. Above all, this is due to the fact that the mass of concrete at first heats up only slowly. After 24 hours, the concrete temperatures have passed through their maximum value and the elongation of the beams is again reduced. It can be estimated with the help of the thermal expansion coefficients (a) shown in Fig. 52.

At an age of 24 hours we arrive at a value of $\Delta l_{[\theta]} = 450 \ \mu m$ (with $\alpha = 5.8 \cdot 10^{-6} / ^{\circ}$ C) for the calcite concrete and $\Delta l_{[\theta]} = 750 \ \mu m$ (with $\alpha = \alpha \ 10.5 \cdot 10^{-6} / ^{\circ}$ C) [sic.] for the gravel-sand concrete. On the 28th day, the length changes due to heat are almost stopped. There remains a shortening due to shrinkage and contraction ($\Delta l_{[s*]}$), which, as shown in Fig. 34, amounts to about 100 $\mu m/m \cdot 2.4 \ m = 240 \ \mu m$ for both types of concrete. This contains a permanent component due to shrinkage in the early stage of hardening.

After the start of heating, the influences of thermal expansion and of contraction and swelling overlap one another, during which time changes in volume also occur which are due to transformations or new formations of hydration products. The length changes due to contraction and swelling, linked with thermal variations and drying on the exposed face, can likewise be estimated by using the values measured with the Invar rod and calculated by taking the thermal expansion coefficients as a basis. Thus, for the period after an approximately linear temperature distribution was reached in the beam, e.g. on the 60th day, calculated length changes due to temperature were obtained which are only slightly greater than the values measured with the Invar rod shown in Figs. 31 and 32, and indeed even taking into consideration the effects of moisture and temperature on thermal expansion (cf. [54]). From this it follows that at this point in time the length changes due to contraction at the ends of the beam and due to swelling in the interior cancel each other out, which is also suggested by the corresponding water balances of Figs. A 21-38 in the appendix. Only with progressive age does the influence of contraction on the total length changes increase, so that the corresponding proportion becomes greater and the two curves in Fig. 58 mcve increasingly father apart.

For the dry state, the expected values can be calculated by means of the degree of contraction for the concrete shown in Fig. 53. For the calcite concrete this is not greater than 200 $\mu\text{m/m}$ and about 450 $\mu\text{m/m}$ for the gravel-sand concrete. After four years of heating--which assumes complete drying-the beams of calcite concrete would accordingly show shrinkage contractions of about 500 μm and about 1100 μm for the gravel-sand concrete beams. Taking into consideration the length changes due to temperature, from these values we can calculate total contractions of about 100 μm for the calcite concrete beams and 300 μm for the gravel-sand concrete beams relative to the start of heating. In this connection, as is obvious from Figs. 31 and 32, the water/cement values for the concretes are especially important in the individual case.

2.5.3. Compressive Strength

Incomparing the compressive strength values which were measured on cores from the split sections of beams 3 and 6, it turned out, at least qualitatively, that higher compressive strength values were present in beam 6 in the region of higher temperatures (cf. Fig. 38 in section 2.2.5.2.), while the distribution of compressive strength values for beam 3 showed an opposite tendency. There was reason to attribute this contrary development to the limestone aggregate. Fig. 38 shows that the compressive strength of the calcite concrete had obviously been impaired up to a distance of about 125 cm from the heated end (corresponding to 80° to about 50°C). To show that the moisture losses were directly connected to the heating effect, another 6 cores measuring 5 cm in diameter and 5 cm in length were removed from sections K/L to Q/X of beam 3 whose changes in moisture content had apparently remained unaffected by the heat. The pressure-bearing surfaces of the cores were smoothed with cement mortar. Three cores for each section were stored for 50 days at 70°C and about 100% relative humidity until being tested for compressive strength along with the other cores in the moist state.

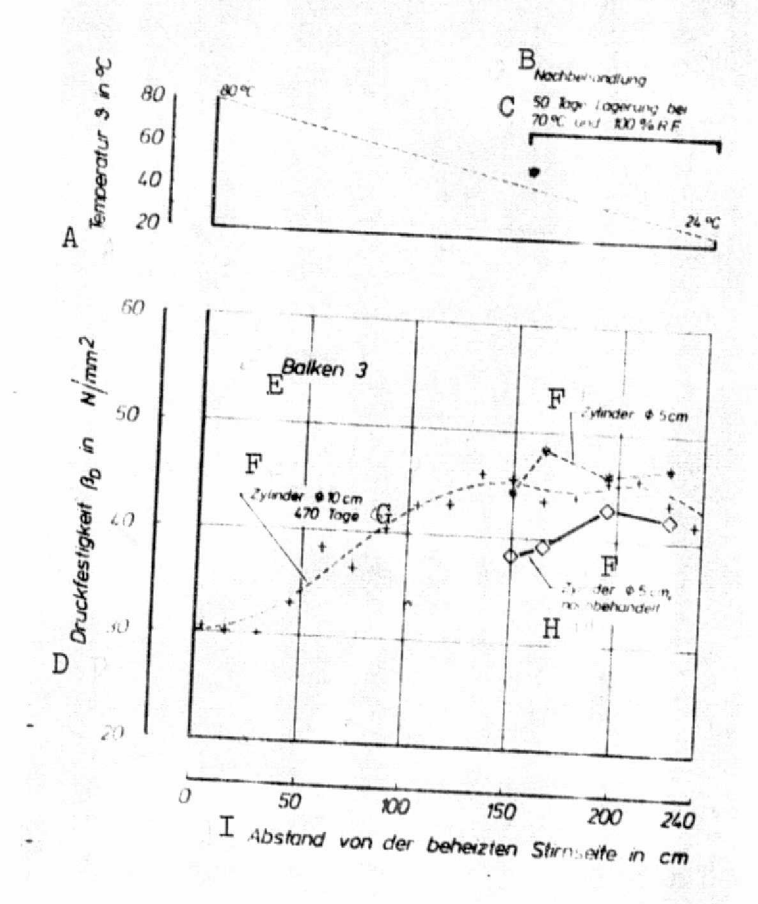
Fig. 59 compares the results of the compressive strength test on the specially stored specimens and the remaining specimens. The top graph shows the temperature distribution in the beam and the type and duration of storage treatment. In spite of the expected large deviations which occur in the compressive strength test on small test specimens, it is clearly obvious that the temperature treatment led to a reduction in compressive strength.

2.5.4. Thermal Conductivity and Water Content

/71

The amount of heat flowing through the beam from the heating plate during the experiment can be used to determine the thermal conductivity of the concrete provided that we may assume that the amount of heat carried through the beam cross-section is constant and independent of its distance from the heated end and that the flow lines of the heat flow run parallel to the long axis of the beam.

According to the theory of heat conduction in solid bodies [68], the heat flux density (q) is proportional to the effective temperature gradient (grad θ) with the thermal conductivity



ORIGINAL PAGE IS OF POOR QUALITY

Fig. 59. Impairment of compressive strength (β_D) of the cores of calcite concrete as a result of heat treatment after removal (also see Fig. 38).

Key: A. Temperature

B. Treatment after removal

C. Storage for 50 days at 70°C and 100% relative humidity

D. Compressive strength

E. Beam

F. Cylinder

G. Days

H. Heat-treated after removal

I. Distance from the heated end

ORIGINAL PAGE IS OF POOR QUALITY

(λ) as a proportionality factor:

The difference equation for the two-dimensional case is written as follows:

$$q = -\lambda \frac{\Delta \sqrt{3}}{\Delta 1} \tag{6}$$

with $\Delta\theta_n=\theta_n-\theta_{n+1}$, e.g. for successive measurement planes and 1 being the distance between the measurement planes.

The heat flow (\emptyset) which occurs during time (t) in the direction of the temperature drop is given by the quantity of heat (Q) with the cross-section (F):

$$\rho = \frac{Q}{1} = \lambda \cdot \frac{\Delta \sqrt{3}}{\Delta T} \cdot F . \tag{7}$$

The assumptions applicable when using the above equation, namely that no heat may be lost or added at the sides and, in particular, also that the body through which the heat flows must act homogeneously and isotropically, could be satisfied in practice only approximately. On the one hand, even by using a thicker layer of thermal insulation with greater thermal resistance and a denser arrangement of counterheating strips, it would not have been possible to completely exclude the impairment of heat conduction by edge effects. On the other hand, with the increasing age of the concrete and as a result of changes in its caloric properties caused by drying and humidification, we had to expect an impairment of the temperature field, i.e. the heat flow. These effect were important throughout the entire time of the experiment These effects after the start of heating. During the heating-up phase, it was to be expected that considerable quantities of heat would be taken up by the concrete and the materials of the experimental apparatus, depending on the thermal capacity, during the development of the temperature field and that as the temperature increased, the heat balance would be affected by physical and chemical processes.

Apart from the simplifications to be made in calculating the thermal conductivity, it was assumed that the heat flux density measurements would provide information on the changes in the temperature distribution and moisture distribution.

As is obvious from the changes in heat flux density shown in Fig. 14 and from the temperature distributions over beam length in Figs. 11 and 12, almost stationary conditions for the heat flow can obviously be counted on for concrete ages above about 140 days, so that Eq. (7) could be used to determine the heat conductivity for the individual beam sections as a function of the age of the concrete. For the 17 sections, after taking into consideration a correction factor determined on the basis of heat flux density control measurements -- in particular, on the exposed end of the beams -we obtained the characteristic $(q \cdot \Delta 1/\Delta \theta)$ values for beams 2 and 5 in Fig. 58 [sic.] as a function of the age of the For the reasons already discussed, the fitted curves are to be regarded as influx curves for the quasistationary case (about after the 140th day) and -- like the equations derived below--are to be regarded as approximations because of the simplifications described. With gradual drying until all of the evaporatable water has been lost, the thermal conductivity as a function of water content may be derived for temperatures between about 20° and 80°C for each beam section using such heat conductivity values as plotted in Fig. 60--assuming stationary conditions. As the water balances (Figs. 57 and A 23, 26, 32 and 35 in the appendix) show, the beams had not yet sufficiently dried out, however, to make such an evaluation worthwhile. By contrast, Fig. 61--in which the heat conductivity values as a function of water content have been plotted, but without taking temperature into consideration--clearly shows that the data are concentrated primarily in the region of high water content. Closer examination of their association with certain temperture ranges revealed relationships which corresponded to the heat transmission equation in moist substances explained by Krischer [59]. Accordingly, beside heat conductivity, processes in the solid structure dependent on moisture content and temperature must be distinguished. So water vapor diffusion is responsible for the increase in heat transmission in moist substances in comparison with dry substances in the hygroscopic range. heat conduction caused by vapor diffusion is strongly dependent on temperature and, under normal pressure conditions at temperatures above 59.3°C, exceeds the heat conductivity of water, Higher values are given by other authors (e.g. [94]).

The graph in Fig. 62 taken from [59] illustrates the phenomena mentioned. It shows the dependence of heat con0 ductivity on moisture content for temperatures $0<59^{\circ}\text{C}$ (case a) and $0>59^{\circ}\text{C}$ (case b). Accordingly, for moisture concentrations between the dry and water-saturated state of a substance, different values for heat conductivity are to be expected. While the curve for temperatures $0<59^{\circ}\text{C}$ constantly rises

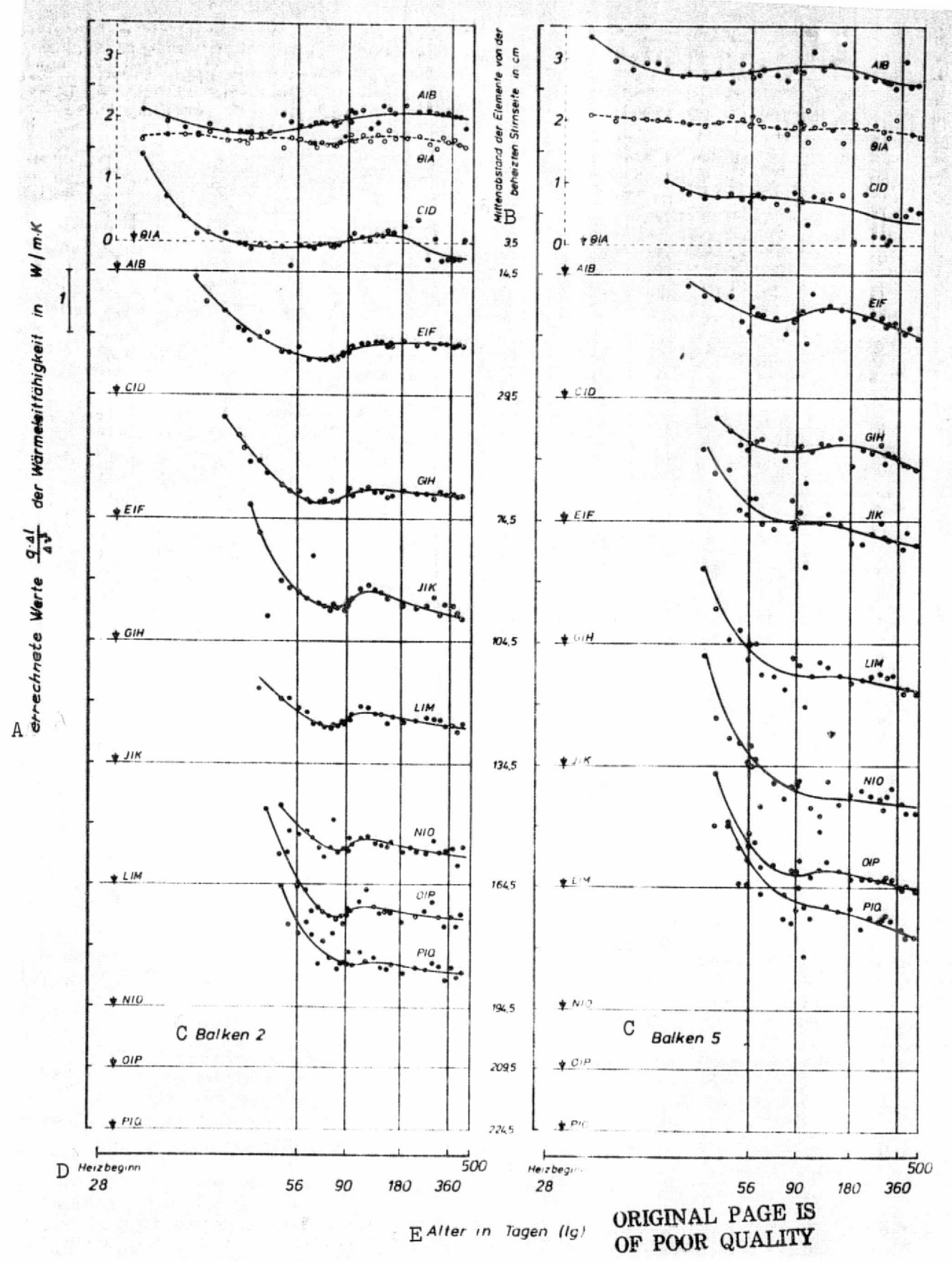


Fig. 60. See caption and key on following page.

Fig. 60. Calculated heat conductivity values $(q \cdot \Delta 1/\Delta \theta)$ for selected sections $\theta/A...$ P/Q of beams 2 and 5 as a function of age.

Key: A. Calculated heat conductivity values

> B. Center distance of the elements from the heated face

C. Beam

D. Start of heating

E. Age in days

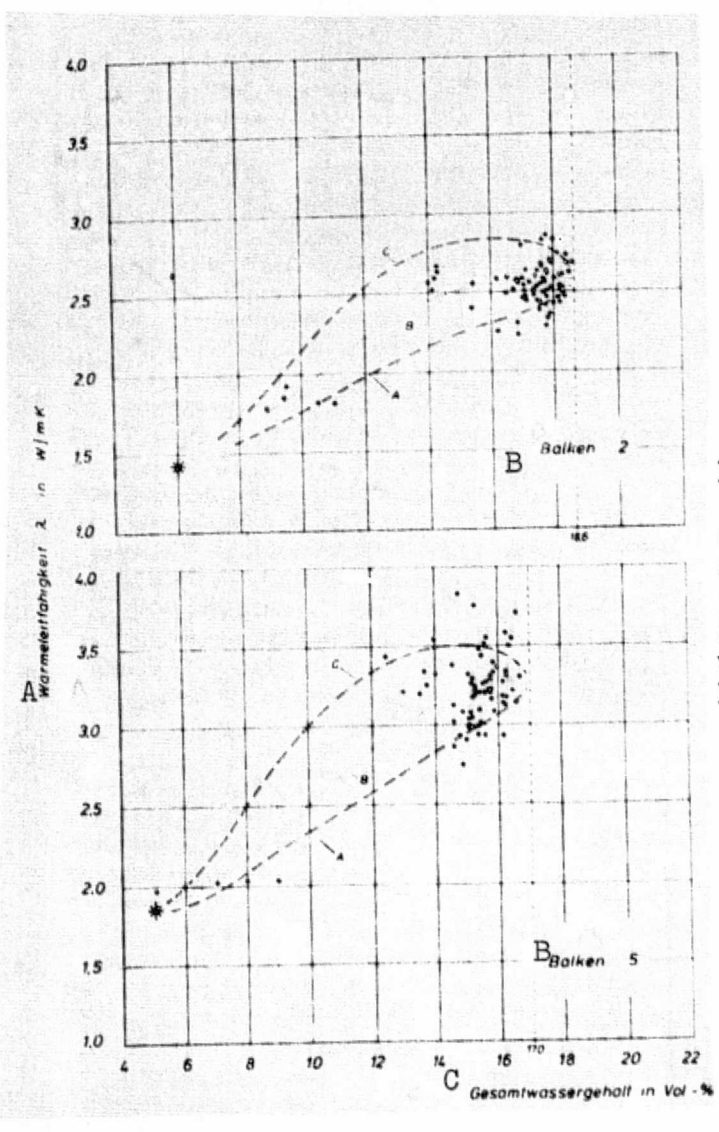


Fig. 61. Graph of heat conductivity (λ) as a function of total water content for temperatures between about 20°C (curve A) and about 80°C (curve C) for calcite concrete (beam 2) and gravel-sand concrete (beam 5) with fitted curve (B). Also see Fig. A 39.

Key: A. Heat conductivity

B. Beam

C. Total water content in % by volume

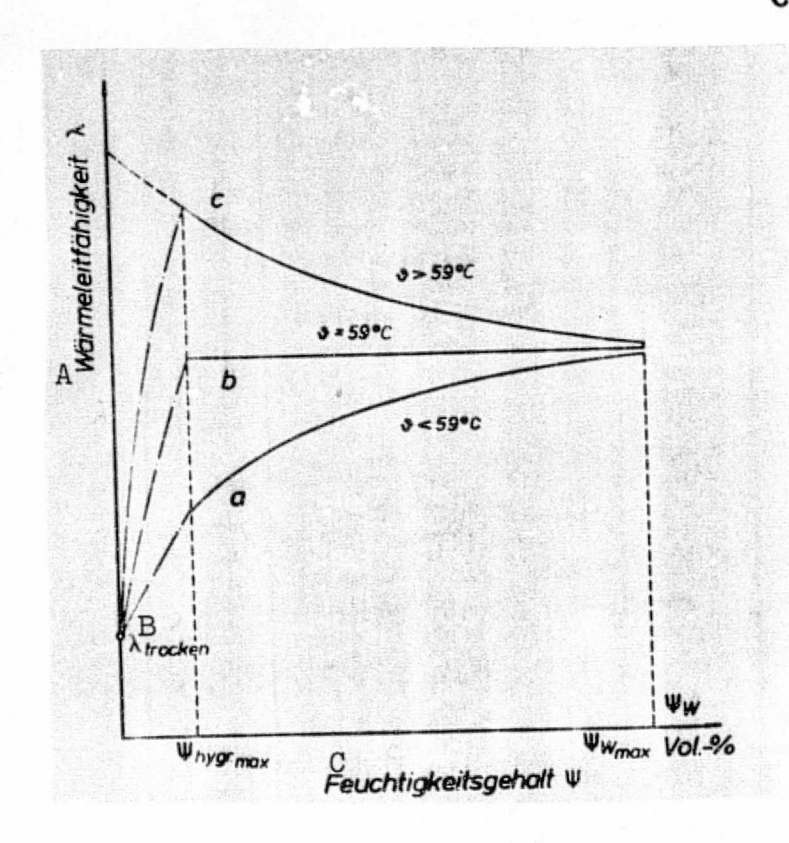


Fig. 62. Characteristic heat conductivity (λ) curve for moist substances at different temperatures, after Krischer.

Key: A. Heat conductivity

B. Dry

C. Moisture content

(case a) for temperatures 0 > 59°C it reaches a maximum in the region of the so-called hygroscopic moisture content [27] and decreases with increasing moisture content. For 0 = 59°C, it remains constant after reaching the hygroscopic moisture content maximum.

Since the pore system is heterogeneous and, for example, in the hygroscopic range diffusion transport does not take place in all pores, the actual path of such measurement curves is smoother than suggested by the graph in Fig. 62 (cf. [60]).

The estimated curves A and C in Fig. 61 indicate the expected curves for calcite concrete (beam 2) and gravel-sand concrete (beam 1) for temperatures of about 20°C and about 80°C respectively. Curve B, which is also plotted in the graphs of Fig. A 39 of the appendix for beams 1, 3 and 4, serves as an auxiliary curve. It was obtained by means of a nonlinear regression (third order polynomial) with the help of a computer.

The results of the heat conductivity measurements (after the test specimens were dried at 105°C until a constant weight was reached) plotted in Fig. 63 were included in the graphs of Fig. 61. It turned out that there was no dependence on

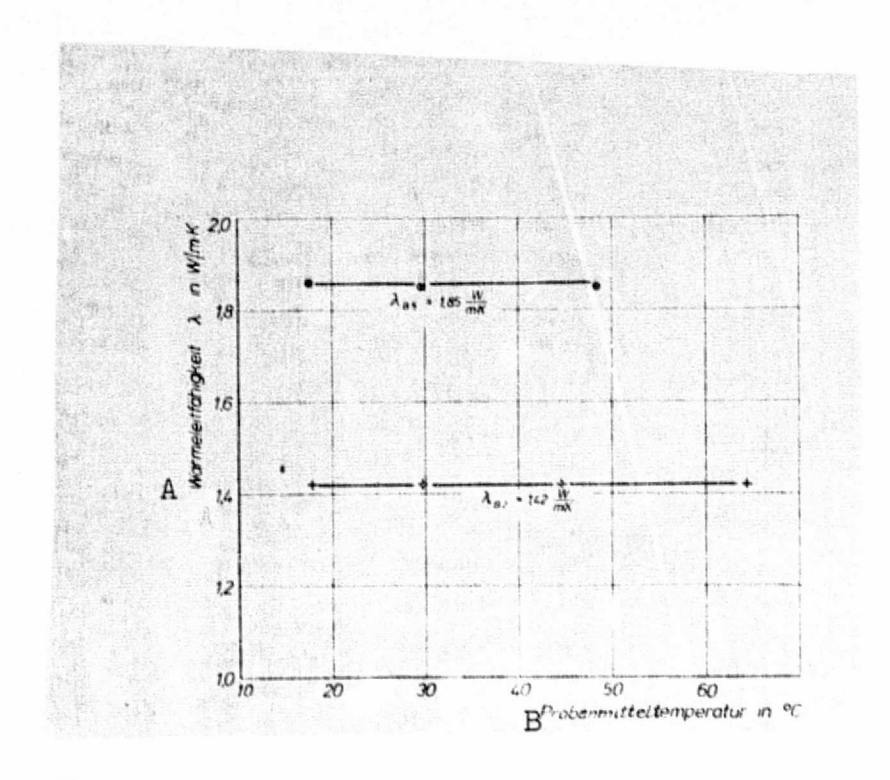


Fig. 63. Heat conductivity (λ) as a function of temperature, measured in accordance with DIN 52 612 on dried specimens. Mean values for calcite concrete (beam 2) and for gravel-sand concrete (beam 5).

Key: A. Heat conductivity

B. Mean specimen temperature

temperature for the temperature ranges from 18° to 48° or 64°C in the measurements made in the plate device, as per DIN 52 612 [7], on test specimens measuring 5 cm thick and 50 cm long. Because of this, the mean values of these measurements of 1.42 W/m·K for the calcite concrete and 1.85 W/m·K for the gravel-sand concrete were plotted in the graphs in Fig. 61. The boundary lines (vertical, dotted lines) for the water-saturated state were estimated on the basis of total water content curves, like those shown in the examples of Figs. A 1-12 of the appendix. They represent the maximum water content achievable under the special temperature and moisture conditions. In conclusion, it should be noted that in the case of the actual shape of heat conductivity curves starting from the dry state, an initially slow rise and then a sharp rise is recorded becasue the effect of vapor diffusion in the pore space increases.

174

3. Discussion of Test Data

3.1. Thermal Processes in the Concrete Beams

3.1.1. Heat of Hydration Effect

As a result of the heat of hydration, temperatures of nearly 60°C were reached in the concrete (Fig. 9), although the beams were not provided with thermal insulation on top. Fig. 2, which compares the change in temperature of a blast furnace cement HOZ 350 L with that of portland cement 450 F used in these experiments, reveals that the portland cement, in spite of the comparatively small heat of hydration of 273 J/g after 7 days for cements with high initial strength (also see the Table in [95]), shows intense production of heat within the first 8 hours after the concrete is poured. Thereafter the temperatures drop rapidly and already after about 20 hours they lie below the temperatures of the HOZ 350 L cement. Even if we consider the fact that the cement paste will show comparatively high strength values in the first hours, the structural stresses resulting from the increase in temperature surely have an adverse effect on the properties of the matrix. This is especially true for the concrete with the calcite aggregate, whose thermal expansion coefficient is about twice as small as that of the cement paste (cf. section 3.4.). Moreover, in the case of massive structural members, problems will especially arise due to the fact that, because of the irregular temperature distribution, stress states must be expected during the initial hardening phase [96].

3.1.2. Heating Effect

Immediately after the start of heating on the 28th day, the temperatures in the beams nearly matched the ambient temperature (Fig. 9); only the core regions still showed slight differences up to a maximum of 2.5°C. After the start of heating, the temperatures in the measurement planes continue to rise in the measurement planes, depending on the distance from the heated surface (Figs. 11 and 12). heat losses on the long sides are largely compensated for by means of the heating strips in the thermal insulation, a nearly straight-line temperature distribution over the beam length is established in all of the beams at an age of about 50-60 days. Figs. 11 and 12 show about the same temperature differences (corresponding to a temperature gradiant of 0.25°C/cm) between the measurement planes. do not reveal specific differences for the types of concrete and the water/cement ratios. A striking feature which indicates the sensitivity of the experimental apparatus is that the set-point corrections, which had to be made on the heating plate regulators, are passed along through the beams in the form of fluctuations in the temperature curves. expected, neither do the graphs of Fig. 13 reveal differences in the temperature distributions as a function of age, but it is clear that for all of the beams there is a "take-off region" next to the heated end which covers a section of the beam measuring about 7 cm (section 0/A) and shows a slight bend in the temperature distribution curves.

As already pointed out (section 2,2,1,2,), the locally somewhat higher temperatures in the lower regions of the /75 beam cross-sections can be explained by the influence of gravity on the moisture distribution. As Pihlajavaara [97] has shown experimentally, gravity influences moisture conduction in cement mortar. Accordingly, an increase in the moisture content from top to bottom--even if slight--would also be expected within the beam cross-sections which, for example for temperatures below 60°C, would lead to an increase in heat conductivity (cf. section 2.5.4.) and consequently to a change in the temperature field. In the context of a theoretical study of this phenomenon, Pihlajavaara and Ranta [98] also discuss the importance of the pore structure in this connection. Lykow [99] reports, for example, that in pores with radii < 104 nm, the influence of gravity can be ignored with a degree of accuracy of 6%. In our experiments, it is assumed that, above all, density differences within the concrete also overlie the influence of gravity, so that a relationship cannot be directly demonstrated. To be sure, the measured values of the content of evaporatable water in planes provided with two moisture measuring elements also

indicate a locally greater concentration in the lower regions of the cross-sections (see, for example, Figs. A 30-38 of the appendix for the gravel-sand concrete beams).

The change in heat flux density as a function of age shows clear differences (Fig. 14) which—since the experimental conditions were identical for all the beams—may likely be a function only of the type of concrete and the water/cement ratios. so the heat flux density for the beams with calcite aggregate is smaller by about 25% with respect to those with gravel—sand aggregate after the heating—up phase. In addition, the heat flux density increases as the water/cement ratio increases, and obviously more so in the case of the gravel—sand concretes than the calcite concretes. All of the curves show the same characteristic shape, which may be interpreted as follows.

The initial high heat flux densities occurring after the start of heating are primarily due to the fact that the concretes and the evaporatable water contained in them "capacitively" absorb heat when the temperature distribution is built up. process is largely completed after 50-60 days, so that only the heat carried to the exposed end is given off by the heating plates onto the beams, i.e. the sharply falling curves break After a few days, however, they rise again and then after reaching a maximum obviously tend towards an asymptotic equilibrium state. The at first unexpected shape of all of the curves. coupled with the appearance of a minimum, towards the end of the heating-up phase suggests that the heat flow is impaired by exothermic processes which emerge as heat sources in the concrete. In the first place, these obviously involve processes accelerated or first introduced by the increased temperature. According to Kuhl [100], we have to "imagine hydraulic hardening as a process in which an energy-rich, unstable system changes into a lower-energy, more stable system." At tempera+ tures above 20° or 30°C, but particularly during the so-called hydrothermal hardening, these are essentially the same processes, however the solution equilibriums are expected to be shifted and the reaction accelerated, during which the production of heat increases. After reaching the above-mentioned temperature gradiant, the reactions do not suddenly come to a stop, but slowly slow down--as shown in Fig. 14--up to about the 120th day where the heat flux density curves drop only slightly and then correspond approximately to a straight line, the slight slope of which is basically due to changes in heat conductivity.

The thermal processes in the beams from the start of heating onward can thus be schematically subdivided into three periods. The first period, the heating-up phase, is finished

after about 50-60 days when an approximately straight-line temperature distribution has become established in the longitudinal direction of the beams. The end of the second period, at an age of about 140 days, is characterized by the fact that the concrete itself can be considered free of heat sources. This is followed by the third period, characterized basically by drying processes, and in view of the fact that structural changes in the cement paste are now perceivable only over longer intervals, it can be regarded as "quasi-stationary".

3.2. Moisture Processes in the Concrete Beams

3.2.1. Moisture Content and Chemical Bonding of Water

Following the terminology of Powers and Brownyard [14], the distinction used between evaporatable and non-evaporatable water conceals—as already mentioned—certain uncertainties due mainly to the fact that as a result of drying at 105°C the water bound adsorptively in the pore space cannot be completely removed.

In section 2.3.1., a thermogravimetric method was used to analyze the dehydration behavior of cement paste during heat treatment. The cement paste was stored in a saturated calcium hydroxide solution until the test dates. Accordingly, the pore space can be regarded as being nearly filled with 176 water. Even the water consumed by hydration could be replaced. With respect to the data plotted in Fig. 40, it must be taken into account that moisture losses cannot be avoided even when extreme care is exercised during the crushing of the test material (200 mg) for the thermogravimetric analysis. Since primarily capillary water is released after the material is crushed, the cement paste with the highest water/cement ratio also shows the greatest error, i.e. the curves shown in the right-hand graph of Fig. 40 for 20°C for cement paste with water/cement ratios of 0.3, 0.4 and 0.5-which respresent the sum of all weight losses up to the final weight of 700°C--are in reality higher, depending on the water/ cement ratio. In view of the comparison with the results obtained in connection with the heat treatment, it should be pointed out that the reference temperature is 1000°C in the case of the heat treatment, which obviously produces a somewhat greater loss in comparison with the final temperature of 700°C in the thermogravimetric analysis.

The curves in the right-hand graph of Fig. 40 were based on measurement routines like that shown in Fig. 39. The reference temperatures were not chosen arbitrarily, but they

delimit characteristic dehydration processes which are superimposed by a continuous course of dehydration.

For the most part, the water expelled between 20° and 110°C is free water and to some extent adsorptively bound water. Czernin [101] refers to the fact that at temperatures around 105°C the gel water is also completely expelled. In addition, longer temperature treatment, even below 100°C, leads to transformation of the calcium sulfoaluminate hydrates (ettringite, monosulfate) with the release of water [102], i.e. it leads to losses which, in view of the calcium sulfate content of the cement listed in Table 2, cannot be ignored.

Above 100°C, the weight loss curve in Fig. 39 is flatter, but to begin with with a nearly constant slope. Moreover, adsorptively bound water is certainly also involved to a small extent in the weight loss between 110°C and 155°C (Fig. 40), but above all, water from the calcium silicate hydrates (CSH phases) is also increasingly involved, since the pore water is already completely expelled. This dehydration curve, characterized by an initial sharp rise followed by a leveling off of the weight loss curve above 155°C (Fig. 39), is confirmed by an estimate made by Harmathy [63] on the basis of thermogravimetric and differential thermal analyses. Thereafter the temperature-dependent change (corresponding to the differential quotient formed from the reaction time and temperature) of the CSH phases increases sharply above 100°C in an idealized cement paste and reaches a maximum between 150° and 200°C. According to an article by Ramachandran [103], a product obtained by complete hydration of C3S gives off the intermediate layer water of the tobermorite-like phase between 170° and 210°C. According to Lea [104], a substantial portion of the dehydration devolves on calcium aluminate hydrates (CAH phases) in the range up to 200°C.

The CSH phases give off water with increasing intensity between 200°C and 650°C, after which dehydration again increases and comes to a stop above about 800°C [63]. Water from the CSH phases is basically responsible for the weight loss shown in Fig. 40 up to 430°C (the sharp rise of the weight loss curve in Fig. 391is due to the high heating rate up to 380°C). The weight loss starting immediately above 430°C, which is characterized by an abrupt rise in the curves shown in Fig. 39 and in Fig. 40 is marked by a jump for the curves within the 430°C temperature stage, is caused by the conversion of calcium hydroxide (Ca(OH)₂) into calcium oxide (CaO).

According to Fig. 40, the weight losses after the break-down of the calcium hydroxide, i.e. up to the 570°C temperature stage, are still only small. What may be happening here is that water is continuously being given off from the CSH phases (see above), as suggested by the flat course of the weight loss curve in Fig. 39. The subsequent rise again matches the data in [63], according to which up to about 700°C a second maximum occurs in the temperature-dependent variations in the CSH phases. The water content, which is no longer measured in the thermogravimetric above 700°C, would be estimated at about 15% of the reaction amount caused altogether by the calcium silicate hydrates.

Harmathy, in his estimates for an idealized coment paste which he uses to evaluate thermal properties of concrete, starts with the simplifying assumption that only two components are involved in the dehydration process, namely CSH phases and calcium hydroxide. All components of the cement paste contribute to the more or less continuous release of water. Apart from the already mentioned calcium sulfoaluminate hydrates, which are converted at comparatively low temperatures, magnesium hydroxide (Mg(OH)2), among other things, which as a rule is present only in a small amount, gives off water below 200°C. As Kuhl states [105], magnesium hydroxide is no longer stable at 190°C, where its dissociation pressure reaches atmospheric pressure. Czernin [106] states, for example, that what occurs first is dehydration of the hydration products containing alumina and iron oxide between about 250° and 350°C, in the process of which, calcium silicate hydrate loses only about 20% of its water component, while the main portion escapes betweer 400° and 700°C.

The stability of the hydration products of the cement paste is a function of temperature and vapor pressure conditions. Additional references can be taken from the literature [107, 108]. In this connection it must be borne in mind that the temperature ranges indicated by many authors depend on the special experimental conditions in each case. For our purposes, the estimate made of dehydration behavior [63], which is qualitatively confirmed by the data plotted in Figs. 39 and 40, should be sufficient.

From the data plotted in the left graph of Fig. 40 for heat treatment at 105°, 550° and 1000°C of cement paste with water/cement ratios between 0.20 and 0.55, the following supplementary remarks can be made.

/77

The weight loss at 105°C (differences with respect to the 20°C lines) becomes smaller with increasing age, above all for water/cement ratios > 0.4, which, among other things, indicates the decrease in pore volume as a function of age.

The weight loss at 550°C (differences with respect to the 105°C lines) obviously also increases with the water/cement ratio. This may be due to the fact that to begin with the hydration tendency becomes greater with an increasing supply of water, so that more water is chemically bound per unit time [15]. More important, however—and this is also verified by the approximately parallel path of the curves at the same distance apart—is that for water/cement ratios <0,4, there is an increasing residue of non-hydrated clinker granules which do not contribute to the chemical bonding. As already shown with respect to the thermogravimetric analysis, a portion of the adsorptively bound water is also contained in this weight loss.

The rest of the weight loss at 1000°C is basically due to the release of water by CSH phases.

With respect to the method of determining the content of evaporatable water by heat treatment at 105°C, it can be said that this method does not measure a portion of adsorptively bound water which cannot be more precisely defined. On the basis of the weight loss curves, however, it can be inferred that this proportion is small in comparison to the amount of water released by CSH phases above 100°C. By means of further heat treatment at 500°C, the substantial portion of the water contained in the CSH phases as well as the hydroxyl water content of Ca(OH)2 are expelled. However, this method does not determine the final dehydration of the CSH phases, which correspond approximately to the weight loss of 3% within the temperature range from 570° to 700° shown in the right-hand graph in Fig. 40.

In spite of the overlapping dehydration processes, the evaporatable water (i.e. free water + adsorptively bound water) is therefore comparatively well represented by the loss due to drying at 105°C. By contrast, the error in the determination of non-evaporatable (i.e. chemically bound) water by heat treatment at 550°C is obviously greater. Since matrix mortars with limestone aggregate were also to be included in the experiments, a temperature greater than 550°C could not be chosen because of the risk of thermal decomposition of CaCO3. In this respect, neither could the approximation method for cement paste suggested by Czernin [109] be used here.

3.2.2. Effects of Hydration and Moisture Conduction on Water Content

3.2.2.1. Changes in a Closed System

The fresh bulk densities listed in Table 3 were measured on six sets of cubes for each of the concretes used to make beams 1-6. These values can be applied to the beam concretes only if the special compacting conditions are taken into account. The dry bulk densities given in parentheses in the upper half of Table ! for the six beams were therefore estimated on the basis of the composition of the concretes and the weights of fresh concrete allowing for a concentration of chemically bound water of about 20% of the weight of the cement. For beams 3 and 6, the values are approximately equivalent to the mean values found for the samples of the beam concrete as described in section 2.5.5. (Table 4, line 1), whose standard deviation of s=±0.13 kg/dm3 is about equal for both beams. The degree of compaction obtained in a beam is a determining factor for the actual total water content of the concrete (line 3, Table 4). This remains the same until the start of heating on the 28th day, during which time, however, the ratio of evaporatable to non-evaporatable water changes due to hydration (beam 1 shows strongly pronounced local differences in compaction and is therefore not to be regarded as characteristic).

That the proportion of non-evaporatable water between the third and 28th day increases only slightly is shown in Fig. 42 for the matrix mortars from the calcite and gravel-sand concrete. In these graphs, the data for beams 1-3 and 4-6 were combined because differences as a function of water/cement ratios could not be detected. Comparison of the two (long dash) curves reveals that the content of non-evaporatable water of the calcite cement, which is primarily due to the high cement content of the calcite concretes (cf. Table 3) and is found in a comparable order of magnitude in the beam concretes themselves (cf. Figs. 57 and A 21-38 of the appendix) [sic.]. The two curves in Fig. 42 extrapolated up to an age of 180 days (short dashes) indicate that under constant temperature and moisture conditions after the 28th day, practically only a small increase would be expected. As is obvious from Fig. 40, the hydration reactions beyond 180 to 360 days increasingly come to a stop.

Fig. 41 gives a differentiated impression of the change in moisture content up to the 28th day. Since up until the start of heating the system can be regarded as closed and the matrix mortar test specimens show practically no changes in weight between the first day and the test date, the maturation progress of the concretes can be inferred from the graphs of

/<u>78</u>

Fig. 41. Obviously in the case of beams 4-6, the decrease in evaporatable water content between the 3rd and 28th day is greater, the higher the water/cement ratio, i.e. the amount of chemically bound water increases as the water/cement ratio increases. The curves for beams 1-3 reveal a corresponding tendency. The determination of non-evaporatable water content by drying at 550°C can only be used for purposes of comparison, because of the reasons explained in section 3.2.1.

3.2.2.2. Changes After the Start of Heating

3.2.2.2.1. Moisture Losses Due to Drying

The total water content on the 28th day is listed in the upper half of Table 4 for the six beams. The distributuion profiles in Figs. 25 and 26 reveal that the distribution curve deviates up to about ±0.5% by volume from the mean values. In the case of beam 1, the deviations are greater because of the reasons explained in section 3.2.2. Such variations in the total water content are linked with variations in bulk density in that a higher content of evaporatable water shows up at points with a greater pore volume.

With the start of heating, the release of moisture takes place unidirectionally through the exposed end of each beam. According to Fig. 16, the calcite concretes different the gravel-sand concretes in this respect in that they have lower initial losses. Thereafter, the curves are qualitatively the same.

The initially high weight losses are caused by the release of moisture at the exposed end--processes which correspond to the characteristic drying curve described by Krischer [110]. Thereafter, given a constant drying rate, water is first of all carried to the surface (exposed face) by capillary conduction until the moisture content at the surface becomes This is connected with an "inflection point" in the drying curve, the drying rate decreases and the "drying level" moves into the beam interior. the drying rate is a functin of external conditions (moisture content and flow velocity of the air) which may be regarded as identical for the six beams. The capillary properties of the concretes are a determining factor for the appearance of the inflection point. In Fig. 16, the change in drying rate for age stages between about 35 and 55 days is indicated by a "deflection" in the weight loss curves, in which connection a dependence on the water/ cement ratio of the cements, which is responsible for the

formation of the capillary pore space, can be detected. perspective graphs of Figs, 28 and 29 (and of Figs, A 13-16 of the appendix) confirm this relationship. For all of the beams, the total water content of the space coordinate lying closest to the exposed face (distance from the heated face = 230.6 cm) changes immediately after the start of heating (also see the change in evaporatable water content plotted in Figs. A 1-12 of the appendix for the space coordinates in question). The shape of the curves in Fig. 16 must not obscure the fact that the appearance of the inflection point does not coincide in time with the end of the heating-up phase. The beam sections involved in the release of moisture indeed experience an increase in temperature, but the quasi-stable state (cf. section 3.1.) is not yet reached. After the deflection of the curves, the weight loss tends to be a linear function of age. An expected continuous loss, in accordance with the theory for a unilaterally drying body [110] (with capillary hygroscopic drying characteristics) may indeed exist, but this is superimposed by a thermally induced moisture supply so that the weight loss curves rise almost in a straight The beams with gravel-sand concretes now obviously show slightly different drying rates and, to be sure, these appear to be all the greater, the higher the water/cement ratio. is not surprising, since the permeability of the pore system increases with the proportion of excess water which is a function of the water/cement ratio.

As the water balances of Figs. A 21-36 in the appendix show, the distribution of evaporatable water in the beam section at the exposed end changes only slowly after the inflection point is reached. To the extent that this can be detected, it is caused by drying in the region of the hygroscopic moisture content. The weight losses are due to processes in which moisture, as a result of the heating, is carried from the beam interior to the drying front which advances only very slowly in the beams. If, to begin with, we ignore the problem of the chemical binding of water influenced by the increase in temperature, then these thermally induced processes can be interpreted as described below on the basis of changes in the total water content (Figs. 28 and 29 as well as the corresponding water balances of Figs. A 21-36 of the appendix).

3.2.2.2. Interpretation of the Drying Curve Under the Effect of a Temperature Gradient

By the addition of heat, the water is placed into an excited state relative to the start of heating and depending on the temperature level reached. In particular, this results

in greater mobility of the water molecules. This system, which is in a state of energy disequilibrium, is striving towards a new equilibrium state. The disequilibrium is characterized by pressure and concentration differences which first of all try to balance themselves within the immediate environment, but they also represent the driving force for the "large-scale" moisture conduction coming into operation towards the exposed end of the beams.

So the initially marked fluctuations in total water content are presumably to be explained by the fact that different types of transport phenomena, changing with time, prevail within small regions of the beams so that, for example, concentrations of free water transported in the direction of a pressure gradient are reversed by capillary conduction in the opposite direction. Especially large variations in the total water content are found in the case of beam 1, which confirms the obvious assumption that these are primarily caused by local differences in the degree of compaction of the concrete. Regional variations in bulk density of this sort can practically not be avoided in concrete and, above all, influence the proportion of large pores. At this point it should be pointed out that what is involved here are certainly variations in the content of free water which, in adcordance with Fig. 20, are indeed also measured by the moisture measuring elements, but because of the simplified plotting in Figs. A 1-12 of the appendix they are evened out. The water absorption values (A) plotted in Fig. 37 for beams 3 and 6 may be used as a measure of the pore volume and the expected variations in density of the calcite and gravel-sand concretes.

Superimposed by the fluctuations, the change in total water content—i.e. the "large—scale" detectable processes whose effect is shown by the weight loss curves of Fig. 16—tends at first to fall linearly up to a concrete age between about 150 and 300 days. This can clearly be seen at the space coordinates in the immediately vicinity of the heated end. In this section the drying rate is constant. Thereafter it decreases and slowly goes to zero.

Fig. 64 shows a schematicized plot of the drying curve as derived from Figs. A 1-12 of the appendix for space coordinates

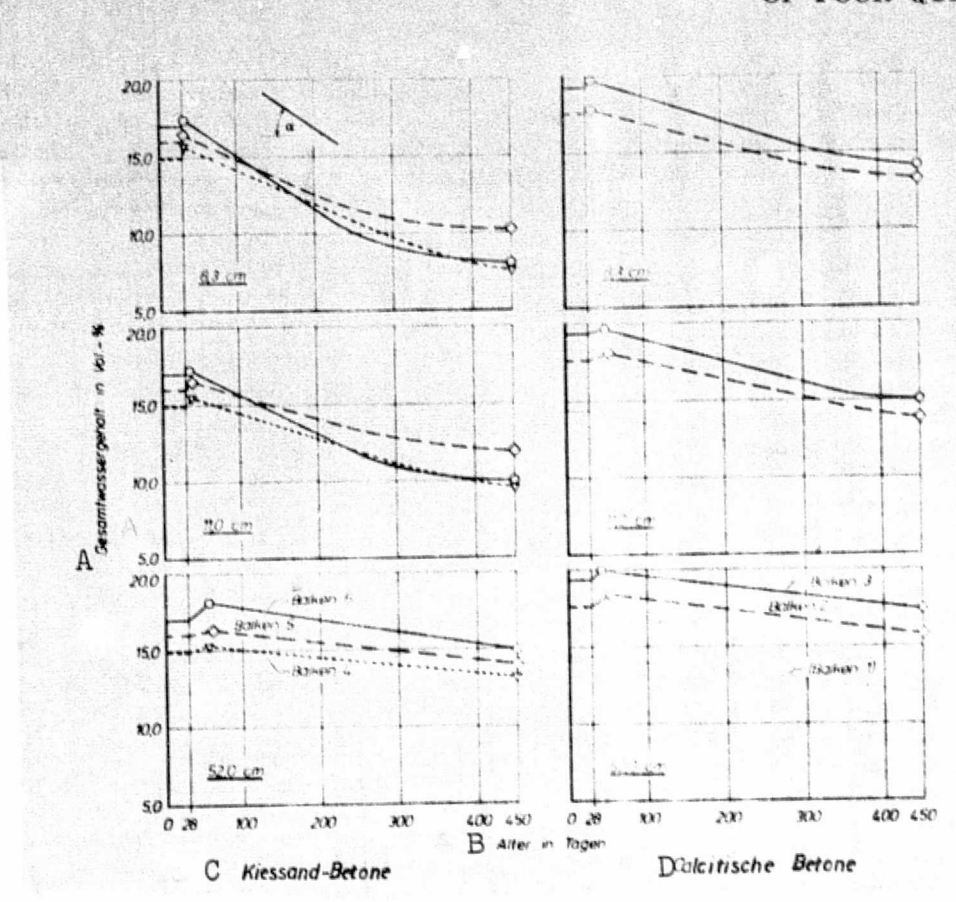


Fig. 64. Diagrams of the change in total water content at distances of 8.3, 11.0 and 52.0 cm from the heated end of beams 4-6 and 1-3 (derived from Figs. A 1-12 of the appendix).

Key: A. Total water content

B. Age in days

C. Gravel-sand concretes

D. Calcite concretes

E. Beam

8.3, 11.0 and 52.0 cm. The age of the concretes is plotted along the abscissus, and the total water content along the coordinates. Up to the 28th day, the total water content is constant, at first increases after the start of heating and then fälls off linearly. The greater the distance of the measurement point from the heated end, the later the inflection point of the curves appears. The increase in total water content which occurs immediately after the start of heating also becomes greater as the distance of the measurement point from the heated end increases, and indeed until the available pore

space has been completely filled with water.

The drying rate of the subsequent (straight line) sections (Fig. 64), is obviously different for the concretes—as can be inferred from the different slopes (tg α) and lengths of the straight—line portions of the curves—and moreover it is also a function of the location in the beam, i.e. temperature as well as the special properties of the pore system affect the drying curve. The section of constant drying rate ends when the larger pores are empty and the hygroscopic water content must be released. Since this water content, which is composed of free water in the tight pores and adsorptively bound water, is only slowly or only partially reduced in volume, drying of all the evaporatable water is not to be expected in the period of the experiments even for the heated end with a temperature of $\theta=80^{\circ}\text{C}$ (cf. the water balances in Fig. 57).

Fig. 64 clearly shows that for space coordinate 52.0 cm for both types of concrete, the period of constant drying rate has not ended even at an age of 450 days. As the distance from /80 the heated end increases, the drying rate becomes slower and the transition to the period of decreasing drying rate is less pro-The drying curves for beams 2 and 3 as well as 4 and 5 are obviously largely similar. They show about the same slope and are apparently shifted with respect to one another only by an amount determined by the respective water/cement ratio. Since the same temperature conditions prevail at corresponding space coordinates, similar transport properties can be expected for the period characterized by the constant drying rate. Variations may exist, however, in view of the hygroscopic region, a fact which can also be deduced from the different duration of the periods along the time axis. Accordingly, differences in the pore structure of the two concretes (primarily in the region of small pores) which affect the drying behavior are to be expected.

3.2.2.2.3. Non-evaporatable Water

The water balances (Figs. 57 and A 21-38 of the appendix) were set up to supplement the water content curves of Figs. A 1-12 of the appendix for the purpose of illustrating the influence of temperature and moisture conditions on the hydration reactions. Because of the failure of a few moisture measuring elements, only a few measurement points are available for beams 1-3. Therefore, the analysis is essentially limited to the distribution of non-evaporatable water in beams 4-6. On the whole, these beams do not reveal considerable differences.

It is possible that the long-lasting supply of evaporatable water leads to a slightly higher content of non-evaporatable water, which of course is not to be expected in the hot regions of the beams -- even with a sufficient supply of moisture -since crystalline formations arise earlier here which have a lower water content [111]. This tendency can also be inferred from Fig. 42 which shows a decrease in the content of non-evaporatable water at a greater age for the matrix mortar of both types of concrete, and this is independent of the local temperature conditions. The striking increase in the content of evaporatable water found immediately after the start of heating for the calcite matrix mortars might be linked with the formation of microcracks discussed in section 3.4., insofar as these cracks were available for absorbing water transported from the hot region. The nonevaporatable water content measured last of all on concrete specimens from beams 3 and 6 (symbols) show only small variations. The mean values corresponding to these data are plotted in all of the water balances (long-dash lines). They lie somewhat below the actual content for the reasons discussed in section 3.2.1. pertaining to the method used.

/81

3.2.3. Comparison of Results

Unfortunately, the experimental data of other authors [44-47] are mostly reported only as lump sum figures (cf. section 1.2.1.). Above all, there is a lack of graphs of the local drying curve as a function of age. England and Ross [47] give water concentration distributions similar to the water balances shown in Fig. 57 for beams ranging in length between 0.6 and 3.1 meters which were heated on the closed end to 80° and 125°C respectively. These disdistributions, ascertained after variable heating times in the beams, agree qualitatively with our data if we take into consideration, for example, the influence of the higher temperature, to which the closed end was exposed, on the drying curve, and bear in mind that, because of the experimental set-ups, a constant and unidirectional flow of heat in the beams was not guaranteed. The fact that McDonald [48] found only slight variations in his experiments in the region of heated end (approximately 65°C), may, among other things be due to the low temperature gradient as well as the short heating time. Therefore, the author also stesses that his experiments are not yet completed.

Yuan, Hilsdorf and Kesler have determined the drying behavior of cement mortar cylinders for different water/cement ratios, temperatures and air humidity values [112]. This systematic study reveals that the moisture loss of concrete is a function of all three variables. As the moisture content

decreases, however, the influence of temperature and relative humidity declines. This essentially corresponds to our data, according to which the drying process is determined by temperature, moisture content and the structure of the pore space. However, the drying diagram supplied by the authors [112] is applicable only for constant external conditions.

With to the dehydration of the beams, we can thus assume that the weight loss curves (Fig. 16) will at first continue to run approximately linearly, and indeed until the pore space of the cooler sections of the beams -- which is filled after the start of heating and then emptied by the release of water at a constant drying rate--contains predominantly hygroscopic water. The time required for this process is a function of the local moisture conductivity of the pore system and of temperature, also of the amount of moisture which must be carried from the respective adjacent, hotter section. Thereupon, the weight loss curves for the beams (Fig. 16) become increasingly flatter and asymptotically approach an end value, i.e. the drying rate goes to zero. The end value is characterized by the temperature-dependent equilibrium moisture concentrations. Reference [112] gives the corresponding values for cement mortar. The period of decreasing drying rate will be considerably longer than the preceding period. Fig. 57 clearly shows that beam 3 as well as beam 6, both of which are still in the period of constant drying rate, have lost only between 1 and 2% by volume of water after more than 400 days of heating in the center (approximately 0.6-2.1 m from the heated end).

3.3. Influence of Heat/Moisture Phenomena on the Pore Structure

3.3.1. Total Porosity and Open Porosity

In section 2.3. we examined the changes in pore space associated with chemical and physical processes in the cement paste. The total porosity (Ut) determined on the basis of density and bulk density measurements can be approximately equated to the actual pore space. By contrast, only a portion of the open pore space, namely in the radius range between about $55 \cdot 10^3$ and 4 nm, is measured with the mercury porosimeter. The pore volumes (UHg) in Fig. 47 are therefore even smaller than the total porosities shown in Fig. 43 (the corresponding pore volumes would be obtained by dividing with ptr $\cdot 10^2 \approx 2.3 \cdot 10^2$ (g/cm³)). On the whole, they correspond to the capillary pore space, whose minimum pore radii presumably measure 3-4 nm [20]. The difference between total porosity (Ut) and pore volume (UHg) thus characterized the gel pore

space with average pore radii between 1 and 2 nm [14] and maximums around 1.5 nm.[21].

The macropores to be attributed to the actual pore volume of the concrete are contained in the water absorption values (A) of Fig. 37, left, (in section 2.2.5.) for concrete samples of beams 3 and 6. Fig. 37, right, shows the order of magnitude of the (open) pore space, which, in addition, can be filled with water under pressure at 150 bars. This proportion is about the same for both types of concrete and is dependent on the water/cement ratio within the range examined, as shown by the values determined on separately produced test specimens.

As shown in Fig. 44, the total porosity (U_t) of cement paste, which is stored in saturated calcium hydroxide solution, is directly dependent on the water/cement ratio. It decreases with increasing age. Both dependencies are to be seen in connection with the development in strength and in this regard are of special technological importance [113]. For cement paste with water/cement ratios > 0.4, the logarithmic dependency of total porosity on age ends after about 28 days, and after about 360 days it reaches a nearly constant value. By contrast, the total porosity decreases further for water/cement ratios < 0.4.

Fig. 43 shows that the continuous decreases over time in the total porosity of the matrix mortar is interrupted by heating. In the case of the calcite concretes, which in comparison with the gravel-sand concrete have a greater total porosity from the outset, the effects of the increase in temperature in the region of windows 1-3 are obviously serious. While for the gravel-sand concrete as well as for the cooler regions of the calcite concretes only a temperature-dependent shift of the curves is indicated, the total porostiy in the hot regions of the concretes does not decrease considerably even during the quasi-stable period with respect to the temperature distribution (cf. section 3.1.). This can only partly be explained by structural changes in the cement paste, and presumably is due to factors caused by the aggregate (crack formation in the bonding region during thermal expansion). This is discussed in section 3.4.

Fig. 47 shows the pore volumes ($U_{\rm Hg}$) and changes in the same measured with the mercury porosimeter on the matrix mortars of beams 1-6. The greater the water/cement ratio, the greater the pore volume. For all water/cement ratios, it decreases similarly with increasing age. Due to the heating begun on the 28th day, the age-induced decrease in pore volume is interrupted. In the region of higher temperatures, the pore

volumes $(U_{\rm Hg})$ at first increase again, but then later decreases. The increase in pore volume caused by the local rise in temperature is also especially large for the matrix mortars of the calcite concretes (see above).

3.3.2. Pore Size Distribution

3.3.2.0. Evaluation of the Measurement Method

The aim of the pore size distribution tests discussed in section 2.3.4. was to characterize the change in pore sizes of the concretes as a function of age and local changes in temperature and moisture conditions in the beams. In analyzing the test data, the error effects peculiar to the mercury porosimeter method had to be taken into account [87]. In particular, we had to bear in mind that the pore radius distribution maximum in the region of the smallest measured pores is only apparent because the detection limit of the method is in this region. This can be shown by measns of sorption measurements [82, 92]. To be sure, Jung [92] assumes that a portion of even smaller pores of the gel pore range is co-detected in the maximums. However, this proportion cannot be large.

Under normal hardening conditions, the capillary pore space decreases because the hydration products penetrate into or form in this space and in this way the gel pore space is simultaneously enlarged (cf. section 1.1.). The re-arrangement of the pore space portions is incompletely reflected by the mercury porosimeter method. So the decrease in pore volume ($U_{\rm Hg}$) shown in Fig. 47 is also a special feature of the measurement method. Diamond [114] estimates the pore volume which can be measured by mercury porosimetry to be 83%-55% depending on the maturation state of the cement paste (also see [16]).

It is not to be assumed that different development stages of the pore space are of considerable influence on the lower limit of the measurement method determined by pore radii of about 4 nm. In this regard, the relative changes in frequency distributions can be regarded as typical for the pore spectra.

3.3.2.1. Cement Paste and Aggregates

For cement paste samples with different water/cement ratios and stored in saturated Ca(OH), solution, Fig. A 19 of the appendix shows that considerable changes in pore structure are to be expected even at an age of 180-470 days. Furthermore, it is obvious from these two graphs that the greater the water/cement

ratio, the greater the (capillary) pore volume measured with the mercury porosimeter. Since at lower water/cement values only a slight shift in pore radius distributions towards smaller radii occurs, it is to be expected under normal hardening conditions that the excess water—not required for hydration—in the main causes the formation of capillary pore space and that the gel pore volume is not influenced by this.

/<u>83</u>

As we can assume on the basis of the data plotted in Fig. A 20, for both types of aggregate even the smallest pores lie within the detection range of the mercury porosimeter. The pore volumes relative to the sample weight measure between 10%-20% of the measurable pore volume of cement paste. The graphs show that the calcite material has a very uniform pore volume frequency distribution, whereas parts of the gravelsand material also have very large pores. Apart from these, the gravel-sand material, like the limestone used, obviously has a high density level.

3.3.2.2. Matrix Mortar

Naturally the pore volume frequency distribution for the matrix mortars of both types of concretes fluctuate more than the frequency distributions for pure cement paste. Therefore, to examine the development tendencies of the mortar for different temperature and moisture conditions, a large as possible number of samples must be used. Although the points on the pore volume frequency distribution curves in Fig. A 17 of the appendix were determined in each case from three individual measurements, the development processes demonstratable for cement paste can be detected only indirectly. In addition, however, the mortars have pore volume frequency distributions which differ considerably from those of the cement paste due to a volume component in the region of larger pore radii. Moreover, the shape and range of sizes differs for the two types of matrix mortar. This is illustrated in the bottom graphs of Fig. 46, in which, using 180-day-old samples from window 8 as an example, a distribution of the pore volumes is plotted. Accordingly, the pore volume frequency distributions are composed of the following:

A - a volume component, due to the cement paste in the range of the smallest measured pores, for the calcite mortars with radii $\langle r_1 \simeq 40 \text{ nm} \rangle$ and for the gravel-sand mortars with radii $\langle r_1 \simeq 52 \rangle$ nm. The considerably larger weight-related pore volume of the calcite mortar is primarily due to the higher concentration of cement paste.

B - the inherent porosity of the aggregate, which in both cases is formed of pores with radii <10 nm and has only a small proportion of the total porosity.

C - the structurally-induced porosity, i.e. the pore volume directly caused by geometrical arrangement, particle shape and surface quality of the aggregates, which in the case of the calcite mortars mainly encompasses pore radii between 40 and 500 nm, and in the case of the gravel-sand mortars covers a radius range between 52 and about 1000 nm. The estimate of the weight-related pore volumes shows that this structurally-induced porosity of the calcite mortar may be about 30% greater than that of the gravel-sand mortars.

Naturally, a quantitative distribution of the measured pore volume as shown in Fig. 46 can yield only reference values.

All of the pore volume frequency distributions measured on the matrix mortars were analyzed with the method illustrated in Fig. 46 (cf. section 2.3.4.2.). In so doing, we characterized the change in cement paste porosity (A) due to the pore volumes (uI) as well as the accompanying central pore radii (rMI), and the change in structurally-induced porosity (C) due to the pore volumes (uII) as well as the accompanying central pore radii (rMI).

Since, as expected, the frequency distributions deviated sharply, it was necessary to combine the results in each case corresponding to both types of aggregate.

Fig. 51, right, shows the development tendency of the structurally-induced porosity (pore volumes uTI) prior to the start of heating. To be sure, the development ranges for the two types of concrete differ in size, but they show the same decreasing course, i.e. in both cases the pore space becomes smaller. In Fig. 51, left, the changes in cement paste porosity (pore volumes u_T) are compared for the same period of time. To be sure, at an age of 28 days the pore volume for both types of concrete reaches the same order of magnitude, but the changes at an early age run in opposite directions. Since the structurally-induced porosity in both cases changed in the same way, this did not have to be explained to begin with and -- moreover, since otherwise the same condition existed -- was presumably due to the expansion behavior of the calcite aggregate during the rise in temperature after the concrete was poured (Fig. 9) which led to crack formation (cf. section 3.4.1.). Moreover, it must also be taken into account that in both cases a direct effect on cement paste porosity at temperatures below 60°C cannot be excluded. The change in cement paste porosity after the

/84

start of heating is plotted in Figs. 48 and 49 on the basis of changes in pore volumes (uI) as well as central pore radii (um), where the results for each two adjacent windows (corresponding to different temperature regions) are combined in a fitted curve. In the case of the mortars with gravelsand aggregates (Fig. 49), a slight reduction in pore volumes (u_T) occurs which is obviously only slightly influenced by the increase in temperature. Moreover, after the start of heating and up to an age of about 100-150 days, the pore volumes are shifted towards smaller central pore radii (uMT) depending on the location in the beam. This is not true for the concretes with the calciteaggregates (Fig. 48). Rather, in this case, the cement paste porosity sharply increases, especially at higher temperatures, and then slowly falls off. Also the central pore radii (rMI) plotted in the top graph of Fig. 48 first increase in size after the start of heating and then decrease. It is worthy of note, however, that the greatest shift results at the pore radii for the lowest temeperature range (windows 7/8). Altogether, both the pore volumes and the accompanying central pore radii show a slightly decreasing tendency up to an age of 471 days.

In comparing the graphs of Figs. 48 and 49, the impression arises that in the case of the calcite concretes the change in cement paste porosity had been superimposed by an obviously temperature-dependent increase in pore volume. Fig. 50 shows that the structurally-induced porosity in the case of both concretes after the start of heating experienced only insignificant changes and the change in cement paste porosity can hardly have discriminately affected the change in cement paste porosity. Since the same development conditions existed for both concretes after the start of heating, here too (as with the changes before the start of heating) the cause is probably to be sought in cracking as a result of the variable thermal expansion behavior of the aggregate and cement paste (cf. section 3.4.1.).

If we assume that the gravel-sand material has influenced the processes in the pore space and the development process of the cement paste only to a small extent, then Fig. 49 admits of other explanations. In the region of the heated side (curves 1/2 and 3/4 in the upper graph) the shift in cement paste porosity towards smaller central pore radii is especially sharp within the heating-up phase, but subsides soon after reaching the straight-line temperature curve. By contrast, the change in the region of the beams only slightly affected by the temperature increase (curve 7/8 of the tor graph) takes place more slowly, but comes to a stop only at a considerably greater age. For this curve, smaller central pore radii on the whole are obtained in the case of curve 1/2. These events are confirmed by the

pore volume curves plotted in the bottom graph of Fig. 49. Curve 7/8 reaches the lowest pore volume, i.e. the number of small pores has increased the most in the cooler region of the beams.

3.3.3. Comparison of Results

The results of the pore structure tests can be summarized as follows:

Pore Volume

- The total porosity (U_t) of cement paste (kept in saturated calcium hydroxide solution) increases as the water/cement ratio increases. With increasing age, the total porosity decreases. At higher water/cement ratios (>0.4) the development comes to a stop earlier than at lower water/cement ratios.
- The total porosity (Ut) of the matrix mortars from calcite and gravel-sand concrete is considerably smaller than that of cement paste with a corresponding water/cement ratio. The decrease in total porosity within the first 28 days is analogous to that of the cement paste.
- For both types of mortars, the age-induced decrease in total porosity (\mathtt{U}_t) is influenced by the temperature increases associated with the heating. The total porosity in the range of higher temperatures at first increases by about 5% to 10% and decreases again with increasing age. In the case of the calcite mortars, an increase in total porosity is also found, the cause of which may be sought in the formation of cracks due to variable thermal expansion of aggregate and cement paste.
- The greater the water/cement ratio, the greater the pore volume ($U_{\rm Hg}$) of the matrix mortars measured with the mercury porosimeter. Up to the 28th day, it increases in the same way for all of the mortars. The age-induced decrease in pore volume is interrupted by the heating. The increase in pore volume in the region of the heated surface, which occurs during the increase in temperature, is especially pronounced in the case of the calcite matrix mortar. With increasing age the pore volumes then again decrease.

Pore Size Distribution

- The pore size distributions measured with the mercury porosimeter on cement paste (kept in saturated calcium hydroxide solution) show that as the water/cement ratio increases, above all the volume of the large pores increases. They also show

that even at an advanced age the pore volume is shifted to still smaller pore sizes. From this it can be concluded that the number of small pores increases as hydration progresses, i.e. the gel pore space is increased at the cost of the capillary pore space.

- The aggregates used have very uniform pore size distributions. The proportion of aggregates in the total pore volume, however, is comparatively small in both cases.
- Besides the cement paste porosity measurable with the mercury porosimeter as well as the inherent porosity of the aggregates, the pore size distributions of the matrix mortars show pore volume components, the production of which is directly dependent on the aggregates. In the case of the calcite matrix mortars, this "structurally-induced porosity" lies in the pore radius range between about 40 and 500 nm, for the matrix mortars from the gravel-sand concretes this range is greater, namely about 52-1000 nm.
- Prior to the start of heating, the structurally-induced porosity of both mortars decreases in the young concretes. The cement paste porosity of the two mortars changes in opposite directions in the same period (up to the 28th day). It becomes larger for the gravel-sand mortars, while it decreases for the calcite mortars, It is assumed that in the case of the calcite mortars, the development curve is superimposed by temperature-dependent deformations which are caused by the behavior of the aggregates.
- After the start of heating, the structurally-induced porosity no longer undergoes substantial changes. By contrast, the change in cement paste porosity is influenced by the temperature increase. However, this also accelerates the hydration processes. The pores produced as a result of these events appear to be larger than is the case with normal hardening temperatures. In the case of the calcite mortars it is assumed that changes with respect to cement paste porosity are superimposed by temperature-induced cracking between the aggregate and cement paste.

Even recently published articles on the pore structure development of cement paste have on the whole confirmed the ideas of Powers (cf. section 1.1.). For example, Winslow and Diamond [20] show that the total porosity decreases with age under normal hardening conditions, while the gel pore space increases because of the number of gel pores. Auskern and Horn [90] confirm that as the water/cement ratio increases, the

excess water causes the increase in capillary pore space. The gel pore space seems to remain largely unaffected by this. The changes in pore structure dependent on the water/cement ratio are by far more important than the developmental events caused by hydration [20]. Our experimental findings are in agreement with the fundamental data.

As temperature increases, the hydration products become coarser [sic.]. Only reently have articles been published on the problem of the influence of temperature on pore structure. In experiments on hydrated tricalcium silicate, Skalny and Odler [115] have found by means of sorption measurements that when the concrete is young the change in the concentration of non-evaporatable water as well as the change in specific surface due to the increase in temperature could be accelerated. Then the hydration rate dropped very rapidly at temperatures of 75° and 100°C, and the reactions came to a stop even before the 28th day. At about 25°C, hydrated samples finally showed a smaller total porosity with greater specific surface. Sellevold [91] observed the same effect on cement paste, which was kept at room temperature in saturated calcium hydroxide solution and subsequently heated to 97°C, namely that -- due to the temperature treatment -- the specific surface became smaller and the pores coarser. Diamond [114] found that initial developmental differences at hydration temperatures between 6° and 40°C are evened out in the following period. From this can be concluded that significant changes in pore structures can be expected only at temperatures above about 40°C.

The rise intemperature not only increases the reaction rate, but it also influences the existence conditions, described by partial vapor pressure and temperature, of the hydration products. This leads to new formations and adjustments of existing faces to altered equilibrium conditions. Since all of these reactions in some way or another affect the flow of heat in the beam, the heat flux densities in Fig. 14 and the calculated heat conductivity values in Fig. 60 provide information on the structural changes over time in the cement paste initiated by heating the beams. In this connection, it turns out that—similar to the changes in central pore radii as shown in Fig. 49—the processes in the high-temperature region come to a stop at an age as early as about 90 days, while they last longer in the region of low temperatures.

As a rule, the permeability of concrete with a dense structure is considerably greater than that of mature cement paste [11]. The gas permeability of cement paste and cement

mortar depends, for example, not only on the degree of compaction and the water/cement ratio, but it is also influenced by curing \(\frac{86}{24}, 116 \)], so that reduced permeability is to be expected as a result of longer storage in water. This is a criterion for the fact that the pore space components must be differentiated depending on their origin (cement paste porosity, inherent porosity of the aggregates, structurally-induced porosity). Moreover, according to Czernin [117], defects in the bonding of aggregate and cement paste cannot always be completely avoided even in careful laboratory experiments. In this connection, the appearance of capillary cavities depends on the nature of the aggregates; limestone aggregate seems to guarantee a better bond than material containing quartz.

With respect to structurally-induced porosity, the pore size distribution of the matrix mortars with calcite or gravelsand aggregate differ distinctly from one another, as expected. Even the observations of Kroone and Crook [118], according to which the pores with radii >200 nm became smaller in young cement mortar after curing at 100% relative humidity, while the volume of small pores ("cement paste porosity") increased, is at least qualitatively confirmed by the development of matrix mortars with gravel-sand aggregate up to the start of heating. In experiments on cement mortars containing different amounts of sand and with different water/cement ratios, the same authors [119] found that by increasing the sand content, the pore cross-sections became less uniform which, for example, might help explain the different sized pore components. parallels could be found in the literature for the assumption made on the basis of our own experiments that the cement paste porosity of the calcite matrix mortars is increased by cracking due to variable thermal expansion of the cement paste and aggregate (cf. the following section, 3.4.1.).

3.4. Change in Technological Properties

3.4.1. Shrinkage, Contraction and Thermal Expansion

In section 2.5.2, we discussed length changes measured on the beams in light of the graph plotted in Fig. 58.

With respect to the lasting contractions before the start of heating on the 28th day as a result of shrinkage and contraction ($\Delta l_{[s*]}$), which were derived from the data plotted in Fig. 34, it must be borne in mind that, above all, the volume changes occurring immediately after the concrete is poured are very difficult to measure. The contraction of

cement paste due to shrinkage, which depends on the water/cement ratio and is usually measured in a volumonometer to characterize the degree of maturity, is practically of no consequent with normal concretes. This process can be regarded as largely completed at an age of 28 days for the water/cement ratios in question here [120]. For both types of concrete, a value of 100 $\mu\text{m/m}$ was determined (corresponds to 240 μm change in length of the beams). DIN 1045 ([1], Table 12) gives degrees of final shrinkage on the same order of magnitude for curing in very moist air.

In comparison to the lasting length changes prior to the start of heating, the amount of counteracting thermal expansion happening before this (at an age of 24 hours) caused by heat of hydration is considerably larger and for the calcite concretes will have measured about 450 µm and about 750 µm for the gravel-sand condretes. While for the gravel-sand concretes, we can expect about the same thermal expansion behavior of the individual components, this cannot be assumed for the calcite concretes. As shown in section 2.4,1.2., the thermal expansion coefficient of the calcite aggregate is about 4.7 10^{-6} /°C, that of the gravel-sand aggregate about 11.5 · 10^{-6} /°C. and according to Dettling [54] the value for the cement paste should be set between 10.0 and 23.0 \cdot 10-6/°C. The expansion of the cement paste inhibited by the limestone by increasing the temperature to about 60°C leads to tensile stresses especially in the area of bonding zones which, according to Czernin [117] show defects from the outset. In spite of high strenght levels at an age of 24 hours (according to Fig. 55, the flexural tensile strength of mortar prisms then measures about 2/3 of the final strength), strain relief cracks obviously It was assumed that the counter-trending cement paste porosity curves (Fig. 51, pore volume u_T) are due to such processes (section 3.3.2.2.). Perhaps a "healing" of the cracks is to be expected if hydration products are formed in them. This could be inferred from the further progression of the cement paste porosity curves up to the 28th day (Fig. 51, left).

In conjunction with losses in strength during temperature treatment of concretes with different sized aggregates, Browne and Blundell [121] report that stresses are to be expected because of the "thermal incompatibility" of limestone and cement paste. On the basis of their own experimental data and those of others, the authors show that precisely at a young age the temperature increase due to heat of hydration leads to high losses in strength in limestone concrete. Wischers [122] has studied the influence of temperature changes on the strength properties of five-month-old cement mortars hardened under water and for temperature increases up to 60°C he did not find any strength

impairment due to different thermal expansion coefficients, although calculations based on elasticity theory suggested that, above all, the flexural tensile strength would be strongly affected.

In the region of the closed end of the beams, temperature increases up to a maximum of 60°C were reached after the start of heating. In the case of the calcite concretes, in these regions at this time even higher structural stresses are to be expected, as a result of which the complicating larger applicable thermal expansion coefficient of the hardened cement paste, due to the lower moisture content, should make itself felt. The stress relief cracks resulting because of the inherent stress state in the already pre-damaged bonding regions, cause a considerable increases in the porosity of the hardened cement paste (pore volume u_I in Fig. 48), a process which was not observed in the case of the matrix mortars from gravel-sand concrete (cf. section 3.3.2.).

After the start of heating, theraml expansion contributes most to the total change in length of the beams (cf. section 2.5.3.). Fig. 52 shows that the thermal expansion coefficients of the concretes depend, as expected, mainly on the nature of the aggregates. Besides the difference due to the aggregate, for all of the concretes the expansion coefficient in the "moist state" (with the unused excess water) is about $1\cdot10^{-6}/^{\circ}$ C higher than in the "dry state". This is in keeping with the relationships discussed in section 1.2.3., according to which the proportion of "apparent thermal expansion" initially becomes larger with decreasing moisture content. At equilibrium moisture levels between 70% and 45%, this proportion reaches a maximum and, according to Dettling [123], is to be set at about 2.10-6/6C for both types of concrete. It becomes smaller as the age of the concrete increases. Taking into consideration the "real thermal expansion" measured in the dry state (Fig. 52), we obtain the following mean thermal expansion coefficients for the period of about one and a half years after the start of heating depending on the moisture content of the concretes examined in this study:

calcite concretes $\alpha = (4.7-6.7) \cdot 10^{-6} / ^{\circ} \text{C}$ gravel-sand concretes $\alpha = (10.1-12.1) \cdot 10^{-6} / ^{\circ} \text{C}$.

The measurements of local length changes in the concrete beams after the start of heating could not yet be included in this paper (cf. section 2.2.4.2.), so that the strains occurring as a result of the heat/moisture processes in the concrete were discussed only in light of the total length changes and of the drying shrinkages shown in Fig. 53 (section 2.5.3.). The

determined drying shrinkages, as a result of drying at 105°C, of 200 $\mu\text{m/m}$ for the calcite concretes and 450 $\mu\text{m/m}$ for the gravel-sand concretes are certainly greater than the values to be expected in the region of the heated end after many years of heating at 80°C. The recommendation to assume a degree of shrinkage of 300-400 $\mu\text{m/m}$ for the inside after the start of heating over a range of 30-50 cm [41] is obviously realistic and guarantees sufficient reliability. In the case of the calcite concretes, about 200 $\mu\text{m/m}$ are sufficient.

The influence of the water/cement ratio on the total length changes of the 2.40 m long beams after the start of the heating is shown in Figs. 31 and 32. If the calcite beams are extended on the order of 400 μm , the value for beam 3 (water/cement ratio = 0.50) is about 100 μm with respect to beam 1 (water/cement ratio = 0.50) [sic.]. If the gravel-sand concrete beams are extended on the order of 750 μm , the values for beam 6 (water/cement ratio = 0.63) and beam 4 (water/cement ratio = 0.52) differ by about 200 μm . It is also obvious for the curve of total length changes that the changes in pore structure, which occur very slowly, obviously do not have a drastic effect on the shrinkage behavior of the concretes—disregarding the heating—up phase.

3.4.2. Compressive Strength

The change in strength of the mortar prisms (Fig. 55, section 2.4.2.) matches expectations for a PZ 450 F cement as per DIN 1164 [3]. At an age of one day (extrapolated values) the flexural tensile strength has reached about 60% of the value at an age of about two years, and the compressive strength has reached about 30% of the two-year-old value. While after 28 days the compressive strength increases by about another 20%, the flexural tensile strength, which is more closely linked to structural stresses, does not show any more significant increases beyond this age.

The age-dependent increase in compressive strength determined on concrete cubes (cf. Fig. 56, section 2.4.2.) reveals clear changes determined by the type of curing and the water/cement ratio. With long-term "moist curing", all of the concretes show the expected logarithmic dependency of compressive strength on age [124]. In the case of "dry curing" started at an age of 7 days, an apparent increase in strength initially results which is due to the rearrangement of stresses as a result of the release of moisture from the pore space. During these processes, the moisture content in the concrete falls below the level necessary for hydration (cf. section 1.1.4.), and the increase in strength comes to

a stop. Taking into consideration these findings as well as the compressive strength levels measured on core samples from split-off sections of beams 3 and 6 (cf. Fig. 38, section 2.2.5.), the change in compressive strength of the concrete in the beams is characterized as follows:

In the temperature ranges up to about 50°C, a temperature-dependent effect cannot be detected. The change in compressive strength in the region of the open end is only insignificantly affected by the drying processes.

While the gravel-sand concrete at temperatures above about 50°C shows a distinct increases in strength (about 15% maximum) with respect to the cooler regions of the beam, this is not found in the case of the calcite concrete. Rather, for this concrete the compressive strength decreases (about 30% maximum) with increasing temperature.

The increase in strength of the gravel-sand concrete is caused by a temperature-dependent acceleration of the hydration processes in the hardened cement paste given a sufficient moisture content (cf. [125] and [126]). This strength-increasing influence is cancelled out in the calcite concrete by the strength-reducing processes of crack formation due to the considerable differences in the thermal expansion coefficients of limestone and hardened cement paste (cf. section 3.4.1.). It is obvious from Fig. 59 that the concrete, already damaged by the temperature cycle due to heat of hydration, experiences a drop in compressive strength of about 10% as a result of heat treatment at 70°C. Browne and Blundell report experiments in which losses in strength of even 35% were found due to a temperature increase on the same order (53°C) [121].

3.4.3. Thermal Conductivity

Fig. 61 shows the dependence of thermal conductivity on moisture content at temperatures between 20° and 80°C expected for the calcite and gravel-sand concretes. The curves are based on equations discussed by Krischer [59], according to which not only the solid structure and the pore space filled with water and air conduct heat, but also vapor diffusion processes contribute to heat conduction. The extent to which this occurs is a function of moisture content and temperature. Taking into consideration moisture content and temperature, the following heat conductivity ranges can be given on the basis of our own experiments:

calcite concrete $\rho_{\rm f} \simeq 2.3 \, {\rm kg/dm}^3$

1.4 $<\lambda<$ ca. 2.8 [W/m.K]

/88

gravel-sand concrete ρ_f ≃ 2.2 kg/dm³ 1.8<λ<ca. 3.5 [W/m·K]

The dependence on the water/cement ratio is abviously insignificant within the range in question (cf. also Fig. A 39 in the appendix). While the literature contains reference values for the thermal conductivity of concretes in the dry state [41], comparable data do not exist on the influence of the moisture content. Only Marechal [62] indicates dependencies for gravel-sand concretes (not further identified), according to which when the moisture content is in equilibrium with the respective saturation vapor pressure at temperatures around 60°C, a thermal conductivity maximum (2.4-3.3 W/m·K) is to be expected.

4. Summary

The temperatures arising during operation in thickwalled concrete reactor vessels alter not only the heat/moisture equilibrium state in the concrete, but they also influence the technilogical properties of the concrete. In this work we have examined the conduction of heat and moisture and the development processes and changes in concrete associated with heat and moisture conduction.

The test specimens used were 6 concrete beams (cf. Fig. 3) measuring 40 cm x 40 cm x 240 cm, which were exposed on one end at an age of 28 days and heated on the opposite end. The nominal temperature on the heated end was 80°C. The prevailing temperature at the open end was 20°C with a relative humidity of 45%. To make it so that the heat and moisture were conveyed only in the direction of the long axis of the beams, the test apparatus was fitted with vapor seals, thermal insulation layers and compensation heating bands. Test specimens of so-called matrix mortar were distributed in cavities on the top of the beams in direct contact with the concrete. These were removed at different intervals for structure tests. Three concretes were made with crushed calcite aggregate with water/cement ratios of 0.50, 0.565 and 0.63 and three concretes were made with uncrushed Rhine gravelsand aggregate with water/cement ratios of 0.52, 0.575 and 0.63. PA 450 F portland cement was used as the binding agent. specimens of hardened cement paste, cement mortar and of various concretes used in the experimental program were used for supplementary tests. This study contains measurements made up

to an age of about 450 days for all of the concretes. Electric resistance elements and a neutron probe were used to determine the water content, including the evaporatable and non-evaporatable portions. In addition, conventional gravimetric analysis methods were also used. A mercury porosimeter as well as other instruments were used to characterize the changes in pore space.

As a result of the heat of hydration, the temperatures in all of the beams reached maximum values of about 60°C within 24 hours after the concrete was poured. In spite of a relatively low heat of hydration of only 273 J/g, the use of cement with high initial strength proved to be a drawback in the case of the calcite concretes.

After the start of heating, an approximately straight-line temperature distribution was established along the long axis within about 30 days in all beams. To be sure, changes in thermal processes over time cannot be distinguished until measured heat flux densities are available. After about 110 days of heating, the temperature fields may finally be regarded as free of heat sinks and heat sources. The movement of moisture beginning after the start of heating is characterized by means of moisture loss curves and balances of the total water content as a function of age and also by means of local changes in the drying curve. In this connection, it turns out that the "large-scale" moisture conduction is at first presumably superimposed by local changes in the concentration of evaporatable water. The drying curve at the open end at first corresponds to the familiar drying equations for capillaryhygroscopic substances and is mainly a function of the constant environmental conditions. For drying under the effect of increased temperature, a diagram was designed, taking into consideration the data available, which expresses the change in time as a function of temperature (i.e. distance from the heated end), the concentration of evaporatable water and the pore structure.

The heat/moisture processes influence the pore structure. The age-induced decrease in total porosity is interrupted after the start of heating. Depending on the local increase in temperature, the total porosity first of all increases and then later decreases. In contrast to the matrix mortars of the gravel-sand concretes, for which the total porosity finally drops to 15%, for the equivalent calcit mortars, with initially higher total porosities, a considerably "more lasting" increase is found. In the course of more than a year, total porosities of about 19% are reached. The pore size distributions measured with the mercury porosimeter also show specific differences.

While the inherent porosity of the aggregates and the hardened cement paste porosity contribute equally to the pore size distributions of both types of concerte, on the other hand a "structurally-induced porosity" can be shown to exist which depends on the nature of the aggregate. For the calcite mortars, this includes the pore volume within a radius range between about 40 and 500 nm; and for the gravel-sand concrete mortars, between about 52 and 1000 nm. Before the start of heating, the structurally-induced porosity of both types of concrete decreases sharply and the temperature increase due to heating results only in insignificant changes. The development of the hardened cement paste porosity (pore volumes within radius ranges between about 4 and 40 or 52 nm) of the matrix mortars of the gravel-sand concretes is characterized by an increase in pore volume up to the start of heating. After the start of heating, the hydration processes are, to be sure, accelerated as a function of the respective temperature increase, but at higher temperatures (>40°C) coarser pores form than under normal hardening conditions. In the case of the calcite mortars, this development is obviously superimposed by the formation of cracks in the bonding regions between aggregate and hardened cement paste. This is caused by the increase in temperature produced by the heat of hydration as well as the externally applied heat. Such processes are due to differences in the thermal expansion coefficients of the calcite aggregate and the hardened cement paste. Already during the temperature increase as a result of the heat of hydration, high levels of structural stress seemed to lead to deformations which, during another temperature increase, appear in the form of defects. This also leads to significant drops in compressive strength in the temperature range of the beam above about 50°C. These losses make up about 30% of the compressive strength of the cooler region of the beam. In contrast to this, the gravel-sand concrete reaches strength increases in the same temperature region up to a maximum of 15%.

The changes in total length measured on the beams are composed of components due to the influence of shrinkage, contraction and thermal expansion. These changes were examined in additional tests on test specimens. Depending on the moisture content, the thermal expansion coefficient should be set at $(4.7\text{-}6.7)\ 10^{-6}/^{\circ}\text{C}$ for the calcite concretes and (10.1-12.1) $10^{-6}/^{\circ}\text{C}$ for the gravel-sand concretes. In the region of the heated end (80°C), degrees of shrinkage have to be taken into account, which in the case of the calcite concretes are no more than about 200 $\mu\text{m/m}$, and in the case of the gravel-sand concretes no greater than about 450 $\mu\text{m/m}$, assuming complete drying.

The heat conductivity of the concretes depends to a considerable extent on the moisture content and temperature. For the concentration range of evaporatable water up to about 12% by volume, values between 1.4 and about 2.8 W/m·K are to be expected for the calcite concretes, and values between 1.8 and about 3.5 W/m·K for the gravel-sand concretes.

/90

In contrast to popular opinion, the results show that changes in the heat/moisture equilibrium with structural development can also significantly prodetermine the technological properties in the temperature range study. Since in this connection the investigation of the course of drying over time is especially important, it is intended to continue making measurements on the beams still in the experiment up to an age of three years. Then, on the basis of moisture loss curves for the beams as well as local drying curves, we will work out the experimental principles for testing heat/moisture models.

REFERENCES

- DIN 1045: Concrete and Reinforced Concrete Construction; Design and Execution, January 1972 edition.
- 2. DIN 1048 Sheet: 1: Testing Methods for Concrete; Fresh Concrete, Set Concrete of Separately Produced Test Specimens, January 1972 edition.
- 3. DIN 1164: Portland Cement, Iron Cement, Blast-Furnace Cement and Trass Cement, June 1970 edition.
 - Sheet 1: Standards, Components, Specifications, Delivery.
 - Sheet 3: Composition Test.
 - Sheet 4: Fineness Test.
 - Sheet 5: Determination of Setting Times Using a Vicat Needle. Sheet 6: Soundness Test Using the Boiling Experiment.

 - Sheet 7: Strength Test.
 - Sheet 8: Heat of Hydration Test Using a Solution Calorimeter.
- 4. DIN 4188 Sheet 1: Screens; Wire Mesh Screens for Sieves; Dimensions. April 1969 edition.
- 5. DIN 52 102: Rock Testing; Determination of Density, Bulk Density, Absolute Density, Degree of Density, Total Porosity. September 1965 edition.
- 6. DIN 52 103: Rock Testing; Water Absorption Test; November 1972 edition.
- 7. DIN 52 612: Thermal Insulation Tests; Thermal Conductivity Tests Using a Plate Apparatus; Thermal Conductivity for Use in Engineering.
- 8. Goffin, H., "Prestressed Concrete Reactor Pressure Vessels, Review of German Research Studies," Beton 10, 378-384 (1974).
- 9. Kuhl, H., Cement Chemistry, Vol. 3, 3rd edition, Berlin, VEB Verlag Technik, 1961, pp. 170-171.
- 10. Czernin, W., Cement Chemistry for the Civil Engineer, 2nd expanded edition, Wiesbaden, Berlin, Bauverlag GmbH, 1964, pp. 39-126.
- 11. Brunauer, S., The Structure of Hardened Portland Cement Paste and Concrete, Proc. 8th Conf. Silicate Ind. (SILICONF). 1966. pp. 205-230.

- 12. Richartz, W., F.W. Locher, "The Morphology and Water Absorption of Calcium Silicon Hydrates and the Structure of Hardened Cement Paste," Zement-Kalk-Gips 18, (1965) 449-459.
- 13. Wischers, G., "Physical Properties of Hardened Paste," Betontechn. Berichte [Concrete Engineering Reports], 1961, ed. K. Walz, Dusseldorf, Beton-Verlag GmbH, 1962, pp. 199-213.
- 14. Powers, T.C., T.L. Brownyard, "Studies of the Physical Properties of Hardened Portland Cement Paste," PCA Bull. 22, (1948) 472.
- 15. Czernin, W., "The Physical Properties of Hydration Froducts," Zement und Beton 16, (1959) 10-15.
- 16. Diamond, S., W.L. Dolch, "Generalized Log-normal Distribution of Pore Sizes in Hydrated Cement Paste," J. Colloid Interface Sci. 38, (1972) 234-244.
- 17. Burnauer, S., P.H. Emmett, E. Teller, "Adsorption of Gases in Multimolecular Layers," J. Amer. Chem. Soc. 60, (1938) 309.
- Romberg, H., "Influence of the Cement Paste on Pore Size Distribution in Hardened Cement Paste," <u>Tonind. -Ztg.</u> 95/4, (1971) 104-115.
- 19. Powers, T.C., "A Few Physical Aspects on the Hydration of Portland Cement," Zement-Kalk-Gips 14/3, (1961) 81-87.
- 20. Winslow, D.N., S. Diamond, "A Mercury Porosimetry Study of the Evolution of Porosity in Portland Cement," J. Mater. 5/3, (1970) 564-585.
- 21. Eipeltauer, E., W. Schilcher, W. Czernin, "Pore Distribution in Cement Hydration Products," Zement-Kalk-Gips 17, (1964) 543-546.
- 22. Loc. cit. [10], pp. 59-60.
- 23. RILEN Technical Committee 15-PM; Determination of Pore Properties of Constructional and Other Materials. <u>Mater. Constr.</u> 6, (1973) No. 33, 167-250.
- 24. Schwiete, H.E., U. Ludwig, "The Determination of Open Porosity in Hardened Cement Paste," Tonind. -Ztg. 90/12, (1966) 562-574.
- 25. Lehmann, H. W. Roesky, "Strength Development and Hydration of Portland Cement and Portland Blast-furnace Cement at 20°C, 5°C and 1°C," Tonind. -Ztg. 89/15-16, (1965) 337-350.

- 26. Copeland, L.E., J.C. Hayes, "Determination on Non-evaporatable Water in Hardened Portland Cement Paste," ASTM Bull. 194, (1953) 40-74.
- 27. Krischer. O., "The Scientific Principles of Drying Techniques,"

 <u>Drying Techniques</u>, Vol. 1, ed. O. Krischer and K. Kroll,

 <u>Berlin, Gottingen</u>, Heidelberg, Springer-Verlag, 1956, p. 52.
- 28. Kroone, B., F.A. Blakey, "Reaction Between Carbon Dioxide Gas and Mortar," J. Amer. Concr. Inst. 31/1, (1959) 497-510.
- 29. Pihlajavaara, S.E., "On the Main Features and Methods of Investigation of Drying and Related Phenomena in Concrete," Diss. Univ. Helsinki, 1965. The State Institute for Technical Research, Finland, Publ. No. 100, Helsinki, 1965, p. 65.
- 30. Klopfer, H., Water Transport by Diffusion in Solids, Wiesbaden, Berlin, Bauverlag GmbH, 1974, pp. 20-23.
- 31. Altmann, K., The Behavior of Concrete Under the Effect of Moisture, Diss., Techn. University, Berlin, 1968 (D 83), pp. 55-61.
- 32. Andreae, G., "Moisture Measurement in Concrete," <u>Materialpruf.</u> 15/3, (1973) 95-97.
- 33. Hummel, A., The ABC's of Concrete, 12th edition, Berlin, Wilhelm Ernst & Son, 1959, pp. 86-97.
- 34. Pilny, F., "The Importance of Pore Space in Concrete," <u>Beton</u> <u>16</u>, (1966) 147-150.
- 35. Powers, T.C., "Principles of Concrete Shrinkage," <u>Betonstein-Ztg.</u> 27, (1961) 45-51.
- 36. Loc. cit. [10], pp. 95-98.
- 37. Bazant, Z.P., "Thermodynamics of Interacting Continua With Surfaces and Creep Analysis of Concrete Structures," <u>Nucl. Eng. Design</u> 20, (1972) 477-505.
- 38. Bazant, Z.P., J.H. Hemann, H. Koller, L.J. Naijar, "A Thin-wall Cement Paste Cylinder for Creep Tests at Variable Humidity or Temperature," Mater. Constr. 6/34, (1973) 277-281.
- 39. Walz, K., G. Wischers, "Concrete as a Radiation Shield for Nuclear Reactors," Betontechn. Berichte [Concrete Engineering Reports], 1961, ed. K. Walz, Dusseldorf, Beton-Verlag GmbH 1962, pp. 91-127.

- 40. Jaeger, Th., "Concrete Radiation Shielding," <u>Technischer Strahlenschutz</u>.[Technical Radiation Protection], Munich, Karl Thiemig, 1959, pp. 16-115. (Series on Atomic Energy, Vol. 2).
- 41. Eibl, J., N.V. Waubke, W. Klingsch, U. Schneider, G. Rieche,
 "Special Concrete Properties in the Construction of Reactor
 Pressure Vessels," Prestressed Concrete Reactor Pressure
 Vessels, Berlin, Wilhelm Ernst & Son, 1974, pp. 3-51.
 (Series published by the German Commission for Reinforced
 Concrete, No. 237).
- 42. Loc. cit. [10], pp. 99-103.
- 43. Wischers, G., Influence of a Change in Temperature on the Strength of Hardened Cement Paste and Cement Mortar with Aggregates with Different Thermal Expansion Coefficients, ed. Verein Deutscher Zementwerke i.V., [Association of German Cement Works], Dusseldorf, Beton-Verlag GmbH, 1961, (Series published by the cement industry, No. 28).
- 44. Browne, R.D., "Properties of Concrete in Reactor Vessels,"
 Conf. on Prestressed Concrete Pressure Vessels, Westminster
 1967, (Group C., Pap. 13), London: The Institution of
 Civil Engineers, 1968, pp. 131-151.
- 45. Ross, A.d. et al., "Short- and Long-term Deformations of Concrete as Influenced by Its Physical Structure and State," Proc. Int. Conf. Structure of Concrete, London: Cement and Concrete Association, 1965.
- 46. Hornby, L.W., "Moisture Measurements in Mass Concrete," Conf. on Prestressed Concrete Reacotr Vessels and Their Thermal Insulation, 18-20 Nov. 1969, Grossbritannien.
- 47. England, G.L., A.D. Ross, "Shrinkage, Mositure and Pore Pressures in Hardened Concrete," Proc. Concrete Nucl. Reactors, Berlin 1970, Detroit: American Concrete Institute 1972, pp. 883-907 (ACI Spec. Publ. SP 34-42).
- 48. McDonald, J.E., "An Experimental Study of Moisture Migration in Concrete," Proc. Concrete Nucl. Reactors, Berlin 1970, Detroit: American Concrete Institute 1972, pp. 957-989 (ACI Spec. Publ. SP 34-45).
- 49. Loc. cit. [30], pp. 52-64.
- 50. Bazant, Z.P. "Constitutive Equation for Concrete Creep and Shrinkage Based on Thermaodynamics of Multiphase Systems," Mater. Constr. 5, (1970) 3-36.

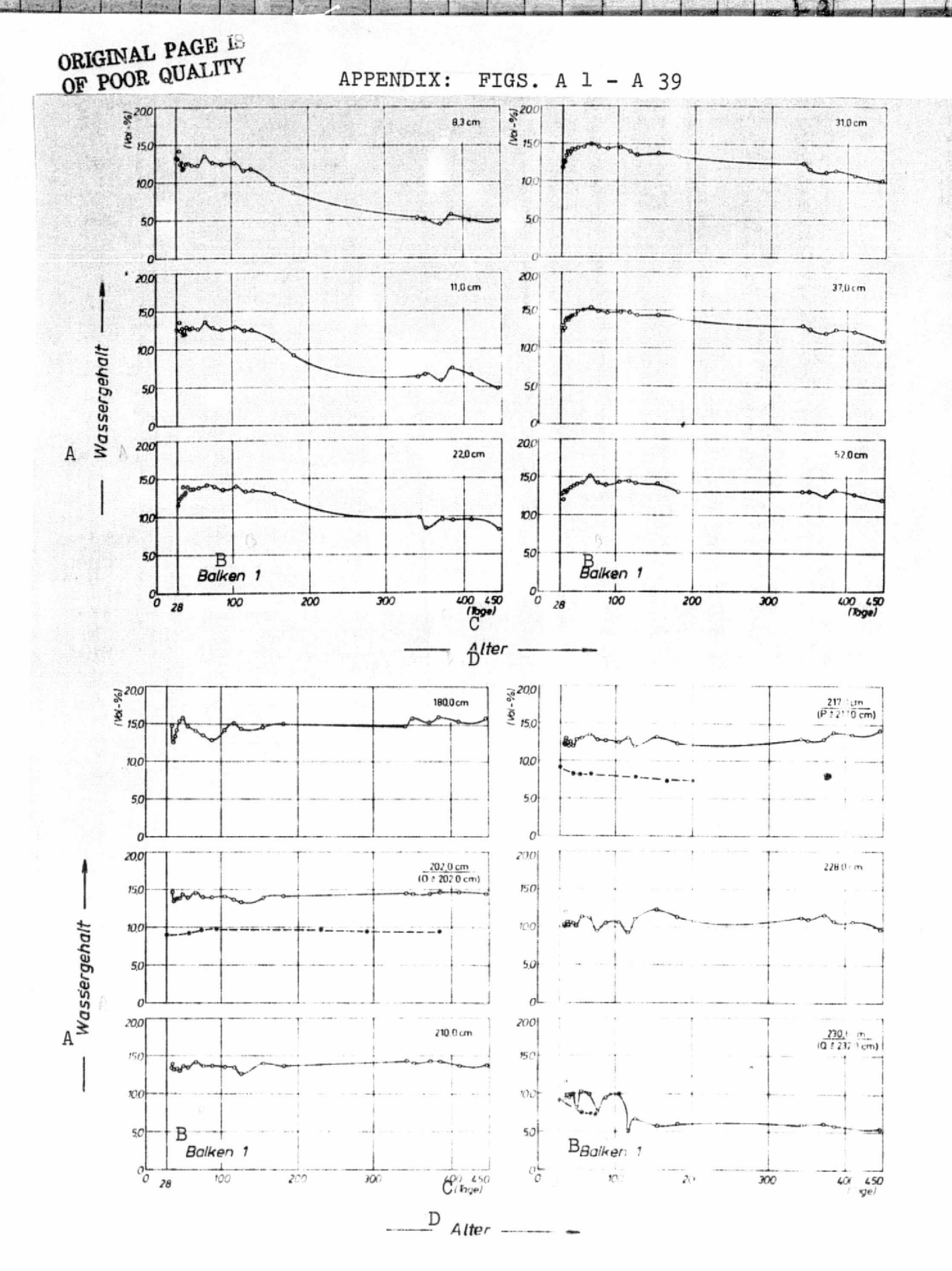
- 51. Ross, A.D., J.D. Parkinson, "Shrinkage in Concrete Pressure Vessels," Nucl. Eng. Disign 5, (1967) 150-160.
- 52. Westphal, W., Physics, 21st/22nd edition, Berlin-Gottingen-Heidelberg, Springer-Verlag, 1959, pp. 220 238.
- 53. Pilny, F., "Concrete Strains Due to Moisture," Zement u. Beton 30, (1964) 1-9.
- 54. Dettling, H., The Thermal Expansion of Hardened Cement Paste, Rocks and Concretes. Series published by the Otto Graf Institute (1962), No. 3, pp. 193.
- 55. Meyers, S.L. "Thermal Expansion Characteristics of Hardened Cement Paste and of Concrete," Proc. Highway Res. Board 30. (1960) 193-203.
- 56. Loc. cit. [54], p. 159.
- 57. Loc. cit. [54], p. 179.
- 58. Loc. cit. [54], pp. 148-153.
- 59. Loc. cit. [27], pp. 223-232.
- 60. Cammerer, W.F., "The Influence of Moisture on the Thermal Conductivity of Structural and Insulating Substances Based on the Current State of Research," <u>Kaltetechnik</u> 13,(1961) 413-420.
- 61. Missenard, A., "Theoretical and Experimental Research on the Thermal Conductivity of Concrete," Ann. Inst. Techn. Bat. Trav. Publ. 18/211-212, (1965) 949-967.
- 62. Marechal, J.C. "Thermal Conductivity and Thermal Expansion Coefficient of Concrete as a Function of Temperature and Humidity," Proc. Concrete Nucl. Reactors, Berlin 1970, Detroit: American Concrete Institute 1972, pp. 1047-1057 (ACI Spec. Publ. SP 34-49).
- 63. Harmathy, T.Z., "Thermal Properties of Concrete at Elevated Temperatures," J. Mater. 5/1, (1970) 47-74.
- 64. Cement Fineness; Determination Guidelines. Ed. Verein Deutscher Zementwerke e.V., [Association of German Cement Works], Dusseldorf: Beton-Verlag GmbH 1967, pp. 40-45 (Cement Industry Series, No. 33).

- 65. Analysis Procedure for Cements. Verein Deutscher Zementwerke e.V. [Association of German Cement Works], Dusseldorf: Beton-Verlag GmbH 1970, 111 pages. (Cement Industry Series No. 37).
- 66. Loc. cit. [29], pp. 97-99.
- 67. Loc. cit. [52], pp. 270-272.
- 68. Grober, H. S. Erk, U. Grigull, <u>The Basic Laws of Heat Transfer</u>. 3rd edition, 3rd printing, Berlin-Gottingen-Heidelberg: Springer-Verlag 1963, pp. 3-15.
- 69. Hundt, J., Buschmann, J., "Moisture Measurement in Concrete," Mater. Constr. 4/22, (1971) 253-259.
- 70. Loc. cit. [31], pp. 59-61.
- 71. Altmann, K., "A New Moisture Measuring Method for Structural Members," Bautechnik 47/8, (1970) 268-272.
- 72. Altmann, K., "The Behavior of Epoxy Polystyrene Concrete (EPS Concrete) and the Testing of It," Materialprufung 16/1, (1974) 3-6.
- 73. Altmann, K., Moisture Measurement in Structural Members of Mortar and Concrete. Dissertation, Construction Department, Technical University, Berlin, 1971, 214 pages.
- 74. Pohl, E., "Moisture Measurement with Neutrons," Nondestructive Testing and Measurement Methods for Concrete, 2nd edition, Berlin, VEB Berlag fur Bauwesen [VEB Publishing House for Construction Engineering], 1969, pp. 167-176.
- 75. Neutron Moisture Gauges. Vienna: International Atomic Energy Agency 1970, 95 pages. (Technical Reports Series No. 112).
- 76. Trost, A., "Industrial Moisture Measurement with Neutrons," Z.f. Instrumentenkunde 73, (1965) 12.
- 77. Mlitz, P., R. Neider, "Using Neutrons to Measure Moisture in Construction Materials," <u>Bautechnik</u> 44, (1967) 77-81.
- 78. Trost, A., "Using Neutrons to Measure Content," Sprechsaal fur Keramik, Glas., Email, Silikate 101/17-18, (1968) 745-752.
- 79. Honig, A. et al., "Comparison of Commercial Portable Gauges for Radiometric Determination of Building Materials Density and Moisture," Confidential Report. Brno. Techn. Univ. 1969, VUT 69 D 1, 194 pages.

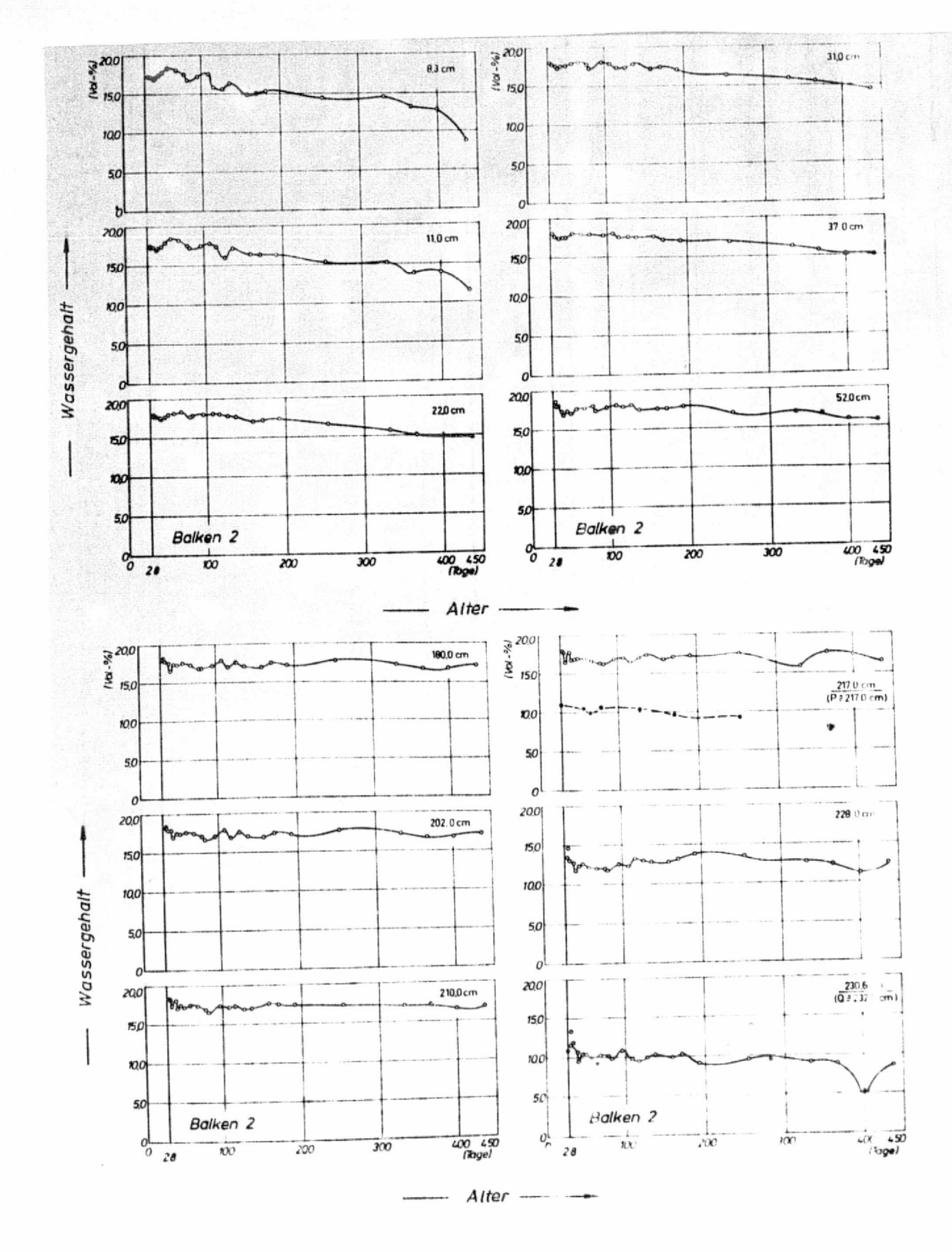
- 80. Sciesinska, E., "The Accuracy of the Neutron Method of Moisture Measurement," Nukleonika 15/9-10, (1970) 593-612.
- 81. Linder, A., Statistische Methoden. Basel, Stuttgart: Birkhauser Verlag 1964, 484 pages.
- 82. Lichtner, B., J. Hundt, "Porosity Measurements on Cement Mortar and Concrete," Tonind.-Ztg. 96/8, (1972) 232-236.
- 83. Kuhne, G., "The Influence of Age on the Solid Pore Space of Concrete," <u>Baustoffindustrie</u> 14/11, (1971) 370-373.
- 84. Konopicky, K., G. Tkotz, F. Kowalcyzk, "Density Determination Using a Comparison Air Pynchometer," Tonind. -Ztg. 89/17-18, (1965) 402-405.
- 85. Ritter, H.L., L.C. Drake, "Pore Size Distribution in Porous Materials," Ind. Eng. Chem., Anal. Ed. 17, (1945) 782-791.
- 86. Guyer, A. Jr., B. Bohlen, A. Guyer, "Pore Size Determination," Helvetica chimica acta 42/6, (1959) 2103-2110.
- 87. Juntgen, H., M. Schwuger, "Usefulness of Mercury Porosimetry for Characterizing Porous Substances," Chemie-Ing.-Techn. 38/12, (1966) 1271-1278.
- 88. Alongi, V., "Determining the Micorostructure of Porous Solids," Chem. Rdsch. 20/49 (1967).
- 89. Hill, R.D., "A Study of Pore Size Distribution of Fired Clay Bodies, II. An Improved Method of Interpreting Mercury Penetration Data," <u>Trans. Brit. Ceram. Soc.</u> 59, (1960) 198-212.
- 90. Auskern, A., W. Horn, "Capillary Porosity in Hardened Cement Paste," J. Testing and Evaluation 1/1, (1973) 74-79.
- 91. Sellevold, E.J., "Mercury Porosimetry of Hardened Cement Paste Cured or Stored at 97°C," Cem. Concr. Res. 4, (1974) 399-404.
- 92. Jung, M., "The Porosity of Hardened Portland Cement Paste," Silikattechn. 22/7, (1971) 222-224.
- 93. 1972 Annual Report of the Bundesanstalt fur Materialprufung (BAM)[Federal Center for Materials Testing], Berlin, Berlin: 1973, p. 49.

- 94. Jespersen, H.B., "Thermal Conductivity Coefficients of Moist Substances and Their Measurements," Ges. -ing. 74, (1953) 187-193.
- 95. Loc. cit. [10], p. 101.
- 96. Loc. cit. [10], p. 99.
- 97. Loc. cit. [29], p. 97.
- 98. Pihlajavaara, S.E., M.A. Ranta, "A Theoretical Study on the Effect of Gravitation on Drying with Special Reference to Concrete," Helsinki: 1965, 61 pages. (The State Institute for Technical Research, Finland, Publ. No. 94).
- 99. Lykow, A.W., Transport Phenomena in Capillary Porous Substances. Ed. K. Steffes, Berlin: Akademie-Verlag, 1958, p. 17.
- 100. Loc. cit. [9], p. 170.
- 101. Loc. cit. [10], pp. 47; 56.
- 102. Loc. cit. [9], p. 120.
- 103. Ramachandran, V.S., Applications of Differential Thermal Analysis in Cement Chemistry. New York: Chemical Publishing Company Inc., 1969, pp. 128-129.
- 104. Lea, F.M., The Chemistry of Cement and Concrete. 3rd edition, (1970), Glasgow: Edward Arnold (Publishers) Ltd., 1970, p. 207.
- 105. Loc. cit. [9], p. 28.
- 106. Loc. cit. [10], p. 127.
- 107. Loc. cit. [9], p. 181 ff.; 248 ff.
- 108. Loc. cit.[104], p. 177 ff.
- 109. Loc. cit. [10], p. 43.
- 110. Loc. cit. [27], p. 233 ff.
- 111. Loc. cit. [9], p. 249.
- 112. Yuan, R.L., H.K. Hilsdorf, C.E. Kessler, "Effect of Temperature on the Drying of Concrete," Dept. Theor. Appl. Mechanics, Univ. Of Illinois 1968, Rep. No. 316, p. 61.

- 113. Loc. cit. [10], p. 56.
- 114. Diamond, S., "Pore Structure of Hardened Cement Paste as Influenced by Hydration Temperature," Proc. Int. Symp. Pore Structure and Properties of Materials, September 18-21, 1973, in Prague, Preliminary Rep., Part I, hrsg. v. S. Modry und Svata, Prag: Academia 1973, S. B 73 bis B -88.
- 115. Skalny, J., I. Odler, "Pore Structure of Hydrated Calcium Silicates. III. Influence of Temperature on the Pore Structure of Hydrated Tricalcium Silicate," J. Colloid Interface Sci. 40/2, (1972) 199-205.
- 116. Riedel, W., C. Gohring, "Pore Distribution in Hardened Cement Pastes and Permeability Measurements on Cement Mortars,"
 Wiss. Z. Hochsch. Arch. Bauwes. Weimar 15/6, (1968) 655-660.
- 117. Loc. cit. [10], p. 105.
- 118. Kroone, B., D.N. Crook, "Studies of Pore Size Distribution in Mortars," Mag. Concr. Res. 13/39, (1961) 127-132.
- 119. Kroone, B., D.N. Crook, "Further Studies of Pore Size Distribution in Mortars," Mag. Concr. Res. 14/40, (1962) 43-46.
- 120. Loc. cit. [10], pp. 77-88.
- 121. Browne, R.D., R. Blundell, "Relevance of Concrete Property Research to Pressure Vessel Design," Proc. Concrete Nucl. Reactors, Berlin 1970, Detroit: American Concrete Institute 1972, pp. 69-102 (ACT Spec. Publ. SP 34-5).
- 122. Loc. cit. [43], pp. 102-109.
- 123. Loc. cit. [54], pp. 172-178.
- 124. Loc. cit. [33], pp. 115-117.
- 125. Loc. cit. [33], p. 113.
- 126. Loc. cit. [9], p. 171.

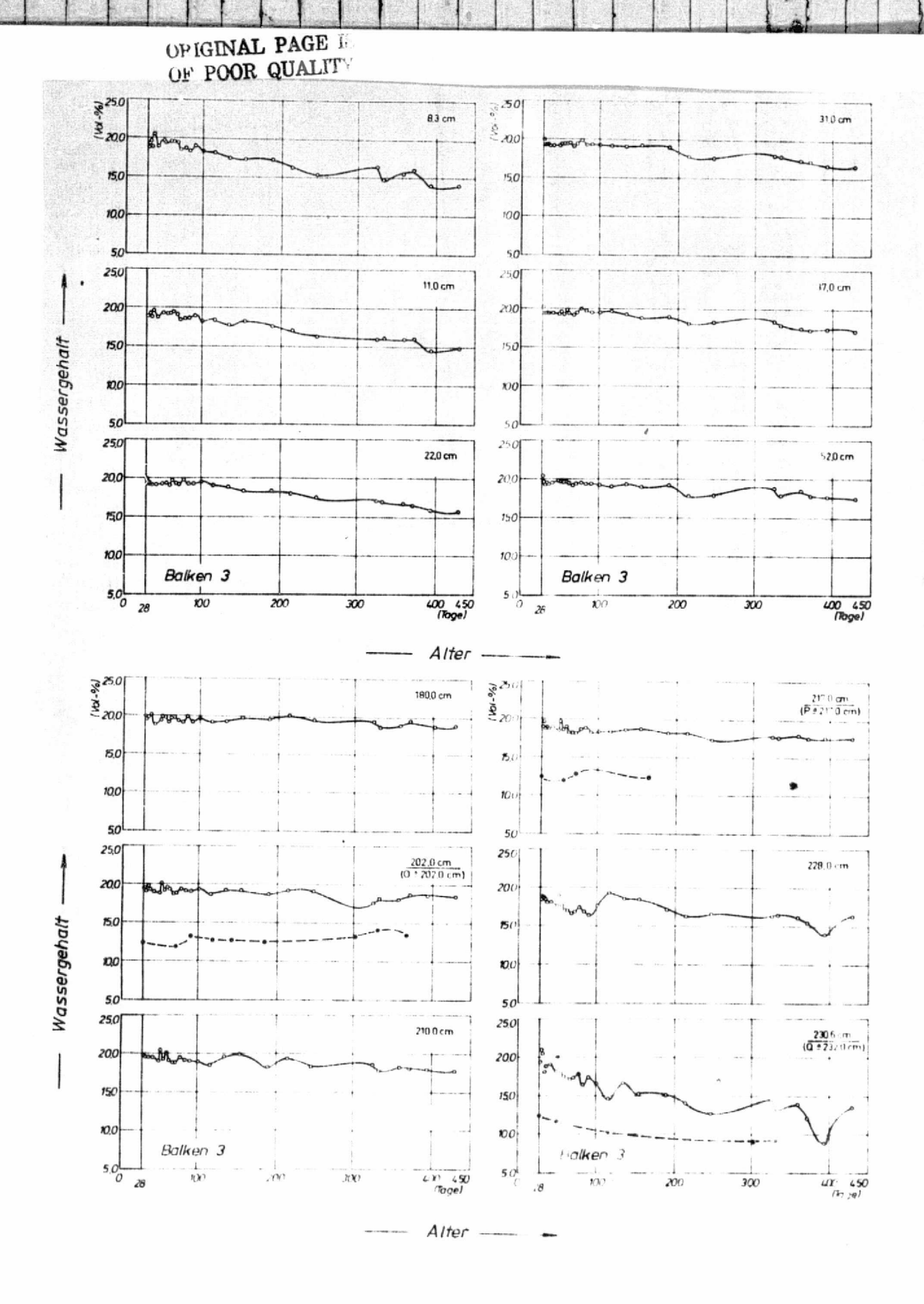


Figs. A 1 and 2. See key and caption on page 171.

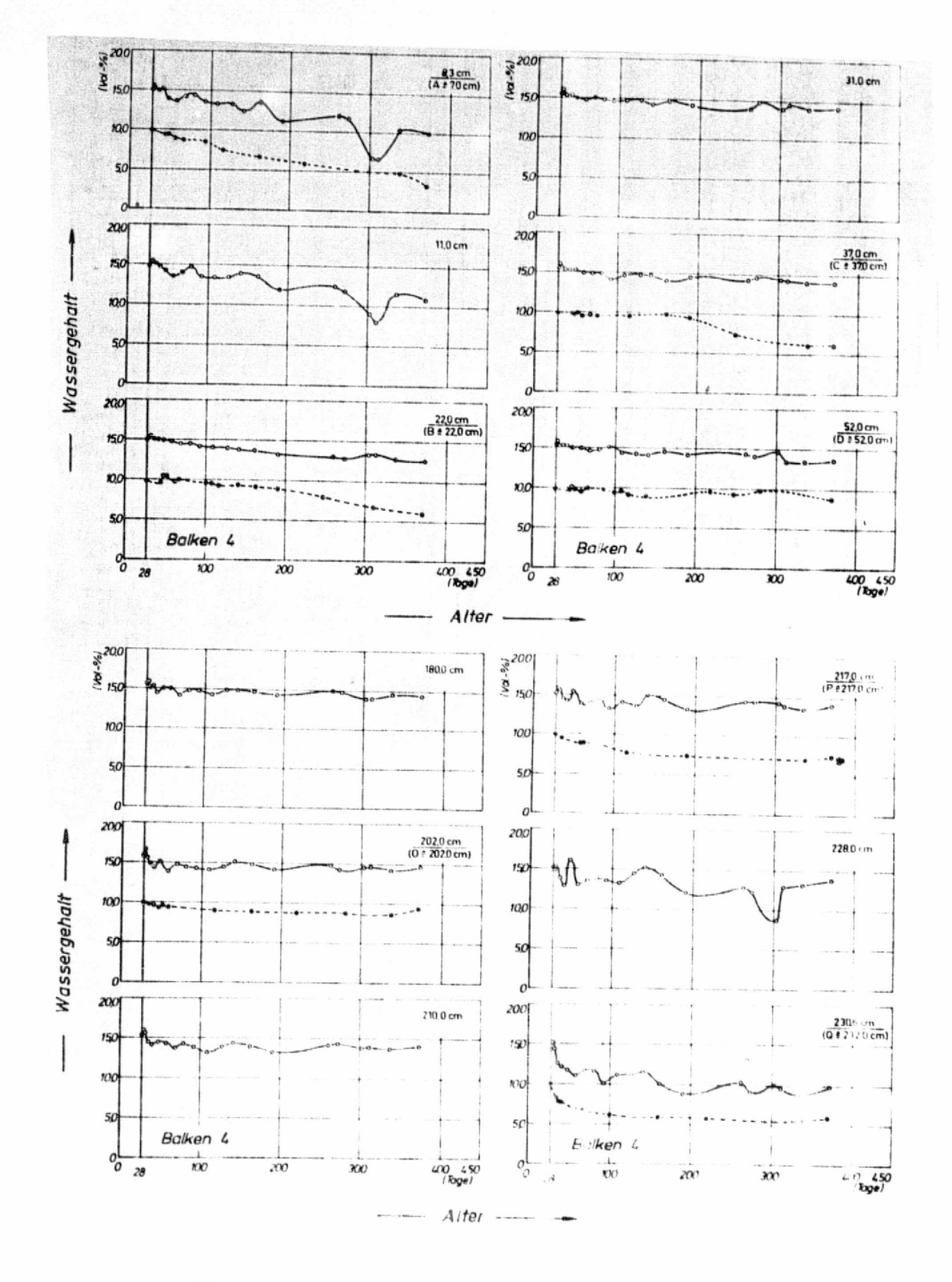


Figs. A 3 and 4. See key and caption on page 171.

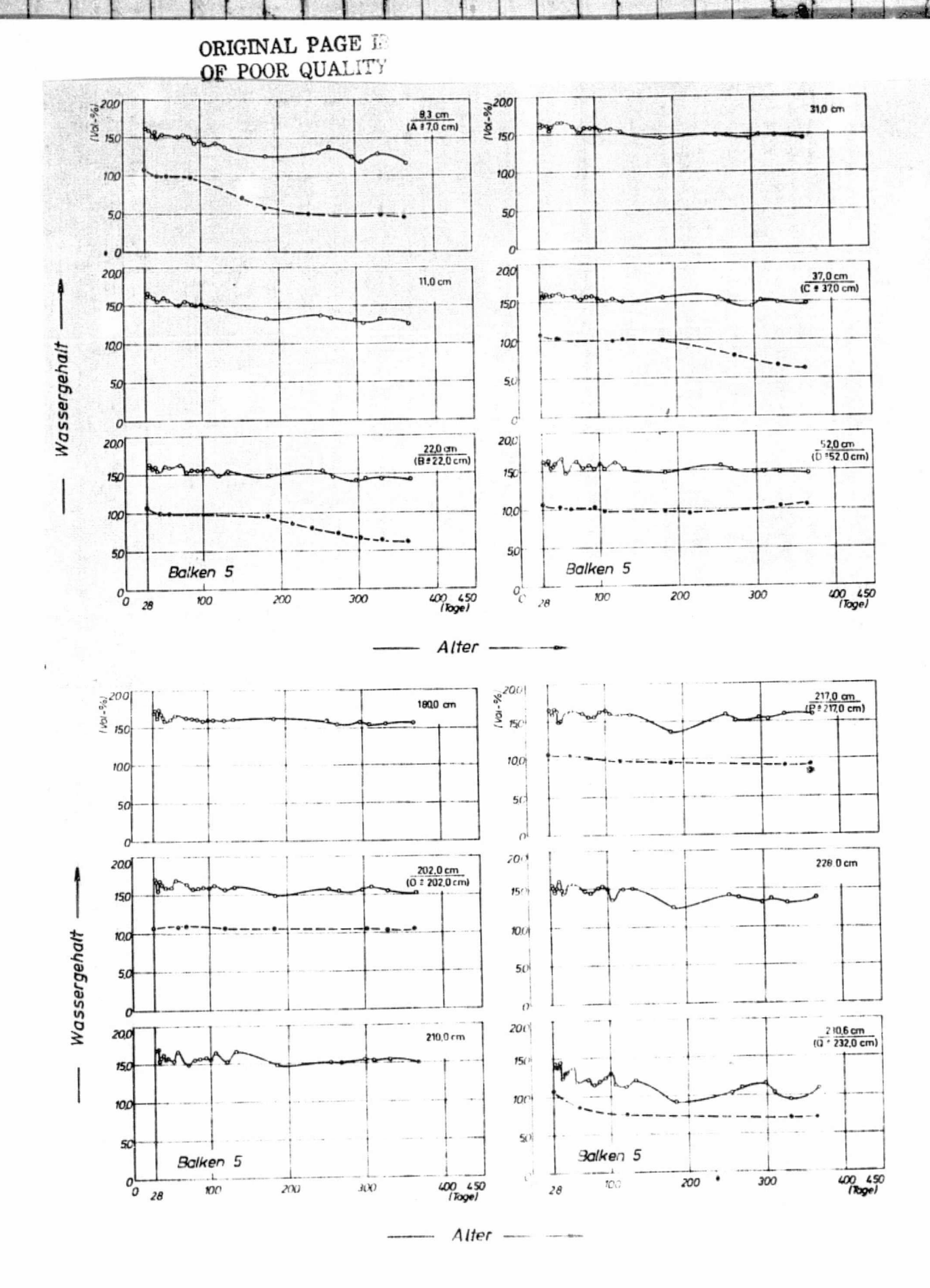
166



Figs. A 5 and 6. See key and caption on page 171.

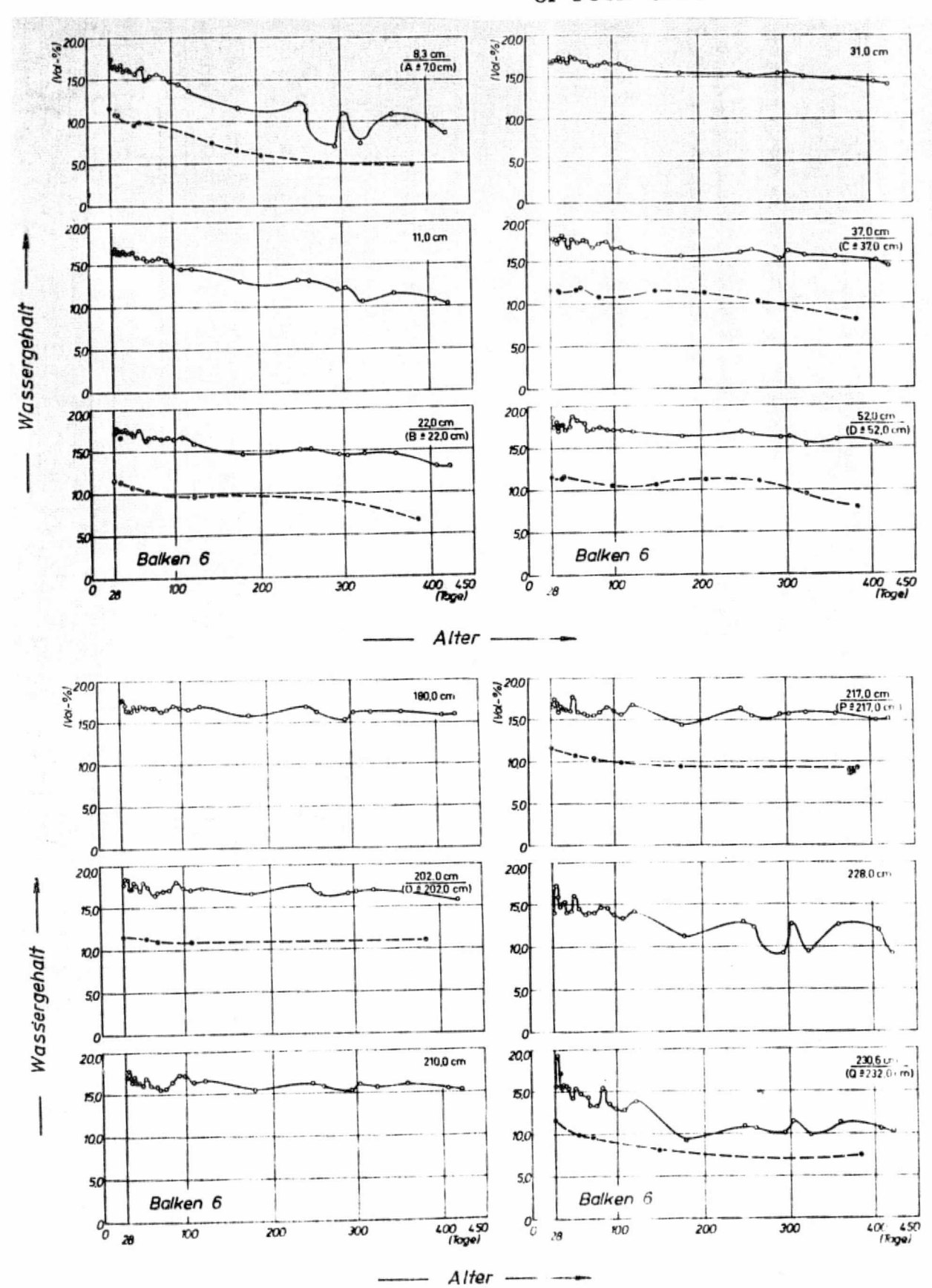


Figs. A 7 and 8. See key and caption on page 171.



Figs. A 9 and 10. see key and caption on page 171.

ORIGINAL PAGE IS OF POOR QUALITY



Figs. A 11 and 12. See key and caption on page 171.

Key, Figs. A 1-A 12: A. Water content

B. Beam

C. Days

D. Age

Captions, Figs. A 1-A 12

Figs. A l and A 2. Solid-line curves: change in total water content as a function of age at different distances from the heated end (space coordinates in cm); cf. section 2.2.3.3.2. Dotted-line curves: change in evaporatable water content as a function of age for measurement planes A to Q (distance from the heated end given in parentheses); cf. section 2.2.3.2.2.

Figs. A 3 and A 4. Solid-line curves: change in total water content as a function of age at different distances from the heated end (space coordinates in cm); cf. section 2.2.3.3.2. Dotted-line curves: change in evaporatable water content as a function of age for measurement planes A to Q (distance from the heated end given in parentheses); cf. section 2.2.3.2.2.

Figs. A 5 and A 6. Solid-line curves: change in total water content as a function of age at different distances from the heated end (space coordinates in cm); cf. section 2.2.3.3.2. Dotted-line curves: change in evaporatable water content as a function of age for measurement planes A to Q (distance from the heated end given in parentheses); cf. section 2.2.3.2.2.

Figs. A 7 and A 8. Solid-line curves: change in total water content as a function of age at different distances from the heated end (space coordinates in cm); cf. section 2.2.3.3.2. Dotted-line curves: change in evaporatable water content as a function of age for measurement planes A to Q (distance from the heated end given in parentheses); cf. section 2.2.3.2.2.

Figs. A 9 and 10. Solid-line curves: change in total water content as a function of age at different distances from the heated end (space coordinates in cm); cf. section 2.2.3.3.2. Dotted-line curves: change in evaporatable water content as a function of age for measurement planes A to Q (distance from the heated end given in parentheses); cf. section 2.2.3.2.2.

Figs. A 11 and 12. Solid-line curves: change in total water content as a function of age at different distances from the heated end (space coordinates in cm); cf. section 2.2.3.3.2. Dotted-line curves: change in evaporatable water content as a function of age for measurement planes A to Q (distance from the heated end given in parentheses); cf. section 2.2.3.2.2.

171

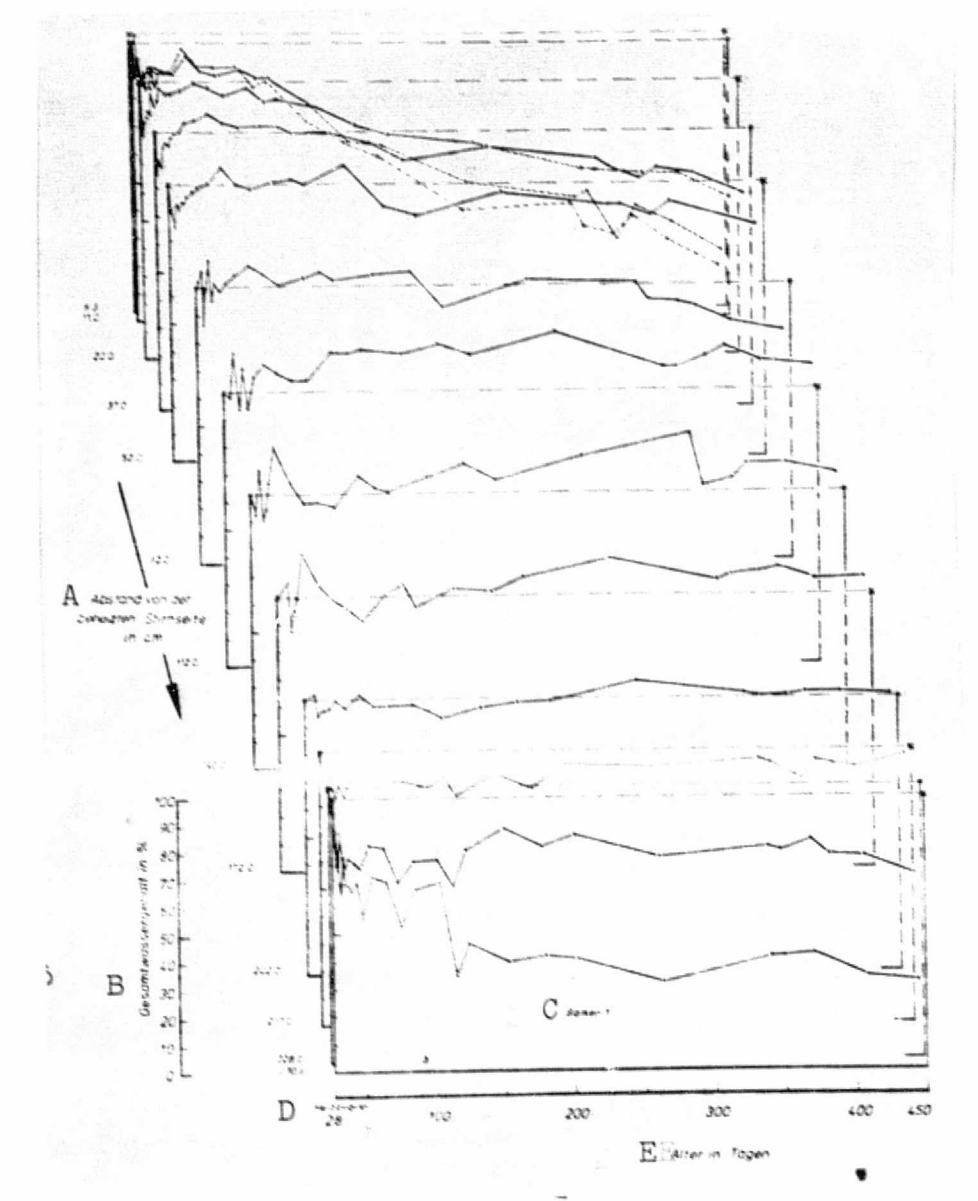


Fig. A 13. Change in total water content (as percentage of the initial value before the start of heating) as a function of the age of the concrete; plotted for 13 space coordinates (distance from the heated end) of beam 1 (cf. section 2.2.3.3.).

Key: A. Distance from the heated end in cm

B. Total water content

C. Beam

D. Start of heating

E. Age in days

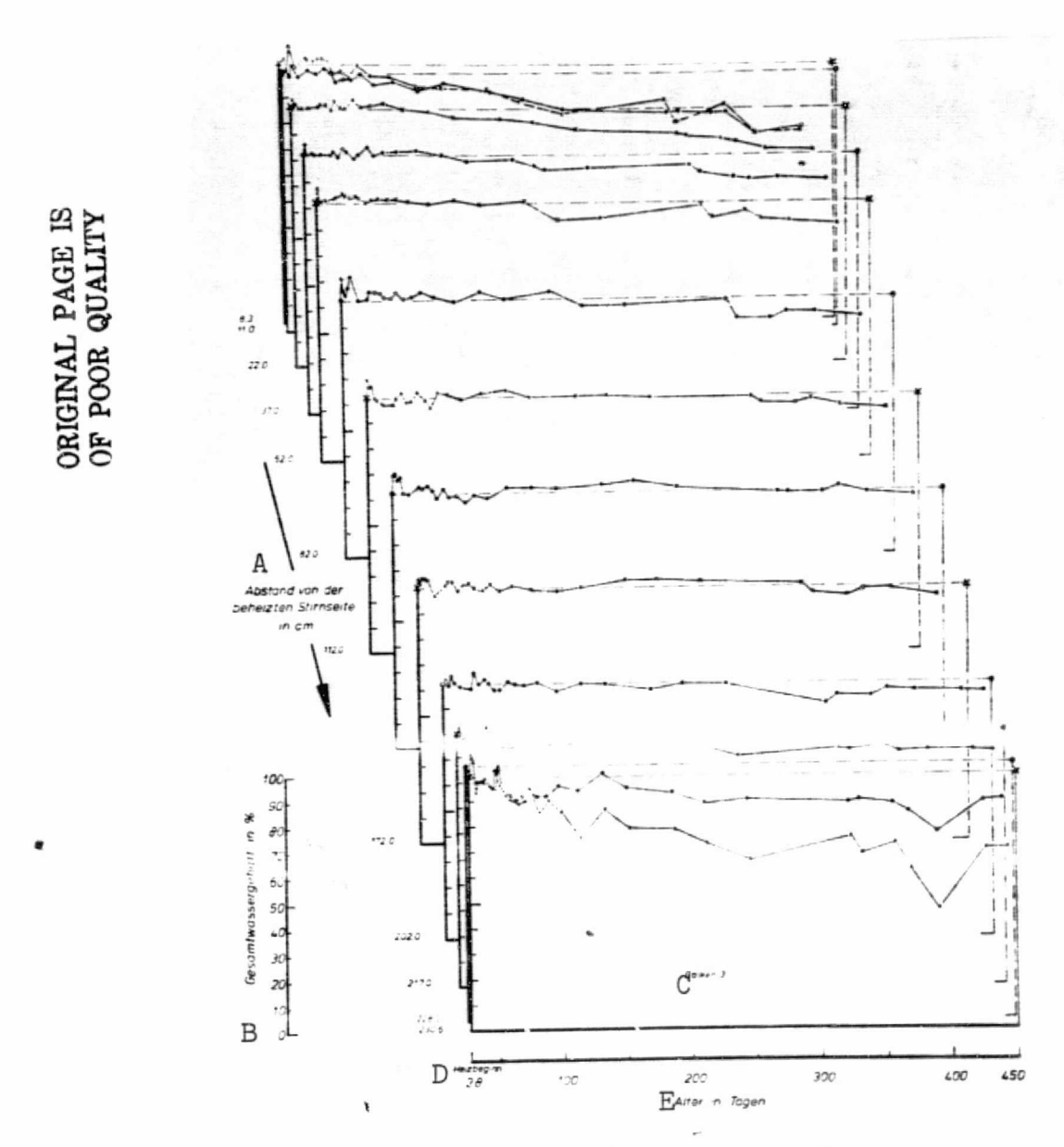


Fig. A 14. Change in total water content (as percentage of the initial value before the start of heating) as a function of the age of the concrete; plotted for 13 space coordinates (distance from the heated end) of beam 3 (cf. section 2.2.3.3.).

Key: A. Distance from the heated end in cm

- B. Total water content
- C. Beam
- D. Start of heating
- E. Age in days



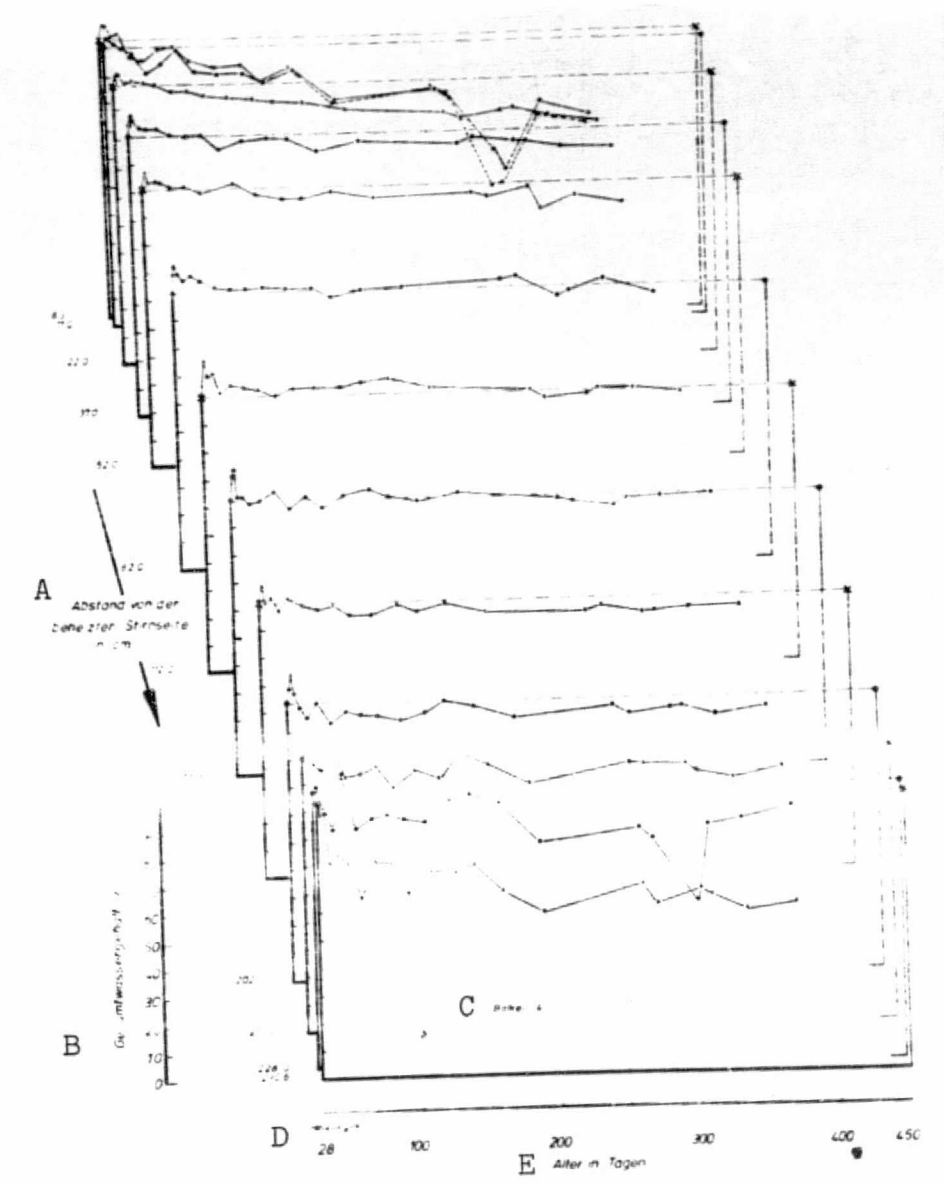


Fig. A 15. Change in total water content (as percentage of the initial value before the start of heating) as a function of the age of the concrete; plotted for 13 space coordinates (distance from the heated end) of beam 4 (cf. section 2.2.3.3.).

Key: A. Distance from the heated end in cm

B. Total water content

C. Beam

D. Start of heating

E. Age in days

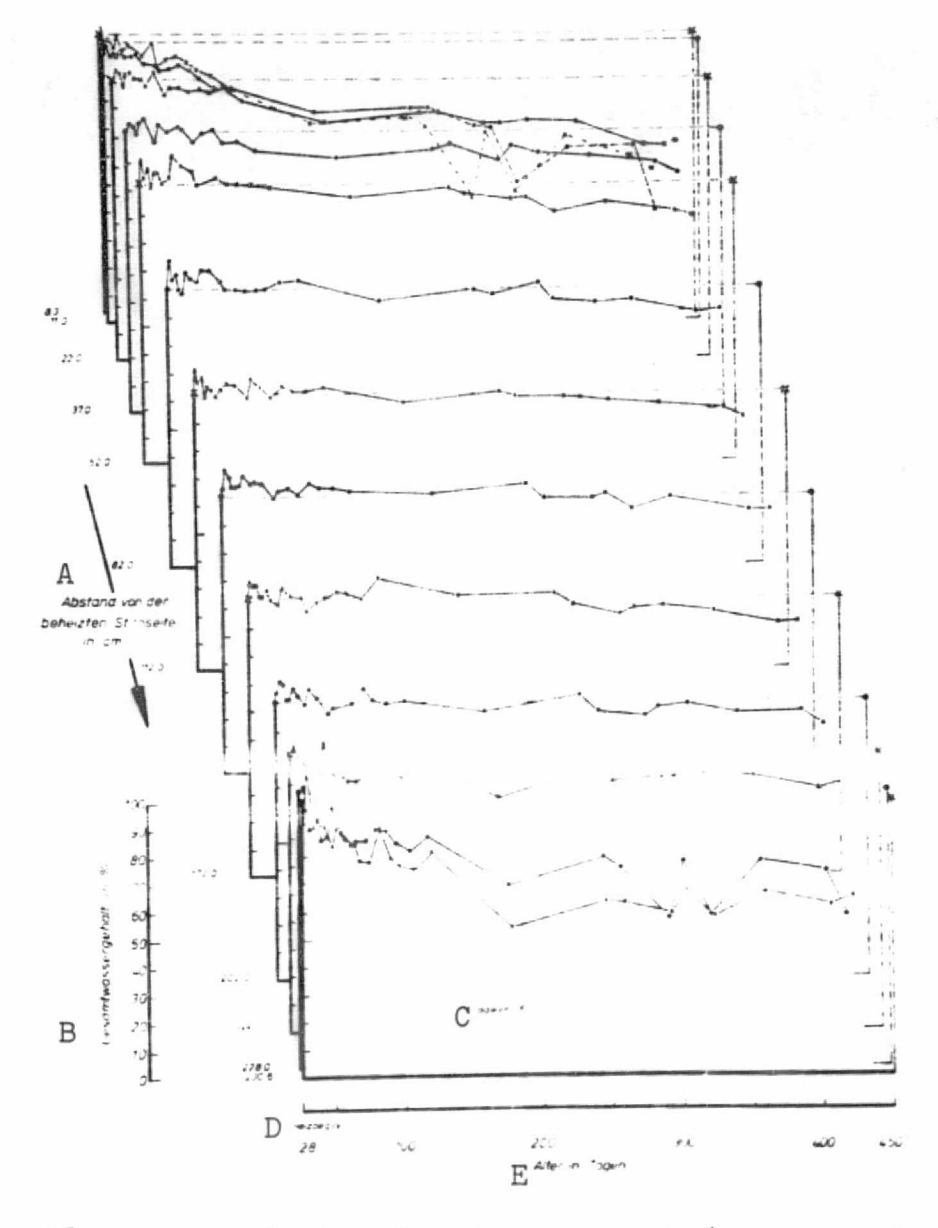


Fig. A. 16. Change in total water content (as percentage of the initial value before the start of heating) as a function of the age of the concrete; plotted for 13 space coordinates (distance from the heated end) of beam 6 (cf. section 2.2.3.3.).

Key: A. Distance from the heated end in cm

B. Total water content

C. Beam

D. Start of heating

E. Age in days

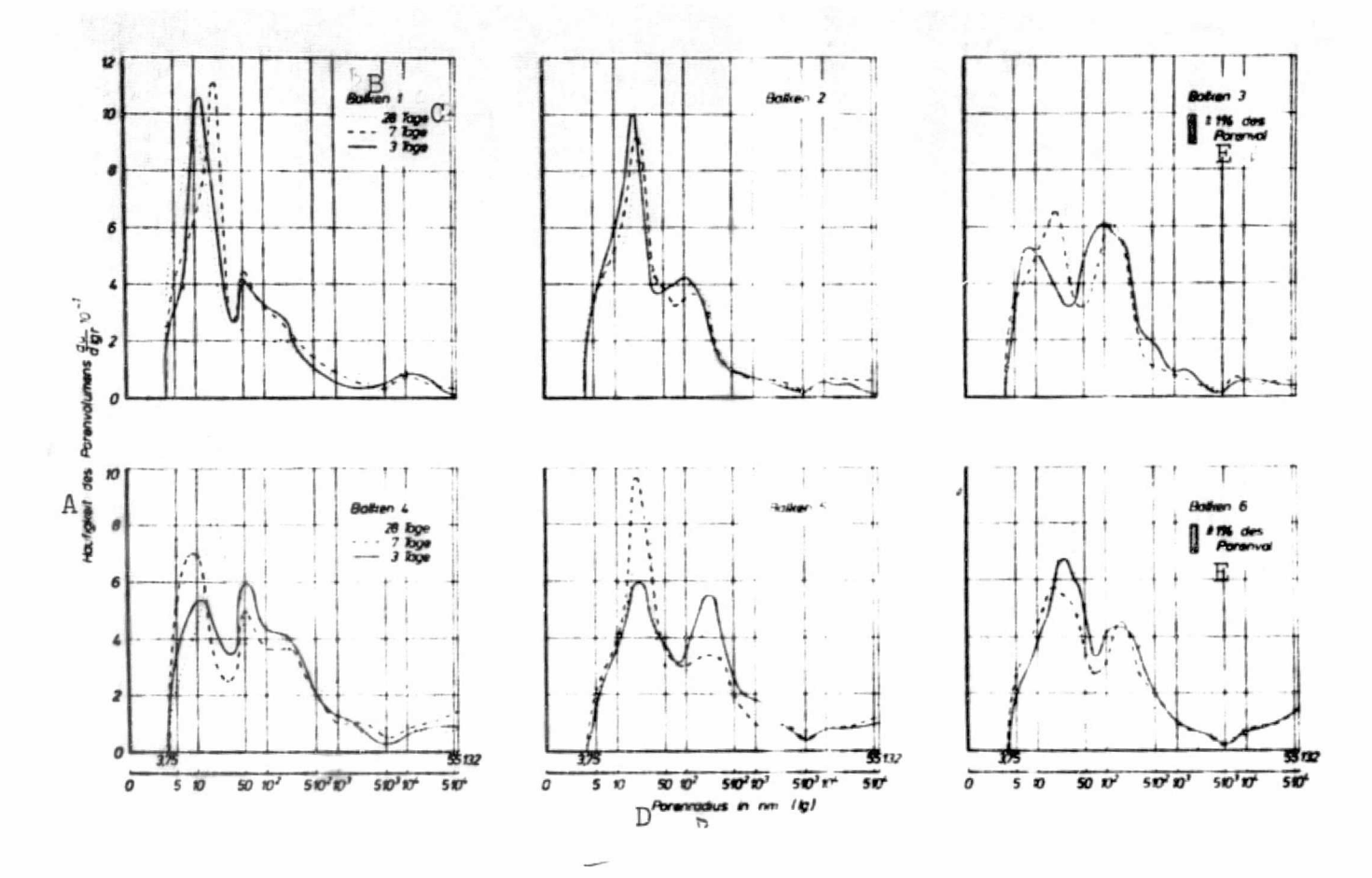


Fig. A 17. Pore volume frequency distribution for matrix mortars of calcite concretes (beams 1-3) and gravel-sand concretes (beams 4-6) at an age of 3, 7 and 28 days (cf. section 2.3.4.2.).

Key: A. Pore volume frequency

B. Beam

C. Days

D. Pore radius

E. One percent of the pore volume

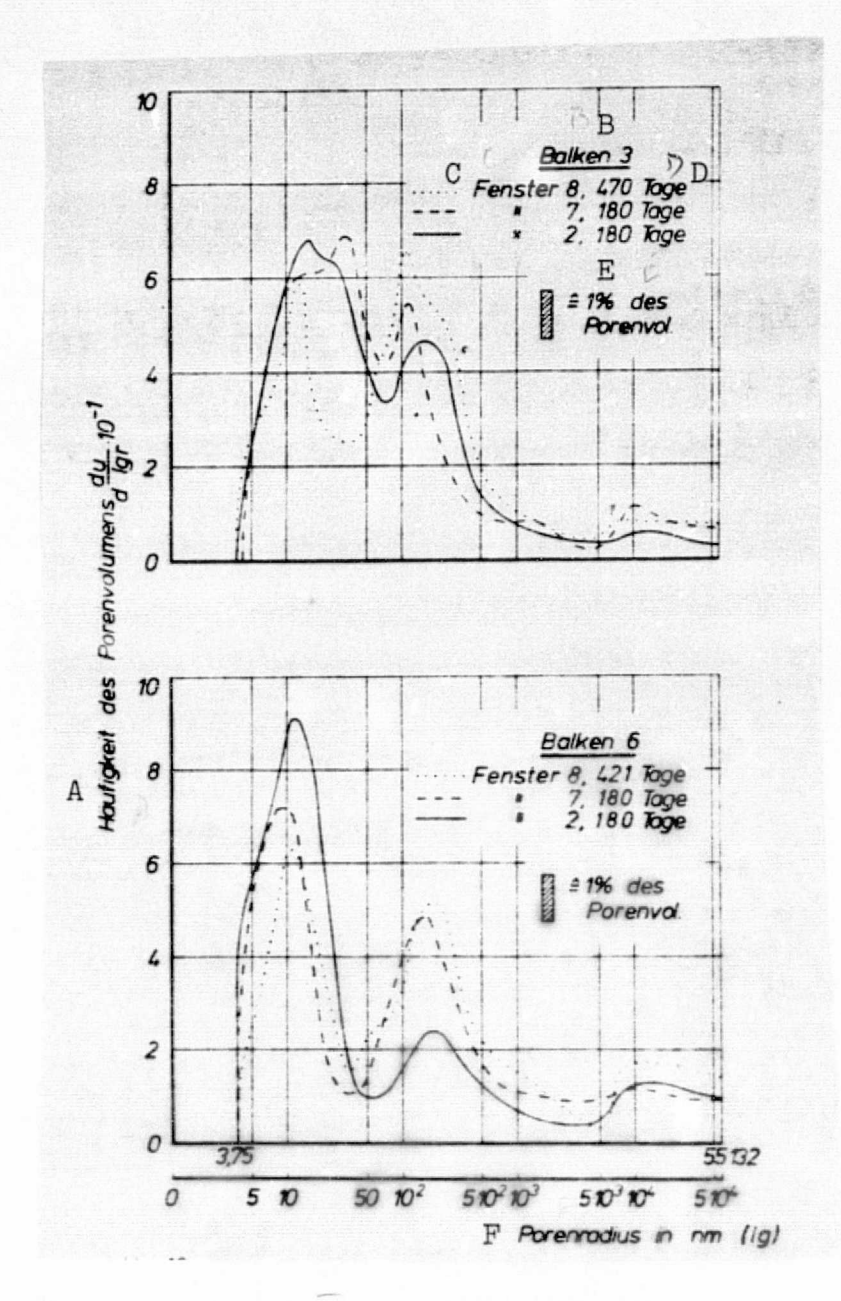


Fig. A 18. Pore volume frequency distribution of the matrix mortars from windows 8, 7 and 2 of beam 3 (calcite concrete; age, 180 and 470 days) and of beam 6 (gravel-sand concrete; age, 180 and 421 days) (cf. section 2.3.4.2.).

Key: A. Pore volume frequency

B. Beam

C. Window

D. Days

E. One per cent of the pore volume

F. Pore radius

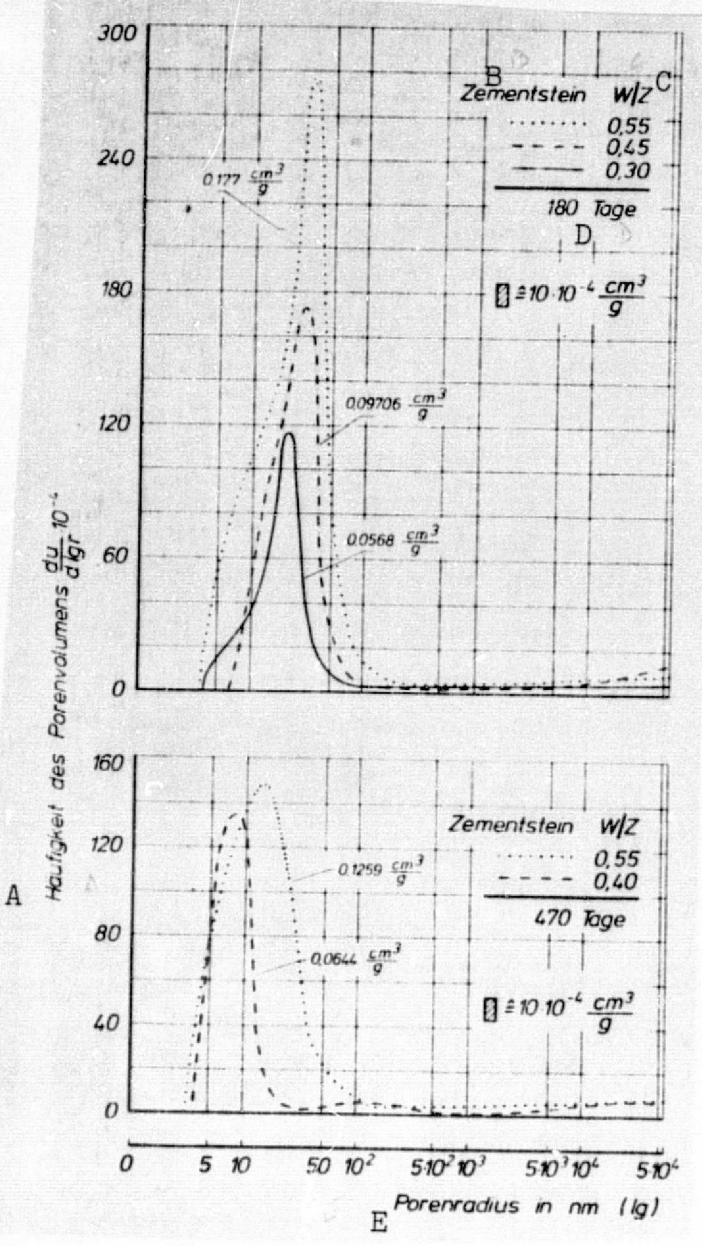


Fig. A. 19. Frequency distributions of the weight-related pore volumes of hardened cement paste with different water/cement ratios at an age of 180 and 470 days (cf. section 2.3.4.2.).

Key: A. Pore volume frequency

B. Hardened cement paste

C. Water/cement ratio

D. Days

E. Pore radius

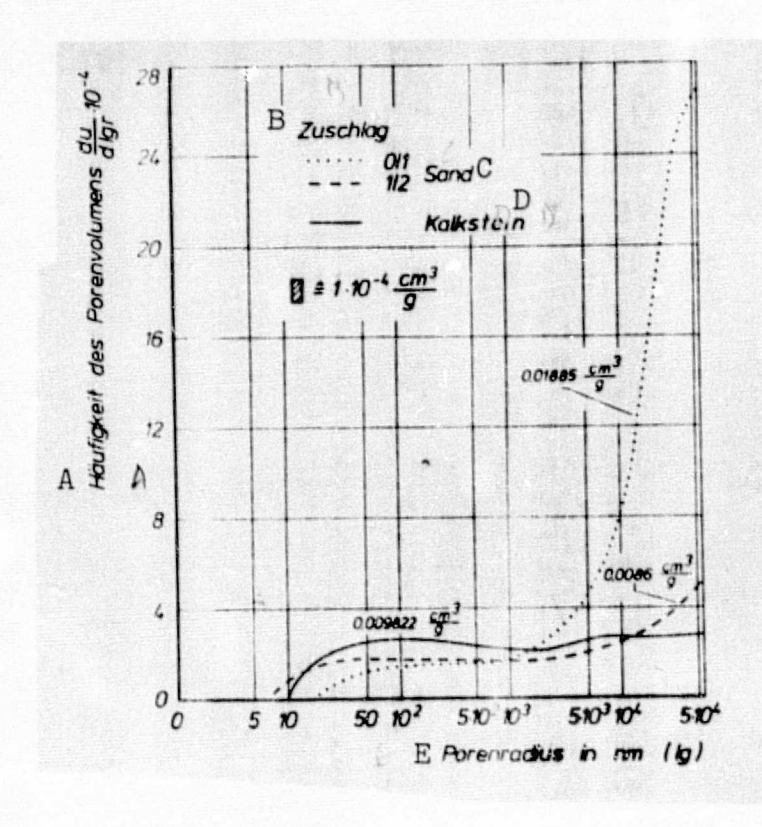


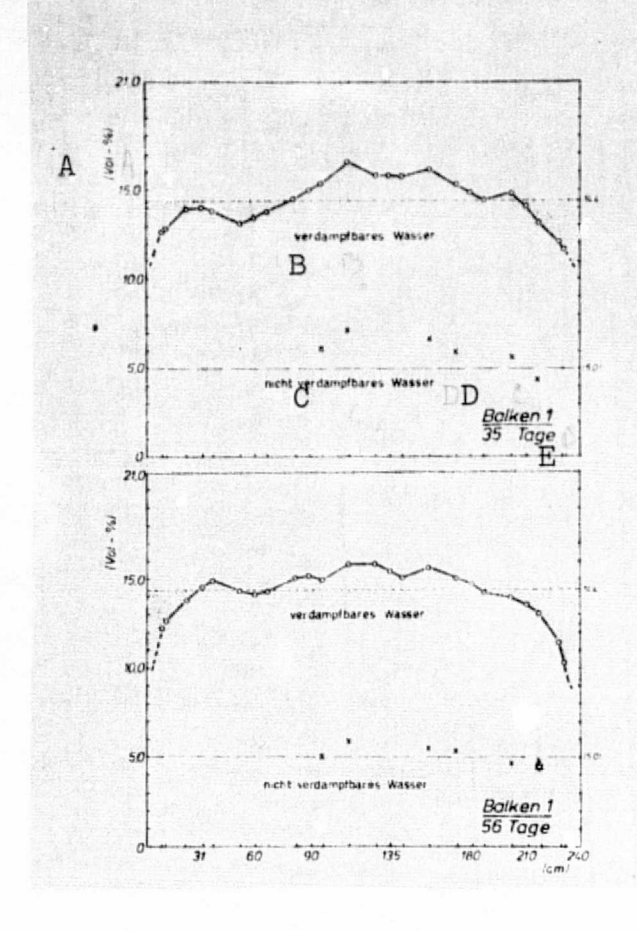
Fig. A 20. Frequency distributions of the weight-related pore volumes of samples of gravel-sand and calcite aggregate (limestone) (cf. section 2.3.4.2.).

Key: A. Pore volume frequency

B. Aggregate C. Sand

D. Limestone

E. Pore radius



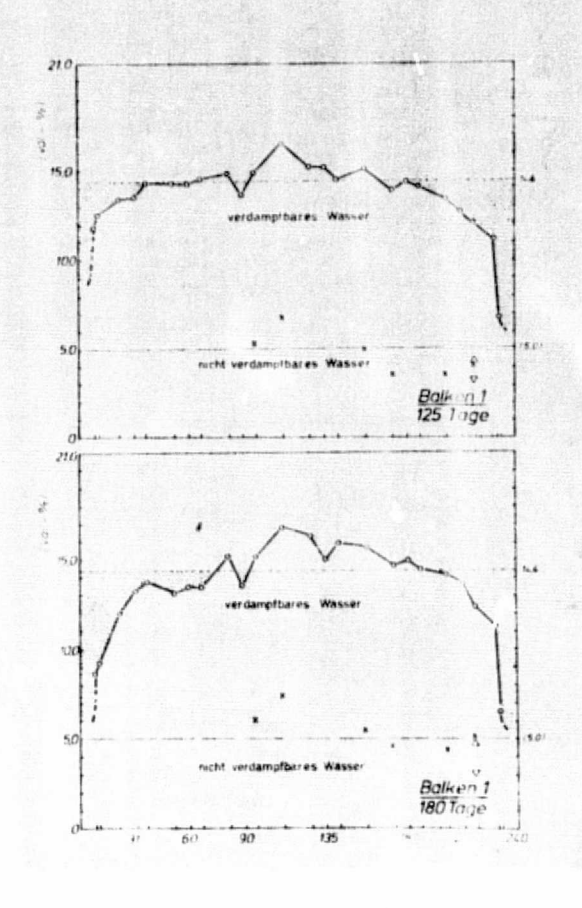


Fig. A 21 and 22. Water content balances over beam length; the upper limit of the dot-shaded fields corresponds to the mean initial water content (cf. section 2.5.1.).

Key: A. % by volume

B. Evaporatable water

C. Non-evaporatable water

D. Beam

E. Days

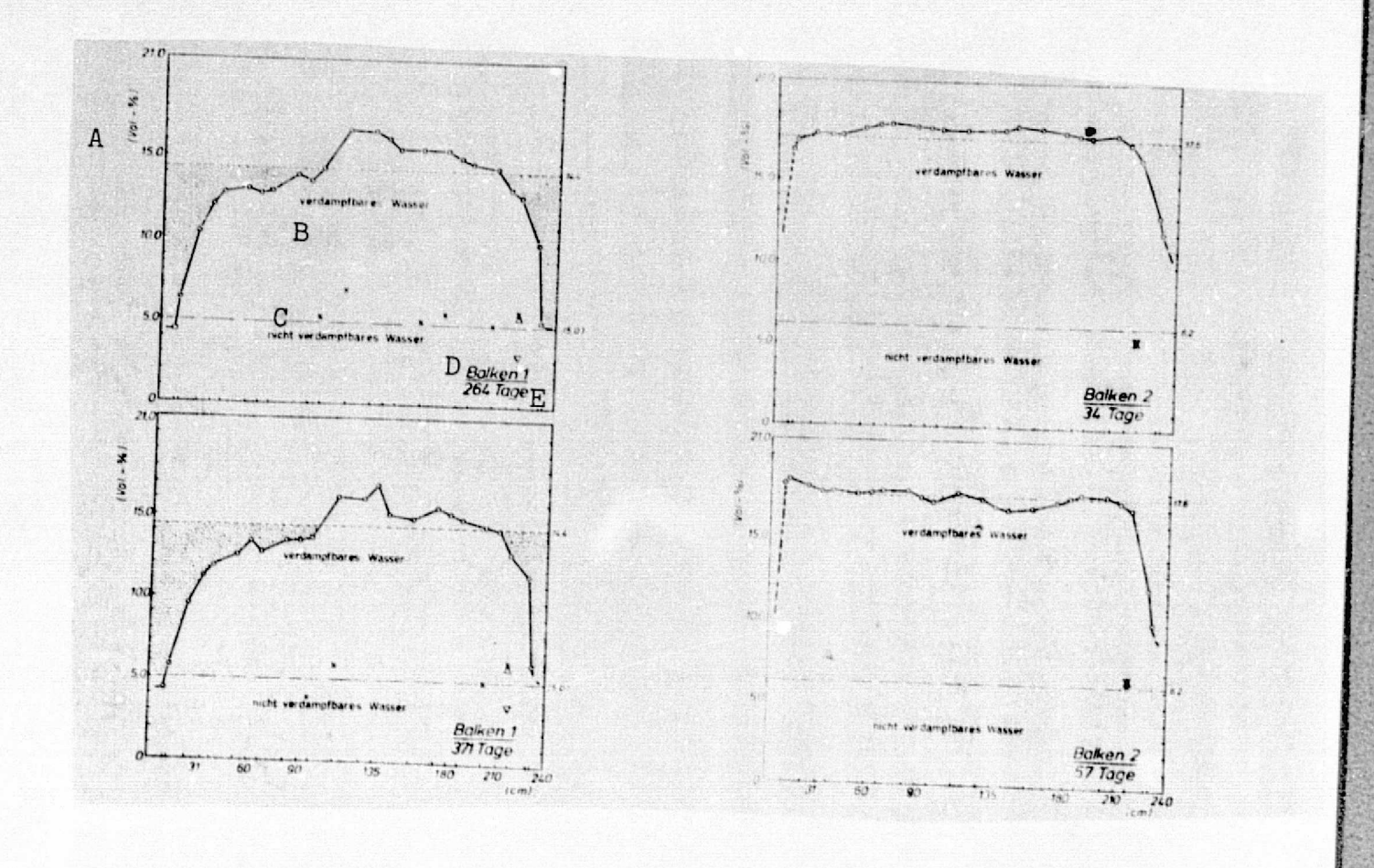


Fig. A 23 and 24. Water content balances over beam length; the upper limit of the dot-shaded fields corresponds to the mean initial water content (cf. section 2.5.1.).

Key: A. % by volume

B. Evaporatable water

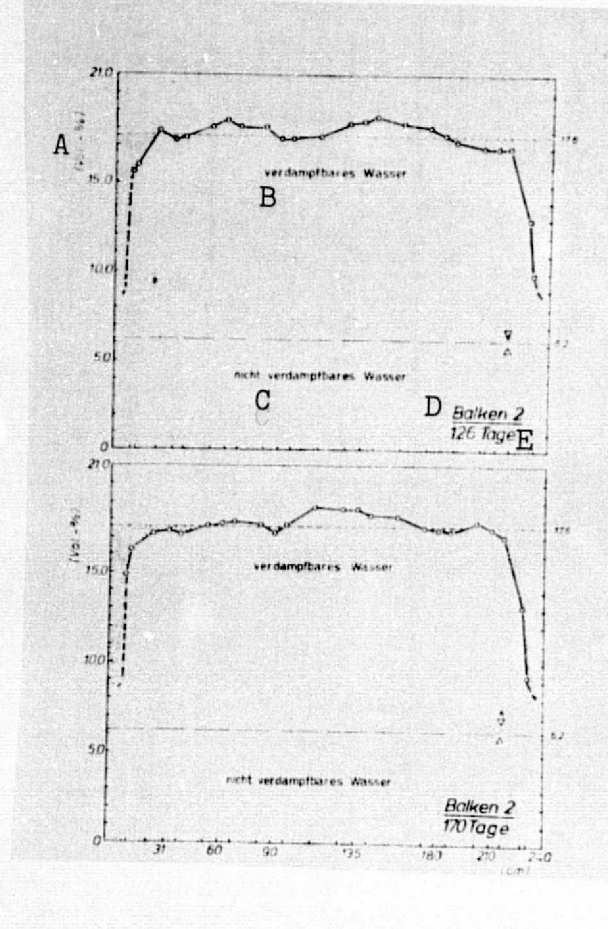
C. Non-evaporatable water

1 80

D. Beam

E. Days

181



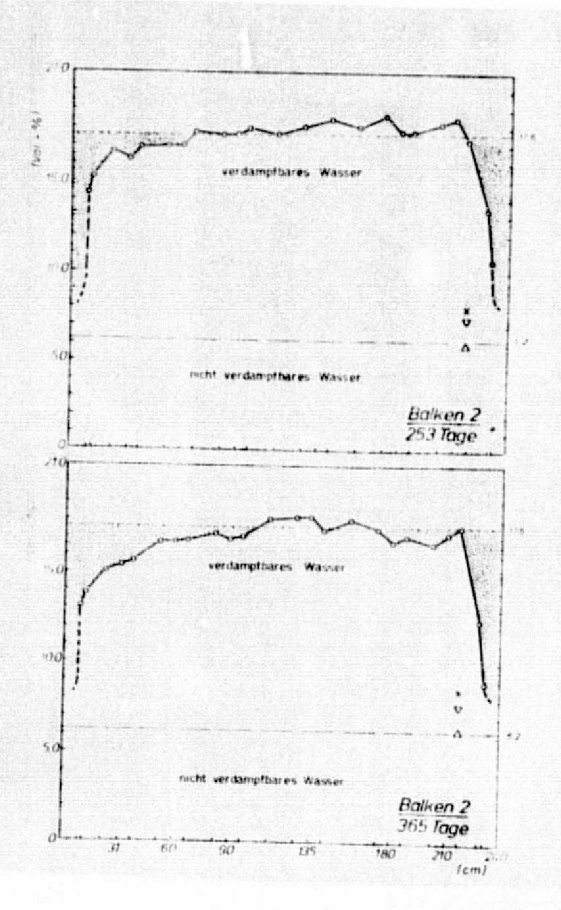


Fig. A 25 and 26. Water content balances over beam length; the upper limit of the dot-shaded fields corresponds to the mean initial water content (cf. section 2.5.1.).

Key: A. % by volume

B. Evaporatable water

C. Non-evaporatable water

D. Beam

E. Days

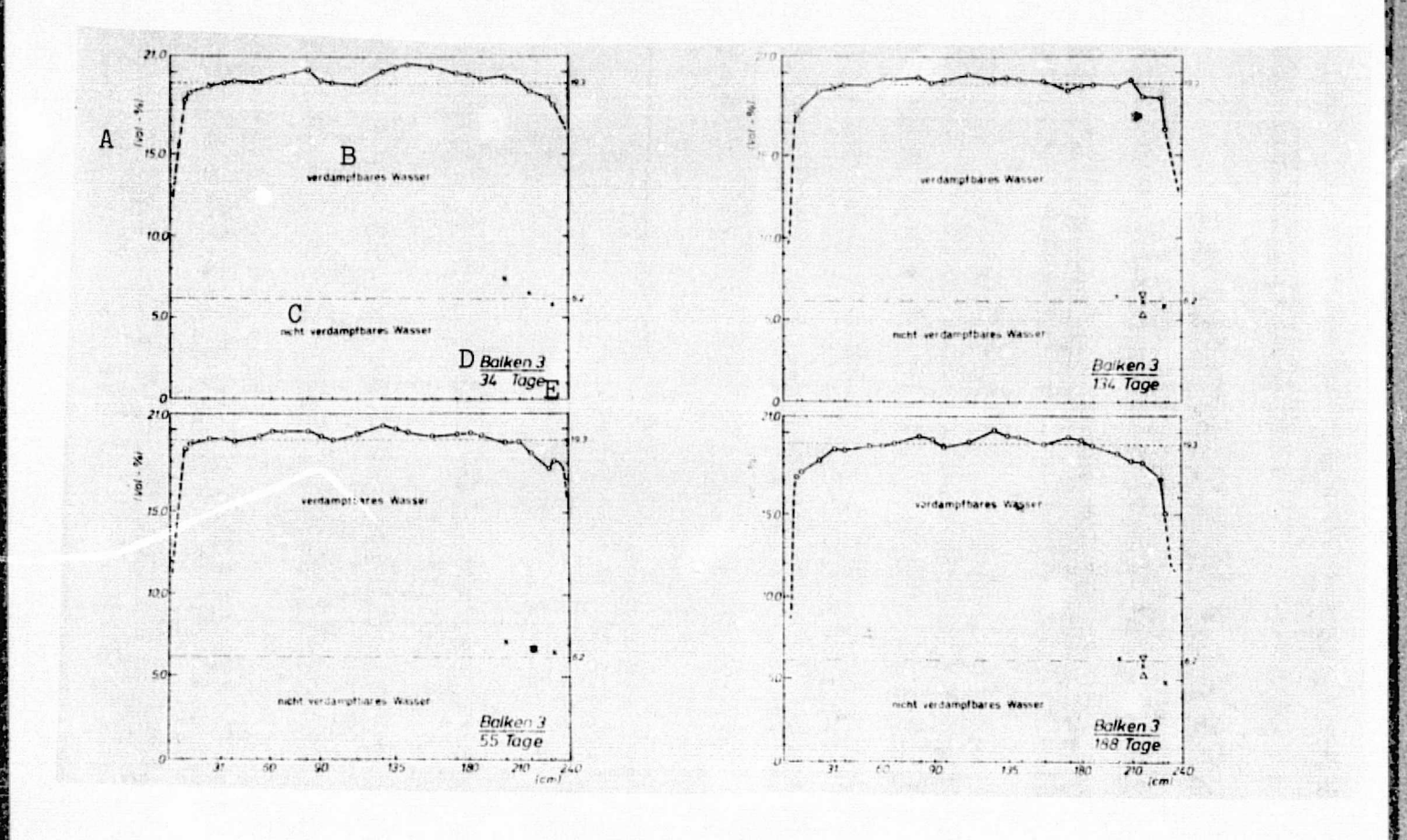


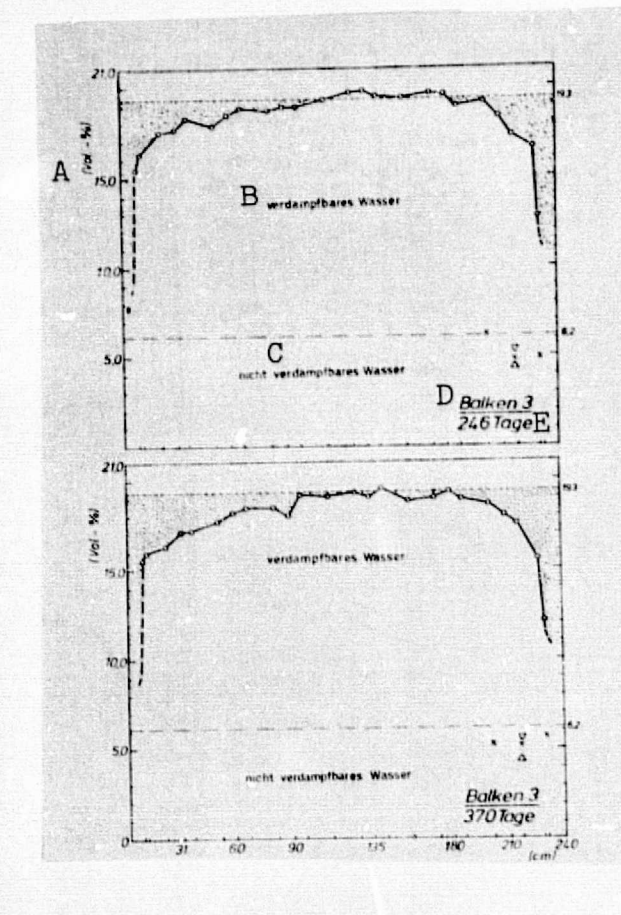
Fig. A 27 and 28. Water content balances over beam length; the upper limit of the dot-shaded fields corresponds to the mean initial water content (cf. section 2.5.1.).

Key: A. % by volume

B. Evaporatable water

C. Non-evaporatable water D. Beam

E. Days



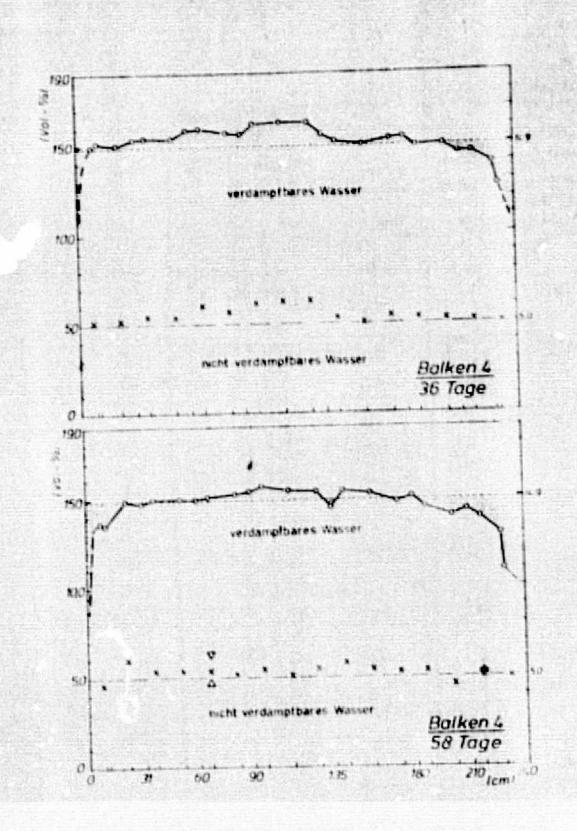


Fig. A 29 and 30. Water content balances over beam length; the upper limit of the dot-shaded fields corresponds to the mean initial water content (cf. section 2.5.1.).

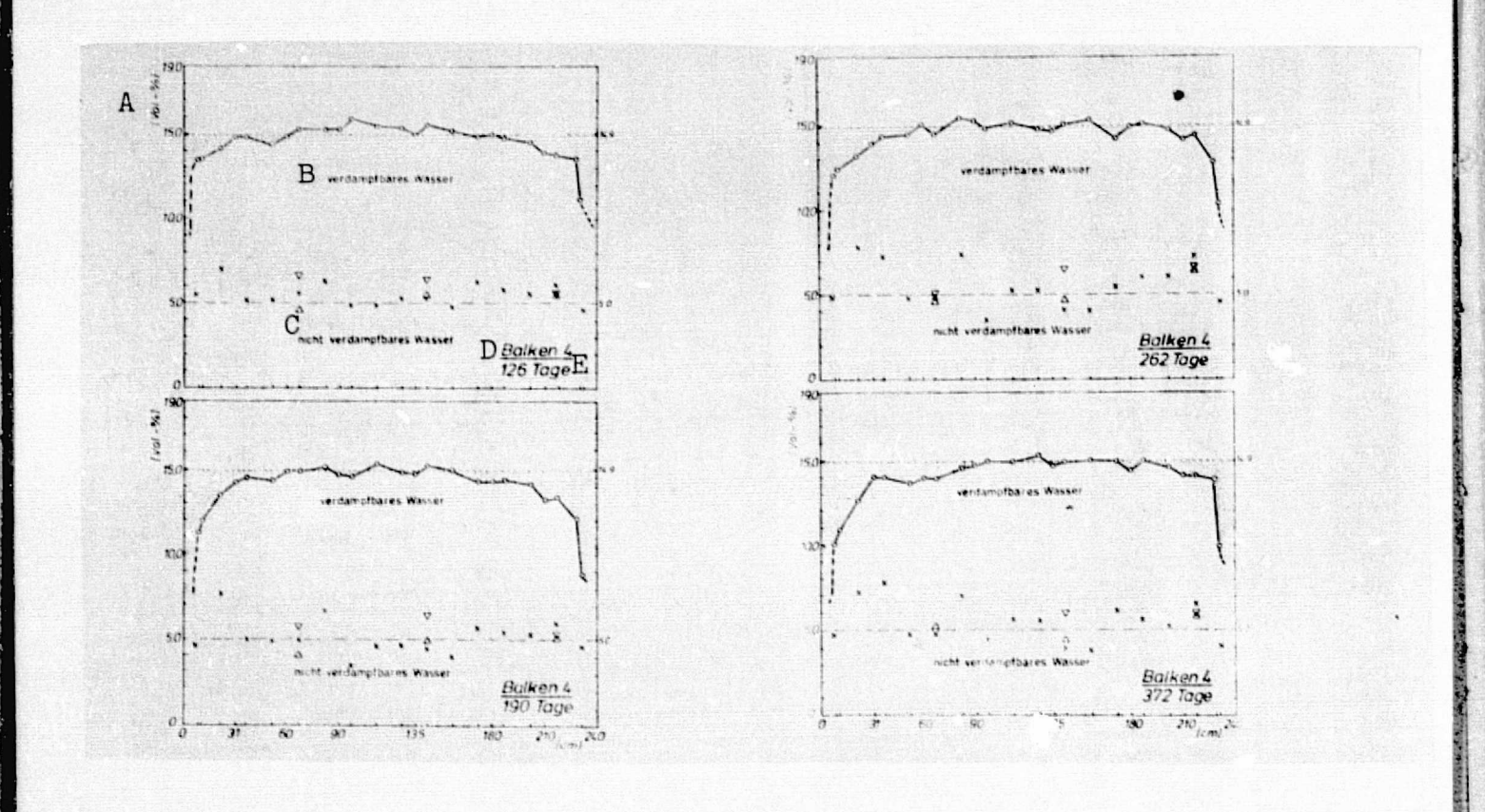
Key: A. % by volume

B. Evaporatable water

C. Non-evaporatable water

D. Beam

E. Days



ma (四日 (日本) 日本 (日本)

Fig. A 31 and 32. Water content balances over beam length; the upper limit of the dot-shaded fields corresponds to the mean initial water content (cf. section 2.5.1.).

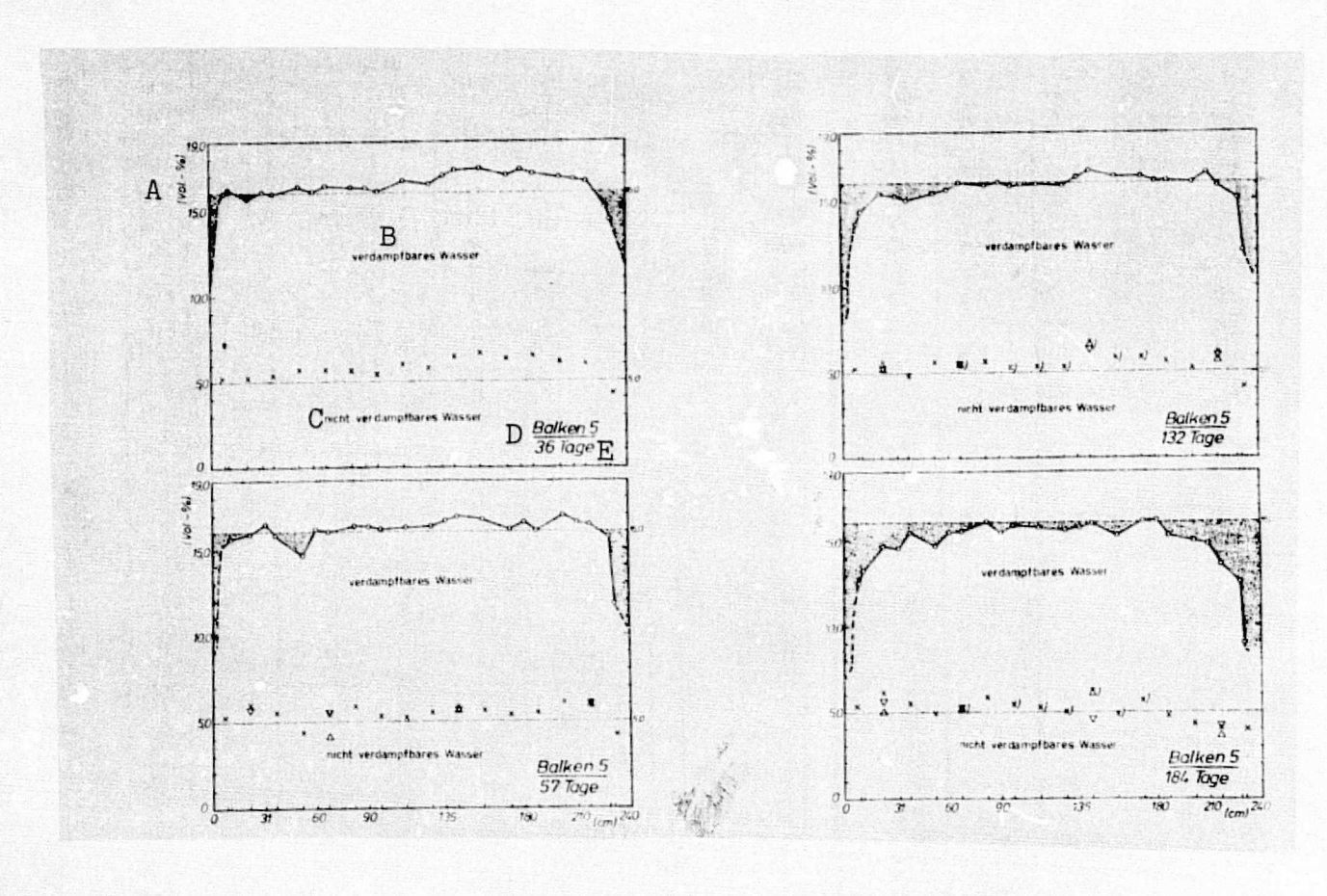
Key: A. % by volume

B. Evaporatable water

C. Non-evaporatable water

D. Beam

E. Days



ORIGINAL PAGE IS

Fig. A 33 and 34. Water content balances over beam length; the upper limit of the dot-shaded fields corresponds to the mean initial water content (cf. section 2.5.1.).

Key: A. % by volume

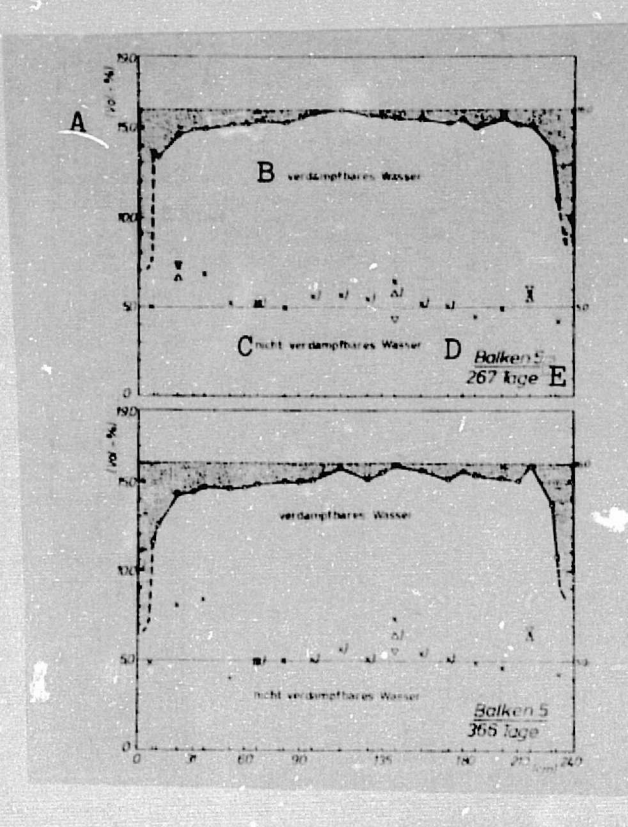
B. Evaporatable water

C. Non-evaporatable water

D. Beam

E. Days

C-3



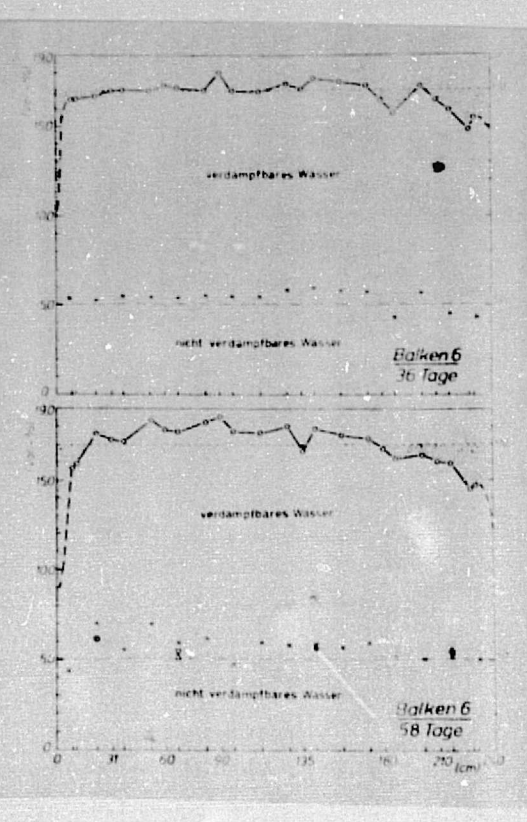


Fig. A 35 and 36. Water content balances over beam length; the upper limit of the dot-shaded fields corresponds to the mean initial water content (cf. section 2.5.1.).

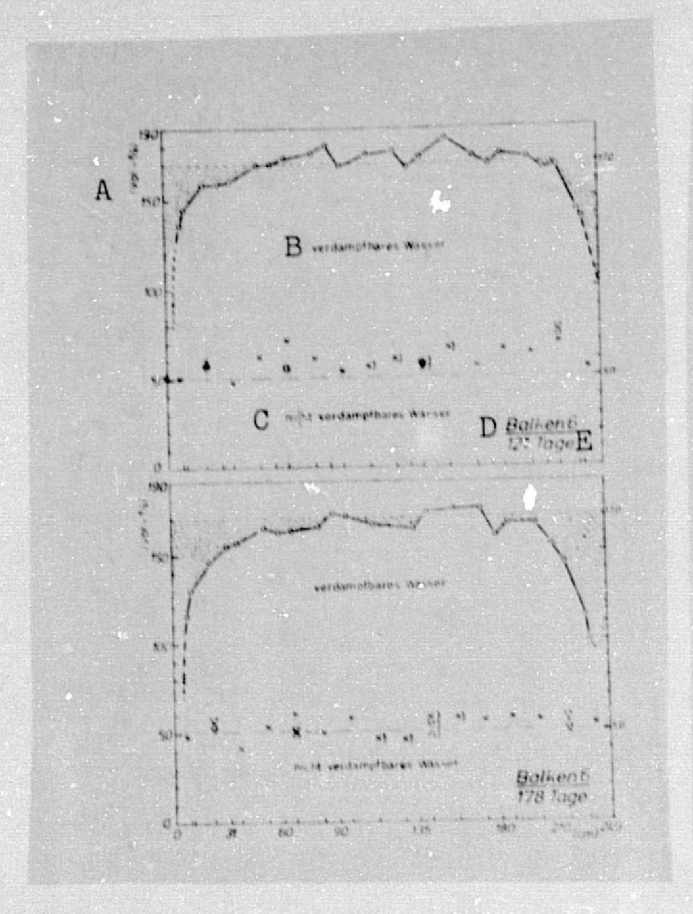
Key: A. % by volume

B. Evaporatable water

C. Non-evaporatable water

D. Beam

E. Days



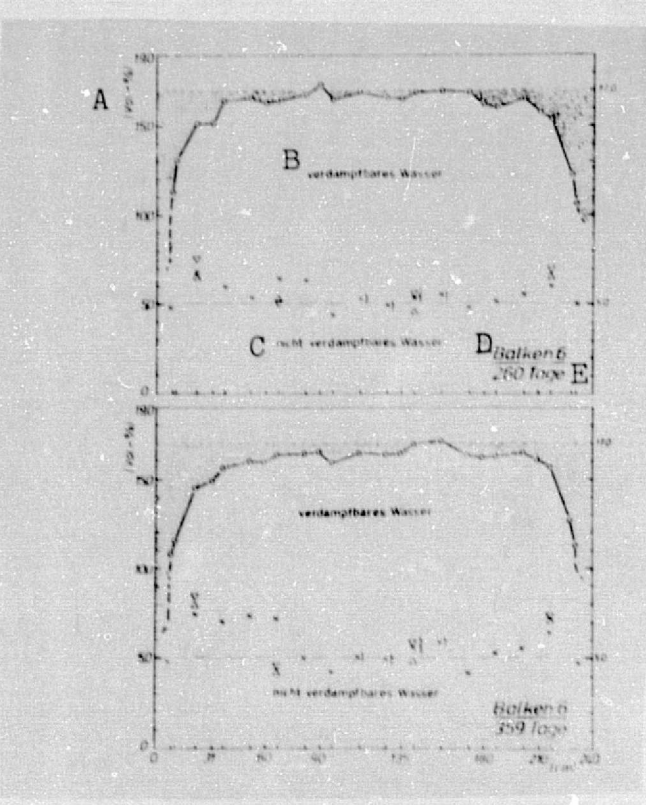


Fig. A 37 and 38. Water content balances over beam length; the upper limit of the dot-shaded fields corresponds to the mean initial water content (cf. section 2.5.1.).

Key: A. % by volume

B. Evaporatable water

C. Non-evaporatable water

D. Beam E. Days

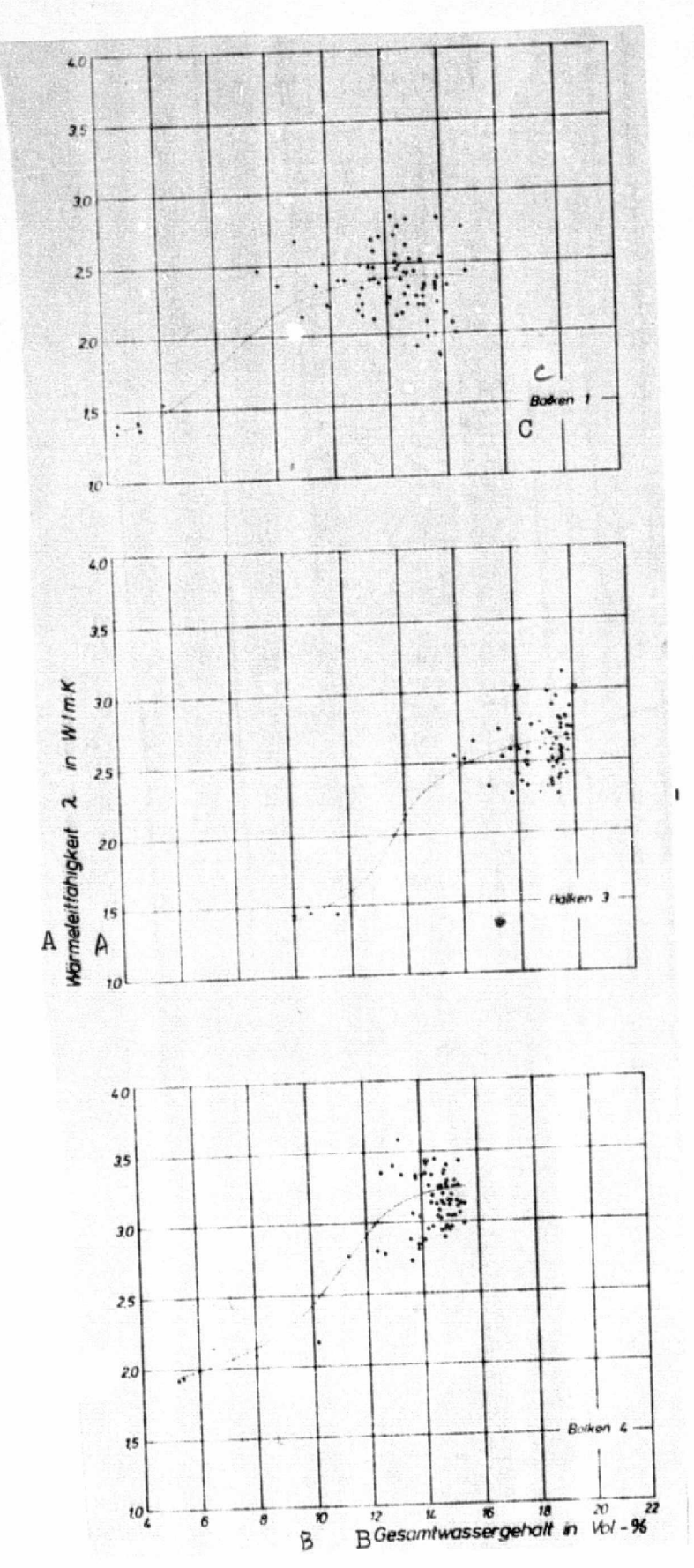


Fig. A 39. Thermal conductivity (λ) as a function of water content with smoothed curve for beams 1, 3 and 4 (cf. Fig. 59 in section 2.5.3.).

Key: A. Thermal conductivity

B. Total water content in % by volume

C. Beam

The following books have been published since 1945 in the series sponsored by the German Commission for Reinforced Concrete:

No. 100: Experiments on Reinforced Concrete Beams to Determine the Reinforcing Limit, by Willy Gehler, Hermann Amos and Erich Friedrich.

Experimental Results and the Dresden Calculation Method for the Plastic Range of Concrete (1949), by Willy Gehler. out of print

No. 101: Experiments to Determine the Degree of Cracking and Strength of Reinforced Concrete Plates with Different Reinforcing Bars with Incrementally Increased Load, by Otto Graf and Kurt Walz.

Experiments on the Swell Tensile Strength of Snaked Reinforcing Bars, by Otto Graf and Gustav Weil.

Experiments on the Behavior of Cold Worked Structural Steels When Bent Back After Treating the Specimens in Various Ways, by Otto Graf and Gustav Weil.

Experiments for Determining the Interaction of Precast Reinforced Concrete Structural Members for Roofs (1948), by Hermann Amos and Walter Bochmann. out of print

- No. 102: Concrete and Cement in Seawater (1950) and further editions, by Alfred Eckhardt and Walter Kronsbein. 8.50 DM
- No. 103: The n-free Method of Calculating a Simple Reinforced, Rectangular Steel Concrete Beam (1951), by K.B. Haberstock. out of print
- No. 104: Binders for Mass Concrete. Studies on Hydraulic Binders Made from Cement, Lime and Trass (1951), by Kurt Walz. out of print
- No. 105: The Experiment Reports of the German Commission for Reinforced Concrete (1951), by Otto Graf. out of print
- No. 106: Calculation Tables for Right-Angled Roadway Plates for Highway Bridges (1952), by Hubert Rusch. 6h revised edition. out of print
- No. 107: The Ball Impact Test for Concrete (1952), by Kurt Gaede. out of print
- No. 108: Compaction of Lightweight Concrete by Vibration (1952), by Kurt Walz.

- No. 109: 503 Concentration of Aggregates (1952), by Kurt Gaede. 6. DM
- No. 110: Crushed Brick Concrete (1952), by Karl Charisius, Walther Drichsil and Alfred Hummel. cut of print
- No. 111: Model Experiments on the Influence of Torsional Rigidity for a T-beam Bridge (1952), by Gerhard Marten. out of print
- No. 112: Prestressed Concrete Railroad Bridges (1953 and 1961)
 2nd enlarged edition, by Rudolf Buhrer. 14.50 DM
- No. 113: Buckling Tests with Reinforced Concrete Columns, by Willy Gehler and Alfred Hutter.
 - Strength and Elasticity of Concrete with High Strength (1954), by Otto Graf. out of print
- No. 114: Heaped Concrete Made from Various Aggregates, by

 Alfred Hummel and K. Wesche.

 Determination of the Granular Stability of Crushed
 Brick and Other Lightweight Concrete Aggregates (1954),
 by Alfred Hummel. 7. DM
- No. 115: The Federal Railway Experiments on Prestressed Concrete Beams in Kornwestheim (1954), by Ulrich Giehrach and Christian Sattele.
- No. 116: Compaction of Concrete with Immersion Vibrators and Vibration Tables, Quality Control of Structural Floor Units (1954), by Kurt Walz. out of print
- No. 117: Aerated and Porous Cement: Bearing Capacity of Walls and Contraction, by Otto Graf and Hermann Schaffler.

 Ball Impact Testing of Porous Concrete (1954), by out of print
- No. 118: Sulfur Bonding in Cinder Concrete (1954), by Adolf Stois, Franz Rost, Helene Zinnert, Fritz Henkel. 13. DM
- No. 119: Experiments on the Bond Between Precast Reinforced Concrete Beams and In-situ Concretes, by Otto Graf and Gustav Weil.

 Experiments on Lightweight Steel Beams for Reinforced Concrete Floors (1955): by Gustav Weil. out of print

- No. 120: Experiments on the Strength of the Bending Pressure Zone (1955), by Hubert Rusch. out of print
- No. 121: Aerated and Porous Concrete: (1956)

 Experiments on Shearing Protection for Beams Made of Reinforced Aerated and Porous Concrete, by Hubert Rusch.

Compensation Moisture of Vapor-Hardened Aerated and Porous Concrete, by Hermann Schaffler.

Experiments to Test the Degree of Shrinkage and Swelling of Aerated and Porous Concrete, by Otto Graf and Hermann out of print

- No. 122: Shape Stability of Concrete Bodies, by Kurt Walz.

 Hot Tensile Tests with Reinforcing Bars, by Dannenberg,
 Deutschmann and Melchior.
 - Concentrated Load Recording in Concrete (1957), by Wolfgang Pohle.
- No. 123: Air Entraining Agents for Concrete (1956), by Kurt out of print
- No. 124: Concrete in Seawater (1956), by Alfred Hummel and K. Wesche.
- No. 125: Studies on Spring Joints (1957), by Karl Kammuller out of print
- No. 126: SO Concentration of Aggregates--Long-term Experiments, by Kurt Gaede. (Supplement to No. 109).

Concrete Penetration Depth in Lightweight Wood Fiber Building Panels (1957), by Kurt Gaede. 10. DM

- No. 127: Weather Resistance of Concrete (1957), by Kurt Walz.
 9. DM
- No. 128: Ball Impact Testing of Concrete (Influence of the Age of the Concrete) (1957), by Kurt Gaede. out of print
- No. 129: Reinforced Concrete Columns Under Short-term and Long-term Load (1958), by Kurt Gaede.
- No. 130: Safety Against Fracture during Prestressing without Bond (1959), by Hubert Rusch, Karl Kordina, Coelestin Zeiger.

- No. 131: The Creep of Unreinforced Concrete (1958), by Otto out of print
- No. 132: Fire Tests with Heavily Reinforced Concrete Columns, by Horst Seekamp.
- Stability of Steel Concrete Structural Members and Ribbed Floors with Hollow Stone Fillers in Fires by Max Hannemann and Heinrich Thoms, (1959). 9 DM
- No. 133: Aerated and Porous Concrete: (1959)

Compressive Strength of Vapor-hardened Aerated Concrete after Various Types of Curing, by Hermann Schaffler.

The Bearing Capacity of Reinforced Panels Made of Vapor-aerated and Porous Concrete, by Hermann Schaffler.

The Interaction of Porous Concrete with Heavy Concrete in Reinforced Heavy Concrete Beams with Porous Concrete Shells on the Sides, by Hubert Rusch and Erhardt Lassas.

9. DM

- No. 134: The Behavior of Concrete in Chemically Corrosive Waters (1959), by Kurt Seidel. out of print
- No. 135: Experiments on the Load Produced on Shuttering during the Pouring of Concrete, by Otto Graf and Ferdinand Kaufmann.

Compressive Strength of Concrete in the Upper Regions after Compacting with an Immersion Vibrator, by Kurt Walz and Hermann Schaffler.

Tests on the Compaction of Concrete on a Vibration
Table in a Loosely Erected Form and in a Fixed Form
by Hermann Schaffler.

out of print

No. 136: Aerated and Porous Concrete: (1960)

Experiments on the Anchorage of Reinforcement in Aerated Concrete, by Hermann Schaffler.

The Creep of Reinforced Slab Made of Vapor-hardened Aerated and Porous Concrete, by Hermann Schaffler. 21. DM

- No. 137: Shearing Tests on Prestressed Concrete Beams without Shear Reinforcement, by Hubert Rusch and Gunnar Vigerust. The Shearing Strength of Prestressed Concrete Beams without Shear Reinforcement (1960), by Gunnar Vigerust. out of print The Principles of Bonding between Steel and Concrete No. 138: (1961), by Gallus Rehm. out of print Theoretical Evaluation of No. 120--Strength of the Bending Pressure Zone (1961), by Gunter Scholz. No. 139:
- 10.70 DM
- No. 140: Experiments with Concrete Shuttering Rods (1963), by Hubert Rusch and Gallus Rehm. 29.80 DM
- No. 141: The Mirror Optics Method (1962), by Hans Weidemann and Werner Koepcke. 18.40 DM
- No. 142: Injection Mortar for Prestressed Concrete (1960), by Walter Albrecht and Hermann Schmidt. 13.50 DM
- No. 143: Aerated and Porous Concrete (1961) Rust Protection for the Reinforcement, by Walter Albrecht and Hermann Schaffler. Strength of the Bending Pressure Zone, by Walter Albrecht and Hermann Schaffler. 28. DM
- No. 144: Tests on the Strength and Deformation of Concrete during Compressive Repeating Load, by Kurt Gaede. The Influence of the Size of Test Samples on the Cube Strength of Concrete (1962), by Kurt Gaede. 27. DM
- No. 145: Shearing Tests on Right-angle Reinforced Concrete Beams with Uniformly Distributed Load, by Hubert Rusch, Finn Robert Haugli and Horst Mayer. Reinforced Concrete Beams under the Simultaneous Effect of Shearing Force and Moment (1962), by Finn Robert Haugli. 29. DM

No. 146: The Influence of the Type of Cement, the Water/Gement Ratio and the Load Duration on the Creep of Concrete, by Alfred Hummel, Karlhaus Wesche and Walter Brand.

The Influence of the Mineralogical Characteristics of Aggregates on the Creep of Concrete (1962), by Hubert Rushc, Karl Kordina and Humber Hilsdorf.

58. DM

No. 147: Test to Determine the Transmission Length of Reinforcing Bars, by Hubert Rusch and Gallus Rehm.

Determination of Latent Stresses and Registered Length

Determination of Latent Stresses and Registered Length for Prefabricated Prestressed Concrete Parts (1963), by Kurt Gaede. 22.60 DM

- No. 148: The Influence of Stirrups and Compression Bars on the Behavior of the Bending Pressure Zone of Reinforced Concrete Beams (1963), by Hubert Rusch and Siegfried Stockl. 27.60 DM
- No. 149: The Relationship between Quality and Safety in Concrete Construction (1962), by Hans Blaut. 18.50 CM
- No. 150: The Behavior of Concrete Joints during Frequently Repeated Compressive Stress and Bending Stress (1962), by Johannes Dix. out of print
- No. 151: Tests on Single-field Reinforced Concrete Beams with and without Shear Reinforcement (1962), by Fritz Leonhardt and Rene Walther. 27290 DM
- No. 152: Tests on T-beams with High Shearing Stress (1962), by Fritz Leonhardt and Rene Walther. 27250 DM
- No. 153: Elastic and Plastic Compressive Strains of Concrete due to Repeating Compressive Load and Static Load (1962), by Alfred Mehmel and Edgar Kern. 25. DM
- No. 154: Stress-Strain Diagram for Concrete and Stress Distribution in the Bending Pressure Zone with a Constant Strain Rate (1962), by Christfried Rasch. 26.30 DM
- No. 155: Influence of the Neat Cement Paste Content and of the Testing Method on the Characteristic Properties of the Bending Pressure Zone of Reinforced Concrete Beams, by Hubert Rusch and Siegfried Stockl.

- No. 156: Shear Tests on T-beams with Different Shear Reinforcement (1963), by Fritz Leonhardt and Rene Walther. 29.60 DM
- No. 157: Studies on the Rupture and Deformation Behavior of Concrete as a Result of Biaxial Stress (1963), by Helmut Weigler and Gerhard Becker. 20.70 DM
- No. 158: Rebound Tests on Dense-structure Concrete, by Kurt Gaede and Ernst Schmidt.

 Measuring the Consistency of Concrete (1964), by Walter Albrecht and Hermann Schaffler. 20.60 DM
- No. 159: The Stress of the Bond between Prestressed Reinforcement Cables in Concrete (1964), by Herbert Kupfer.

 12.30 DM
- No. 160: Tests with Deformed Reinforcing Bars (1963), by Hubert Rusch and Gallus Rehm. 21.80 DM
- No. 161: Model Statistics Study of Point Supported Obtuseangle Beams, with Special Consideration of the Yieldingness of the Support (1964), by Alfred Mehmel and Hans Weise. out of print
- No. 162: The Behavior of Reinforced Concrete and Prestressed Concrete in Fire (1964) by Horst Seekamp, Wolfran Becker, Werner Struck, Karl Kordina and Hans-Joachim Wierig.
- No. 163: Shearing Tests on Continuous Beams (1964), by Fritz Leonhardt and Rene Walther. 38.00 DM
- No. 164: Behavior of Concrete at High Temperatures (1964), by Helmut Weigler, Rudolf Fischer and Heinz Dettling. 24.60 DM
- No. 165: Tests with Deformed Reinforcing Bars (Part III) (1964), by Hubert Rusch and Gallus Rehm. 22.60 DM
- No. 166: Calculation Tables for Obtuse-angle Roadway Beams for Highway Bridges (1967), by Hubert Rusch, Arnfried Hergenroder and Thean Mungan. 38.---DM
- No. 167: Frost Resistance and Pore Structure of Concrete, Relationships and Testing Methods, by Axel Schafer.

The Influence of Fine Aggregates on the Properties of Injection Mortars for Prestressed Concrete Conduits, Injection Tests on Long Prestressed Concrete Conduits (1965), by Walter Albrecht. 27.60 DM

No. 168: Tests with Gap Gradations, by Walter Albrecht and Hermann Schaffler.

The Influence of Hardened Cement Paste Pores on the Resistance of Concrete in Seawater, by Karlhaus Wesche.

The Behavior of Young Concrete with Respect to Frost, by Friedrich Henkel.

The Use of Stud Drivers to Determine the Compressive Strength of Concrete (1965), by Kurt Gaede. 24.50 DM

No. 169: Tests on the Influence of Crack Width on the Formation of Rust on the Reinforcing Material of Reinforced Concrete Sturcutural Members, by Gallus Rehm and Hans Moll.

The Corrosion of Steel in Concrete (1965), by Hans Leonhardt Moll. 25.60 DM

No. 170: Observations on Old Reinforced Concrete Structural Members with Respect to Carbonation of the Concrete and Rusting of the Reinforcement Material, by Gallus Rehm and Hans Leonhardt Moll.

Study on the Progress of Carbonation on Concrete Structures, Conducted on behalf of the Waterways Division of the Federal Ministry of Transportation, compiled by Hans-Joachim Kleinschmidt.

Depth of the Carbonated Layer in Old Concrete Structures, Tests on Concrete Samples, performed by the Research Institute for Blast Furnace Slag, Rheinhausen, and by the Laboratory of the Westfalian Cement Industry, Beckum, compiled in the Cement Industry Research Institute of the Association of German Cement Works, Dusseldorf (1965).

No. 171: Buckling Tests with a Double-hinged Rigid Frame made of Reinforced Concrete (1965), by Walter Bochmann and Siegfried Robert. 19.10 DM

- No. 172: Impact Curve Studies on Reincforced Concrete Supports and Framing Studs Struck by Vehicles (1965), by Camillo Popp. 20.---DM
- No. 173: Determining the Biaxial Strength of Concrete, Summary and Critique of Previous Tests and a Proposal for a New Test Method, by Hubert Hilsdorf. 15.60 DM
- No. 174: The Bearing Capacity of Mesh-reinforced Concrete Columns (1965), by Helmut Weigler and J. Henzel.
- No. 175: Concrete Hinges Test Report, Design and Construction Proposals, by Fritz Leonhardt and Horst Reimann.

Critical States of Stress in Concrete during Multiaxial Static Short-term Load (1965), by Horst Reimann. out of print

- No. 176: The Fatigue Strength of Prestressed Concrete Structural Members (1966), by Martin Mayer. 17.80 DM
- No. 177: Rearrangement of the Cutting Forces in Reinforced Concrete Structures: Calculation Principles for Statically Indeterminate Support Structures, Taking into Consideration Plastic Deformations (1966), by P.S. Rao.
- No. 178: Wall-type Supports (1966), by Fritz Leonhardt and Rene Walther. 40.---DM
- No. 179: Variability of Bending Strength and Shear Strength in Reinforced Concrete Support Structures and Their Influence on the Distribution of Cutting Forces and Load during Statically Indeterminate Curing (1966), by Walter Dilger. 24.50 DM
- No. 180: Buckling of Reinforced Concrete Posts with a Rectangular Cross-section under Short-term Load (1966), calculation using automatic digital computers, by Albrecht Blaser. 15.60 DM
- No. 181: Burning Behavior of Reinforced Concrete Beams--Influence of Protective Coatings, by Karl Kordina and Paul Bornemann.

Principles for Determining the Fire Resistance Time for Reinforced Concrete Beams (1966), by Paul Bornemann.

No. 182: Carbonation of Heavy Concrete, by Adolf Meyer, Hans-Joachim Wierig and Klaus Husmann.

Influence of Atmospheric Carbon Dioxide and Moisture on the Condition of Concrete as Corrosion Protection for Steel Inserts (1967), by Fritz Schroder, Heinz-Gunter Smolczyk, Karl Grade, Reinhard Vinkeloe and Rudolf Roth.

- No. 183: Creep of Hardened Cement Paste in Concrete and How It is Affected by Simultaneous Contraction (1966), by Walter Ruetz. 15.60 DM
- No. 184: The Influence of Secondary Compaction and of a Coating on the Strength, Creep and Shrinkage of Concrete (1966), by Hubert Hilsdorf and Klemens Finsterwalder.
- No. 185: The Variable Deformation Behavior of Marginal Regions and Core Regions of Concrete (1966), by Siegfried Stockl.
- No. 186: Aged Concretes made from Slag-sulfate Cement (1966), by Karlhaus Wesche and Wilhelm Manns. 15.60 DM
- No. 187: The Influence of the Form of the Support on the Shear Force Bearing Capacity of Reinforced Concrete Beams, by Kurt Gaede.

Oscillation Measurements on Reinforced Concrete Bridges (1966), by Bruno Bruckmann. 17.80 DM

- No. 188: Deformation Tests on Reinforced Concrete Beams with Highly Refractory Reinforcing Bars (1967), by Gotthard Franz and Heinrich Brenker. 22.30 DM
- No. 189: The Carrying Capacity of Floors made of Reinforced Concrete Glazing (1967), by Colestin Zelger. 20. --- DM
- No. 190: Strength of the Bending Pressure Zone--Comparison of Prism and Beam Tests (1967), by Hubert Rusch, Karl Kordina and Siegfried Stockl. 15.60 DM
- No. 191: Experimental Determination of Stress Distribution in the Bending Pressure Zone, by Christfried Rasch.

Supporting Moments of Cross-wise Reinforced Continuous Rectangular Concrete Beams (1967), by Heinz Schwarz. 17.80 DM

- No. 192: The Effective Flange Width of T-beams (1967), by Werner Koepcke and Gunter Denecke. 27.80 DM
- No. 193: Structural Damage as a Result of the Deflection of Reinforced Concrete Structural Members (1967), by Horst Mayer and Hubert Rusch. 24.50 DM
- No. 194: Calculating the Bending under Load of Reinforced Concrete Structural Members (1967), by Horst Mayer. 24.50 DM
- No. 195: 5 Tests for Studying Deformations in the Shearing Force Region of a Reinforced Concrete Beam (1967), by Hubert Rusch and Horst Mayer. 22.20 DM
- No. 196: Preliminary Experiments on the Influence of Previous Long-time Loads on the Short-time Strength of Concrete (1967), by Siegfried Stockl.

Characteristic Numbers for the Behavior of a Rectangular Bending Pressure Zone of Reinforced Concrete Beams under Short-time Load, by Hubert Rusch and Siegfried Stockl.

25.30 DM

No. 197: Burning Behavior of Continuous Reinforced Concrete Rib Floors, by Horst Seekamp and Wolfram Becker.

Burning Behavior of Cross-wise Reinforced Concrete Rib Floors, by Jurgen Stanke.

Increasing the Thickness of Concrete Flooring as Fire Protection of Reinforced Concrete Beams, Parts 1 and 2 (1967), by Horst Seekamp and Wolfram Becker.

25.25 DM

- No. 198: Strength and Deformation of Unreinforced Concrete under Constant Long-time Load (1968), by H. Rusch, R. Sell, Ch. Rasch, E. Grasser, A. Hummel, K. Wesche and H. Flatten. 24.90 DM
- No. 199: The Calculation of Flat Continuums Using the Framework Method--Use of Beams with a Rectangular Opening (1968), by Albrecht Krebs and Friedrich Haas. 20.---DM
- No. 200: Long-term Oscillation Resistance of Reinforcing Bars <u>Imbedded in Concrete</u> (1968), by Helmut Wascheidt.

Concrete Hinges Subjected to Repeated Hinge Rotation by Gotthard Franz and Hans-Dieter Fein. 21.80 DM

- No. 201: Shear Tests on Indirectly Supported, Single-field and Continuous Reinforced Concrete Beams (1968), by Fritz Leonhardt, Rene Walther and Walter Dilger. 17.80 DM
- No. 202: Torsion and Shear Tests on Prestressed Box Girders by Fritz Leonhardt, Rene Walther and Otto Volger.

 Torsion Tests on a Synthetic Resin Model of a Box Girder (1968), by Diethelm Feder. 22.20 DN
- No. 203: Strength and Deformation of Concrete Subjected to Tensile Stresses (1969), by Hans Georg Heilmann, Hubert Hilsdorf and Klemens Finsterwalder. 26.70 DM
- No. 204: Bearing Behavior of Off-center Loaded Reinforced Concrete Compression Members (1969), by Alfred Mehmel, Heinz Schwarz, Karl-Heinz Kasparek and Joszef Makovi. 22.30 DM
- No. 205: Tests on Circular Reinforced Concrete Columns Subject to Short-time and Long-time Centric Loads (1969), by Hubert Rusch and Siegfried Stockl. 22.20 DM
- No. 206: Statistical Analysis of Concrete Strength (1969), by Hubert Rusch, Rudolf Sell and Rudiger Rackwitz.

 15.60 DM
- No. 207: Tests on the Fatigue Strength of Lightweight Concrete, by Rudolf Sell and Colestin Zelger.
 - Tests on the Strength of the Bending Pressure Zone, Influence of the Cross-sectional Shape (1969), by Steffried Stockl and Hubert Rusch. 24.50 DM
- No. 208: Cracking Caused by Latent and Induced Stresses Due to Temperature in Reinforced Concrete Structural Members (1969), by Horst Falkner. out of print
- No. 209: Strength and Deformation of Aerated Concrete Subjected to Biaxial Compressive-Tensile Stress, by Rudolf Sell.
 - Bonding Tests on Reinforced Aerated Concrete (1970), by Rudolf Sell and Colestin Zelger. 22.30 DM

- No. 210: Shear Tests with Indirectly Induced Forces: Tests to Study the Dowelling Effect of Flexural Tensile Reinforcement of a Reinforced Concrete Beam (1970), by Theodor Baumann and Hubert Rusch. 26.70 DM
- No. 211: Electronic Calculation of the State of Forces in a Cracked Reinforced Concrete Beam, Especially Taking Into Consideration the Shearing Force Region (1970), by Dieter Jungwirth.
- No. 212: Influence of the Bend of the Reinforcement on Steel Elongation, by Colestin Eelger and Hubert Rusch.

 The State of Preservation of 20-year-old Prestressed Concrete Beams (1970), by Karl Kordina and Nils Valerian Waubke.
- No. 213: Hollow Reinforced Concrete Beams Supported on Four Sides-Tests, Calculation and Design (1970), by Relmut Aster.
- No. 214: Increasing the Fire Resistance Time of Reinforced Concrete Supports by the Use of Coverings or Jackets, by Wolfram Becker and Jurgen Stanke.
 - The Behavior of Cement Mortar and Concrete at Higher Temperatures (1970), by Rudolf Fischer. 28.50 DM
- No. 215: Fire Tests on Prefabricated Reinforced Concrete Supports (1970, by Wolfram Becker and Jurgen Stanke. 28.50 DM
- No. 216: Cutting Force Tables for Designing Circular Cylinder Barrel Roofs (1971), by Alfred Mehmel, Wolfgang Kruse, Sabri Samaan and Heinz Schwarz. 39.00 DM
- No. 217: Structural Conditions of Orthagonal Reinforcement

 Meshes of Any Direction in Load-bearing Slabs made

 of Reinforced Concrete (1972), by Th. Baumann.

 18.30 DM
- No. 218: The Shear Safety and Satisfaction of Moment Requirement for Profiles Reinforced Concrete Beams (1972), by R. Kupfer and Th. Baumann. 20.50 DM
- No. 219: The Carrying Capacity of Ribbed Floors with Hollow Stone Fillers, by C. Zelger and F. Daschner.

Reinforced Brick Supports (1972), by C. Zelger. 18.90 DM

- No. 220: Design of Concrete and Reinforced Concrete Parts in Accordance with DIN 1045, January 1972 Edition-Bending with Longitudinal Force, Shear, Torsion; Buckling Safety Tests (1972). 31.00 DM
- No. 221: Strength and Deformation of Interior Wall Joints in Construction Using Panels, by H. Kupfer.

The Compressive Strength of Mortar Joints between Prefabricated Concrete Parts, by E. Grasser and F. Daschner.

Carrying Capacity (Shear Strength) of Roof Supports
Using Prefabricated Parts (1972), by R.v. Halasz
and G. Tantow. 26.60 DM

- No. 222: Pressure Shocks of Reinforcing Rod--Reinforced Concrete Supports with Highly Refractory St 90 Steel (1972), by Fritz Leonhardt and K.-Th. Teichen.
- No. 223: Reinforcement Anchorages in the Interior of Structural Members, by J. Eibl and G. Ivanyi.

 Partial Prestressing (1973), by R. Walter and N.S. Bhal.
- No 224: Interaction of Individual Prefabricated Part in the Form of a Large Disc (1973), by G. Mehlhorn.

 30.20 DM
- No. 225: Microconcrete for Model Statistical Studies (1972), by A.-Hilmar Burggrabe. 24.70 DM
- No. 226: Bearing Capacity of Tensile Loop Butt Joints, by F. Leonhardt, R. Walter and H. Deiterle.

Hook and Loop Joints in Flexurally Stressed Beams, by G. Franz and G. Timm.

Overlapping Full Butt Joints with Hook-shaped Bent Ribbed Reinforcing Bars (1973), by K. Kordina and G. Fuchs. 26.20 DM

- No. 227: Shear Tests on Prestressed Concrete Beams (1973), by Fritz Leonhardt, Rainer Koch and Ferdinand-S. Rostasy.
- No. 228: Relationship between Surface Quality, Bonding and the Splitting Effect of Reinforcing Steels Subject to Short-time Load (1973), by Horst Martin.
- No. 229: The Behavior of Concrete Subject to Multiaxial Short-time Load, with Special Attention to Biaxial Load, by Helmut Kupler.

Construction and Testing of a Test Apparatus for Biaxial Load (1973), by Helmut Kupfer and Colestin 36.00 DM

- No. 230: Heating Phenomena in Beam-like Reinforced Concrete Parts Subject to Fire Stress (1975), by H. Ehm, K. Kordina and R.v. Postel. 37.80 DM
- No. 231: The Test Reports of the German Commission for Reinforced Concrete, summaries of Nos. 1-230 (1973), by Otto Graf and Herbert Deutschmann. 18.80 pm
- No. 232: Determining the Physical Properties of Hardened

 Cement Paste, by F. Wittmann.

 Deformation and Rupture of Porous Structural Materials

 Subject to Short-time Load and Long-time Load (1974),

 by F. Wittmann and J. Zaitsev. 26.60 DM
- No. 233: Random Sample Test Plans and Acceptance Characteristic Curves for Concrete (1973), by Hans Blaut.14.70 DM
- No. 234: Finite Elements for Calculating Reinforced Concrete Reactor Pressure Vessels (1973), by J.H. Argyris, K.J. William. Szimmat, E.F. Warnke and 24.50 DM
- No. 235: Studies on the Hot Liner as the Interior Wall for Prestressed Concrete Pressure Vessels for Lightwater Spandick.

 26.75 DM
- No. 236: Bearing Capacity and Safety of Reinforced Concrete Supports Subjected to Eccentric Uniaxial and Biaxial Warner.

 Warner. 15.50 DM

- No. 237: Prestressed Concrete Reactor Pressure Vessels: Study
 to Determine Special Concrete Properties in the Construction of Reactor Pressure Vessels, by J. Eibl,
 N.V. Waubke, W. Klingsch, U. Schneider, G. Rieche.
 Parameter Calculations on a Reference Container, by
 J. Szimmal and K. William.
 Influence of Material Properties on Stress States and
 Deformation States of a Prestressed Concrete Vessel,
 by V. Hansson and F. Stangenberg (1974). 24.50 DM
- No. 238: Influence of Simulated Material Characteristics on the Critical Tipping Loads of Narrow Reinforced Concrete and Prestressed Concrete Beams, by G. Mehlhorn.

 Calculation of Reinforced Concrete Discs in State II by Assuming Realistic Material Characteristics(1974), by K. Dörr, G. Mehlhorn, W. Stauder and D. Uhlisch. 31.10 DM
- No. 239: Torsion Tests on Reinforced Concrete Beams (1974), by Fritz Leonhardt and Günther Schelling. 37.80 DM
- No. 240: Calculation of Section Sizes and Shape Changes for Reinforced Concrete Supporting Structures in Accordance With DIN 1045, January 1972 edition, by E. Grasser and G. Thielen.
- No. 241: Scaling Tests on Specimens of Concrete, Reinforced Concrete and Prestressed Concrete under Different Temperature Stresses (1974), by C. Meyer-Ottens.
- No. 242: Characteristics of Galvanized Prestressing Reinforcement and Reinforcing Rods, by G. Rehm, A. Lämmke, U. Nürnberger, G. Rieche, H. Martin and A. Rauen.

 Brazing Concrete Reinforcing Bars (1974), by D. RuBwurm.

 37.80 DM
- No. 243: Ultrasonic Pulse Technique on Prefabricated Farts, by G. Rehm, N. V. Waubke and J. Neisecke.

 Tests on Completed Prestressing Reinforcement (1975), by A. Röhnisch. 28.90 DM
- No. 244: Electronic Calculation of the Effects of Creep and Shrinkage in Combination Frameworks Produced in Sections (1975), by D. Schade and W. Haas.
- No. 245: The Granular Strength of Synthetic Aggregates and its Influence on Concrete Strength, by R. Sell.

 Compressive Strength of Light Weight Concrete (1974), by K. D. Schmidt-Hurtienne. 32.50 DM
- No. 246: Tests on the Side Impact on Foundation Posts of Reinforced Concrete and Steel When Hit by Vehicles (1974), by C. Popp. 32.00 DM

- No. 247: Temperature and Induced Stress in Lightweight
 Construction Concrete as a Result of Hydration, by
 H. Weigler and J. Nicolay.
 Long-time Expansion Stability and Operation Stability
 of Lightweight Structural Concrete (1975), by
 H. Weigler and W. Freitab. 24.50 DM
- No. 248: Scaling on Structural Members Made of Concrete Subjected to Fire Stresses (1975), by C. Meyer-Ottens.
- No. 249: Impact Bending Tests with Variously Reinforced Concrete Beams (1975), by C. Popp. 18.50 DM
- No. 250: Long-time Experiments on Reinforced Concrete Supports, by K. Kordina.

 Influence of Creep on the Lateral Buckling of Narrow Reinforced Concrete Supports, by K. Kordina and R. F. Warner.
- No. 251: Tests on Circular Reinforced Concrete Columns Subject to Eccentric Load (1975), by S. Stöckl and B. Menne. 20.00 DM
- No. 252: Stability of Different Types of Concrete in Seawater and in Water Containing Sulfate, by H. Th. Schröder, O. Hallauer and W. Scholz.
- No. 253: Prestressed Concrete Pressure Reactor Vessels:

 Instrumentation, by J. Nemel and Rudolf Angeli.

 Test to Further Develop a Deformeter (1975), by

 CBlestin Zeiger. 19.00 DM
- No. 254: Stability and Deformation Behavior of Concrete
 Subjected to High Biaxial Long-time Loads and Longtime Expansion Loads
 Stability and Deformation Behavior of Lightweight
 Concrete, Aerrated Concrete Cement Paste and Plaster
 Subjected to Short-time Biaxial Load, by D. Linse and
 A. Stegbauer.
- No. 255: Permissable Crack Widths and the Concrete Covering Required in Reinforced Concrete Construction, with Special Attention to the Carbonation Depth in the Concrete, by F. Schiebl.
- No. 256: Heat and Moisture Flow in Concrete as a Function of Temperature (1975), by J. Hundt. 29.40 DM